FAULT TOLERANT STRATEGY FOR ACTIVELY CONTROLLED RAILWAY WHEELSET

Mohammad Mirzapour

School of Computing, Science and Engineering College of Science and Technology
University of Salford, Salford, UK

Submitted in Partial Fulfilment of the Requirements of the Degree of Doctor of Philosophy, June 2015

CONTENTS

List of Figures

List of Tables

List of Equations

List of Abbreviations

AVL	Vehicle with active control, trailing wheelset
AVT	Vehicle with active control, leading wheelset
FDI	Fault detection and isolation
FDI 1	Fault detection and isolation through vehicle model-based approach
FDI 2	Fault detection and isolation through actuator model-based approach
FH	Fail hard
FS	Fail soft
FTC	Fault tolerant control
KF	Kalman Filter
LFS	Leading actuator fail-soft
LH	Leading actuator fail-hard
LH1	Leading actuator fail-hard at conicity of 0.1
LH2	Leading actuator fail-hard at conicity of 0.2
LH3	Leading actuator fail-hard at conicity of 0.35
LHL	Leading actuator fail-hard, leading wheelset
LHR	Leading actuator fail-hard, trailing wheelset
LKF	Local Kalman Filter
LSC	Leading actuator with short circuit failure
LSC	Trailing actuator with short circuit failure
NC	Normal condition
NC2	Normal condition at conicity of 0.2
NC3	Normal condition at conicity of 0.35
NCL	Normal condition, leading wheelset

NCT	Normal condition, trailing wheelset
OC	Open circuit
PVL	Passive vehicle, leading wheelset
PVT	Passive vehicle, trailing wheelset
RC	Re-configuration control
RCO1	Actuator open circuit failure with re-configuration control, leading wheelset
RCO2	Actuator open circuit failure with re-configuration control, trailing wheelset
RCS1	Actuator short circuit failure with re-configuration control, leading wheelset
RCS2	Actuator short circuit failure with re-configuration control, trailing wheelset
RMS	Root mean square
S_1	Failure of the lateral accelerometer sensor on the front wheelset
S_7	Failure of the relative yaw displacement sensor on the front wheelset
S_8	Failure of the relative yaw displacement sensor on the rear wheelset
SC	Short circuit
SF1	Failure of the motor sensor
SF2	Failure of the motor current
SF3	Failure of the motor torque
STD	Standard deviation
TFS	Tailing actuator fail-soft
TH	Trailing actuator, fail-hard
THL	Trailing actuator fail-hard, leading wheelset
TOC	Trailing actuator with open circuit failure

List of Symbols

A_r	Track roughness factor
C_g	Gearbox drive damping
C_m	Motor gearbox shaft damping
C_s	Primary lateral damping
C_{sc}	Secondary lateral longitudinal damping
f	Temporary frequency
f_{11}	Longitudinal creepage coefficient
f_{22}	Lateral creepage coefficient
f_{33}	Spin creep coefficient
F_{1L}	Longitudinal contact force of the left hand side wheel
F_{1R}	Longitudinal contact force of the right hand side wheel
F_{2L}	Lateral contact force of the left hand side wheel
F_{2R}	Lateral contact force of the right hand side wheel
f_n	Kinematic frequency
$F_{f_{wg}}$	Lateral force between front wheelset and bogie
$F_{r_{wg}}$	Lateral force between rear wheelset and bogie
F_{gv}	Lateral force between wheelsets and half body
F_{fm}	Gravity force, front wheelset
F_{rm}	Gravity force, rear wheelset

F_{gm}	Gravity force, bogie frame
F_{vm}	Gravity force, half body
F_{fc}	Centrifugal force, front wheelset
F_{rc}	Centrifugal force, rear wheelset
F_{gc}	Centrifugal force, bogie frame
F_{vc}	Centrifugal force, half body
$F_{f_{1L}}$	Longitudinal contact force, left wheel (front wheelset)
$F_{r_{1L}}$	Longitudinal contact force, left wheel (rear wheelset)
$F_{f_{1R}}$	Longitudinal contact force, right wheel (front wheelset)
$F_{r_{1R}}$	Longitudinal contact force, right wheel (rear wheelset)
$F_{f_{2L}}$	Lateral contact force, left wheel (front wheelset)
$F_{r_{2L}}$	Lateral contact force, left wheel (rear wheelset)
$F_{f_{2R}}$	Lateral contact force, right wheel (front wheelset)
$F_{r_{2R}}$	Lateral contact force, right wheel (rear wheelset)
g	Gravity
i_a	Motor's current
I_g	Bogie yaw inertia
I_m	Motor's rotor moment of inertia
I_{ma}	Motor's stator moment of inertia
I_w	Wheelset yaw inertia

k	Yaw stiffness from the passive spring
K_b	Motor back e.m.f constant
K_f	The material stiffness in the connections of the actuators to the bogie frame and wheelset in the event of the actuator fail hard
K_g	Gearbox drive stiffness
K_s	Primary lateral stiffness
K_{sc}	Secondary lateral longitudinal stiffness
K_t	Motor torque constant
L_a	Motor armature inductance
l_g	Half gauge of wheelset
l_v	Half spacing of axle
m_g	Bogie mass
m_w	Wheel mass
m_v	Half vehicle mass
N	Window size
n	Gear ratio
r_0	Wheel radius
R_1	Track curve, front wheelset
R_2	Track curve, rear wheelset
R_a	Motor armature resistance
r_L	Contact radii of he left wheel

r_R	Contact radii of the right wheel
Q_1	Variance of the lateral track irregularities
V_a	Motor voltage
V_s	Vehicle forward speed
$V_{x_l}^{\ t}$	Longitudinal velocity of the left hand side track
$V_{x_r}^{\ t}$	Longitudinal velocity of the right hand side track
$V_{y_l}^{\ t}$	Lateral velocity of the left hand side track
$V_{y_r}^{\ t}$	Lateral velocity of the right hand side track
$V_{x_l}^{\ w}$	Longitudinal velocity of the left hand side wheel
$V_{x_r}^{\ w}$	Longitudinal velocity of the right hand side wheel
$V_{y_l}^{\ w}$	Lateral velocity of the left hand side wheel
$V_{y_r}^{\ w}$	Lateral velocity of the right hand side wheel
V_x^t	Longitudinal velocity of the track
V_y^t	Lateral velocity of the track
V_x^w	Longitudinal velocity of the wheel
V_y^w	Lateral velocity of the wheel
x_i	The sampling point of the raw signal
y_g	Lateral displacement, bogie frame
$\dot{y}_g$	Lateral velocity, bogie frame
$\ddot{y}_g$	Lateral acceleration, bogie frame

y_{t_1}	Random track (irregularities) lateral displacement, front wheelset
$\dot{y}_{t_1}$	Random track (irregularities) lateral velocity , front wheelset
y_{t_2}	Random track (irregularities) lateral displacement, rear wheelset
$\dot{y}_{t_2}$	Random track (irregularities) lateral velocity, rear wheelset
y_v	Lateral displacement, half body
$\dot{y}_v$	Lateral velocity, half body
y_{w_1}	Lateral displacement, front wheelset
$\dot{y}_{w_1}$	Lateral velocity, front wheelset
$\ddot{y}_{w_1}$	Lateral acceleration, front wheelset
y_{w_2}	Lateral displacement, rear wheelset
$\dot{y}_{w_2}$	Lateral velocity, rear wheelset
$\ddot{y}_{w_2}$	Lateral acceleration, rear wheelset
Ω_{3_L}	Spin creepage at left hand side wheel
Ω_{3_R}	Spin creepage at right hand side wheel
Ω_z^w	Rotational velocity of the wheel
Ω_z^t	Rotational velocity of the track
$\Omega_{z_l}^{\ w}$	Rotational velocity of the left hand side wheel
$\Omega_{z_r}^{\ w}$	Rotational velocity of the left hand side wheel
$\Omega_{z_l}^{\ t}$	Rotational velocity of the left hand side track

$\Omega_{z_r}{}^{t}$	Rotational velocity of the right hand side track
α_1	Radial angular position of the leading wheelset, fail hard
α_2	Radial angular position of the trailing wheelset, fail hard
γ_1	Longitudinal creepage
γ_2	Lateral creepage
γ_{1_L}	Longitudinal creepage at left hand side wheel
γ_{1_R}	Longitudinal creepage at right hand side wheel
γ_{2_L}	Lateral creepage left hand side wheel
γ_{2_R}	Lateral creepage right hand side wheel
λ	Conicity
$\lambda_{0.1}$	The conicity at 0.1
$\lambda_{0.2}$	The conicity at 0.2
$\lambda_{0.35}$	The conicity at 0.35
λ_L	Conicity of the right wheel
λ_R	Conicity of the right wheel
θ_{c_1}	Track cant angle, front wheelset
θ_{c_2}	Track cant angle, rear wheelset
θ_m	Motor's rotor displacement
$\dot{\theta}_m$	Motor's rotor velocity
$\ddot{\theta}_m$	Motor's rotor acceleration

τ_{f_1}	Torque of leading wheelset, when leading actuator fail-hard
τ_{f_2}	Torque of trailing wheelset, when trailing actuator fail-hard
τ_g	Gearbox torque
τ_m	Motor torque
τ_{w_1}	Produced a torque opposing the yaw motion of the front wheelset
τ_{w_2}	Produced a torque opposing the yaw motion of the rear wheelset
ω	Angular velocity of the wheelset
ω_3	Spin creepage
ψ_g	Yaw motion bogie frame
$\dot{\psi}_g$	Yaw velocity bogie frame
$\ddot{\psi}_g$	Yaw acceleration bogie frame
ψ_{w_1}	Yaw motion, front wheelset
$\dot{\psi}_{w_1}$	Yaw velocity, front wheelset
$\ddot{\psi}_{w_1}$	Yaw acceleration, front wheelset
ψ_{w_2}	Yaw motion rear wheelset
$\dot{\psi}_{w_2}$	Yaw velocity, rear wheelset
$\ddot{\psi}_{w_2}$	Yaw acceleration, rear wheelset
$\Delta\psi_{w_1}$	Relative yaw motion between front wheelset and bogie frame
$\Delta\psi_{w_2}$	Relative yaw motion between rear wheelset and bogie frame

Acknowledgements

This thesis is submitted in partial fulfilment of the requirements for a Doctorate's Degree in control system engineering. The work in this thesis was carried out between June 2011 and June 2014 at the Research Centre for Control and Systems Engineering at Salford University, Salford, UK.

I would like to acknowledge the support of the Engineering and Physical Science Research Council (EPSRC) and Rail Research UK Association (RRUKA) for funding/ supporting the project, which has made this study possible. Particularly, I am thankful to my supervisor, Professor TX Mei, for providing me the opportunity to do this work, for guiding me through the field of condition monitoring and for lots of great inspiration, ideas, and comments.

In addition, I want to gratefully acknowledge all my friends, and especially Marc Whalley, for his remarkable ability to cheer me up when I was in desperate need of it.

Finally, I want to show my most heartfelt gratitude to my family, especially my Dad and Mum, for all your support and encouragement during my study. Your efforts are beyond any words that can be expressed!

March 2015

Mo

Abstract

Traditionally, solid axle railway wheelsets are stabilised by using passive suspensions on a conventional rail vehicle, but such additional stiffness affects the pure rolling action of the wheelset around the curve. It has been theoretically proven that this design conflict between stability and curving performance can be solved by applying active control instead of conventional passive components, resulting in the reduction of the wear of the wheels and track by minimising the track shifting forces. In the active approach, the use of actuators, sensors and data processors to replace the traditional passive suspension raises the issue of the system safety in the event of a failure of the active control, which could result in the loss of stability and in more severe cases, derailment. Further on, in active control systems for railway vehicles the actuators tend to be significantly more expensive and require more additional space than sensors, and an electronic control unit. Therefore, developing an analytical redundancy-based fault tolerance technique for an actively controlled wheelset that minimises the number of actuators will clearly be more beneficial. Thus the emphasis of this research is to develop a fault-tolerant system of active control for a railway vehicle in the event of actuator malfunction in order to guarantee stability and good curving performance without using additional actuators. The key achievements of this research can be summarised as follows:

- The research considers three of the most common types of actuator failure for the electro-mechanical actuators: fail-hard (FH), short circuit (SC) and open circuit (OC). The fail-hard is a failure condition when the motor shaft of the actuator becomes immovable, whereas the short circuit and open circuit are failures that occur in the electrical parts of the actuator which correspond to zero voltage and zero current in the motor respectively.

- The research investigates and develops a thorough understanding of the effect of actuator faults and failure modes on the vehicle behaviour that provides the necessary foundation for the development of the proposed fault-tolerant strategy.
- An effective fault detection and isolation methods for actuator faults through two different approaches is developed; the vehicle model-based approach and the actuator model-based approach. Additionally, the research takes into account the reliability and robustness of the FDI schemes in the presence of sensor failures and parameter uncertainties in the system.
- The research develops the control re-configuration in order to cope with the identified failure mode of the actuator in order to maintain the vehicle stability and desired curving performance.

Chapter 1 INTRODUCTION & LITERATURE REVIEW

A conventional railway vehicle is stabilised through the use of the passive suspensions, but such additional stiffness has an adverse impact on the curving performance (Polach, 2004); resulting in the severe wear of the wheel and rail during curving and fatigue due to the high stress related with rolling contact during curve negotiation. On the other hand, there is a limitation to the design of an optimum passive suspension that limits the extent to which contact forces can be minimised in wheel-rail contact patches in order to solve this conflict for the railway vehicle.

More recent studies have suggested that the active control for the railway wheelset in the primary suspensions can be used to overcome this design conflict by stabilising the wheelsets without compromising the vehicle performance on curved track (Pearson, Goodall, Mei, & Himmelstein, 2004); by affecting/ minimising the dynamic forces between wheel and rail.

In this new method, the use of actuators and sensors to replace the traditional passive suspensions raises the concern of system safety in the event of a malfunction of the active control, which could result in the loss of stability and in more severe cases derailment (Mirzapour & Mei, 2014).Therefore, the active controls for safety-critical applications have to achieve a high level of integrity through appropriate fault tolerance solutions that guarantee the basic functionality and safety of the overall system whilst permitting component fault(s) (Mirzapour & Mei, 2014).

This chapter presents a brief background of the actively controlled wheelset with different vehicle configuration and control methodologies. Meanwhile, a full description of the proposed fault-tolerant strategy will be provided as it represents an important issue in maintaining the safety and reliability of the active suspension for the railway vehicle. Finally, the research objective of this study as well as thesis structure will be given.

1.1 Background and Overview of Active Control

A conventional railway wheelset is composed of two coned (or profiled) wheels rigidly connected to a common axle to rotate at the same angular velocity, as shown in Figure 1.1 (Wickens, 1998). When an unconstrained wheelset travels through a curved track, it is displaced laterally and the rolling radii of the two wheels are therefore different because of the profiles of the wheelsets. Consequently, different forward speeds are obtained for each wheelset due to the difference in rolling radii that provide a natural centring/curving action. However, this arrangement has the disadvantage of presenting a problem of kinematic instability, known as "Kinematic Oscillation" or wheelset "hunting", as illustrated in Figure 1.2 (Brickle, 1986).

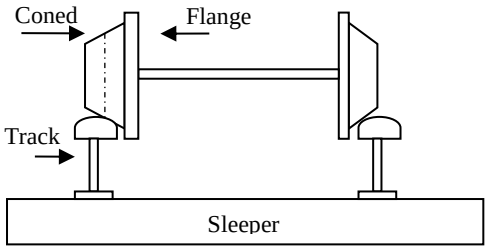

Figure 1-1: Conventional wheelset for railway vehicles

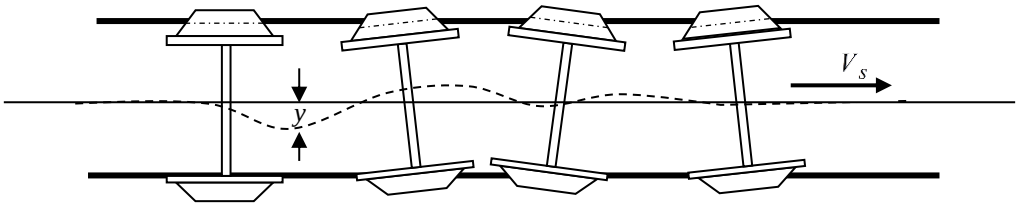

Figure 1-2: "Kinematic Oscillation" or wheelset "hunting"

The dynamic performance of conventional railway vehicles is determined by the basic geometry and mechanical parameters such as mass, springs, dampers and contact mechanics,

etc., the values of which are constrained in all manner of ways (Goodall & Kortum, 2002; Iwnicki, 2003). The instability problem is solved on conventional railway vehicles by using passive springs connected between the wheelset and the body/bogie frame of the vehicle, but the added stiffness also interferes with the movement of the wheelset on curves (Anon, 1997; Mei & Goodall, 1999a) and is known to be a main cause of severe wheel and rail wear (Mei & Goodall, 2001). There is therefore a difficult trade-off to be made between the vehicle's stability and curving performance in the design of railway vehicles/suspensions (Pearson, Goodall, Mei, & Himmelstein, 2004).

A detailed study shows that there are limitations to designing such optimum basic geometry and mechanical parameters to overcome the perceived conflict for the railway vehicle (Wickens, Stability of High Speed trains, 1973). A number of more recent investigations have concluded that this design conflict can be solved by applying active control within the primary suspensions to stabilise the wheelset and control laws can be formulated not to interfere with the natural curving actions of the wheelset; leading to a significant reduction in the wear of the wheelset and track, and minimised track-shifting forces (Mei & Goodall, 2000a). Therefore, there has been increasing interest in the use of active control in the railway industry as opposed to its passive counterparts (Bruni, Goodall, Mei, & Tsunashima, 2007).

With active suspensions, actuators can be used to deliver the desired forces or torques that are reliant upon measurements from a combination of sensors and a controller, as given in Figure 1.3 (Goodall, 1997). The use of active control leads to higher levels of dynamic performance that may be completely impractical with passive approaches (Goodall & Kortum, 2002). In the passive suspensions, the relationship between inputs and outputs only determined by the value of masses, springs, dampers and the geometrical arrangement (Goodall & Mei, 2006a, p. 328) whereas, in the active approach, the dynamic performance becomes dependent upon

the number and positioning of the actuators, the number and type of sensors, and the software that implements the control algorithms to provide a link between the controller and physical/vehicle system to be controlled (Goodall & Mei, 2006b).

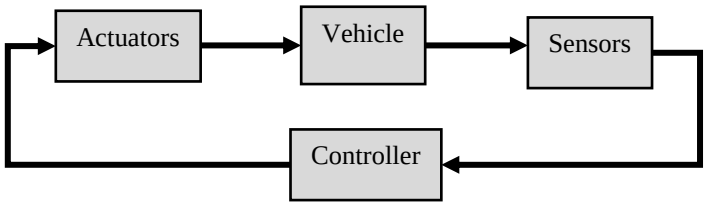

Figure 1-3: Active control strategy

Recently, a number of different wheelset configurations and active control methodologies have been developed to maintain stability without compromising the steering performance of the vehicle, which offers greater scope of possible approaches for the active primary suspensions (Goodall, Bruni, & Mei, 2006; Bruni, Goodall, Mei, & Tsunashima, 2007). These proposed technologies can significantly improve the future efficiency of rail vehicles in terms of cost, energy consumption, maintenance, weight and reduced complexity in vehicle configurations (Kortüm, Goodall, & Hedrick, 1998). This section reviews various options for the actively controlled wheelset. Different actuation configurations for the active control of railway wheels, and different control approaches and control design methods are provided in subsections 1.1.1 and 1.1.2, respectively.

1.1.1 Vehicle configuration and actuation scheme

A number of different vehicle (mechanical) configuration schemes for controlling the wheels and the wheelset have been proposed recently. These options are illustrated diagrammatically in figures 1.4 to 1.9.

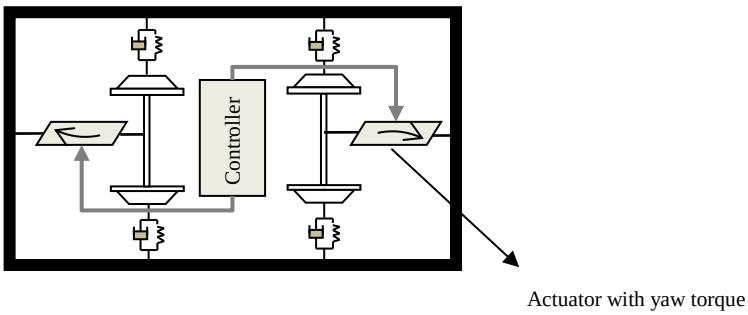

Figure 1-4: Actuated solid-axle wheelset (ASW) via yaw torque

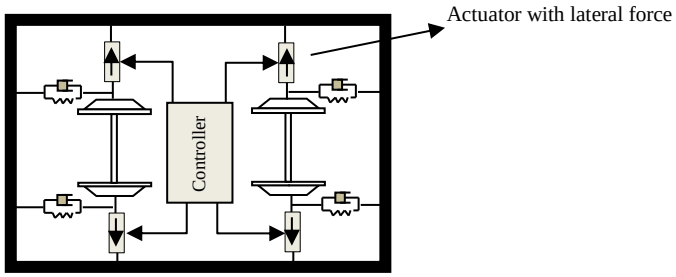

Figure 1-5: Actuated solid-axle wheelset (ASW) via lateral force

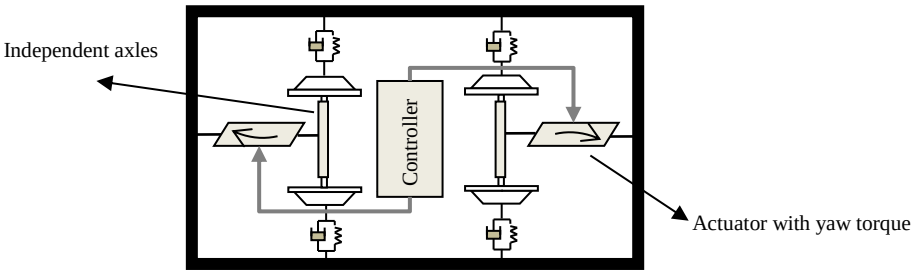

Figure 1-6: Actuated independently rotating wheels (AIRW)

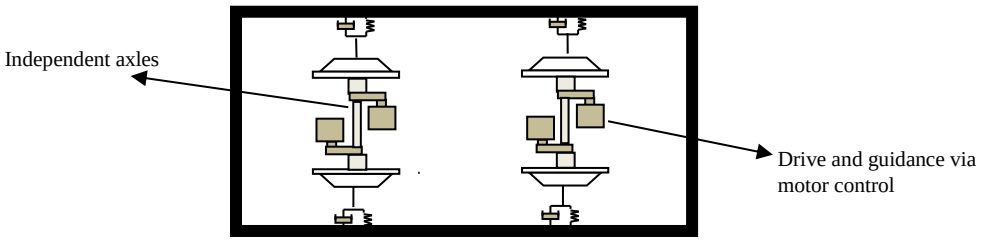

Figure 1-7: Driven independently rotating wheels (DIRW)

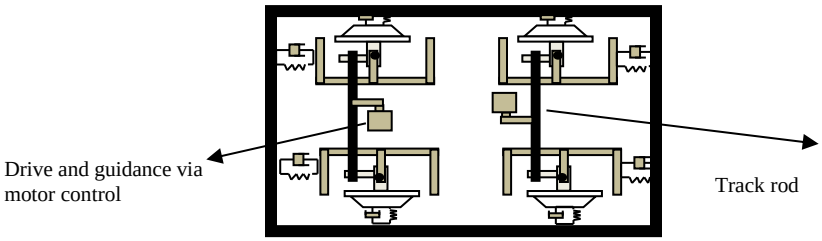

Figure 1-8: Directly steered wheels (DSW)

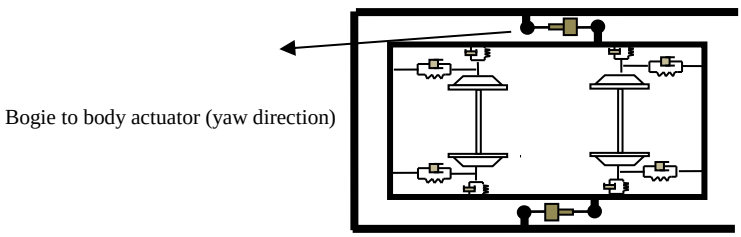

Figure 1-9: Secondary yaw control (SYC)

- **Actuated solid-axle wheelset (ASW):** The first concept was investigated through the use of controlled traction rods to provide a yaw relation of coned wheelsets in order to

improve curving performance without compromising stability (Shen & Goodall, 1997). In the ASW configuration, the actuator provides a controllable force or torque to a conventional wheelset to maintain the stability and curving performance of the railway vehicle. The actuated solid-axle wheelset via yaw torque and lateral force schemes are shown in figures 1.4 and 1.5, respectively. It has been suggested by Mei and Goodall (1999a) that yaw actuation is preferable to lateral actuation, with the former requiring a lower control force to achieve the same level of stability and provide better ride comfort experienced by the passengers. In recent years, several studies have focused on the advantages of applying the ASW concept to conventional bogie-based architectures for high speed service compared to the passive vehicle. For example, a study in (Perez, Busturia, & Goodall, 2002) investigated the problem of sensors' requirements and required state estimation for the implementation of the active control strategies with the main emphasis on improved curving performances. A comprehensive study (Pearson, Goodall, Mei, & Himmelstein, 2004) studied both stability and curving performance, and requirements for actuators and sensors, as well as the required state estimation for practical implementation. The demonstrated concept has also been tested on a full size vehicle (Pearson, et al., 2003).

- **Actuated independently rotating wheelset (AIRW):** The use of independently rotating wheelsets (IRW) allows the two wheels on the same axle to rotate independently from each other. This configuration eliminates the cause of hunting due to the decoupling of the yaw motion and lateral displacement (Dukkipati, Narayanaswamy, & Osman, 1992), as shown in Figure 1.6, but the removed constraint between the two wheels also lead to the loss of guidance and natural curving of the solid-axle wheelset (Goodall & Li, 2000) Therefore, some form of steering control becomes necessary but this tends to require a lower control torque

(actuation effort) when compared to a conventional solid wheelset (Mei & Goodall, 2001).

- **Driven independently rotating wheelset (DIRW):** For the independently-rotating wheelset, there is a possibility of controlling the wheelset via an active torsional coupling, as shown diagrammatically in Figure 1.7, where independently driven, independently rotating wheelsets provide drive and guidance via motor control (Gretzschel & Bose, 1999). The other study in (Mei, Li, Goodall, & Wickens, 2002) investigates the implementation of the DIRW on two-axle vehicle (without bogie) on a low speed vehicle through the use of permanent magnet electric motors embedded inside the wheels.
- **Directly steered wheels (DSW):** The concept was initially treated by (Aknin, Ayasse, & Devallez, 1991). In this configuration, the axles of the independently-rotating wheelset are mounted onto a wheel frame, as shown in Figure 1.8. This configuration offers the possibility of applying a lateral force between the frame and the wheels to steer the angle directly via a track rod. Study in (Wickens, 1994) considered a vehicle configuration with a carbody and two bogies, and each bogie equipped with DSW which is guided by feedback on the lateral wheel/rail displacement, with the main emphasis on the vehicle stability and curving performance, where very good curving performance can be obtained compared to a conventional passive vehicle. A recent application of the DSW concept is proposed by (Suda, Wang, Nishina, Lin, & Michitsuji, 2012), where independently rotating wheels with inverse tread conicity have been considered in order to improve steering ability without any complex bogie structure, and the effectiveness of the concept has been demonstrated using a vehicle with two single-axle bogies in a 1/10 scale model experiment.

- **Secondary yaw control (SYC):** This concept is based on applying a yaw torque on the bogie, to improve stability and/or curving performance, as shown in Figure 1.9. The actuator may be designed to replace the traditional passive yaw dampers, and therefore active control of the running gear can be introduced without fundamental redesign of the bogie (Diana, Bruni, Cheli, & Resta, 2002), but this approach is less beneficial in tackling the trade-off between the stability and curving performance than what is possible when the control is applied directly to wheelsets.

1.1.2 Control strategies

The different vehicle configurations reviewed in subsection 1.1.1 present several practical challenges that have to be considered in order to develop the controller (Goodall & Mei, 2006b). One of the most important challenges relates to providing essential feedback signals for the controller as that some of the feedback variables are very difficult and expensive to measure, such as the relative movement between the wheels and rail-track and the wheelset angle of attack (Bruni, Goodall, Mei, & Tsunashima, 2007; Li H. , 2001). Therefore, it is necessary to find cost-effective solutions with the use of practical sensors (Mei, Li, & Goodall , 2001). Furthermore, railway vehicles are subject to parameter variations when the vehicle is running along a track, especially at the wheel-rail interface. Another issue is related to the order of the dynamic models of railway vehicle, which is usually high, which may lead to a complex controller (Zolotas & Goodall, 2007, p. 4). For the configuration of yaw actuation, which is also considered in this study, control strategies that have been proposed include intuitively formulated control methods and model-based control approaches.

- **Active yaw damping:** where the vehicle stabilisation can be achieved by applying a yaw torque to each axle proportional to its lateral velocity (Mei & Li, 2007).
- **Sky-hook spring:** where the control torque of each actuator is set to be proportional to the yaw angle of the corresponding wheelset (Mei & Goodall, 2007).
- **Model base full state feedback control:** where the controllers for the two actuators are designed with full-state-feedback, where the feedback states may be provided through the use of an estimator (Mei & Goodall, 2003a).

Although the control requirements as well as control possibilities are mostly reliant on the vehicle and wheelset configurations as outlined above, an important challenge relates to the strategies for the safety and reliability of the active control (Goodall & Mei, 2006b; Goodall, 2010).

In the active approach, the use of actuators, sensors and data processors to replace the traditional passive suspensions raises the issue of system safety in the event of a failure of the active control, which could result in the loss of stability (i.e., wheelset hunting) and, in more severe cases, derailment. The practical implementation for such technology can only be made possible if the safety and reliability requirements can be addressed satisfactorily. Therefore, actively controlled wheelsets for such a safety-critical application have to attain a high level of integrity through fault tolerance approaches that ensure the basic functionality of the entire system, whilst being capable of tolerating potential faults (Mirzapour, Mei, & Xuesong, 2014).

1.2 Fault-Tolerant Control

More recently, fault-tolerant control has drawn significant attention due to the growing demand for safety, reliability, and productivity in many engineering applications (Jiang, 2005). In recent years, an increasing number of survey papers on fault-tolerant control

systems have appeared (Blanke, Izadi Zamanabadi, Bogh, & Lunau, 1997; Steinberg, 2005; Isermann, Schwarz, & Stolzl, 2002; Zhang & Jiang, 2008; Patton, 1997) and text books on this subject have been published (Benıtez, Hector, García, & Fabián, 2005; Isermann, 2011; Ding, 2014; Patton, Frank, & Clark, 2000; Patton, Clark, & Frank, 1989; Gertler, 1998). Literature reviews indicated that the research on fault-tolerant control systems was first motivated by aircraft flight control system designs (Steinberg, 2005; Lombaerts, Saili, & Breeman, 2010, pp. 2-3), where the objective was to provide "self-repairing" capability in order to ensure that a safe landing in the incident of severe faults in aircraft can be achieved (Zhang & Jiang, 2008; Chandler, 1984). Historically, the notion of a fault-tolerant control system has been inspired by reported commercial aircraft accidents in the late 1970s (McMahan, 2005; Montoya, et al., 1982). In one accident, Delta Flight 1080 (April 12, 1977) (McMahan, 2005), the captain experienced a serious control problem in the pitch axis immediately after take-off. The malfunction was later determined to be the left elevator jammed in the up position (at 19°), but the pilot had been given no indication of this malfunction. However, based on his experience and knowledge about actuation redundancy in the L-1011 airplane, the pilot was able to reconfigure the remaining control elements to land safely. In another accident, American Airlines Flight 191 (May 25, 1979) (Montoya, et al., 1982) crashed, and subsequent investigation by the National Transportation Safety Board reported (1979) that the crash could have been avoided if the engine failure had been separated/isolated, a mechanism that the DC-10 did not have. More recently, fault-tolerant control has begun to draw more widespread attention in a variety of industrial applications, as can be seen from a number of existing publications such as in the aerospace (Briere, Favre, & Traverse, 2001; Goupile, 2011; Tarnowski, 2008), automotive (Isermann, Schwarz, & Stolzl, 2002), railway vehicles (Goodall & Kortum, 2002; Goodall & Mei, 2006b; Goodall, 2010), manufacturing and other process industries (Bruccoleri, Amico, & Perrone, 2003; Mehrabi,

Ulsoy, Koren, & Heytler, 2002). In fact, the concept of a fault-tolerant system is a vital part of a control design and complex system in order to make feasible the implementation of the new innovation (Muenchhof, Beck, & Isermann, 2009), whereas without developing the fault-tolerant control the production of such a new innovation cannot be justified in terms of the reliability and cost for the high volume of production. Such an example can be seen for clutch-by-wire (eClutch) in the automotive industry (Gallagher, Paciotti, Ribichini, & Struve, 2012). The objective of the eClutch is to provide sufficient damping through controlling the slip between the engine and driveline in order to minimise the excited driveline oscillation which occurs during synchronisation of the engine and drivetrain (Albers, Meid, & Ott, 2010). Although the concept has been implemented successfully, it requires substantial consideration to develop fault-tolerant control in the incident of the components' failures to ensure that the actuator and sensors are functioning in order to engage/disengage the clutch by driver request.

In general, redundancy is fundamental to achieve fault tolerance which can be classified on the basis of redundancy in hardware and analytical redundancy (Nelson, 1990; Patton, 1991).

1.2.1 Hardware redundancy

In hardware redundancy at least two modules are required in order to re-configuration take place. One module is usually in operation with the other module used as the standby or backup unit. If the operation module fails, the backup unit takes over. This requires a fault detection and isolation (FDI) scheme to identify if an operational component has become faulty, in order for the reconfiguration to switch to the standby component. The fault detection scheme is usually performed by the use of an output signal for consistency checking, cross testing or voting system through the use of information in computers (Isermann, Schwarz, & Stolzl, 2002) . Another way is to use self-validating sensors or actuators to perform fault detection technique (Henry & Clarke, 1993; Clarke, 1995), where

sensor/ actuator has an in-built microprocessor and therefore the self-diagnosis take place within sensor/ actuator (Isermann, Schwarz, & Stolzl, 2002).

Hardware redundancy can be performed with “cold-standby” or “hot-standby” methods (Furman, Chutani, & Nussbaumer, 1995; Isermann, 2011, p. 22). In the “cold-standby” the back-up component comes to operation when the fault appears, as shown in Figure 1.10. Although this method saves the lifetime of the component, it does not guarantee that the backup module is functioning at the time when it is required to be in the operation. The other disadvantage with this re-configuration is that a transition time is required to switch from the faulty component to the intake module (Isermann, Schwarz, & Stolzl, 2002).

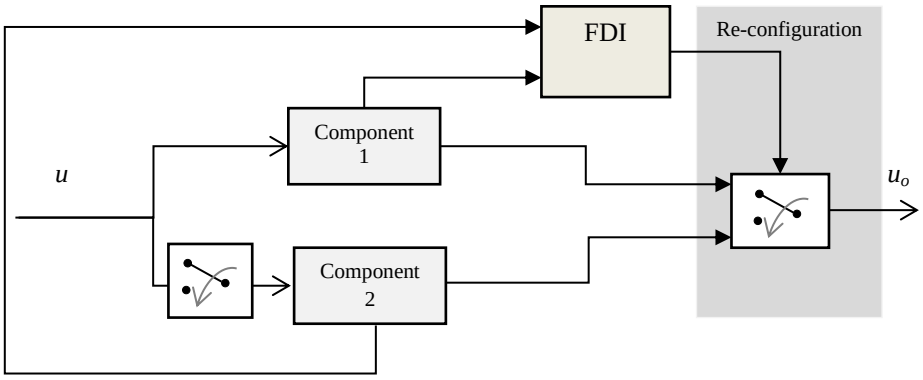

Figure 1-10: Hardware redundancy with “cold-standby”

In the cease of “hot-standby”, the standby unit is continuously running as shown in Figure 1.11. In contrast to the “cold-standby” method, the continuous operation of the backup module ensures that the intake unit is available for operation at the expected time, and this strategy also minimises the transition time to start-up procedure (Isermann, 2008).

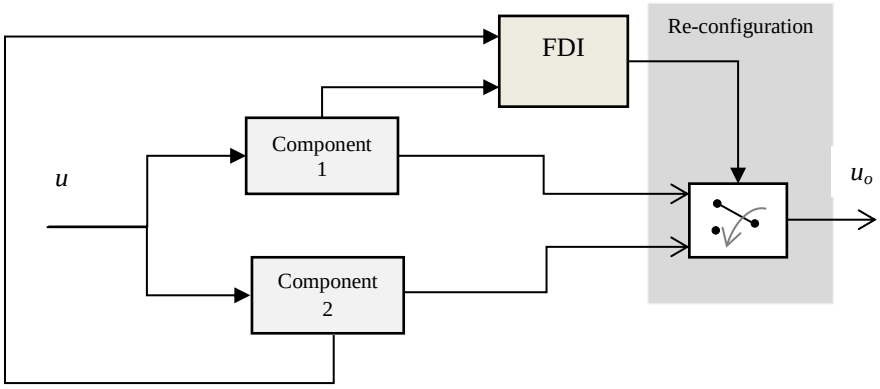

Figure 1-11: Hardware redundancy with "hot-standby"

An example of hardware redundancy can be given in military aircraft applications and the new generation of civilian aircrafts such as the Boeing 777 and Airbus A320/330/340/380 (Briere, Favre, & Traverse, 2001), where the control surfaces are controlled by multiple actuators and motion sensors in the yaw, roll and pitch directions to maintain the required level of safety. The decision is made by a "voting plan" which determines the available components to control the system (Goupile, 2011). However, this type of redundancy requires multiple components to be used, and also an additional space is needed to accommodate the redundant components within the limited space of the system; therefore the cost, complexity, power consumption, weight and maintenance scheduling of the overall system could significantly increase (Crepin & Kress, 2000). Nevertheless, it should be noted that sometimes the use of hardware redundancy is unavoidable in order to be able to develop a fault-tolerant strategy. A practical example can be given in a brake-by-wire system, which presents the concept of hardware redundancy for safety-critical applications, where a fault-tolerant strategy with hardware redundancies with hot-standby for the real-time communication system and power system were employed (Isermann, Schwarz, & Stolzl, 2002; Schwarz, Isermann, Böhm, Nell, & Rieth, 1998). A prototype concept of an electro-mechanical brake was developed by Continental Teves, Germany, and the system consists of

four electro-mechanical wheel brake modules with local microcontrollers, an electromechanical brake pedal module, a duplex communication bus system and a central brake management computer (Isermann, Schwarz, & Stolzl, 2002).

1.2.2 Analytical redundancy

In contrast to hardware redundancy, the analytical redundancy method can help to considerably reduce the use of hardware redundancies (number of components) in order to keep the overall cost down in terms of design and development (Frank, 1990). In an analytical redundancy, the re-configuration is achieved through software without adding extra components in the incident of fault(s) (Patton, 1991; Patton, 1997) in order to maintain stability and the current dynamic performance of the system close to the desired performance (Guenab, Weber, Theilliol, & Zhang, 2011). However, in order to allow a reconfiguration to take place, FDI methods must be performed to diagnose the faulty components. FDI may be classified depending on the dynamical availability of the model associated with the applications into the model-based approach, direct-signal approach and intelligent (knowledge) -based approach (Isermann, 2011, p. 24).

1.2.2.1 Direct computation

Many measured signals of processes show oscillations that are either of harmonic or stochastic nature, or both. If changes in these signals are related to faults in the actuators, the process and sensors, then signal based fault detection methods can be applied in order to detect an abnormal change in time or frequency domain. Therefore, in this approach FDI is based merely on the analysis of the output signal (measured signal) (Isermann, 2005). This method is well suited for detecting abnormal changes in the stator current and magnetic fields inside the motor of an actuator due to its periodic behaviour, but it might not be able to provide reliable fault detection for the bearings due to noise, gear teeth and temperature

changes, etc. (Muenchhof, Beck, & Isermann, 2009). Studies in (El Hachemi Benbouzid, 2000; Zhongming , 2000) survey the detection of abnormal changes in the electrical (rotor, stator) and mechanical (bearing) parts of an induction motor through the use of the signal-based approach in both the time and frequency domains.

1.2.2.2 Model-based approaches

If a physical system is sufficiently understood and a set of dynamic equations that capture its essential responses can be developed, a model-based approach can be appropriate (Patton, Uppal , & Lopez-Toribio, 2000). This approach captures human knowledge explicitly within the model, and a mathematical model enables powerful parameter-estimation techniques to be developed using concepts of parameter estimation or state-estimation techniques such as least square or parity equation for parameter estimation(s), or the Kalman Filter (KF) for linear systems, or the Extended Kalman Filter in the case of non-linearity for the state estimation (Isermann, 1997). In general, in the model-based approach, fault detection can be determined by fixed threshold(s) on residuals—the difference between real measurements and their estimation obtained from a mathematical model. The analysis of each residual which exceeds the threshold can then be used to help with fault isolation (Simani, 2006, p. 28). Figure 1.12 shows the general structure of a model-based approach for FDI. It illustrates that the model-based approach in FDI solves the problem at two levels: first, residuals generation are used to generate symptoms, and then the fault isolation is achieved through residual evaluation. This structure was first proposed by Chow and Willsky (1980).

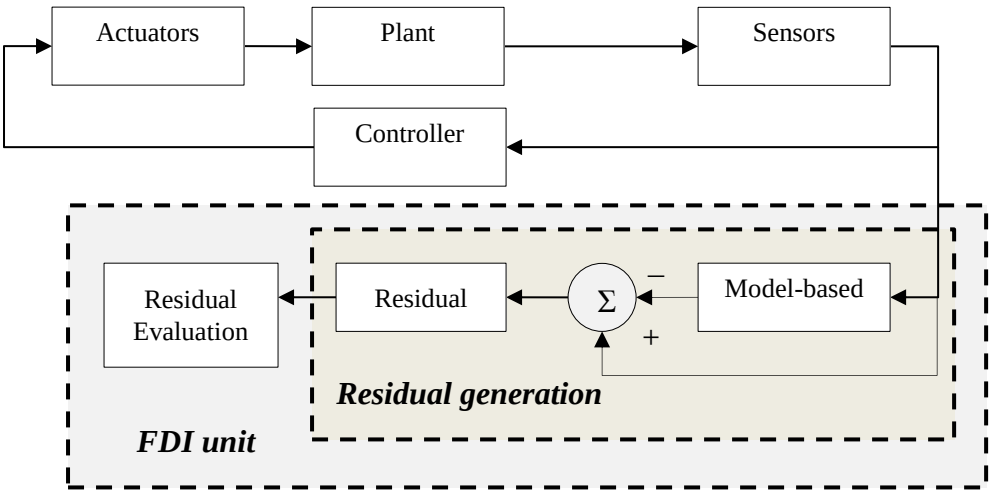

Figure 1-12: Fault detection and isolation structure

This approach presented in Figure 1.12 is widely applied in many industrial applications. For example, the fault detection of automotive vehicle suspensions and hydraulic brakes was examined in (Borner, Straky, Weispfenning, & Isermann, 2002) by using the parameter estimation technique through parity equations and least square method. An example of the model-based approach for a non-linear system is given in (Zhang, et al., 2013), where FDI for the sensor failure is achieved through the use of the Extended Kalman Filter to ensure that the system reliability can be guaranteed in the event of sensor failure.

1.2.2.3 Knowledge-based approaches

Knowledge based approaches can be very efficient when a dynamical model of the system or process is unknown or very complex if the majority of real industrial applications/ processes are non-linear and cannot readily be modelled by applying a model-based approach (Chen, 1995, pp. 67-70; Sobhani & Khorasani, 2009, p. 39) . This knowledge based methods attempt to evaluate system knowledge to develop rule-based decision making, which is also known as heuristic knowledge (Isermann, 2011, pp. 22-23). A number of different

knowledge-based methods are possible to diagnose fault(s) depending on the available analytical and heuristic information of the model (Simani, 2006, pp. 57-60):

- **Fuzzy logic**: if the dynamic model or parameters are not known, diagnosis is mainly based on heuristic information, and fuzzy system theory seems to be a natural tool to handle these uncertain conditions (Simani, Fantuzzi, & Patton, 2003, p. 52; Mendonça, Sousa, & Costa, 2006, p. 82). Instead of using a complex non-linear model through modelling techniques, a plant can be described by a collection of local affine fuzzy and non-fuzzy models (Leontaritis & Billings, 1985; Simani, Fantuzzi, & Patton, 2003, p. 52), where parameters are determined through identification techniques (Simani, 2006, p. 58). In order to extract the features for FDI, a logic decision process can be developed to transform residual information (quantitative knowledge) into qualitative statements (e.g. fault or normal conditions) (Simani, 2006, p. 58). Research studies in (Ulieru & Isermann, 1993; Meneganti, Saviello, & Tagliaferri, 1998) investigated the residual evaluation primarily in the decision making for releasing the final yes–no decision. Further studies in (Rich & Venkatasubramanian, 1987; Chen & Patton, 1999, p. 68) exploited the rule-based method to diagnose fault(s), where being rule-based required a database of rules and the accuracy of FDI depended on the inferred rules. However, in order to develop FDI through the fuzzy logic approach both rule-based and decision making should be developed at two levels in order to generate the symptoms and fault detections (Dexter & Benouarets, 1997). An example of using fuzzy logic for FDI in turbine engines can be given in (Gayme, Menon, Ball, & Mukavetz, 2003), where the fuzzy logic rule-based method incorporates both sensed engine parameters that represent engine normal operation, and fault conditions related to engine performance such as

high pressure turbine, high pressure compressor and fault condition related to engine performance such as high pressure.

- **Neural Networks**: In pattern recognition, the neural network is considered primarily for fault classification (Sobhani & Khorasani, 2009, p. 40), and this approach was suggested by (Himmelblau, 1979) (Pau, 1981). Studies (Li, Chow, Tipsuwan, & Hung, 2000), that considered the bearing vibration in both time and frequency domains are applied to build an automatic motor bearing fault diagnosis machine, and other studies (Hoskins & Himmelblau, 1988) (Venkatasubramanian & Chan, 1989), considered the neural network-based methodology in order to provide a potential solution to the preceding problems in the area of process fault diagnosis. These studies demonstrated the use of neural-networks' pattern recognition for FDI. In these applications, the neural networks' pattern recognition is only trained to examine the possibility of a fault or abnormal features in system measurements and give a fault classification system signal to determine the normal condition (no fault) of the system (Sobhani & Khorasani, 2009, p. 40). It demonstrated that the performance of the FDI is significantly affected by the dynamic behaviour of the systems. Therefore, the use of neural networks through pattern recognition for the purpose of the fault diagnosis, especially for the non-linear systems, may produce incorrect fault information since the inputs' signals to the systems are subject to change (Simani, 2006, p. 52) (Sobhani & Khorasani, 2009, p. 40). This drawback can be resolved by using a neural network-based residual generation decision-making scheme (Sobhani & Khorasani, 2009, p. 40) or using the combination of neural network and fuzzy logic in order to minimise the perceived problem (Simani, 2006, pp. 52-53). The former approach was initially suggested by Patton et al (Patton, Chen, & Nielsen, 1995). In this method, the fault diagnosis system uses both analytical and heuristic knowledge of the monitored

system and the knowledge can be determined in terms of residual (analytical knowledge) and feature extraction (heuristic knowledge) (Simani, 2006, p. 52). Furthermore, a fuzzy-neuron has the same structure as the artificial neuron, except that some or all of its parameters may de described by fuzzy logic (Simani, Fantuzzi, & Patton, 2003, pp. 53-54). Different structures for neuro-fuzzy networks can be considered (Nelles, 2001) in order to combine the advantages of both fuzzy-logic and neural networks (Simani, 2006, p. 53).

An example of knowledge-based approaches in rail applications can be found in (Lehrasab, Roberts, & Goodman, 2002), where the health of the control system of train doors is determined by extracting features from the trajectory profiles of the train doors. Detailed diagnostics can then be carried out once a fault has been detected through a neural network. Another study in (Balaban, Bansal, Stoelting, & Saxena, 2009) performed condition monitoring tasks to identify and categorise the fault mode for an electromechanical actuator in the aerospace industry. A subset of the faults, i.e., actuator jam, sensor bias, sensor drift and sensor scaling were selected for detailed study, with the features for fault detection determined through a neural network.

Table 1-1 summarised the fault-tolerant control to a different range of engineering applications. Further on, a comprehensive research survey in (Zhang & Jiang, 2006; Blanke, Izadi Zamanabadi, Bogh, & Lunau, 1997; Zhang & Jiang, 2008) shows that most research on fault tolerant control have treated the concepts of the fault detection and isolation and re-configuration control as two distinct issues due to the complexity of the problem. From a practical point of view, the integration of a fault detection and isolation scheme and an appropriate re-configurable control technique should be designed in an integrated manner in order to analyse systematically the interaction between fault detection and isolation and re-configuration control. On the other hand, the majority of the publications have primarily

considered the analytical redundancy approaches for the sensors' failure whilst comparatively little attention has been paid to the actuators' failure (Zhang & Jiang, 2008; Blanke, Izadi Zamanabadi, Bogh, & Lunau, 1997; Frank, 1990; Patton, Uppal , & Lopez-Toribio, 2000; Isermann, 2011). Therefore, this research study aims to fill the following gap in the research field:

- The analytical redundancy for the actuator failure.
- Designing fault detection and isolation and re-configuration control in an integrated manner.

Table 1-1: Summarised list of published studies in different applications, Fault-tolerant strategy (FTS), Fault Detection and Isolation (FDI)

Application	Type of redundancy	Objective	Failures	Design approach	References
Aircraft	Analytical/ Model-based approach	R-configure the controller	Sensor failures, wind components	Reconfiguring control is implemented by making use of adaptive nonlinear dynamic inversion for autopilot control.	(Lombaerts, Looye, Chu, & Mulder, 2012)
Aircraft	Analytical redundancy/ Knowledge-based	FDI	Actuator and sensor failures	The fault-tolerant flight control system through a neural network to identify sensor and actuator failures.	(Napolitano, An, & Seanor, 2000)
Railway	Analytical redundancy/ Model-based	FDI	Vehicle suspensions	The developed Rao–Blackwellized Particle Filter (RBPF) based method is used for parameter estimation to provide an early warning of a fault or performance degradation.	(Li P. , et al., 2007)
Railway	Analytical redundancy	FDI	Track circuit failures	The proposed method uses a hybrid quantitative/qualitative technique known as the neuro-fuzzy system to detect and diagnose the failure of the track circuits for railway.	(Chen, Roberts, & Weston, Fault detection and diagnosis for railway track circuits using neuro-fuzzy systems, 2008)

Railway	Direct signal approach	FDI	Motor failure of wheel-motor	A measurement from torque transducer considered in order to implement range of winding failures	(Ifedi, et al., 2011)
Articulated vehicles	Hardware redundancy	Fault-tolerant strategy	Electronic control unit failure	The electro-hydraulic (EH) power circuit is controlled by two embedded electronic control modules (ECM): the primary ECM and backup ECM. The two ECMs monitor each other's condition. If one detects fault in the other, it takes over the control functions. The finite state machine (FSM) concept is used to design the fault handling algorithms for both the component level and the system level failure.	(Haggag, Rosa, Huang, & Cetinkunt, 2007)
Motor and drive	Analytical redundancy/ Model-based approach	Fault-tolerant strategy	Stator failure	A fault-tolerant control design based on a sliding mode observer for induction motors has been developed. The proposed sliding mode observer detects and reconstructs the faults, and also estimates the flux.	(Djeghali, Ghanes, Djennoune, & Barbot, 2010)
Air conditioning	Analytical redundancy/ Knowledge-based approach	Fault-tolerant strategy	Terminal boxes and controller unit	The fault-tolerant control scheme has been established through a knowledge-based approach. The fuzzy models relate the performance of the terminal boxes, the air-handling unit and the chiller to fuzzy descriptions of the cooling load, the supply air and chilled water temperature set-points, and the amount of air-side and water-side fouling.	(Liu & Dexter, 2001)
Gas turbine	Hardware redundancy/ Hot stand-by	Re-configuration control	Controller unit	Classical methods for fault tolerance, such as error checking and n-module redundancy have been used to implement a fault-tolerant controller module.	(Thompson & Fleming, 1990)

1.3 Research Objectives

In active control systems for railway vehicles, the actuators tend to be significantly more expensive and require more additional space than sensors and an electronic control unit. Therefore, developing an analytical redundancy-based fault tolerance technique for actively controlled wheelset that minimise the number of actuators will clearly be more beneficial. The emphasis of this research is therefore to develop a fault-tolerant system of active control for a railway vehicle in the event of actuator malfunction in order to guarantee stability and good curving performance without using additional actuators. Figure 1.13 shows the basic components for an actively controlled railway system (without fault-tolerant measures). Each solid-axle wheelset is equipped with an electro-mechanical actuator to deliver the desired torque demand to the wheelset. A selected number of sensors are mounted on the bogie frame to minimise the need to install sensors on the wheelset axles where the working environment is known to be extremely harsh.

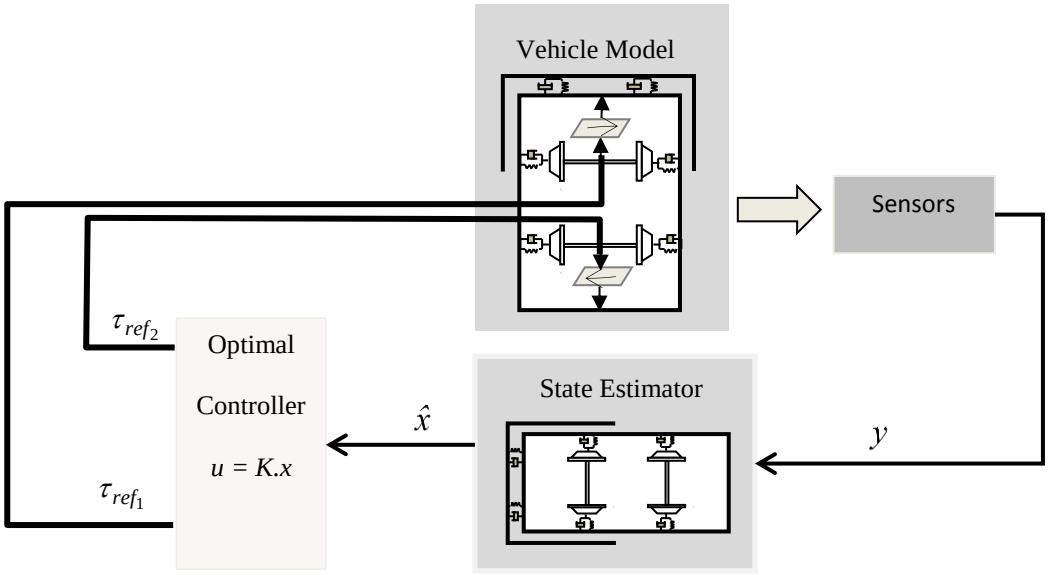

Figure 1-13: Overall control strategy

A control strategy based on the optimal control approach is used in this study and an observed model-based observer is developed to provide the necessary full state feedback, although other control strategies may also be used.

However, the scheme in Figure 1.13 does not guarantee the vehicle stability and desired performance if one of the actuators fails to deliver the desired torque to the wheelset. In the development of a fault-tolerant scheme for actively controlled wheelsets, two key issues are investigated in this study. The first issue is to develop an accurate FDI scheme that monitors the actuators' status in the system and raises a flag (or alarm) if a fault is identified. The second key issue is to develop Re-configuration Control (RC) methods to deal with different fault conditions and preserve stability conditions and maintain the vehicle performance, in the presence of a fault, close to that desired, or at least not worse than the passive system in the normal condition. This study considers the three most common types of actuator failure: Fail-Hard (FH), Short Circuit (SC) and Open Circuit (OC). The fail-hard is a failure condition where the motor shaft of the actuator becomes immovable, which could be caused by a mechanical jam possibly due to the lack of lubrication. The short circuit and open circuit are failures that occur in the electrical parts of the driving motor of the actuator, which correspond to zero voltage (e.g. short circuit in the motor windings) and zero current (e.g. failures in the power supply/amplifier) in the motor, respectively; resulting in re-generative braking or the absence of motor torque from the actuator. Furthermore, one of the critical design aspects is that the features of FDI depend on the reliability and availability of the information that is provide by the sensors. Therefore, this study also considers the sensor fault(s), although the scope of the study is limited to the failure mode of zero output for the sensors concerned. In this study, two different approaches are investigated in the development of condition monitoring tasks: the vehicle model-based approach and the actuator model-based approach.

- The vehicle model-based approach (Approach 1) as illustrated in Figure 1.14 is considered to monitor the actuators and sensors' status as the modelling technique and specified models for the railway vehicle system dynamics are well developed. In this approach, a Kalman Filter (KF) developed to provide state estimation feedback for the active controller will also be used for the purpose of fault diagnosis and condition monitoring tasks, where the FDI scheme for the actuators and sensors will be developed.
- The actuator model-based approach (Approach 2) as shown in Figure 1.15 through the use of a Local Kalman Filter (LKF) is considered to detect abnormal changes in the actuators, while the generated residuals between the estimated data and measured data will be used to provide the information for the FDI scheme.

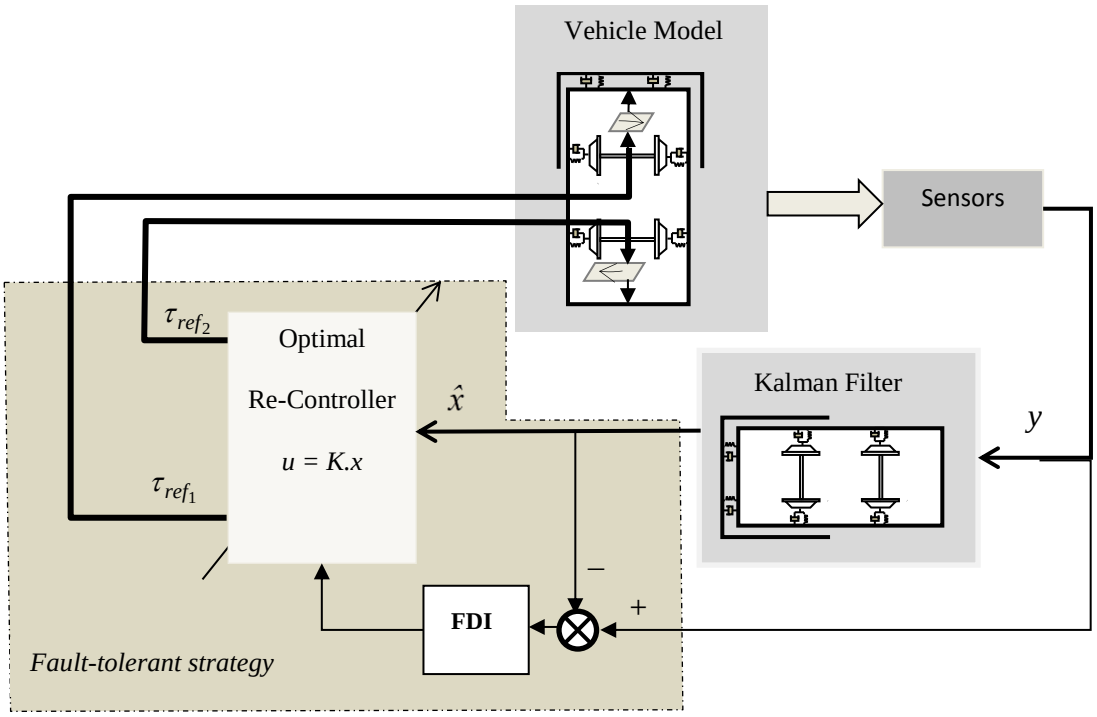

Figure 1-14: Fault-tolerant strategy through Approach 1

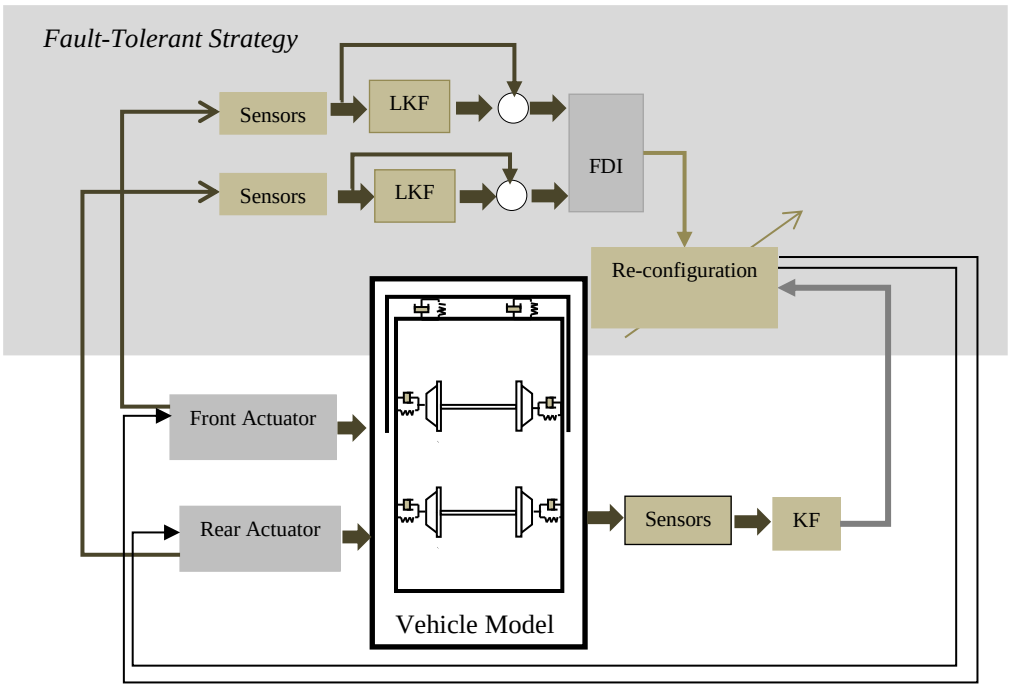

Figure 1-15: Fault-tolerant strategy through Approach 2

In either approach, if an abnormal change is detected based on the information provided by the FDI filters, the active wheelset controller will be re-configured in order to adjust the structure and the control gains in respect to the type of the actuator failure in order to maintain stability and the desired performance. It should be noted that some level of degradation in the event of actuator failure is inevitable as the actuator's availability is reduced, but the development of the control re-configuration must ensure a performance at least not worse than that of the vehicle with passive suspensions.

1.4 Thesis Structure

This thesis is organised as follows. Chapter 2 presents the development of the mathematical models that represent the vehicle dynamics and a control strategy for the implementation of the actively controlled wheelset. The dynamical model of an electromechanical actuator will be presented.

Chapter 3 presents the development of the approach 1 for the FDI, where a condition monitoring task is performed by the use of Kalman Filters that are also used to provide the full state feedback for the controller. One of the critical design aspects for the features of FDI is related to the reliability of the sensors; therefore, the given FDI for the actuator will be used to detect the sensors' failure in order to show the effectiveness of the approach. Furthermore, the FDI will be assessed on both random and deterministic track inputs.

Chapter 4 presents the development of the approach 2 for the FDI, where the condition monitoring task is performed based on the use of a local Kalman filter for the individual actuators. The proposed approach also attempts to address the key issue for the sensor's failure. The performance assessment will be provided to show the robustness of the scheme.

Chapter 5 provides a full description for the development of control re-configuration in the event of actuator failure in order to preserve stability and curving performance to a level at least not worse than a vehicle with passive components. Also the integration of the proposed control reconfiguration strategies with the fault detection and isolation schemes as developed in the previous chapters will be presented in order to demonstrate how the two parts of the entire fault tolerant strategy work together in a simulated 'real situation' environment.

Chapter 6 concludes the research. The major contribution and novelty aspects of the work will also be highlighted, together with recommendations and suggestions for future work.

Chapter 2 VEHICLE DYNAMICS AND CONTROL STRATEGY

2.1 Introduction

This chapter presents the development of the modelling and the basic active control strategy for a conventional railway vehicle that provides a research platform for the study of the fault tolerant control for the active primary suspensions. The characteristic of railway track is first discussed in section 2.2. The wheel–rail contact and mathematical model for the dynamics of a half vehicle is then provided in section 2.3. The basic control strategy and design performance for the active primary suspensions in the normal condition (i.e. no faults) is presented in section 2.4. The model of the actuator dynamics is provided in section 2.5. Section 2.6 details the design of a model-based estimator to provide the controller with the required full state feedback variables. Finally, summary of the work will be provided.

2.2 Characteristic of Railway Track

The wheelsets of the railway vehicle respond to the track excitations and therefore the track geometry has a direct impact on the wheelset's behaviour and the performance of the railway vehicle as assessed through track input (Mei, Li, & Goodall , 2001). In the railway industry, two distinct input characteristics of the railway track are considered: random and deterministic track inputs (Mei & Goodall, 2003b). Deterministic track inputs are intended features that represent the design alignment associated with the curves (R), cant angle (θ) and transition time that a train takes to connect the straight track to a curved/gradient track. These characteristics are defined in order to satisfy the requirements for passenger comfort. Figures 2.1 and 2.2 show a curved track with a radius of 1250 (m) and a cant angle of 6°, respectively, at the vehicle speed of 50 (m/s) and transition time of 2 (s).

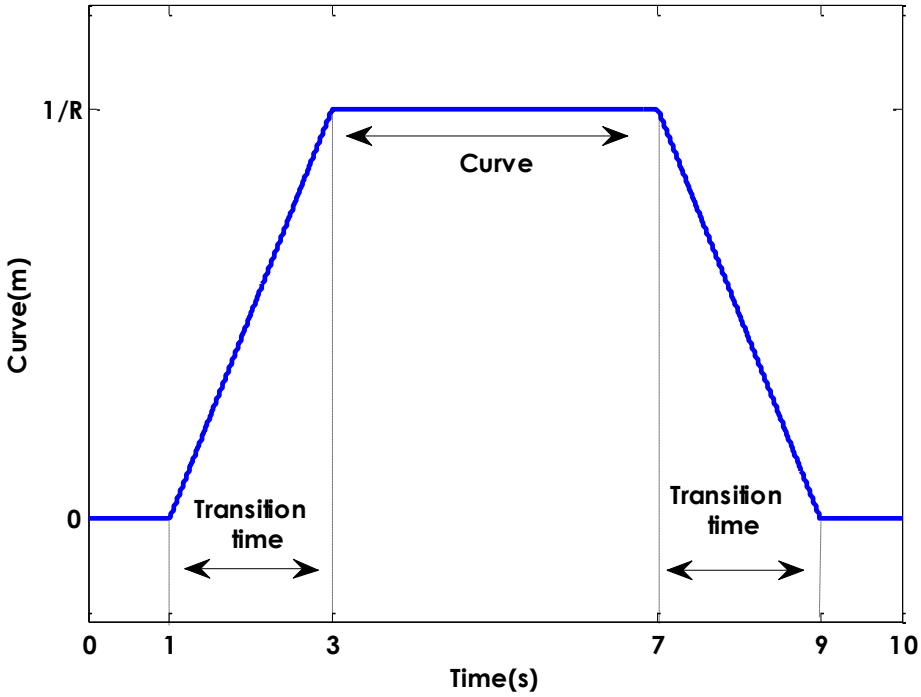

Figure 2-1: Curve track (R =1250 m)

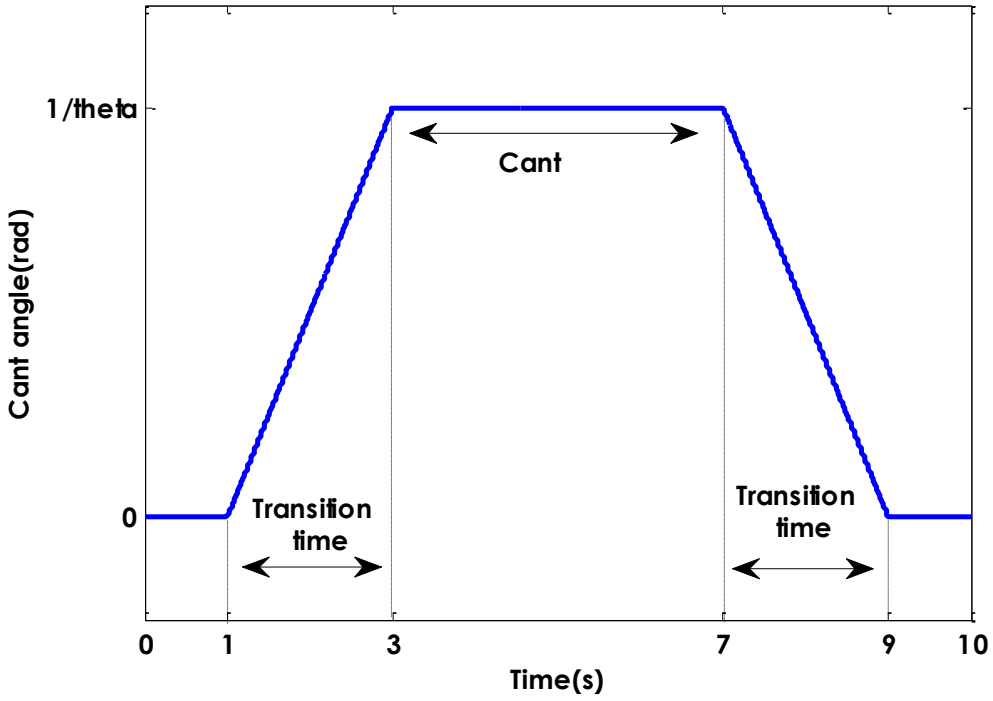

Figure 2-2: Cant angle (theta = 6°)

Random inputs are the track irregularities that represent the unintended deviations from the intended alignment in both lateral and vertical directions (Mei & Goodall, 2003b). In this

study only the lateral irregularities are of prime interest due to the fact that this study focuses on the stability and steering control of the primary suspensions, i.e. the plan-view dynamics. The lateral track irregularities used in this study to represent the roughness of typical track are generated from filtered white-noise in order to provide a broad frequency spectrum with a relatively high level of irregularities (Zheng Jiang , Z. Matamoros-Sanch, Goodall, & Smith, 2012). The lateral track irregularities can be approximated as the zero mean white Gaussian noise with variance, as described in Equation (2.1).

$$Q_1 = \frac{4\pi^2 A_r {V_s}^2}{f^3} \qquad \left(\frac{m}{s}\right)^2 (Hz)^{-1} \qquad \textbf{Eq. 2-1}$$

where A_r is the track roughness factor, V_s is the vehicle forward velocity and f is the temporal frequency. This equation can be used to generate time domain random sequences as the input excitation to the vehicle dynamic models in the computer simulations (Li P. , et al., 2007). Figure 2.3 shows the generated random lateral track irregularities at the vehicle speed of 50 (m/s).

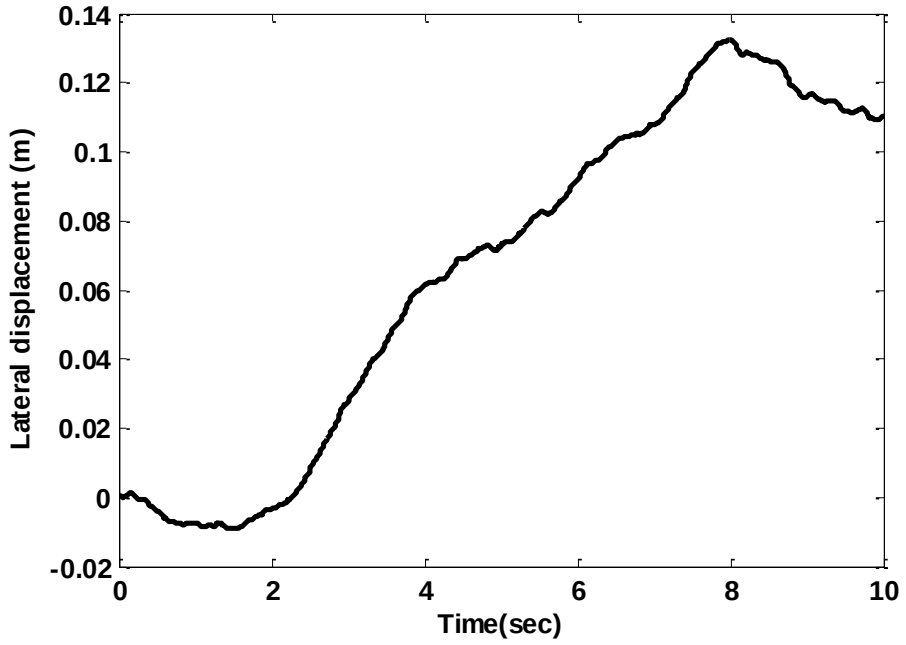

Figure 2-3: Random track irregularities

Although it is possible to use the measured real track data, one of the main drawbacks is that their frequency content is limited and is normally less representative (Mei & Goodall, 2001). Therefore, the use of the generated random track data would ensure full coverage of the relevant frequency range (Mei, Li, & Goodall , 2001).

2.3 Wheel–Rail Contact and Modelling of Vehicle Dynamics

2.3.1 Wheel–rail contact

The dynamic behaviour of railway vehicles is significantly affected by the contact forces at the wheel–rail interfaces (Wickens, 2006). These forces have an impact on the adhesion (Polach, 2005), creep and wear characteristics (Mei & Goodall, 2003a), and also provide the fundamental forces for wheel guidance (Wickens, 2003, p. 1). These contact forces are due to micro-slippage or creepage in the contact region, which can be expressed as the ratio of sliding velocity to forward velocity due to rolling (Note, sliding velocity is the difference between the circumferential velocity of a driven wheel and the translational velocity of the wheel) (Iwnicki, 2003). In a railway wheel, the creepage can occur in three directions (Garg & Dukkipati, 1984, p. 104): longitudinal (γ_1), lateral (γ_2) and spin (ω_3), as defined in Equations (2.2), (2.4) and (2.4), respectively, where V_x^w, V_y^w and Ω_z^w represent the longitudinal, lateral and rotational velocities of the wheel; V_x^t, V_y^t and Ω_z^t represent the longitudinal, lateral and rotational velocities of the track; and V_s represents the forward velocity of the wheel.

$$\gamma_1 = \frac{V_x{}^w - V_x{}^t}{V_s} \qquad \textbf{Eq. 2-2}$$

$$\gamma_2 = \frac{V_y{}^w - V_y{}^t}{V_s} \qquad \textbf{Eq. 2-3}$$

$$\omega_3 = \frac{(\Omega_z{}^w - \Omega_z{}^t)}{V_s} \qquad \textbf{Eq. 2-4}$$

In order to calculate the creepage, the velocity for each wheel (i.e. the left and right side of the wheels) can be derived in terms of the lateral displacement and the yaw motion of the wheelset in respect to the track centreline as given in Equations (2.5) and (2.6), — the concept of the creepage has been extensively explained in a number of publications (Garg & Dukkipati, 1984, pp. 103-132; Wickens, 2003, pp. 19-43; Iwnicki, 2003) and the full details of the calculation can be found in Appendix A.

Left-hand side wheel:	**Right-hand side wheel:**	
$V_{x_l}{}^w = V_s(1-\frac{L_g}{R}) + L_g.\dot{\psi}_w$	$V_{x_r}{}^w = V_s(1+\frac{L_g}{R}) - L_g.\dot{\psi}_w$	
$V_{y_l}{}^w = \dot{y}_w - V_s.\dot{\psi}_w$	$V_{y_r}{}^w = \dot{y}_w - V_s.\dot{\psi}_w$	**Eq. 2-5**
$\Omega_{z_l}{}^w = \dot{\psi}_w + \frac{V_s.\lambda_l}{r_0}$	$\Omega_{z_r}{}^w = \dot{\psi}_w + \frac{V_s.\lambda_r}{r_0}$	

Left-hand side track:	**Right-hand side track:**	
$V_{x_l}{}^t = \omega.r_L$	$V_{x_r}{}^w = \omega.r_R$	
$V_{y_l}{}^t = 0$	$V_{y_r}{}^t = 0$	**Eq. 2-6**
$\Omega_{z_l}{}^w = 0$	$\Omega_{z_r}{}^w = 0$	

where $\dot{y}_w$ is the lateral velocity of the wheelset; $\dot{\psi}_w$ the yaw velocity of the wheelset; L_g represents the half-gauge of the wheelset; R represents the curve radius; ω the angular velocity of the wheelset ($=V_s/r_0$); and r_L and r_R represent the contact radii (i.e. the distance between the wheel-central axis and wheel–rail contact) on the left and right wheels, respectively, as shown in Figure 2.4.

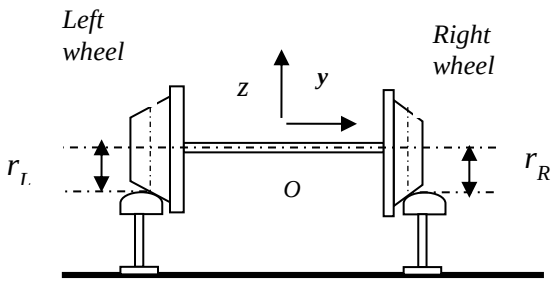

Figure 2-4: Lateral and vertical direction of a wheelset

The contact radii for the left and right wheels vary as the wheelset displaces laterally. When the wheelset is in the centre position to the track centreline, the contact radii for the left and right wheels are equal to the constant value of r_0. In practice, the contact profile of the wheel rim and rail head is nonlinear, but linear approximations using conicity λ_L, λ_R are often used in the study of wheelset dynamics to provide a linear relationship between the differences in rolling radii and the lateral displacement of the wheels, as given in Equation (2.7), in which $(y\text{-}y_t)$ is the relative lateral movement between the wheel and rail (Ayasse & Chollet, 2006).

$$\lambda_R = +\frac{(r_R - r_0)}{(y - y_t)};$$
$$\lambda_L = -\frac{(r_L + r_0)}{(y - y_t)};$$

Eq. 2-7

Equations (2.2), (2.3) and (2.4) are used to compute the creepage for the two wheels, as given in Equations (2.8), (2.9) and (2.10), respectively.

$$\gamma_{1_L} = 1 - \frac{L_g}{R} + \frac{L_g.\dot{\psi}_w}{V_s} - \frac{\omega.r_L}{V_s}$$

$$\gamma_{1_R} = 1 + \frac{L_g}{R} - \frac{L_g.\dot{\psi}_w}{V_s} - \frac{\omega.r_R}{V_s}$$

Eq. 2-8

$$\gamma_{2_L} = \frac{\dot{y}_w}{V_s} - \psi_w$$

$$\gamma_{2_R} = \frac{\dot{y}_w}{V_s} - \psi_w$$

Eq. 2-9

$$\Omega_{3_L} = \frac{\dot{\psi}_w}{V_s} + \frac{\lambda_L}{r_0}$$

$$\Omega_{3_R} = \frac{\dot{\psi}_w}{V_s} - \frac{\lambda_R}{r_0}$$

Eq. 2-10

The creep forces at the contact patches are generated due to the creepages (Garg & Dukkipati, 1984, p. 105; Iwnicki, 2003), which exist in both longitudinal and lateral directions as illustrated in Figure 2.5. At small values of creepage the relationship can be considered to be linear. However, at larger values of creepage, the relationship becomes highly nonlinear and the creep force approaches a limiting value determined by the normal force and coefficient of friction in the contact area (Ayasse & Chollet, 2006). When working in the nonlinear regions, it would be necessary to use different modelling methods. However, this study uses the linearised models of the wheel–rail contact mechanics exclusively for control law design, principally because nonlinearities are relatively small unless there is flange contact, a condition which the actively controlled wheelset avoids (Li & Goodall, 1998). The contact forces are determined as given in Equations (2-11)-(2-14):

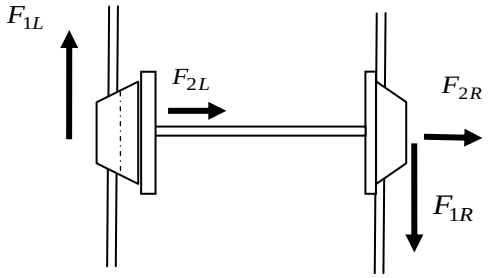

Figure 2-5: Contact forces

$$F_{1L} = -f_{11}.\gamma_{1L}$$

Eq. 2-11

$$F_{2L} = -f_{22}.\gamma_{2L} - f_{23}.\gamma_{3L}$$

Eq. 2-12

$$F_{1R} = -f_{11}.\gamma_{1R}$$

Eq. 2-13

$$F_{2R} = -f_{22}.\gamma_{2R} - f_{23}.\gamma_{3R}$$ **Eq. 2-14**

where F_{1L}, F_{1R} correspond to the longitudinal contact forces for the left and right wheelset, respectively; and F_{2L}, F_{2R} represent the lateral forces for the left and right wheelset, correspondingly; and f_{11} , f_{22} and f_{23} represent the longitudinal, lateral and spin creep coefficient, respectively.

2.3.2 Vehicle dynamics

In this study, a half vehicle model (consisting of a two-axle bogie and a half-body frame) is used as the focus is on the primary suspensions (i.e. between the wheelsets and the bogie frame). Also, as the investigation of the primary suspensions of the vehicle only affects the lateral and yaw motions, only the plan view dynamics of the half vehicle require consideration. Figure 2.6 gives a simplified plan view diagram, where the modelled scheme mainly consists of two solid-axle wheelsets, a bogie and a half body of the vehicle. The wheelsets are connected to the bogie frame through springs (K_s) and dampers (C_s) in the lateral direction, while the bogie is also connected to the body frame via secondary springs (K_{sc}) and dampers (C_{sc}) in the lateral direction (Pearson, Goodall, Mei, & Himmelstein, 2004). Although in practice some form of longitudinal connection is needed to transmit the traction and braking forces to the vehicle, this is not included in the model as it is not the concern of the current study (Mei & Goodall, 2001).

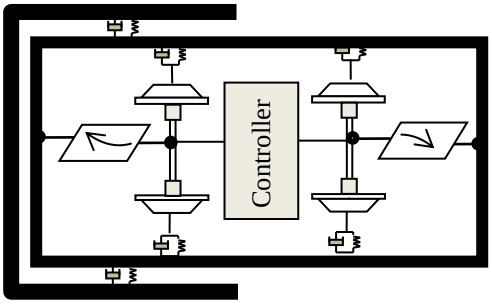

Figure 2-6: Plan view diagram of half vehicle

The stabilisation of the wheelset can be obtained through the use of the yaw connection between the bogie frame and each wheelset in the longitudinal direction on either side that effectively produce a torque (τ_{w_1}, τ_{w_2}) opposing the yaw motion of the wheelset. This could be a yaw stiffness in the case of passive suspensions and actuator torque in the active case.

The lateral forces between wheelsets and the bogie frame $F_{f_{wg}}$ and $F_{r_{wg}}$ for the leading and trailing wheelsets are those of the springs and dampers connected the wheelset to the bogie, as given in Equations (2.15) and (2.16). Note, all variables in the equations are related to local track references. Four sets of Cartesian coordinate system are shown in Figure 2.7 with respect to their four different local frames of references, where the frame references by $O_{wf}\, x_{wf}\, y_{wf}$, $O_{wr}\, x_{wr}\, y_{wr}$, $O_g\, x_g\, y_g$, $O_v\, x_v\, y_v$ move synchronously with the front wheelset, the rear wheelset, the bogie and the vehicle body respectively. Those coordinate systems have their origins (O_{wf}, O_{wr}, O_g, O_v) at the track centre line and move at a constant forward velocity with respect to ($O_{wf}\, x_{wf}$, $O_{wr}\, x_{wr}$, $O_g\, x_g$, $O_v\, x_v$), and axis of ($O_{wf}\, y_{wf}$, $O_{wr} y_{wr}$, $O_g y_g$, $O_v\, y_v$) pointing to right-hand sides.

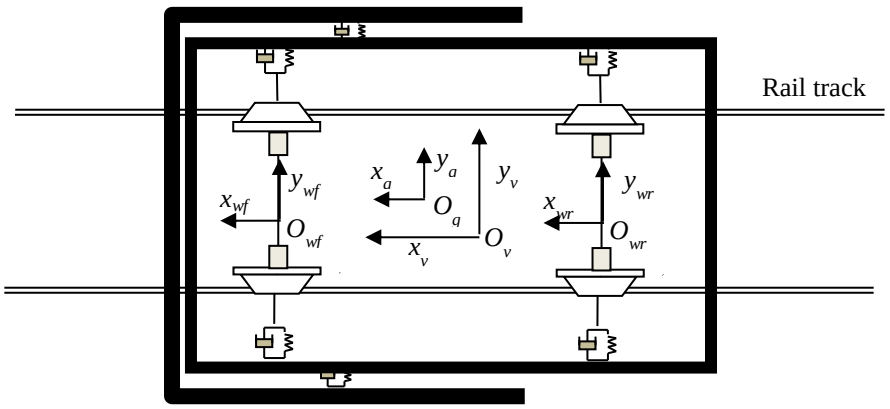

Figure 2-7: Axes systems

$$F_{f_{wg}} = -K_s.(y_{w_1} - y_g - L_v.\psi_g) - C_s.(\dot{y}_{w_1} - \dot{y}_g - L_v.\dot{\psi}_g)$$ **Eq. 2-15**

$$F_{r_{wg}} = -K_s.(y_{w_2} - y_g + L_v.\psi_g) - C_s.(\dot{y}_{w_1} - \dot{y}_g + L_v.\dot{\psi}_g)$$ **Eq. 2-16**

In addition, the lateral force between the bogie frame and half-body vehicle is due to the springs and dampers which connect those rigid bodies, and can be written as Equation (2.17).

$$F_{gv} = -K_{sc}.(y_g - y_v) - C_{sc}.(\dot{y}_g - \dot{y}_v)$$ **Eq. 2-17**

According to Newton's second law, the dynamics of the two wheelsets, bogie and the body frame can be derived in Equations (2.18)-(2.24).

For the front wheelsets:

$$I_w.\ddot{\psi}_{w_1} = F_{f_{1L}}.L_g - F_{f_{1R}}.L_g + \tau_{w_1}$$ **Eq. 2-18**

$$m_w.\ddot{y}_{w_1} = F_{f_{2L}} + F_{f_{2R}} + F_{fc} + F_{fm} + F_{f_{wg}}$$ **Eq. 2-19**

For the rear wheelsets:

$$I_w.\ddot{\psi}_{w_2} = F_{r_{1L}}.L_g - F_{r_{1R}}.L_g + \tau_{w_2}$$ **Eq. 2-20**

$$m_w.\ddot{y}_{w_2} = F_{r_{2L}} + F_{r_{2R}} + F_{rc} + F_{rm} + F_{r_{wg}}$$ **Eq. 2-21**

For the bogie frame:

$$I_g.\ddot{\psi}_g = -F_{f_{wg}}.L_v + F_{r_{wg}}.L_v - (\tau_{w_1} + \tau_{w_2})$$ **Eq. 2-22**

$$m_g.\ddot{y}_g = -F_{f_{wg}} - F_{r_{wg}} + F_{gv} + F_{gc} + F_{gm}$$ **Eq. 2-23**

For a half-body:

$$m_v.\ddot{y}_v = -F_{gv} + F_{cr} + F_m$$ **Eq. 2-24**

By substituting the forces associated with creep, dampers and springs in the above equations, the dynamic equations of the vehicle can be obtained as presented in Equations (2.25)-(2.31), where all the variables are related to local track references. There are a total of seven degrees of freedom (14th order), i.e., the lateral and yaw motions for each wheelset, and for the bogie and lateral displacement for the vehicle body (Pearson, Goodall, Mei, & Himmelstein, 2004).

$$\ddot{y}_{w1} = -\frac{1}{m_w}[(\frac{2f_{22}}{V_s} + C_s)\dot{y}_{w1} - K_s y_{w1} + 2f_{22}\psi_{w1} + C_s\dot{y}_g + K_s y_g + C_s L_v\dot{\psi}_g + K_s L_v\psi_g - m_w(\frac{V_s^2}{R_1} - g\cdot\theta_{c1})], \quad \textbf{Eq. 2-25}$$

$$\ddot{\psi}_{w1} = -\frac{1}{I_w}[\frac{2f_{11}L_g^2}{V_s}\dot{\psi}_{w1} + \frac{2f_{11}\lambda L_g}{r_0}y_{w1} - \frac{2f_{11}L_g^2}{R_1} - \frac{2f_{11}\lambda L_g}{r_0}y_{t1} - \tau_{w1}], \quad \textbf{Eq. 2-26}$$

$$\ddot{y}_{w2} = -\frac{1}{m_w}[(\frac{2f_{22}}{V_s} + C_s)\dot{y}_{w2} - K_s y_{w2} + 2f_{22}\psi_{w2} + C_s\dot{y}_g + K_s y_g - C_s L_v\dot{\psi}_g - K_s L_v\psi_g - m_w(\frac{V_s^2}{R_2} - g\cdot\theta_{c2})], \quad \textbf{Eq. 2-27}$$

$$\ddot{\psi}_{w2} = -\frac{1}{I_w}[\frac{2f_{11}L_g^2}{V_s}\dot{\psi}_{w2} + \frac{2f_{11}\lambda L_g}{r_0}y_{w2} - \frac{2f_{11}L_g^2}{R_2} - \frac{2f_{11}\lambda L_g}{r_0}y_{t2} - \tau_{w2}], \quad \textbf{Eq. 2-28}$$

$$\ddot{y}_g = -\frac{1}{m_g}[(2\cdot C_s + C_{sc})\cdot\dot{y}_g + (2\cdot K_s + K_{sc})y_g - C_s\dot{y}_{w1} - K_s y_{w1} - C_s\dot{y}_{w2} - K_s y_{w2} - C_{sc}\dot{y}_v - K_{sc}y_v - m_g V_s^2(\frac{1}{2R_1} + \frac{1}{2R_2}) + m_g g(\frac{\theta_{c1}}{2} + \frac{\theta_{c2}}{2})], \quad \textbf{Eq. 2-29}$$

$$\ddot{\psi}_g = -\frac{1}{I_g}[2L_v^2 C_s\dot{\psi}_g + 2L_v^2 K_s\psi_g - L_v C_s\dot{y}_{w1} + L_v C_s\dot{y}_{w2} - L_v K_s y_{w1} + L_v K_s y_{w2} + \tau_{w1} + \tau_{w2}], \quad \textbf{Eq. 2-30}$$

$$\ddot{y}_v = -\frac{1}{m_v}[C_{sc}\dot{y}_v + K_{sc}y_v - C_{sc}\dot{y}_g - K_{sc}y_g - m_v V_s^2(1/2R_1 + 1/2R_2) + m_v g(\theta_{c1}/2 + \theta_{c2}/2)], \quad \textbf{Eq. 2-31}$$

There are two different types of track inputs at the wheelsets: random inputs (y_{t1},y_{t2}) that represent lateral track irregularities along the route track at the leading and trailing wheelsets and deterministic inputs that represent the track curvature (R_1,R_2) and cant angle of the track (θ_{c1},θ_{c2}) for the two wheelsets.

The control torques for the two wheelsets (τ_{w_1}, τ_{w_2}) are given in Equations (2.32) and (2.33), where *k* represents the effective yaw stiffness from the passive springs and the third term in the equations represents the additional relative yaw displacement between the wheelsets and the bogie frame due to track curvature.

$$\tau_{w1} = -k.(\psi_{w1} - \psi_g + L_v / R_1) \quad \textbf{Eq. 2-32}$$

$$\tau_{w1} = -k.(\psi_{w2} - \psi_g - L_v / R_2) \quad \textbf{Eq. 2-33}$$

However, after setting up a set of mathematical equations that represents the vehicle dynamics, it is necessary to analyse and validate those equations of motion in order to ensure that there is no mistake. In this study two methods are considered to analysis the vehicle model. The fist method is an eigenvalue analysis that indicates the natural frequencies of the various modes of motion. In the second method, a comparison of curving performance against published work has been considered. Both methods are briefly examined in sections 2.4.1.1 and 2.4.1.2 respectively in order to avoid repeating what is required to be described for the active approach.

2.4 Active Control Strategy and Design Performance

2.4.1 Active approach

The active wheelset control can be used to stabilise the wheelsets without compromising performance during curve negotiation, with much reduced contact forces in comparison to passive suspensions (Mei & Goodall, 2003a). In active control, the yaw torque for each wheelset will be determined by the specific control algorithms from a selected set of sensor measurements to maintain stability and curving performance (Bruni, Goodall, Mei, & Tsunashima, 2007). As shown in Figure 2.6, two actuators are placed between the wheelsets

and the bogie frame in the yaw direction for the implementation of the active controls — these are illustrated as rotational torque-producing actuators, although in practice they might be a pair of linear actuators. A number of control strategies are possible, but in this study the optimal control approach with full state feedback is used to design the active control (Mei & Goodall, 1999b; Mei & Goodall, 2003a). The design of the optimal controller is fairly standard, and for the wheelset control it has been found that the minimisation of the lateral displacements and the angle of attack of the wheelsets result in a controller that provides the desired degree of stability and performance (Mei & Goodall, 2000b). A general diagram of the control structure is shown in Figure 2.8.

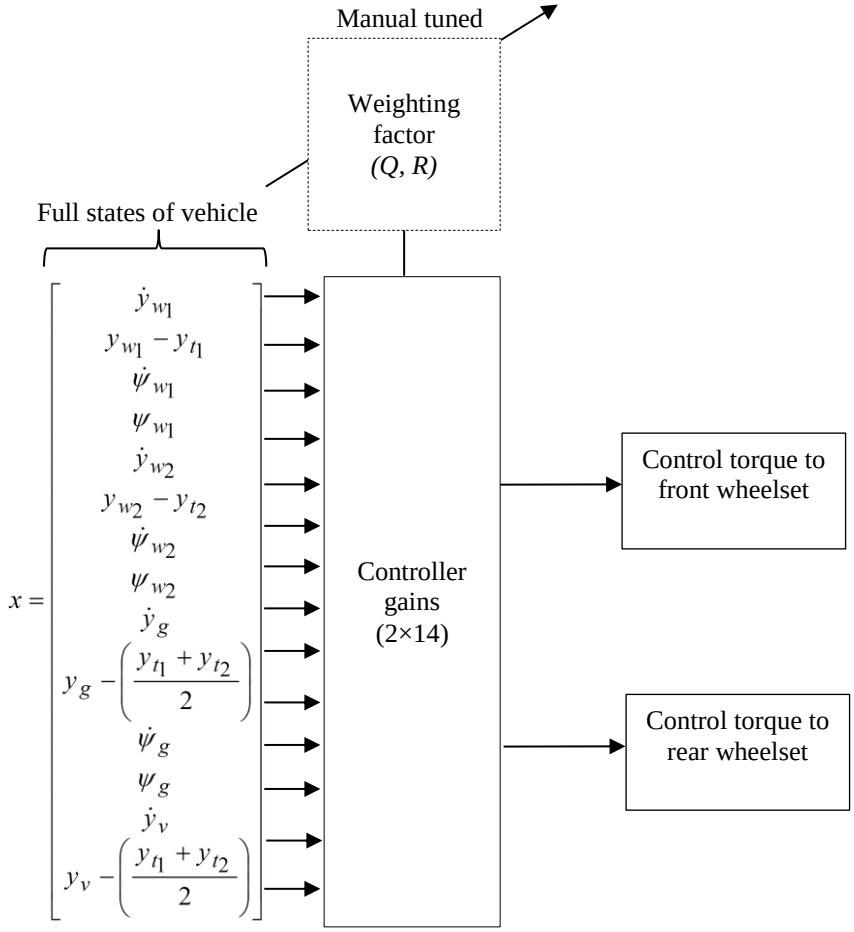

Figure 2-8: A general diagram of the control structure

Equations (2.34) and (2.35) define a state–space representation of the vehicle model suitable for the optimal control design, where *x* is a vector of state variables, *u* is the control input vector, *w* is a vector of track inputs, and *y* is a vector of outputs or measurements. In the state space model represented in Equation (2.34), the lateral deflection of the wheelset, bogie and vehicle body to the lateral track irregularities are part of the state in order to control the vehicle to follow the track (Mei, Li, & Goodall , 2001). For designing the optimal controller, it is not necessary to minimise all the states. It has been found that minimisation of the lateral displacements or the yaw motion of the wheelsets results in a controller that provides the desired performance and stability.

$$\dot{x} = A \cdot x + B \cdot u + \mu \cdot w, \qquad \textbf{Eq. 2-34}$$

Where;

$$x = \left[\dot{y}_{w_1} \quad y_{w_1} - y_{t_1} \quad \dot{\psi}_{w_1} \quad \psi_{w_1} \quad \dot{y}_{w_2} \quad y_{w_2} - y_{t_2} \quad \dot{\psi}_{w_2} \quad \psi_{w_2} \quad \dot{y}_g \quad y_g - \left(\frac{y_{t_1} + y_{t_2}}{2} \right) \quad \dot{\psi}_g \quad \psi_g \quad \dot{y}_v \quad y_v - \left(\frac{y_{t_1} + y_{t_2}}{2} \right) \right]^T ;$$

$$u = \left[\tau_{w_1} \quad \tau_{w_2} \right]^T ;$$

$$y = C \cdot x + D \cdot u; \qquad \textbf{Eq. 2-35}$$

Where;

$$y = \left[y_{w_1} \quad \psi_{w_1} \quad y_{w_2} \quad \psi_{w_2} \right]^T$$

The cost function is given in Equation (2.36), where the first term reflects the expected performance of the controller and the second term reflects the control effort requirement.

$$J = \int (y^T . Q . y + u^T . R . u) dt \qquad \textbf{Eq. 2-36}$$

By tuning the weighting matrices *Q* and *R* the performance of the optimal control can be studied thoroughly. In this study the weighting matrices *Q* and *R* tuned manually although some studies of intuitively formulated control with GA (Genetic Algorithm) optimisation are

also carried out and reported elsewhere. The weighting factors R and Q can be tuned to provide a compromise between the tracking performance and control effort requirements and it is found that a small value of R is to be reasonable, as the small size of these reflecting the large size of the control torques which must be applied to the wheelsets. However, the tuning of Q is not straightforward and the trial-error tuning has been used to give the best results by achieving the following forces on curves tracks (Bruni, Goodall, Mei, & Tsunashima, 2007):

- Zero longitudinal creep force on steady curve.
- Equal lateral creep force.

By choosing the weighting matrices Q and R in Equation (2.37), a control gain matrix K is obtained that provides desirable creep forces on curved tracks; the control input vector consisting of the two actuator torque signals is defined by Equation (2.38).

$$Q = \begin{bmatrix} 45.5 & 0 & 0 & 0 \\ 0 & 0.01 & 0 & 0 \\ 0 & 0 & 3.5 & 0 \\ 0 & 0 & 0 & 0.01 \end{bmatrix}; \qquad \textbf{Eq. 2-37}$$

$$R = \begin{bmatrix} 10^{-12} & 0 \\ 0 & 10^{-12} \end{bmatrix};$$

$$u = -K.x; \qquad \textbf{Eq. 2-38}$$

2.4.1.1Stability analysis

An unconstrained solid-axle wheelset is known to be inherently unstable and the natural frequency of the unstable mode (kinematic frequency) can be approximated in Equation (2.39), which is proportional to the speed and square root of the slope (conicity) of the wheel tread; and inversely proportional to the square root of the wheel radius and half distance of the two wheels (Goodall & Li, 2000; Wickens, 2003, p. 6).

$$f_n = \frac{V_s}{2\pi}\sqrt{\frac{\lambda}{r_0 L_g}} \qquad \textbf{Eq. 2-39}$$

The stabilisation of the conventional wheelsets may be provided through the use of passive suspensions or active control (Mei & Li, 2007). Table 2-1 compares the natural frequency and damping ratios of the vehicle dynamics associated with each mode between the vehicles without stability control, the vehicle with passive suspension and the vehicle with active control. The results reveal that in the case of the vehicle without stability control, the two modes associated with each wheelset are unstable at the kinematic frequencies of 5 and 5.8 Hz. On the other hand, the vehicle with the passive suspension (kinematic frequencies of 4.8 and 6.6 Hz) and active control (kinematic frequencies of 5.3 and 7.1 Hz) can provide sufficient damping for the kinematic modes. It can be seen that the high frequency modes of the wheelsets are highly damped, and their frequencies are significantly higher than the kinematic frequencies. It also indicates that the dynamic modes of a bogie frame and the body are sufficiently damped as expected. Note that the results in Table 2-1 are obtained with the nominal parameter values given in Appendix B, and the vehicle forward velocity of 50 (m/s).

Table 2-1: Natural frequencies and damping ratios of the vehicle dynamic modes with different approaches

Eigenvalues	Speed of 50 (m/s)					
	Without stability control		***passive control***		***Active control***	
	Damping (%)	Frequency (Hz)	Damping (%)	Frequency (Hz)	Damping (%)	Frequency (Hz)
Wheelset high frequency	99.3	48.4	100	46.8	99.3	48.4
	99.3	48.4	99.8	46.8	99.3	48.4
	99.3	48.4	99.8	46.8	99.3	48.4
	99.3	48.4	100	46.8	99.3	48.4
Bogie lateral and yaw	100	38.3	79.3	27.4	22	11.4
	20.7	7.3	79.3	27.4	22	11.4
	20.7	7.3	83.7	9.5	40	7.2
	100	3.3	83.7	9.5	40	7.2
Kinematic mode 1	-0.1	5.8	36	6.6	20.3	7.1
	-0.1	5.8	36	6.6	20.3	7.1
Kinematic mode 2	-15.5	5	11.4	4.8	15	5.3
	-15.5	5	11.4	4.8	15	5.3
Body lateral	19.4	0.9	19.1	0.9	19.5	0.9
	19.4	0.9	19.1	0.9	19.5	0.9

2.4.1.2 Curving performance

Principally, the control strategy for a good curving performance is concerned with minimising/ eliminating the creep forces, and therefore the idea of a good curving performance can be expressed as follows (Bruni, Goodall, Mei, & Tsunashima, 2007):

- No longitudinal creep force, as it tends to cause unwanted yaw motion, and therefore it is desirable to be eliminated.

- Equal lateral creep force, as some force in the lateral direction is demanded to compensate for the cant deficiency. It is preferred to distribute the lateral forces between all wheelsets.

The use of passive suspensions for stability control is known to produce undesirable contact forces when a rail vehicle negotiates curved track (Pearson, Goodall, Mei, & Himmelstein, 2004). To study the responses of the actively controlled vehicle on a curved track, a curve radius of 1250 (m), connected to straight track via a transition of 2 (s) with a speed of 50 (m/s) are used. Note also that the track is canted during the curve to reduce the lateral acceleration experienced by the passengers (Mei, Perez, & Goodall, 2000). Figure 2.9 compares the lateral displacements at the leading and trailing wheelsets on the curved track between the active scheme and the passive vehicle system; where PVL and PVT depict the vehicle with passive suspension at the leading and trailing wheelsets, respectively; and AVL and AVT denote the vehicle with active control at the leading and trailing wheelsets, respectively. It clearly shows that the lateral displacement of both the leading and trailing wheelsets with the use of the active controller is approximately 1.4 (mm), which is the theoretical pure rolling line for this particular curve; whereas the two wheelsets of the passive vehicle behave differently, at 5.2 (mm) and 0.8 (mm), respectively, and are forced away from the pure rolling line due to the use of yaw stiffness for stabilisation.

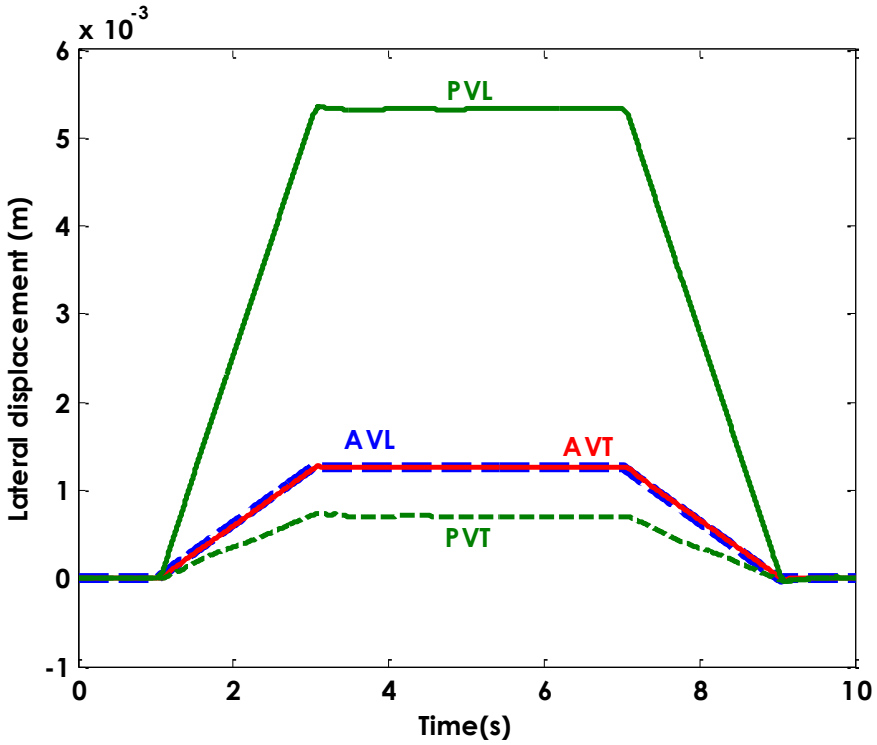

Figure 2-9: Lateral displacement- active control vs passive

Figure 2.10 shows the angle of attack (yaw motion) for the leading and trailing wheelsets with the use of active controllers and passive suspension. The actively controlled wheelsets have an equal angle of attack when running around the steady curve, to provide the appropriate lateral creep for the cant deficiency. For the passive vehicle, the angles of attack of the two wheelsets are deviated from the ideal position.

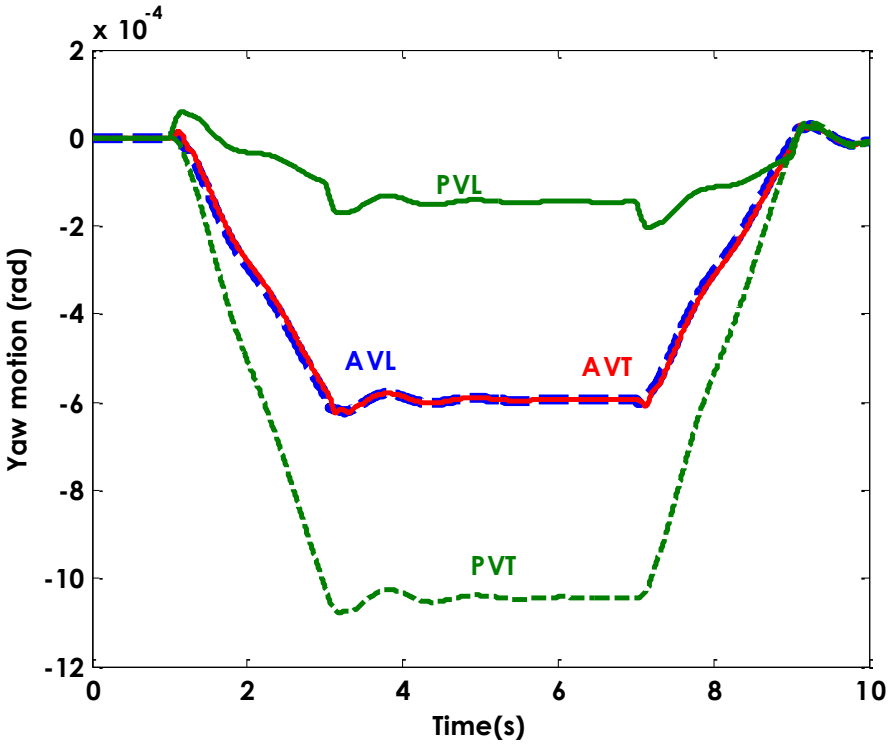

Figure 2-10: Angle of attack- active control vs passive

The lateral displacement of the two wheelsets on the pure rolling line in the case of the actively controlled vehicle minimises the longitudinal contact force, as shown in Figure 2.11, where the longitudinal contact forces on a steady curve are nearly zero, whereas for a passive vehicle this is significantly higher for the leading and trailing wheelsets (Figure 2.12).

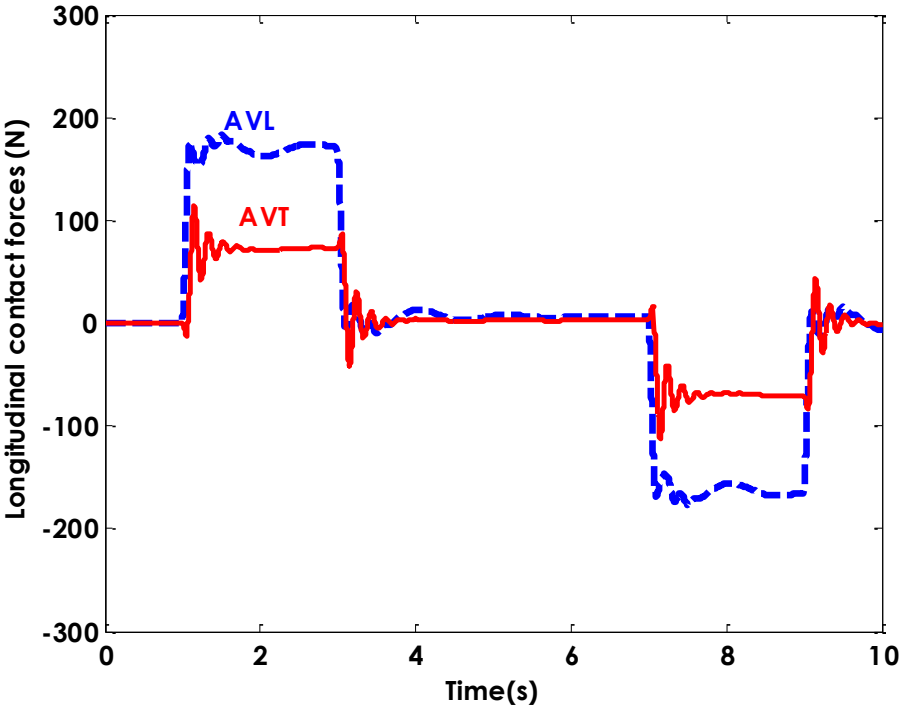

Figure 2-11: Longitudinal contact force–active control

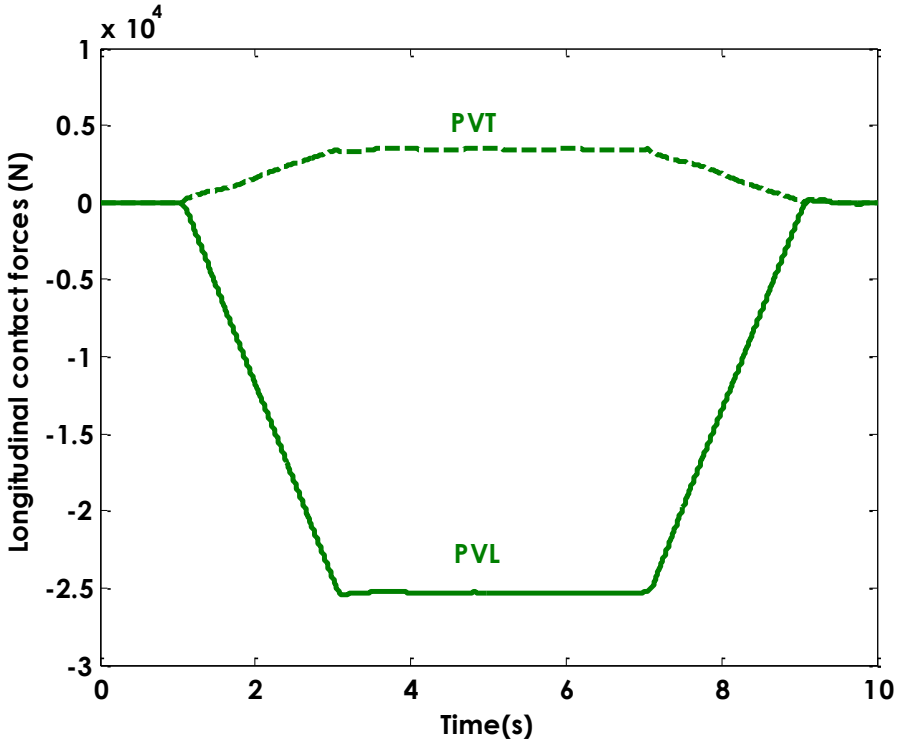

Figure 2-12: Longitudinal contact force–passive vehicle

In the lateral direction, some creep forces will be required to provide the necessary curving force to compensate for any cant deficiency, but this should be ideally equally shared between the wheelsets as in the case of the active control in Figure 2.13. In the passive case, however, the lateral creep force of the trailing wheelset is significantly higher than that of the leading wheelset.

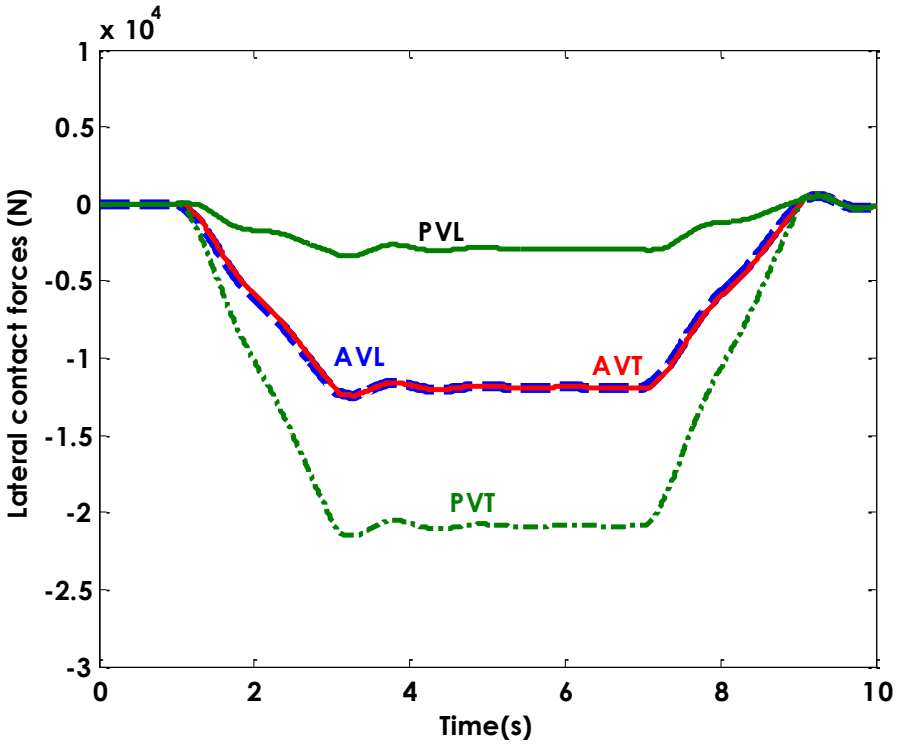

Figure 2-13: Lateral contact forces–active control vs passive vehicle

2.5 Actuator Dynamics

The implementation of the active control requires the use of an actuator for each wheelset to deliver the control action in the yaw direction. There are a number of different actuator technologies such as pneumatic actuation, electro-hydraulic actuation, electro-mechanical actuation and electro-magnetic actuation (Pacchioni, Goodall, & Bruni, 2010). However, in this study electro-mechanical actuation is chosen to meet the main requirements for the active control in order to stabilise the wheelset kinematic modes, which are relatively high frequency (5-10 Hz) (Pearson, Goodall, Mei, & Himmelstein, 2004).

Although the actuator models are not included in the control design to avoid the extra complexity of the control structures, the actuator dynamics will be included in the simulation to evaluate the vehicle performance (Mei, Nagy, Goodall, & Wickens, 2002). The actuator model dynamics consist of two parts: the electrical part, i.e. a dc motor, and mechanical part consisting of the rotor, gearbox. Figure 2.14 shows the key elements of the actuator and the connections to the wheelset and bogie.

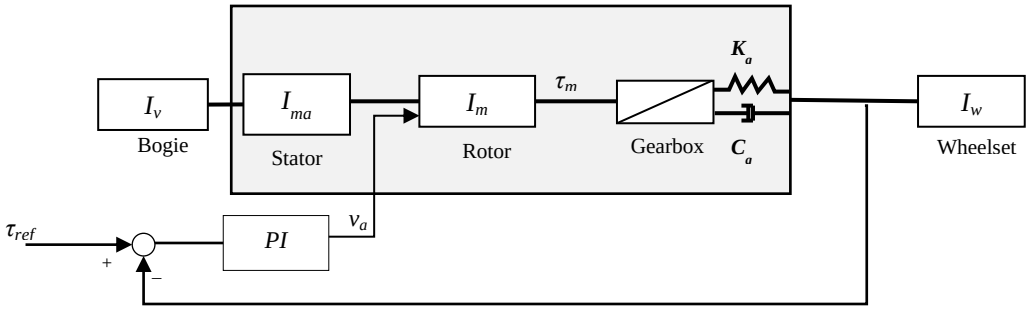

Figure 2-14: Actuator model

The electrical and mechanical parts of the actuator are presented in Equations (2.40) and (2.41).

$$\frac{di_a}{dt} = \frac{V_a}{L_a} - \frac{R_a}{L_a} i_a - \frac{K_b . \dot{\theta}_m}{L_a} \qquad \textbf{Eq. 2-40}$$

$$I_m \ddot{\theta}_m = \tau_m + \frac{\tau_g}{n} - C_m \dot{\theta}_m \qquad \textbf{Eq. 2-41}$$

Where;

$$\tau_m = K_t . i_a$$

$$\tau_g = K_g (\psi_w - \theta_A) + C_g (\dot{\psi}_w - \dot{\theta}_A)$$

$$\theta_A = \psi_g + \frac{\theta_m}{n}$$

$$\tau_w = -\tau_g$$

In the above equations, θ_A represents the combination of the rotor displacement (θ_m) and bogie's yaw motion (ψ_g) due to the fact that the stator of the motor is considered to be

mounted to the bogie frame. The nomenclatures for the symbols used in Equations (2.40) and (2.41) are given in the Appendix B—together with the parameter values used for all calculations presented in this section.

The torque output of the actuator must be maintained as closely as possible to the torque demand as calculated by the controller and therefore a local proportional-integral (PI) controller is used for each actuator to track the desired torque (τ_{ref}) from the wheelset controller as given in Equation (2.42).

$$C(s) = e(K_p + \frac{K_i}{s}) \qquad \textbf{Eq. 2-42}$$

where *e* represents an error value as the difference between the measured torque (τ_m) of the dc motor and the desired torque (τ_{ref}). The proportional ($k_p=0.025$) and integral gain ($k_i=0.567$) are tuned to obtain a fast response necessary for wheelset control.

This model is then added to the vehicle dynamics model in the computer simulations to assess the performance of the active control system. Figures 2.15 and 2.16 compare the lateral displacements and yaw motions of the leading and trailing wheelsets with and without the actuator dynamics, respectively. They clearly justify the design approach with and without actuator dynamics, as the desire curving performance is maintained.

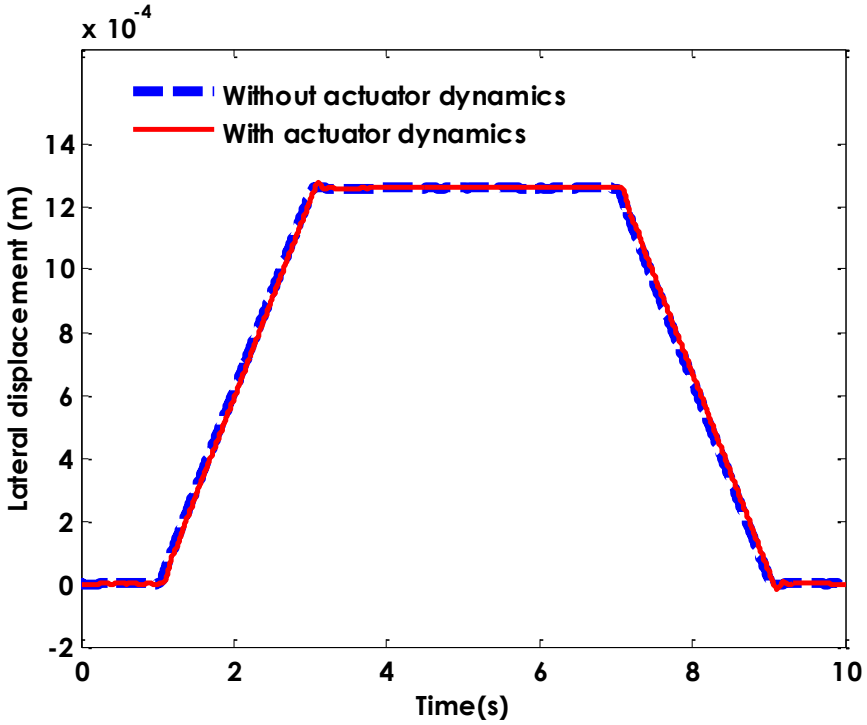

Figure 2-15: lateral displacement with and without actuator dynamics

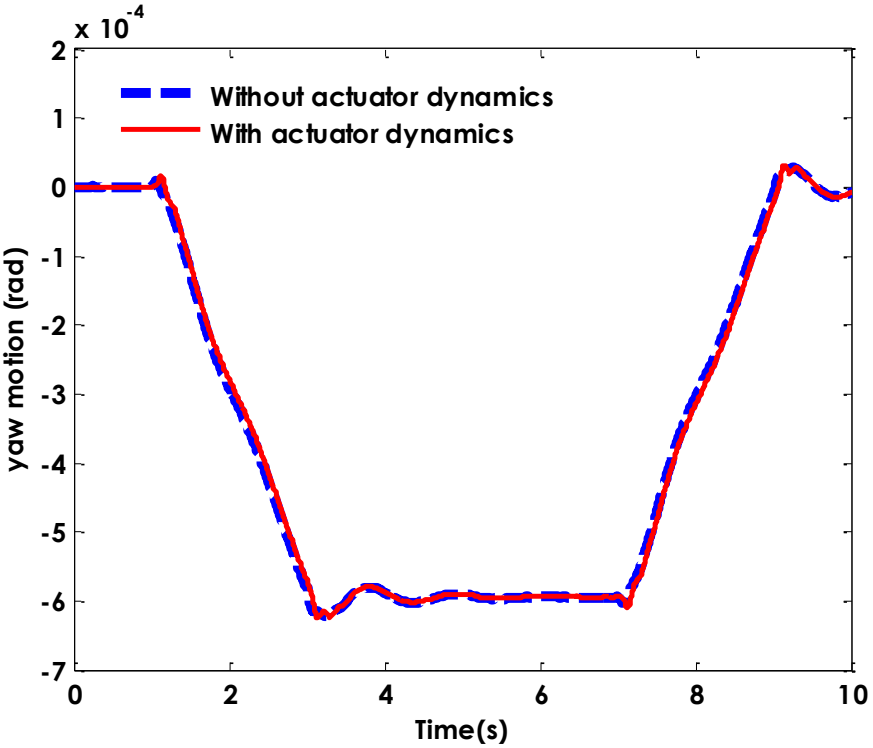

Figure 2-16: Angle of attack with and without actuator dynamics

2.6 Estimator Design

For the optimal control approaches, full state feedback (14 variables) is required. In practice, it would be very difficult and not cost effective to measure parameters such as wheel–rail deflection and wheelset angle of attack (Pearson, Goodall, Mei, & Himmelstein, 2004). Therefore, some form of state estimation is required to provide accurate/ optimise state estimates in order for the controller to calculate the torque demands, one of the most well-known and often used tools is known as the Kalman Filter (Kalman, 1960). The Kalman Filter (KF) is a model-based state estimator and uses a linear dynamic model that is formulated in the state space model, which is known as an *"optimal recursive data processing algorithm"* that is able to estimate unavailable process variables/measurements with an optimal/minimum error through combining all available process variables in real time, plus prior knowledge of the measurements (Maybeck, 1979, p. 4). In this research, the use of a Kalman Filter in a continuous time, which is known as Kalman-Bucy Filter, is considered to provide the required feedback variables for the controller. Figure 2.17 shows the basic structure of the system, where the vehicle is stabilised by an optimal controller and the output of the KF is used to provide the feedback signals required by the controller.

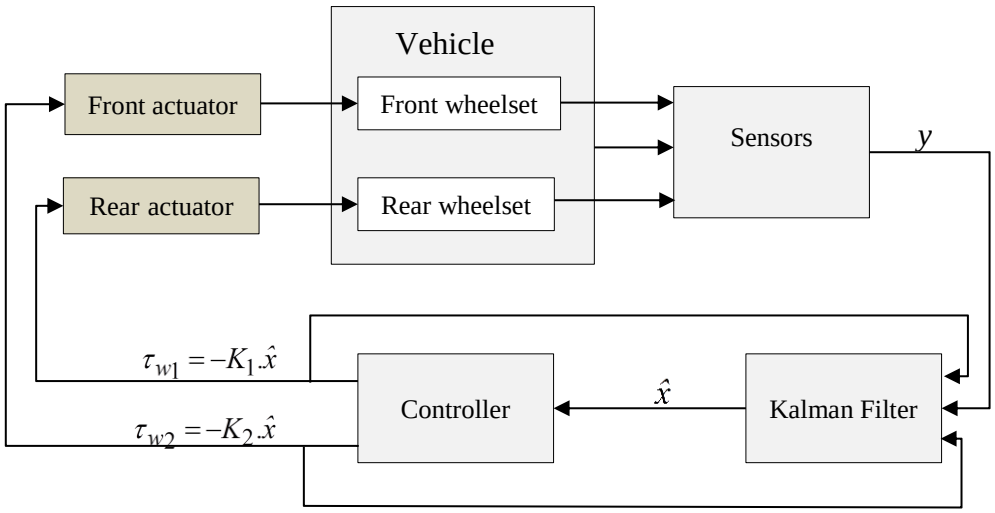

Figure 2-17: The overall control strategy

The proposed Kalman Filter for the estimation of the states is re-formulated from the state equation in (Mei, Li, & Goodall , 2001) such that the deterministic features of the track have been included as a part of the control input to the Kalman Filter as those can be readily made available in practice. The re-formulated equation for the design of the Kalman Filter is given in Equation (2-43).

$$\dot{x}_k = A.x + B_k.u_k + H_k.w_k \qquad \textbf{Eq. 2-43}$$

$$x = \left[\dot{y}_{w_1} \quad y_{w_1} - y_{t_1} \quad \dot{\psi}_{w_1} \quad \psi_{w_1} \quad \dot{y}_{w_2} \quad y_{w_2} - y_{t_2} \quad \dot{\psi}_{w_2} \quad \psi_{w_2} \quad \dot{y}_g \quad y_g - \left(\frac{y_{t_1} + y_{t_2}}{2} \right) \quad \dot{\psi}_g \quad \psi_g \quad \dot{y}_v \quad y_v - \left(\frac{y_{t_1} + y_{t_2}}{2} \right) \right]^T ;$$

Where;

$$u_k = \left[\tau_{w_1} \quad \tau_{w_2} \quad \frac{1}{R_1} \quad \theta_{c_1} \quad \frac{1}{R_2} \quad \theta_{c_2} \right]^T$$

$$w_k = \left[\dot{y}_{t_1} \quad \dot{y}_{t_2} \right]^T$$

In Equation (2-43), x is the vector of state variables from Equation (2.34) and the derivative of the track irregularities considered as the input white noise in the design process w_k. A total of eight sensors (six accelerometers and two displacements) are used. The accelerometers are used to measure the lateral and yaw acceleration of the leading and trailing wheelsets and the bogie frame and the two displacement sensors are used to measure the yaw motion between the bogie frame and each wheelset — the latter is used to provide information regarding the wheelset, but to avoid the need for axle-mounted sensors which would be problematic in practice due to the hostile working environment (Mirzapour, Mei, & Xuesong, 2014). The output equation for the measurements is given in Equation (2.44).

$$y_k = C_k.x_k + D_k.u_k + v_k; \qquad \textbf{Eq. 2-44}$$

Where;

$$y_k = \left[\ddot{y}_{w_1} \quad \ddot{\psi}_{w_1} \quad \ddot{y}_{w_2} \quad \ddot{\psi}_{w_2} \quad \ddot{y}_g \quad \ddot{\psi}_g \quad \Delta\psi_{w_1} \quad \Delta\psi_{w_2}\right]^T;$$
$$\Delta\psi_{w_1} = \psi_{w_1} - \psi_g;$$
$$\Delta\psi_{w_2} = \psi_{w_2} - \psi_g$$

where v_k represents the measurement noise vector and all measurement noises are set to 2% of their maximum value which is representative of real sensors of this type (Mei, Li, & Goodall , 2001); and the measurement matrix C_k is obtained readily from the system matrix A. The provided states can be used to determine the Kalman gain and a general structure of the Kalman-Bucy Filter (Maybeck, 1979) is given in Figure 2.18.

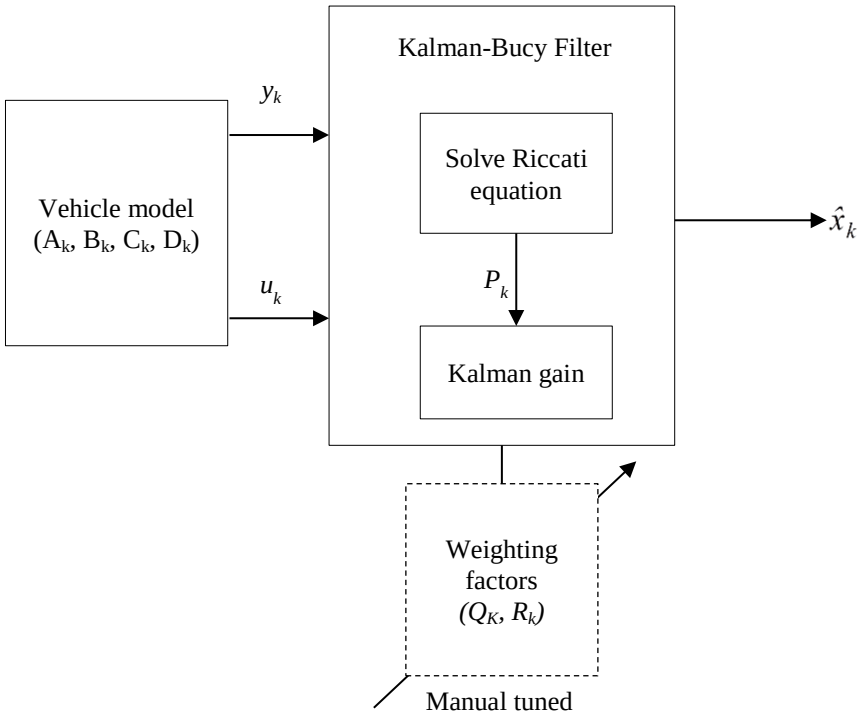

Figure 2-18: A general structure of the Kalman-Bucy Filter

The state-equation of the Kalman-Bucy Filter can be written as:

$$\dot{\hat{x}}_k = A \cdot \hat{x}_k + B_k . u_k + K_k (y_k - C_k . \hat{x}_k - D_k . u_k) \quad \textbf{Eq. 2-45}$$

where K_k is called Kalman gain and it must be determined through an algebraic Riccati equation as given in Equation (2.46).

$$\dot{P}_k(t) = AP_k(t) + P_k(t)A^T - K_k . C_k . P_k(t) + Q_k \quad \textbf{Eq. 2-46}$$

Where

$$K_k = P_k {C_k}^T {R_k}^{-1}$$

where P_k is an estimate of the covariance of the measurement error, and Q_k and R_k represent process and measurement covariance, respectively. The performance of the Kalman Filter will be assessed by the fine-tuning of the measurement noise covariance R_k and process disturbance (track noise) Q_k. Here, the measurement noise covariance matrix can be calculated directly from the measurement noise (v_k) as given in the Equation (2-47).

$$R_{ac} = \sum_{i=1}^{n} \frac{(v_{k_i} . v_{k_i}^T)}{n} \quad \textbf{Eq. 2-47}$$

Where

n = 8; total number of sensors

However, the determination of the track noise Q_k is generally not straightforward and trial-error tuning has been used to find the best result such that the performance and robustness of the Kalman Filter can be assessed and final value are given in Equation (2.48).

$$Q_k = \begin{bmatrix} 1 \times 10^{-7} & 0 \\ 0 & 1 \times 10^{-7} \end{bmatrix} \quad \textbf{Eq. 2-48}$$

By tuning Q_k and R_k, a Kalman gain matrix (K_k) is obtained that generates optimal full state estimations. Table 2-2 summarises the root mean square of the measurements' data along with their estimation error in order to study the performance of the Kalman Filter on a

random track. An analysis of the generated data shows that the Kalman Filter can provide good estimation results and that the estimation errors are small and mainly due to sensor noises in the measurement.

Table 2-2: Root mean square of the measurements, estimation and error data

		Root mean square (r.m.s)		
		Measurement	*estimation*	*error*
Leading wheelset	Lateral acceleration (m/s^2)	3.56e-1	3.15e-1	5.37e-2
	Yaw acceleration (rad/s^2)	4.15e-1	4.17e-1	1.78e-1
	Relative yaw displacement (rad)	5.58e-4	5.27e-4	1.07e-4
Trailing wheelset	Lateral acceleration (m/s^2)	5.51e-1	5.21e-1	1.54e-1
	Yaw acceleration (rad/s^2)	5.99e-1	6.18e-1	2.37e-1
	Relative yaw displacement (rad)	2.84e-4	2.21e-4	9.12e-5
Bogie	Lateral acceleration (m/s^2)	6.14e-1	6.07e-1	2.59e-2
	Yaw acceleration (rad/s^2)	7.66e-1	7.50e-1	6.20e-2

Figures 2.19 and 2.20 give the estimated lateral displacement (wheel–rail), yaw motion and the estimation errors of the leading wheelset respectively and similar results are obtained for the trailing wheelset. Clearly, the Kalman Filter estimates the wheel–rail lateral deflection and yaw motion (angle of attack) very effectively.

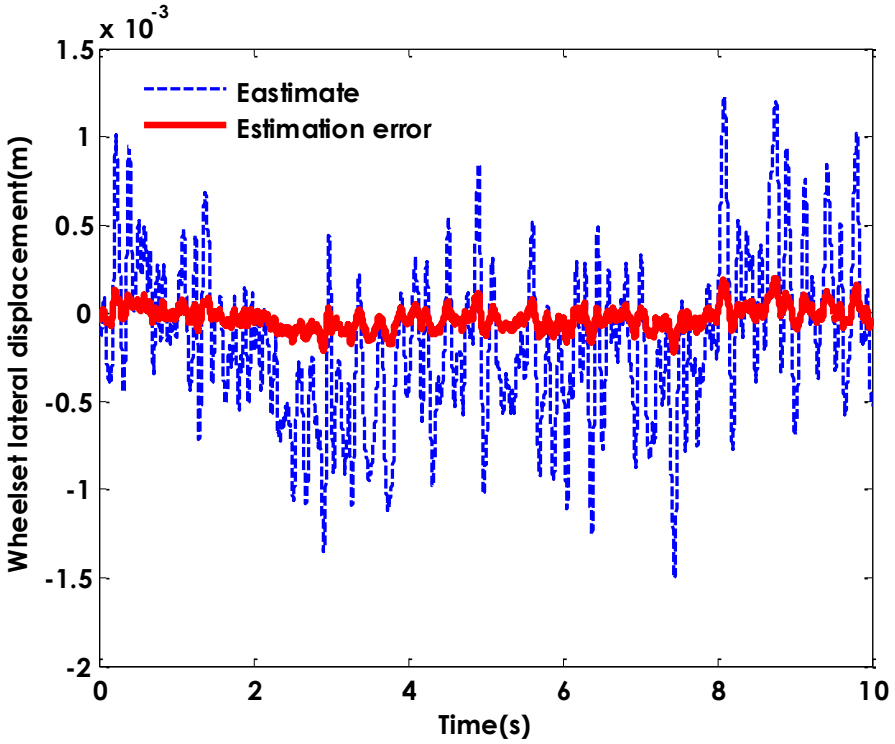

Figure 2-19: Estimated lateral displacement–front wheelset

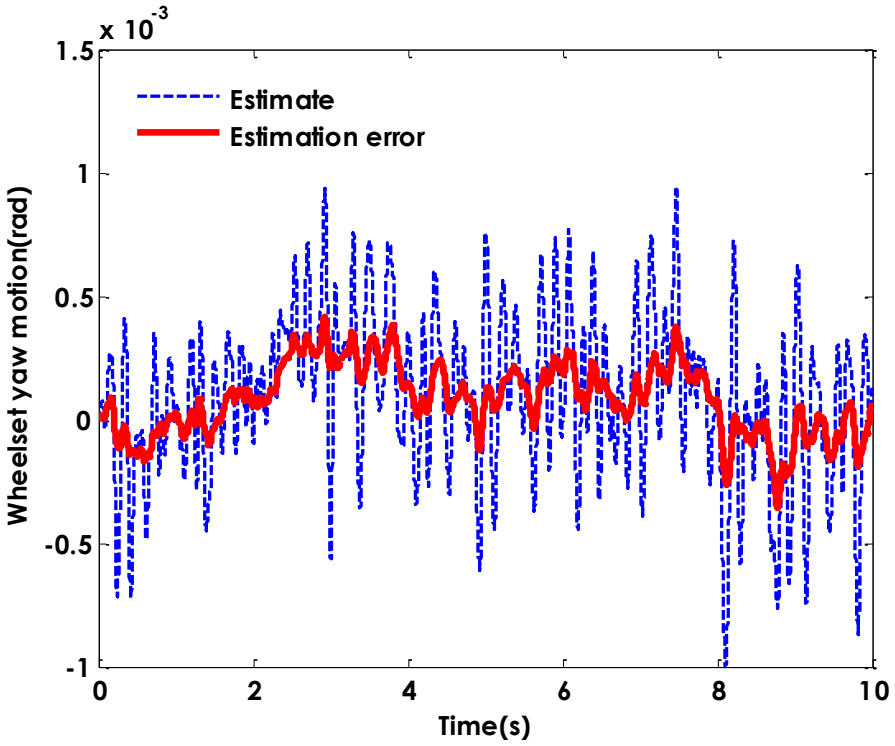

Figure 2-20: Estimated yaw motion–front wheelset

2.7 Summary

This chapter represents the development of the modelling and the basic active control strategy for a conventional railway vehicle that provides a research platform for the study of the fault tolerant control for active primary suspensions. A control strategy (controller and estimator) that provides stability and good curving performance was designed and verified by studying the results.

Chapter 3 FAULT DETECTION AND ISOLATION (APPROACH 1)

3.1 Introduction

When a fault occurs in an actuator, the actuator may become dysfunctional or at least less effective in delivering the desired torque to the wheelsets of the vehicle. Therefore, it is essential to detect and isolate actuator failure for safety critical systems such as wheelset control in order to enable the controller to cope with the corresponding fault (Mirzapour, Mei, & Hussain, 2012). This study considers two types of actuator failures that are likely to occur: Fail-Hard (FH) and Fail-Soft (FS). A fail-hard is a failure condition in a mechanical part of the actuator where the motor shaft of the actuator becomes stuck or immovable; possibly due to lack of lubrication. This type of failure is considered in (Alwi, Christopher, Tan, & Chee, 2011, pp. 8-10), and such an incident was reported for Flight 1080 (McMahan, 2005) (Montoya, et al., 1982), where one of the horizontal stabilisers jammed in the trailing edge-up position, and Flight 96, where the rudder jammed with an offset (Aircraft Accident Report: American Airlines 1972, 1973) . A fail-soft is a failure that is most likely to occur in the electrical parts of the motors' actuator due to either an Open Circuit (OC) or Short Circuit (SC), as a result of the power switch devices and/or the motor winding failing into a state of open or short circuit (Wolfgang, 2015, p. 163). The short circuit and open circuit correspond to zero voltage and zero current in the motor, respectively—resulting in re-generative braking or no motor torque from the actuator. This chapter presents the study of a fault detection scheme for actuator(s) through a vehicle model-based approach taking advantage of the fact that the dynamic properties and associated mathematical models for the railway vehicles are well established. Principally, this approach is proposed to explore the changes in vehicle dynamics in response to actuator failure(s) and hence the full vehicle model is used. The same Kalman Filter (KF) presented in the previous chapter to provide full state feedback for

the optimal controller will be used as the basis for the condition monitoring of the actuator status. In addition, sensor fault(s) are considered as the reliability of the fault detection and isolation scheme is highly dependent upon the information from the sensors. Figure 3.1 illustrates the overall strategy for the fault detection and isolation purposes. In this approach, the residuals will be generated in order to capture changes in the difference between the estimated signals ($\hat{y}$) and measured data (y) from the sensors (Patton, Chen, & Nielsen, 1995). Due to the actuator or sensor malfunction, the model used in the design of the Kalman Filter and the real vehicle dynamics would deviate from each other and therefore the estimation errors between the outputs of the Kalman filter and the measurements from the sensors are expected to increase. The data delivered by the estimator and measurements will be processed in the computation unit to extract the features specifically related to different fault conditions in order to detect and isolate any abnormal behaviour in the actuator(s) and sensor(s) (Isermann, 2005).

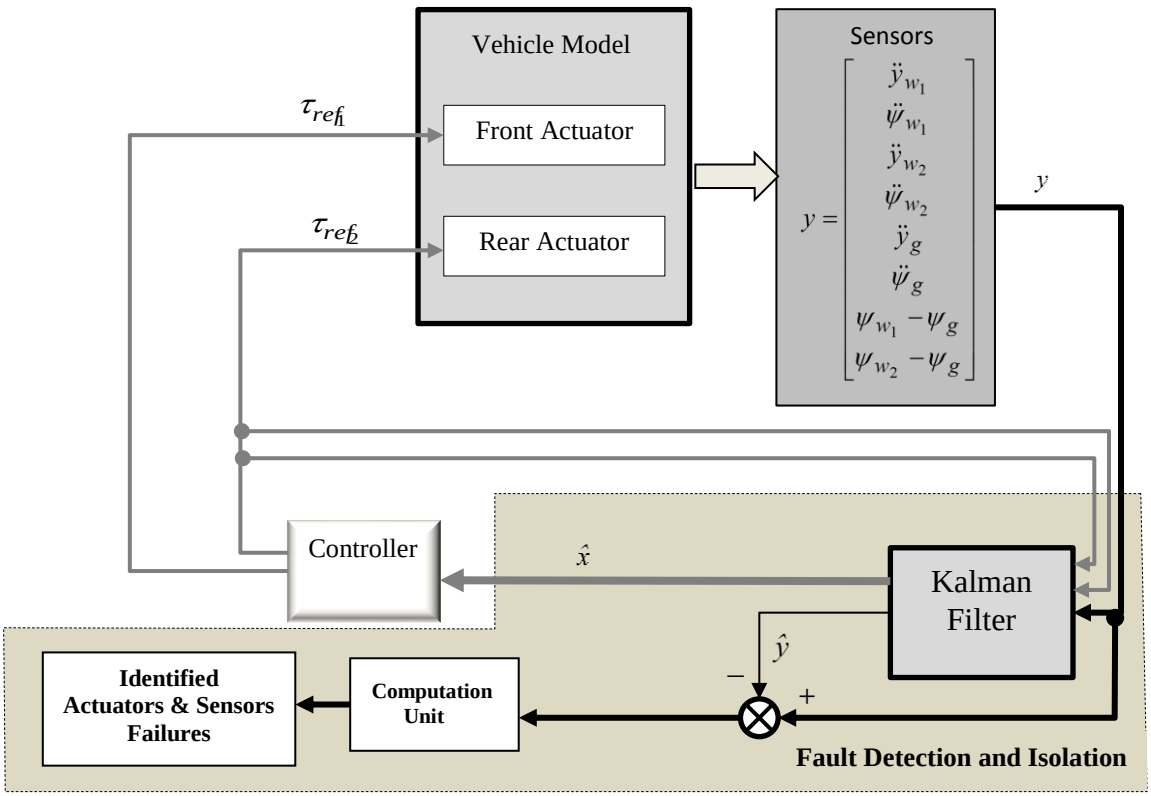

Figure 3-1: Overall fault detection and isolation strategy–Approach 1

3.2 Influence of Failure on Vehicle

This section examines changes in the dynamic behaviour of the vehicle in the presence of the actuator failures in order to first establish a better understanding of how fault(s) will affect the vehicle dynamics, and then to develop a fault detection and isolation (FDI) scheme.

3.2.1 Fail-hard

In the case of actuator fail-hard, the motor is jammed at a constant position, with the relative motion between the wheelset and the bogie constrained only by the material stiffness in the actuator connections. Figure 3.2 shows the relative yaw angle of the front wheelset when the leading actuator fails in hard mode at the position zero (at the time zero). It is clear that the relative yaw motion of the front wheelset, when the front actuator fails hard, is significantly reduced compared to the normal condition where both actuators are functioning. Similar results will be obtained if the rear actuator fails hard.

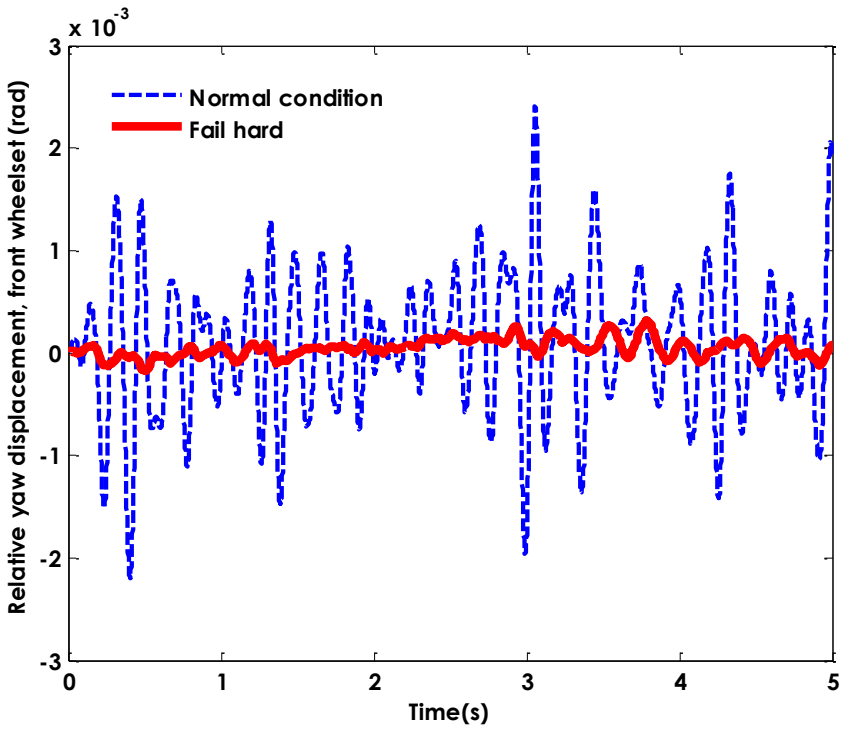

Figure 3-2: Relative yaw displacement–front wheelset (fail-hard)

Further investigation shows that the vehicle stability is not necessarily a major concern in such an incident, even though the level of the damping may be reduced (Mirzapour, Mei, & Xuesong, 2014). Figure 3.3 compares the minimum damping ratio of the wheelset modes between the normal condition, where both actuators are functioning effectively, and when one of the actuators fails hard. It clearly shows that in the normal condition where both actuators are functioning, the bogie is designed to be stable. Although an actuator with hard failure would reduce the stability margins, it does not present a major concern for the stability—even in the case of trailing actuator failure, the critical speed is still around 85 (m/s) or 306 (km/h) (Mirzapour, Mei, & Xuesong, 2014).

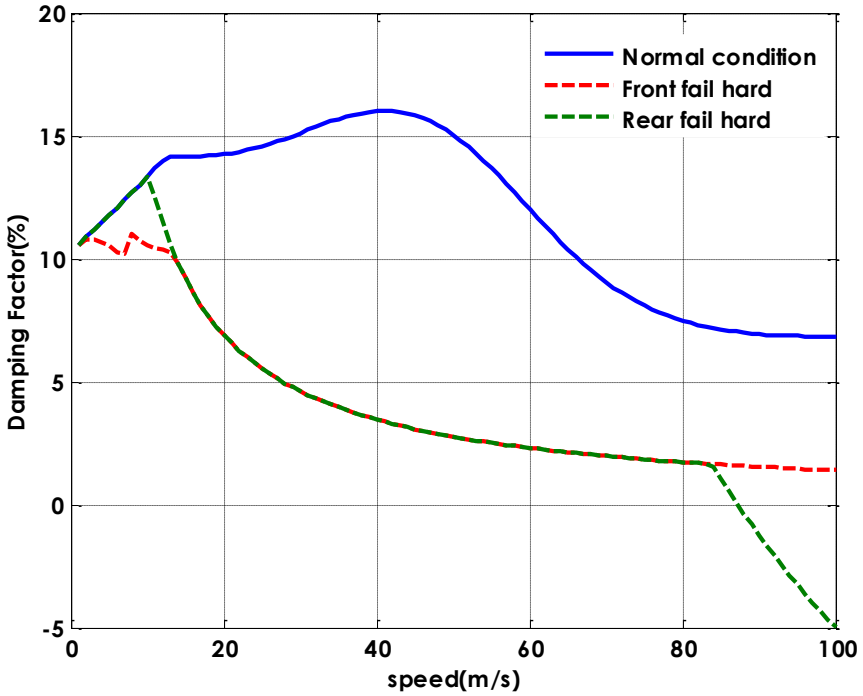

Figure 3-3: Minimum damping fail-hard vs normal condition–original controller

However, the fail-hard condition presents a much greater challenge for ensuring desirable curving performance due to much constrained motion for the wheelset concerned. Figures 3.4 and 3.5 compare the longitudinal contact forces in both the normal condition and in the event of actuator fail-hard.

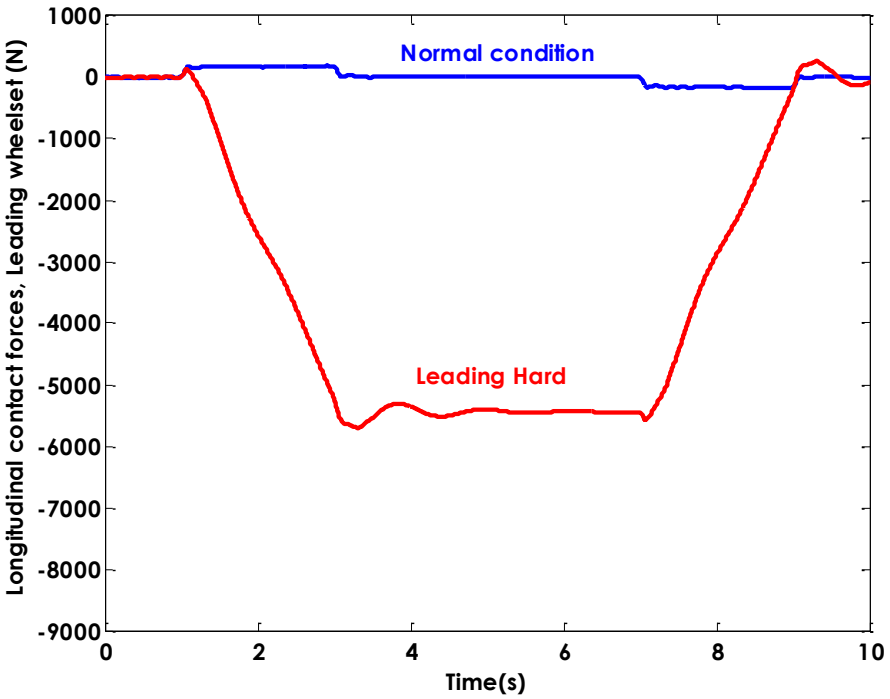

Figure 3-4: Longitudinal contact force of leading wheelset–locked actuator on curved track (V_s = 50 m/s, R = 1250 m, θ = 6°)

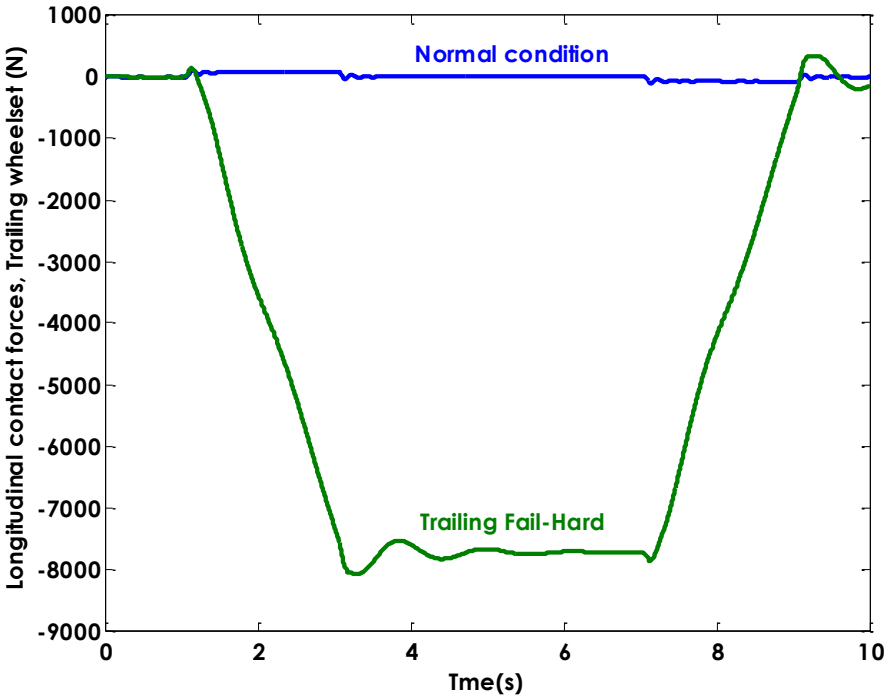

Figure 3-5: Longitudinal contact force of trailing wheelset–locked actuator on curved track (V_s = 50 m/s, R = 1250 m, θ = 6°)

The figures above clearly show that in the scenario of fail-hard in either the leading or trailing actuator, the contact creep forces at both the leading and trailing wheelsets significantly increase during curve negotiation due to the fact that the damaged actuator has very limited freedom of motion, resulting in poor steering performance. The generated forces in the lateral direction for the leading and trailing wheelsets should ideally be equal in order to achieve a good curving performance, because such equality can maintain the wheelsets in position to follow a curved track without deviating from each other (Bruni, Goodall, Mei, & Tsunashima, 2007). Figures 3.6 and 3.7 clearly show that the generated forces at the contact region in the lateral direction for the two wheelsets are far from being equal when one of the actuators fails hard for the leading and trailing wheelsets, where the normal condition is denoted by NC, leading fail-hard of the leading wheelset LHL, leading fail-hard of the trailing wheelset LHR, the trailing fail-hard of the leading THL and trailing wheelsets (THT).

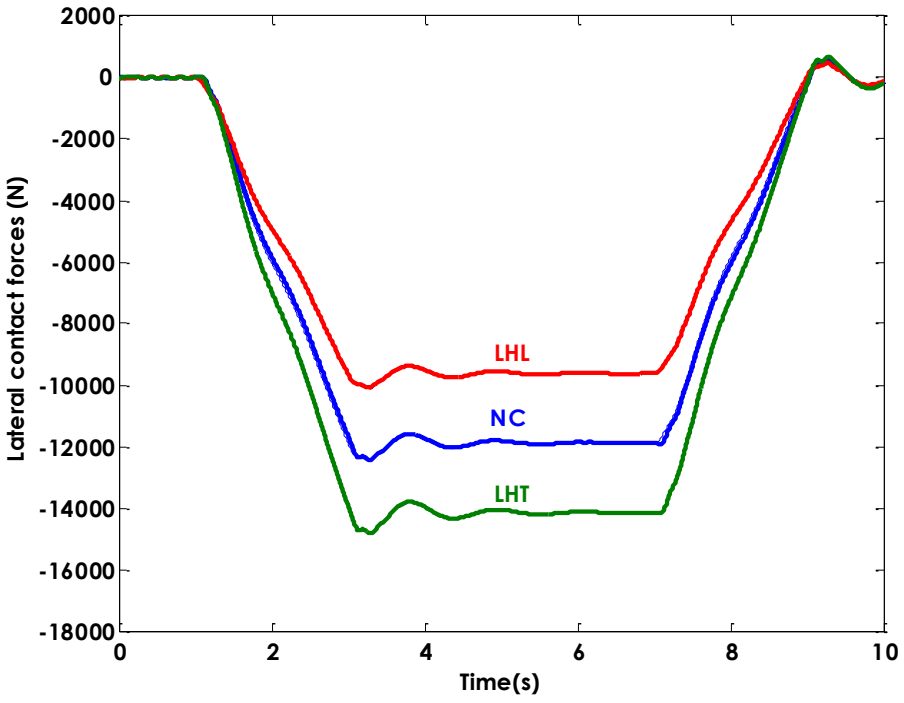

Figure 3-6: Lateral contact force–leading actuator (fail-hard)

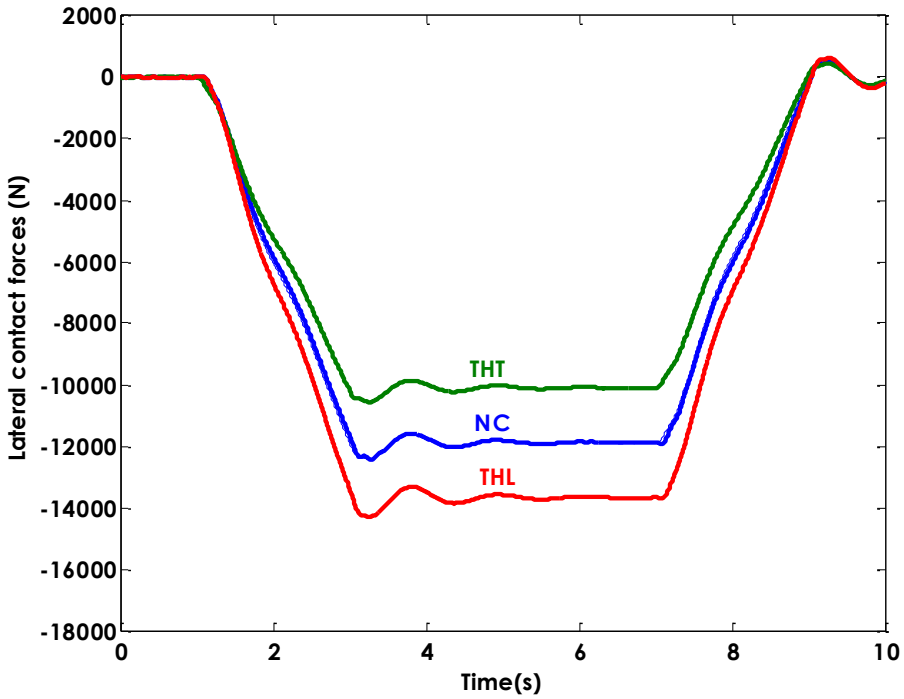

Figure 3-7: Lateral contact force–trailing actuator (fail-hard)

It can be deduced from the equation of motion given in chapter 2 that the increase of forces in the contact region is the result of the wheelset behaviour, especially on tight curves in terms of lateral displacement and angle of attack (Mei & Goodall, 2001). Figures 3.8 and 3.9 indicate the lateral displacement of the leading and trailing wheelsets associated with actuator fail-hard, respectively. They reveal that the wheelset related to the faulty actuator resulted in a larger lateral displacement compared to that in the normal no fault condition. This is due to the fact that the movement of the wheelset concerned is severely restrained by the corresponding broken actuator, and the wheelset is forced away from the pure rolling line.

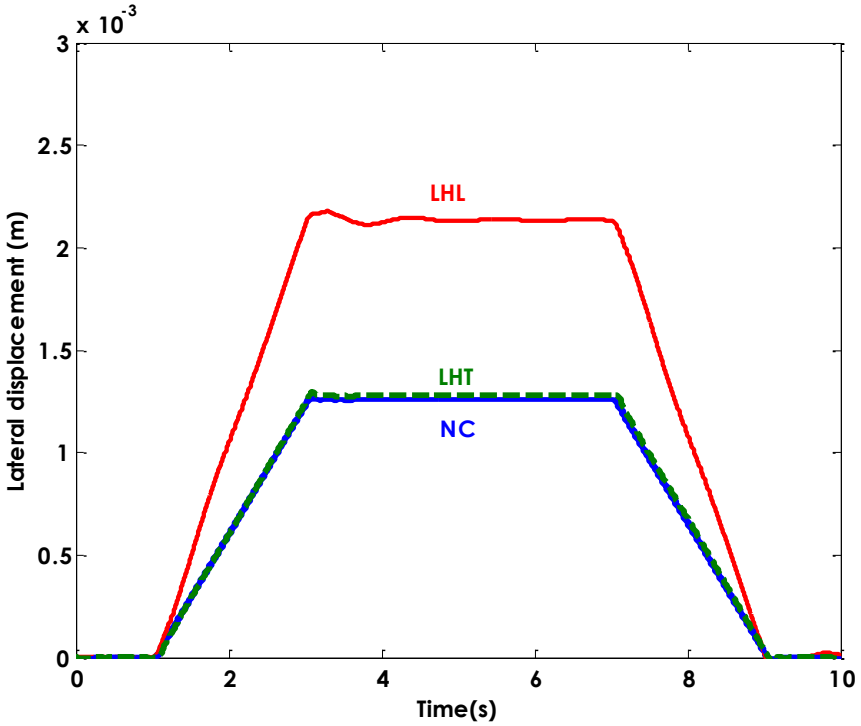

Figure 3-8: Lateral displacement–leading actuator (fail-hard)

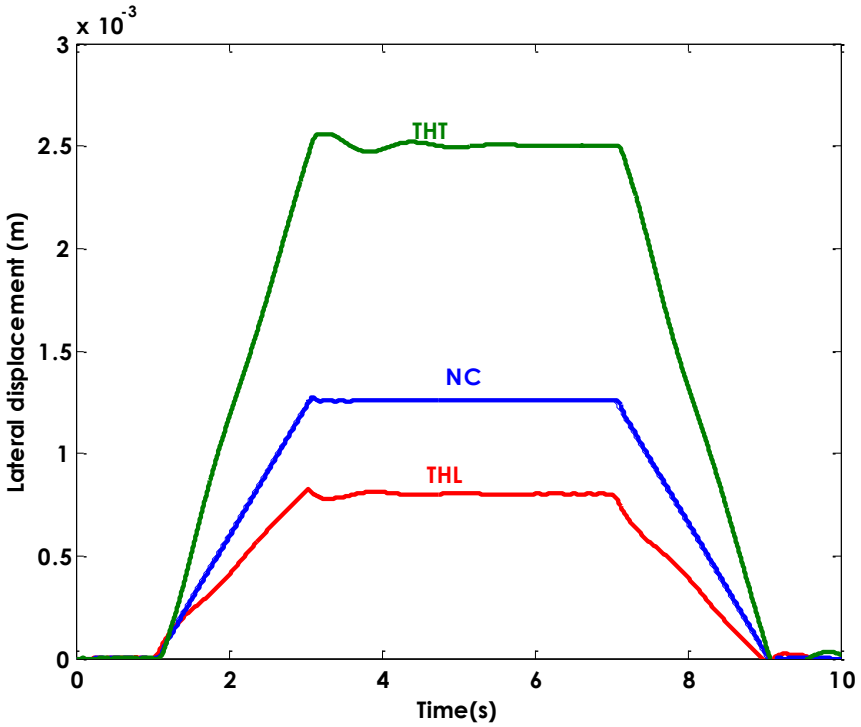

Figure 3-9: Lateral displacement–trailing actuator (fail-hard)

Further investigation at lower speeds shows that when the railway vehicle negotiates tighter curves, the effect of actuator failure on the vehicle performance becomes more obvious, as

indicated in Figures 3.10 and 3.11 where the curve radius of 300 (m) is used and NCL, NCT stand for the lateral displacements of the leading and trailing wheelsets under the normal condition. In this case, the large lateral displacement for the vehicle with actuator fail-hard would lead to flange contact which would cause damage to both the wheelset and track and may increase the risk of derailment in more severe cases (Wickens, 2003, p. 4).

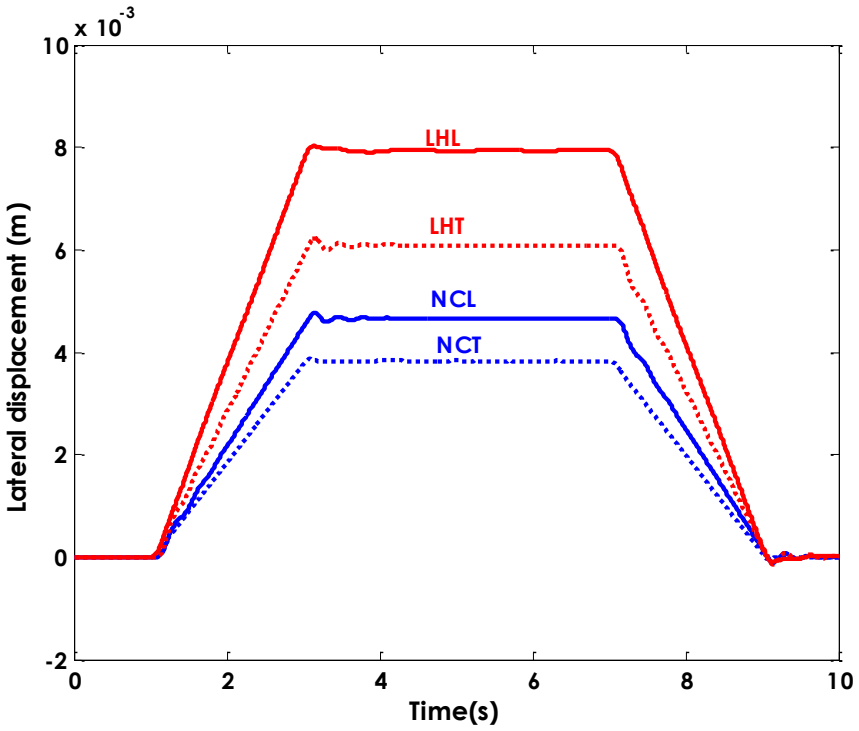

Figure 3-10: Lateral displacement–curve radius 300 (m)

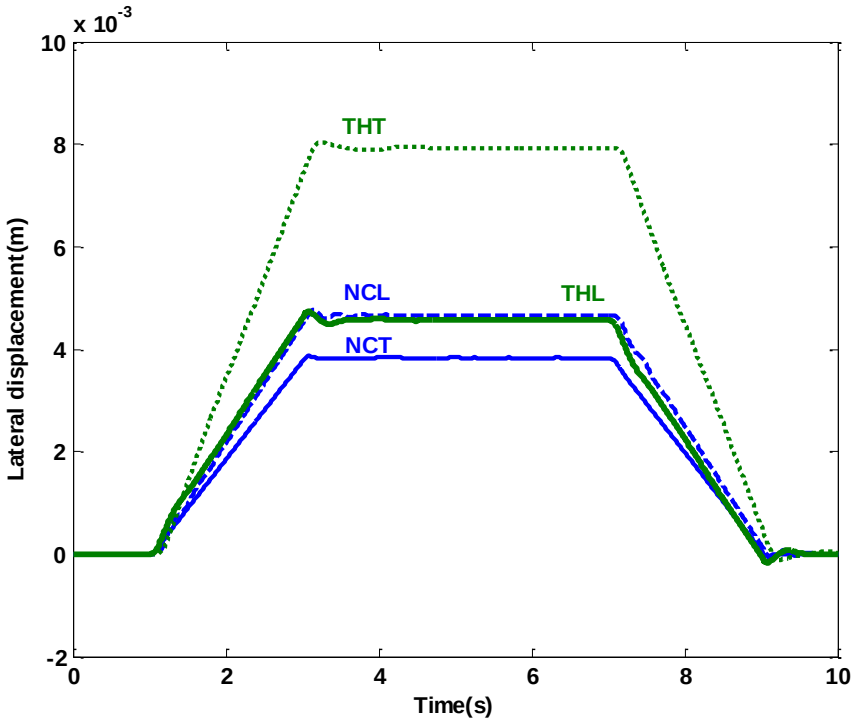

Figure 3-11: Lateral displacement–curve radius 300 (m)

Therefore, the priority of the fault tolerance in the fail-hard scenario, on detection of the actuator fault, will be to re-configure the controller to minimise the adverse impact of the actuator failure on the curving performance.

3.2.2 Fail-soft

In the event of fail-soft, in either the short circuit or the open circuit case, the actuator will not be able to provide the required control torque to stabilise the kinematic mode of the wheelset (Mirzapour, Mei, & Hussain, 2012). Figure 3.12 compares the minimum damping ratio in the normal no fault, leading actuator fail-soft and the trailing actuator fail-soft conditions. In either of the fault conditions, the stability of the bogie is compromised significantly and the critical speed of the vehicle is reduced to less than 10 (m/s) (Mirzapour, Mei, & Xuesong, 2014). In practice, the operational speed will have to be kept at a very low level to avoid any potential compromise of safety if no other corrective control actions are taken (Mirzapour, Mei, & Hussain, 2012).

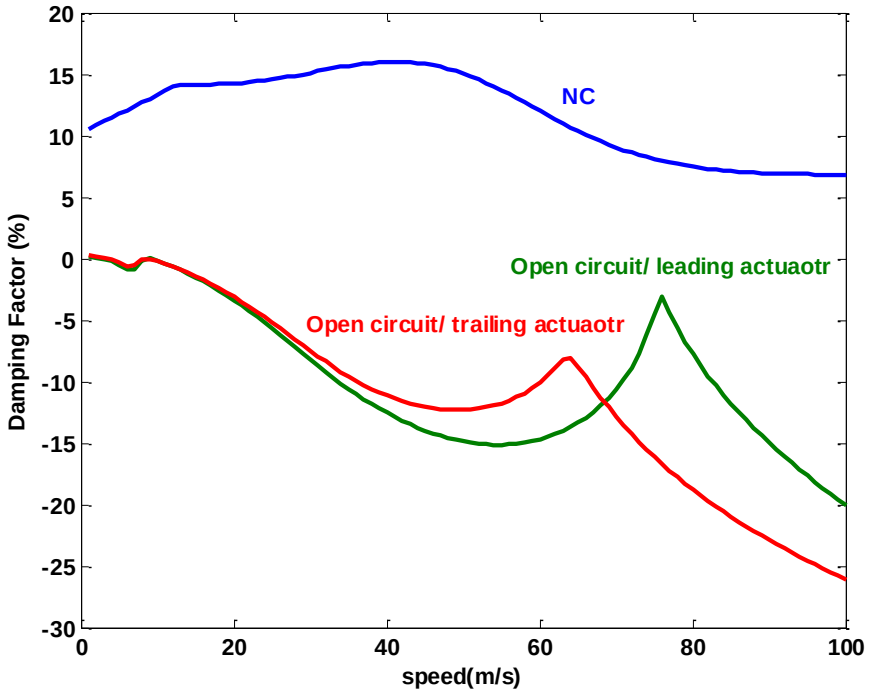

Figure 3-12: Minimum damping open circuit vs normal condition–original controller

Clearly, in the event of the short circuit and open circuit conditions, the priority of any fault tolerance strategy for the active control system is to preserve the stability control, whereas the curving performance is a secondary design issue (Mirzapour, Mei, & Xuesong, 2014).

3.3 Actuator Fault Detection and Isolation

It is clear that the fail-hard condition leads to a much constrained motion of the actuators, whereas the fail-soft fault results in an instability condition in the wheelset. Whilst the measurements of the actuator displacement and wheelset motion may be used to detect and identify the actuator fault(s), this kind of direct approach is problematic if sensor faults are also included for consideration. A fault detection and isolation method is therefore proposed that combines the sensor measurement and the knowledge of the dynamics of the system in order to provide a more robust solution.

3.3.1 Fault detection

In the event of actuator fail-hard, the motion of the wheelset (relative to the bogie frame) associated with the faulty actuator is severely constrained. This will lead to increased estimation error between the estimated data and measured data (i.e. the residual) because of the difference between the model used in the design of the Kalman Filter (for the normal no fault conditions) and changes in the real vehicle dynamics due to the fault. Figure 3.13 shows that in comparison to the normal no fault condition (NC), there is an increase in the generated residual of the relative yaw displacement of the leading wheelsets when the leading actuator fails hard (LH). On the other hand, the actuator fault at the leading wheelset is not expected to have any significant impact on the trailing wheelset, as shown in Figure 3.14. Similarly, in the scenario of the trailing actuator failing hard (TH), the generated residual of the yaw displacement at the leading wheelset is only marginally affected, but that at the trailing wheelset will be increased in comparison to the normal condition, as shown in Figures 3.13 and 3.14. Further examination shows that the error between estimated data and measured data from lateral and yaw accelerometers on the wheelsets and the bogie frame in the event of the actuator fail-hard do not show a significant change compared to the normal condition. For example, Figures 3.15 and 3.16 reveal that the changes are relatively small in the generated residuals of the lateral accelerometer of the leading and trailing wheelsets in the event of actuator fail-hard and normal condition.

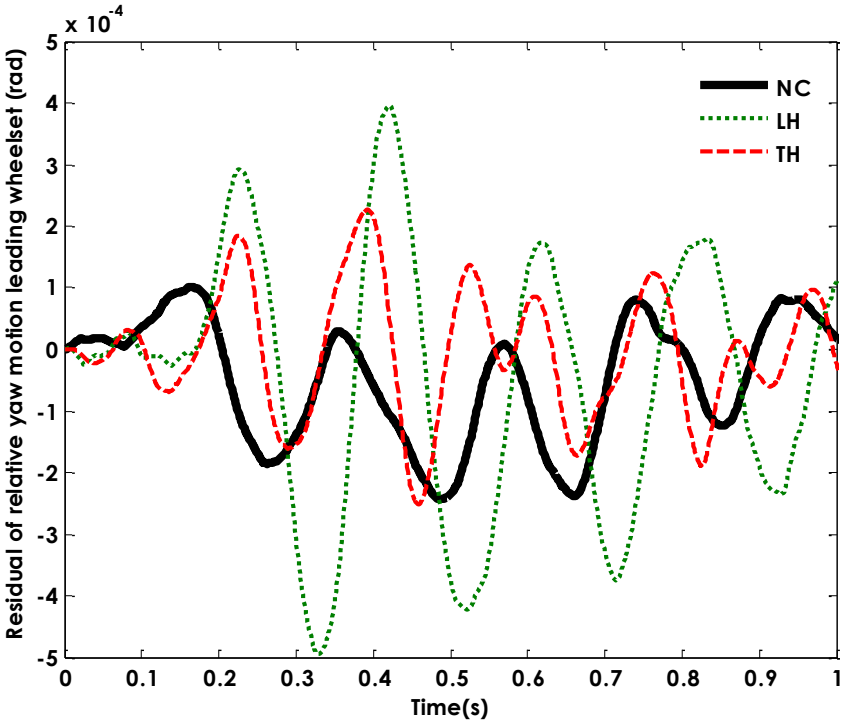

Figure 3-13: Residual of relative yaw displacement–leading wheelset (fail-hard)

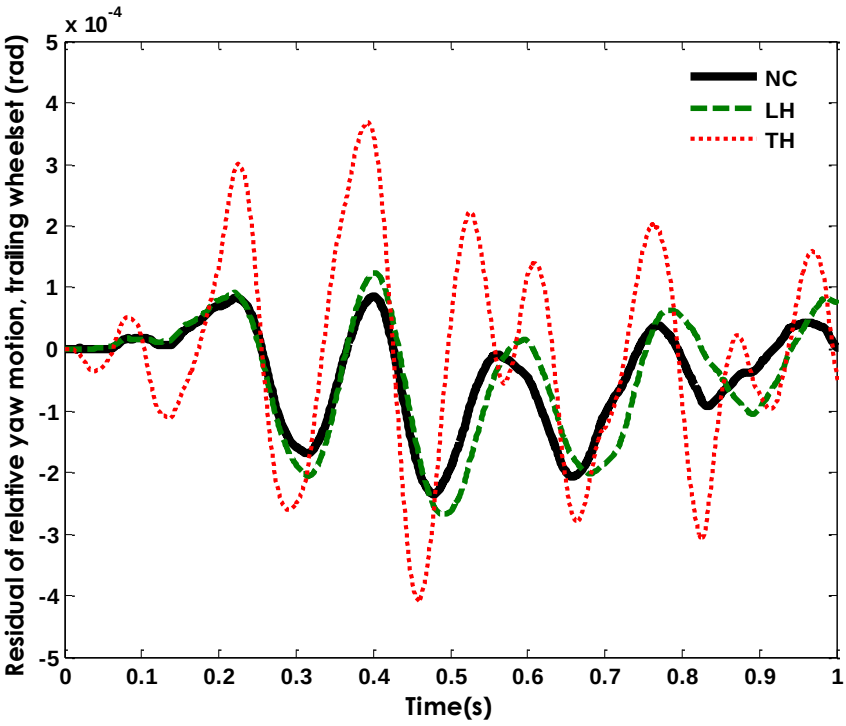

Figure 3-14: Residual of relative yaw displacement–trailing wheelset (fail-hard)

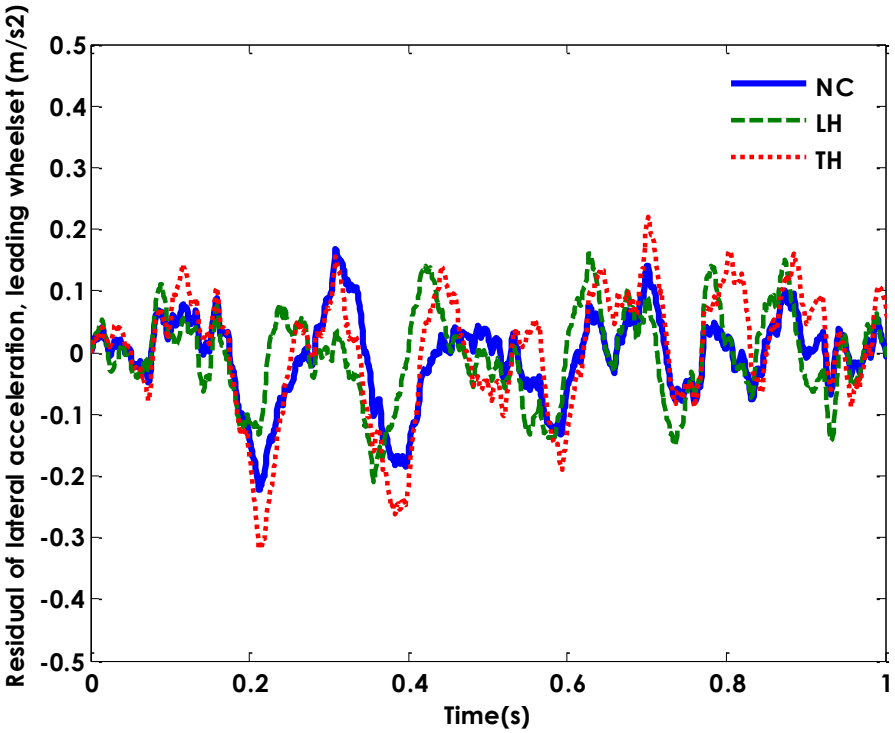

Figure 3-15: Residual of lateral acceleration–leading wheelset (fail-hard)

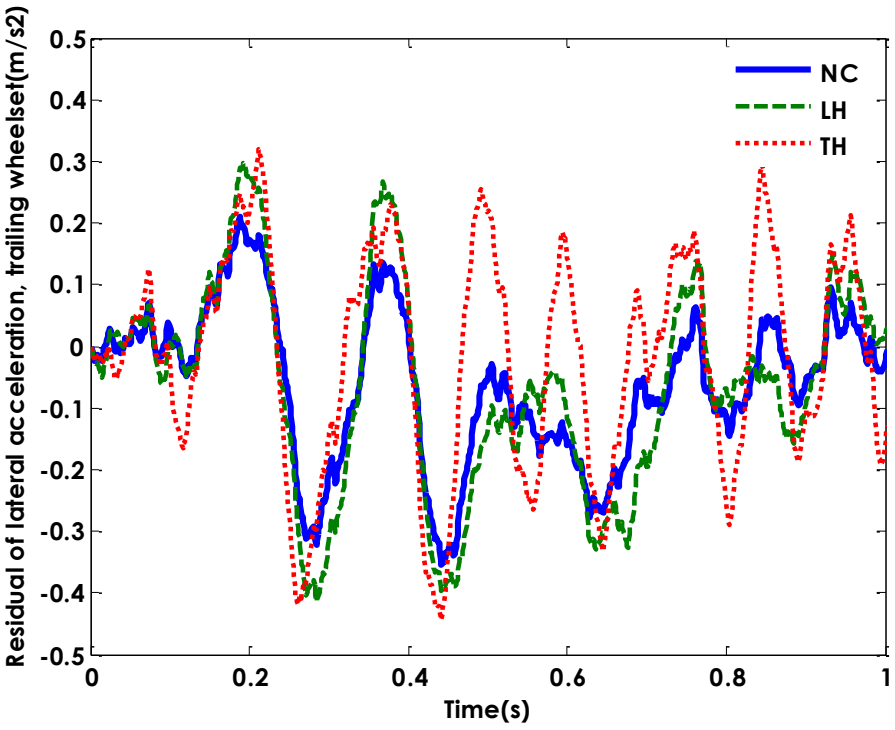

Figure 3-16: Residual of lateral acceleration–trailing wheelset (fail-hard)

On the other hand, in the event of fail-soft, the actuator failure leads to the system instability and therefore all generated residuals from the estimator will be expected to show an

oscillation (or limit cycle if the nonlinearity of the wheelset profile is concerned) because of the close interactions between the different modes of the vehicle (Mirzapour, Mei, & Xuesong, 2014) . Figure 3.17 presents the generated residuals from the relative yaw displacement between the wheelset and the bogie frame where the actuator is depicted with leading open circuit (LOC), leading short circuit (LSC), trailing open circuit (TOC), and trailing short circuit (TSC). It shows that in the case of either actuator fail-soft (i.e. open and short circuit) at the leading or trailing wheelsets, there is a significant increase in the generated residuals.

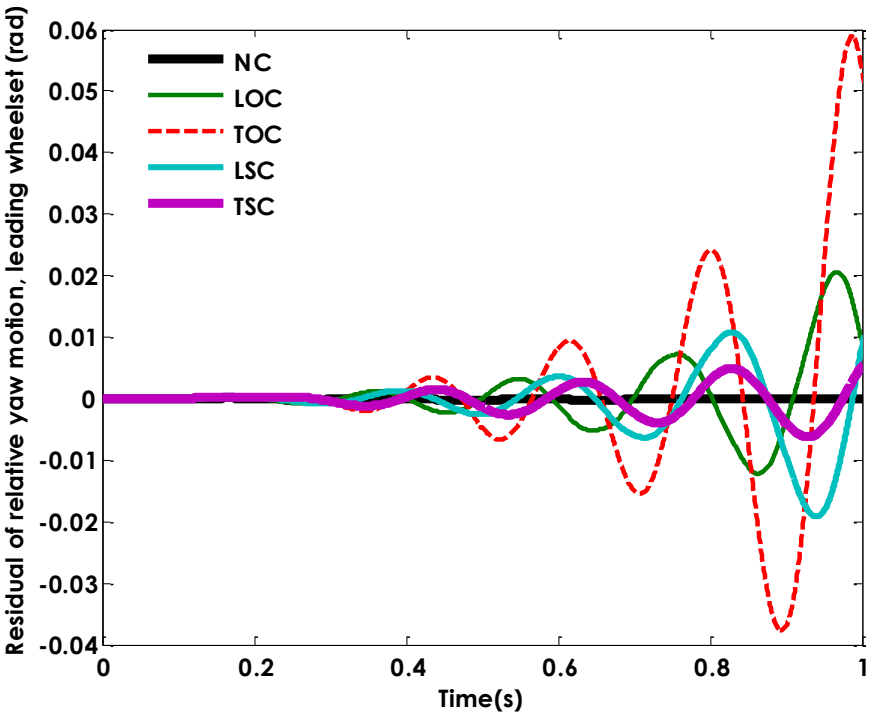

Figure 3-17: Residual of relative yaw displacement–leading wheelset (fail-soft)

Table 3-1 summarises how different possible actuator faults will affect the generated residuals from the estimator, where r_1, r_2, r_3, r_4, r_5, r_6, r_7 and r_8 represent the generated residuals from leading lateral accelerometer, leading yaw accelerometer, trailing lateral accelerometer, trailing yaw accelerometer, bogie lateral accelerometer, bogie yaw accelerometer, leading relative yaw displacement and trailing relative yaw displacement, respectively.

Table 3-1: The generated residuals from measured signals

Actuator conditions		**Residuals**							
		r_1	r_2	r_3	r_4	r_5	r_6	r_7	r_8
Normal condition		0	0	0	0	0	0	0	0
Fail-hard	Front actuator	0	0	0	0	0	0	+	0
	Rear actuator	0	0	0	0	0	0	0	+
Fail-soft	Front actuator	++	++	++	++	++	++	++	++
	Rear actuator	++	++	++	++	++	++	++	++

(0) no change, (+) increase, (++) significant increase

In Table 3-1, (+) stands for the increased residuals in respect to the normal condition (nominal value), (++) means that the fault leads to a significant increase of the residual, and (0) indicates that there is little influence of an actuator condition on the residual . It can be seen from Table 3-1 that the fail-soft condition can be readily differentiated from the fail-hard and normal conditions through evaluation of the generated residuals from any of the lateral or yaw accelerometers on the wheelsets or the bogie frame, as those generated residuals are considerably increased in the incident of the fail-soft condition. In addition, the fail-hard condition shows that the error from the measurement of the relative wheelset yaw displacement increases compared to the normal condition, and therefore can be identified from the normal condition. However, the use of residuals alone is not sufficient to classify the location of the actuator fail-soft as all generated residuals are subject to significant increase. Therefore, it is necessary to include extra information in order to identify the location of the soft failure. Further investigation shows that, in the event of fail-soft, the measurement of the lateral accelerometer of the wheelset associated with the damaged actuator increases much faster than its residual, whereas the measurement of the lateral accelerometer of the wheelset with the operational actuator is almost identical to its residual (Mirzapour, Mei, & Xuesong, 2014). This is due to the fact that when the actuator fail-soft occurs either in the leading or

trailing wheelset, the faulty actuator is not able to deliver any torque to the wheelset and therefore the lateral oscillation of the wheelset without actuator torque significantly increases in the wheelset concerned in the incident of fail-soft. Note, in the case of short circuit, the actuator would work in the regenerative (passive) mode and the torque produced will be quite small as the back e.m.f of the motor is low due to the low velocity. As far as the wheelset is concerned, there is no controlled output from the faulty actuator to influence the stability of the vehicle – note that damping does not stabilise the wheelsets.

For example, Figures 3.18 and 3.19 show the measurements and residuals of the lateral accelerometers. They clearly show that the measured signal associated with the defective actuator increases much faster than its estimated error, whereas the measurement from the healthy actuator is similar to its residual. A similar result will be generated for the trailing actuator in fail-soft (i.e. open and short circuits). Therefore, in order to isolate the location of the actuator fail-soft, the measurement data from the lateral acceleration of either the leading or trailing wheelset can be taken into consideration (Mirzapour, Mei, & Xuesong, 2014).

Note that the proposed FDI scheme treats the actuator open circuit and short circuit as a single case of fail-soft as there is little difference in the changes of the dynamic behaviour of the vehicle between the two and the control requirements to stabilise the vehicle are more or less the same in both cases – more will be explained in chapter 5.

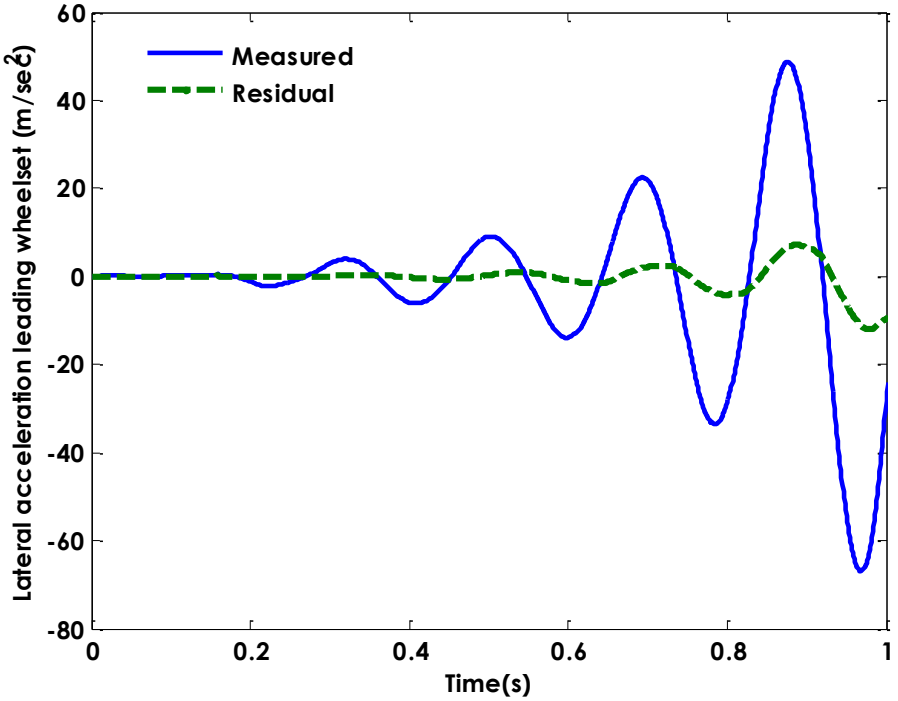

Figure 3-18: Measured and residual of lateral acceleration–leading wheelset (leading actuator open-circuit)

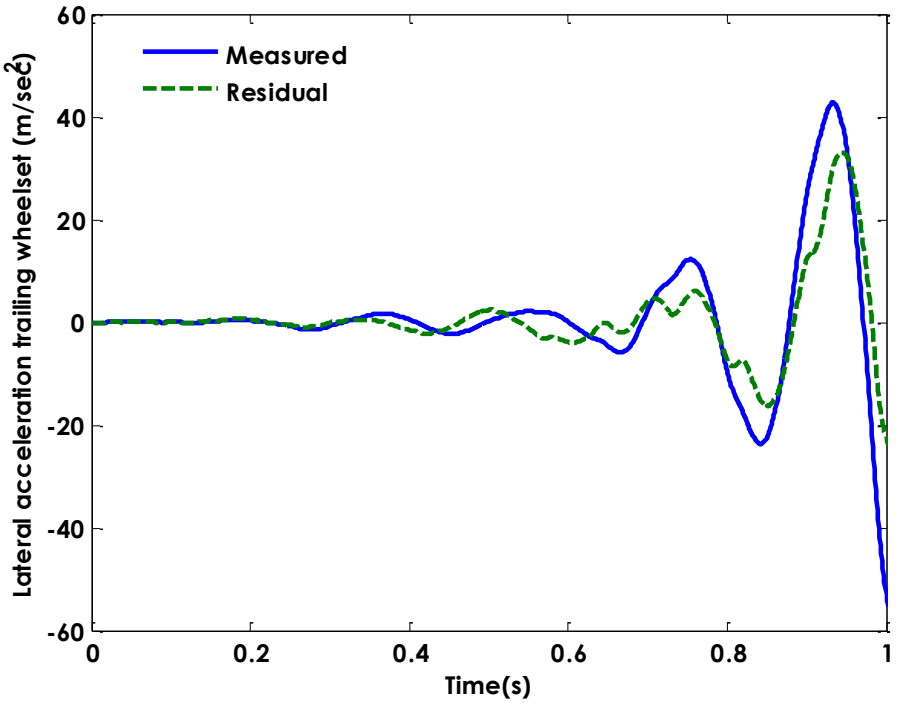

Figure 3-19: Measured and residual of lateral acceleration–trailing wheelset (leading actuator open-circuit)

3.3.2 Data processing

Having established the links between the fault conditions and the symptoms through sensorial devices and the estimation of the dynamic system, it is necessary to develop a computation (processing) method to extract related features from the raw data (Rauber, Nascimento, Wandekokem, & Varejão, 2010). Standard Deviation (STD) or Root Mean Square (RMS) are possible candidates for smoothing out the fast varying vibration signals, before further processing for the different fault conditions. In this study, standard deviation is preferred as, in the presence of fail-hard, the actuator's motor may become locked in different positions, rather than zero position and the use of standard deviation can extract the features by determining the level of variation from its average value. For example, Figure 3.20 shows the angular displacement of the motor's actuator locked-up at the position of -1.5×10^{-2}(rad) when the leading actuator fails at the time of 1 (s).

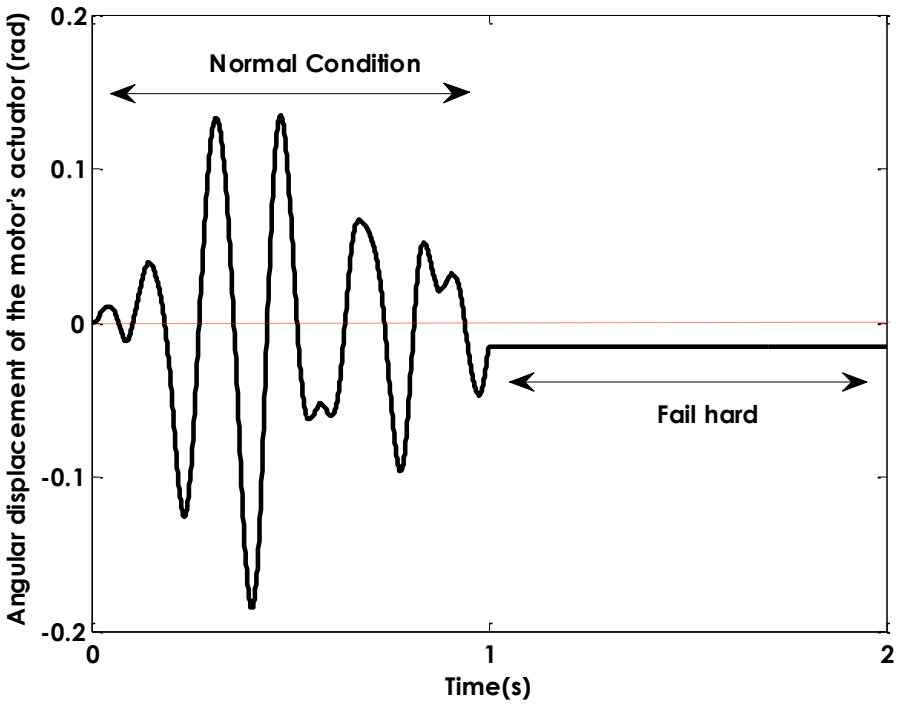

Figure 3-20: Angular displacement of the motor's actuator- front actuator fail-hard (time=1s)

A standard deviation with a window size of N is given in Equation 3.1, where x_i represents the sampling point of the raw signal (Chapra & Canale, 2009, pp. 441-444).

$$STD = \sqrt{\frac{1}{N-1}\left[\left(\sum_{i=1}^{N} x_i - \frac{\sum_{i=1}^{N} x_i}{N}\right)^2\right]} \quad \textbf{Eq. 3-1}$$

For the fail-hard condition, although the errors from the measurement of the relative wheelset yaw displacement increase in comparison with the normal condition, it turns out that the level of the obtained residual is not significant enough to define a distinct threshold that consistently separates the fault from the non-fault condition. Figure 3.21 shows the standard deviation, using a moving window with the size of 1 (s), of the residual from the relative yaw displacement of the rear wheelset when the front actuator fails in hard mode at a time of 2 (s). It shows a clear overlap in the magnitude between the two conditions. Note, the use of a moving window with the length of 1 (s) requires a buffer, in order to compute the standard deviation from raw data. Therefore, the calculation of the standard deviation moving window from the buffer to delay 1 (s) its processing while the buffer refills. Hence, in the following figure(s), which indicate the standard deviation moving window, the gap in data between 0 (s) and 1 (s) is due to the use of buffer that cause 1 (s) delay. In addition, the window size of 1 (s) on the standard deviation moving window has been chosen to provide a compromise between the vehicle performance requirement in the incidence of the actuator fail soft and to extract a distinguished threshold in the presence of the actuator fail hard. For example, Figure 3.22 indicates the relative lateral displacement of the front wheelset when the rear actuator fail-soft at the time of 2 (s). It clearly shows that the relative lateral displacement of the wheelset reaches 8 (mm) after 1 (s) of the actuator failure. In practice, it means that there is severe flange contact between wheelset and rail, resulting in the vehicle derailment. Therefore, the window size larger than 1 (s) is not suitable in the event of fail soft. On the

other hand, the larger buffer size is required in the event of fail-hard in order to make a distinctive threshold (Figure 3.21) while increasing the length of the buffer more than 1 (s) would increase the risk of the vehicle derailment in the event of the actuator fail-soft (Figure 3.22) .

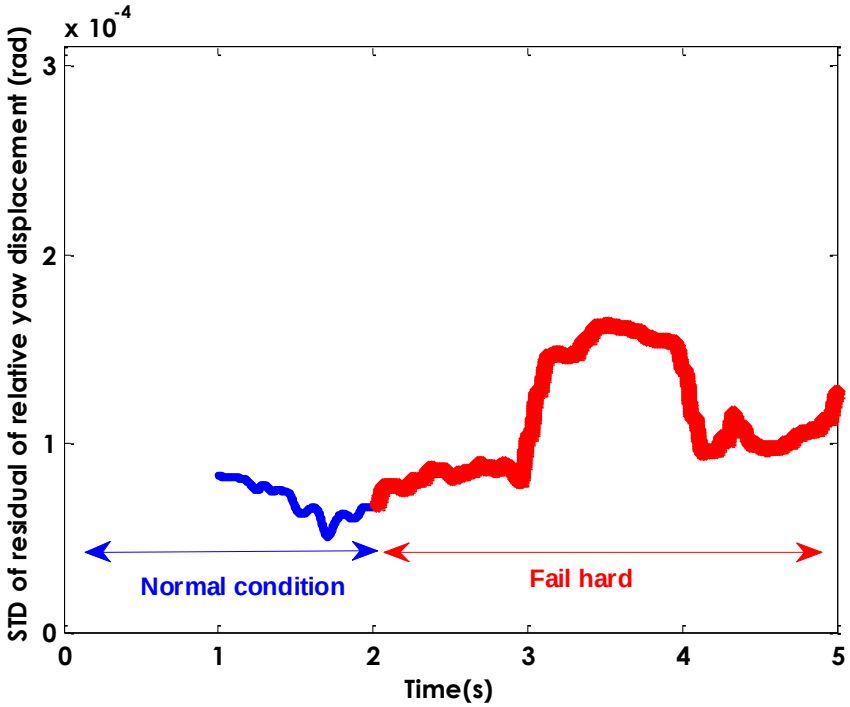

Figure 3-21: STD of relative yaw displacement–front wheelset fail-hard (time=2s)

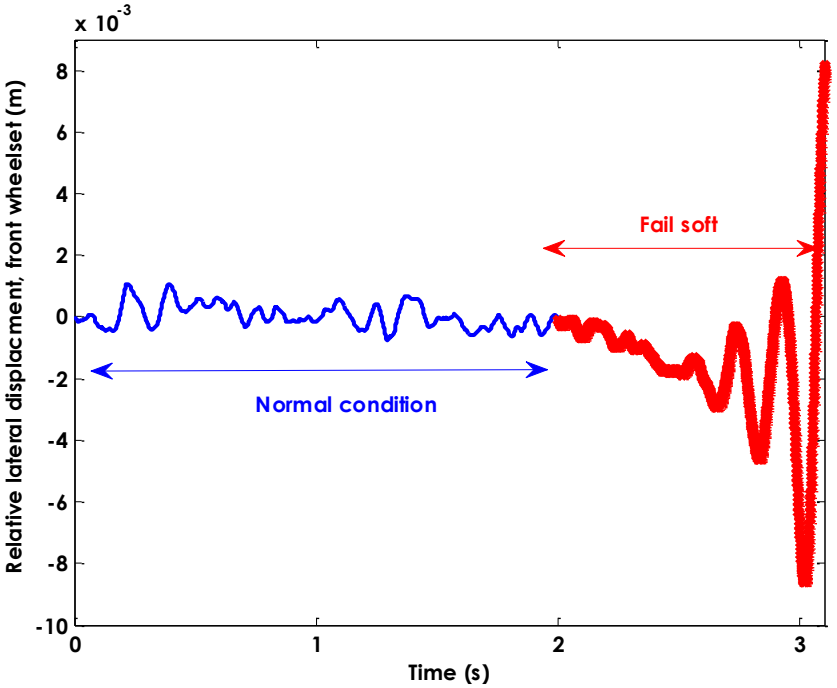

Figure 3-22: relative lateral displacement of the front wheelset- rear actuator fail-soft (time=2s)

Therefore, it seems that the other information must be taken into account in order to improve the sensitivity to detect and isolate the actuator fail-hard within 1 (s). For this reason, the measured data from the relative wheelset yaw displacement is also included as the magnitude of the relative yaw displacement associated with the immovable actuator notably reduces compared to the normal condition. The inclusion of the latter measurement can ensure that the fault detection and isolation scheme is capable of responding quickly to the fail-hard condition. Further on, the information of the measurement and the associated residual cannot be evaluated individually in order to define a threshold as the residual does not show significant change compared to the measurement. Therefore, the use of a ratio to make a comparison between the measurement and its residual has been considered for the fault detection and isolation purpose. In the data processing, the ratio of the measurement from the relative yaw displacement to its corresponding residual is proposed to extract the feature for the actuator fail-hard condition, as shown in Equations (3.2) and (3.3), where (ε) is a very small value.

Leading actuator fail-hard:

$$\frac{STD(\Delta\psi_{w_1})}{STD(\Delta\psi_{w_1} - \Delta\hat{\psi}_{w_1})} \approx \varepsilon < Threshold_1 \qquad \textbf{Eq. 3-2}$$

Trailing actuator fail-hard:

$$\frac{STD(\Delta\psi_{w_2})}{STD(\Delta\psi_{w_2} - \Delta\hat{\psi}_{w_2})} \approx \varepsilon < Thrershold_2 \qquad \textbf{Eq. 3-3}$$

Figures 3.23 and 3.24 show the standard deviations (using the same moving window as above) of the ratio of the measured relative yaw displacement to its residual in the event of fail-hard where the incident occurs at a time of 2 (s). They clearly show that thresholds can be

readily set and an actuator fail-hard can be detected and identified if the monitored variable is reduced to below a (pre-definable thresholds).

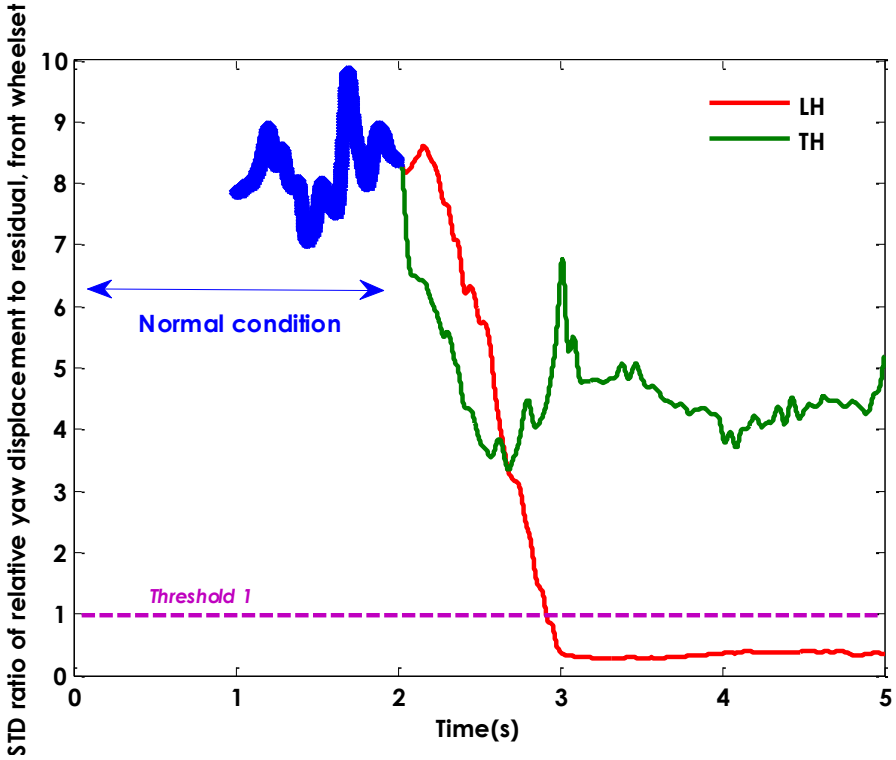

Figure 3-23: STD ratio of relative yaw displacement–front wheelset fail-hard (time=2s)

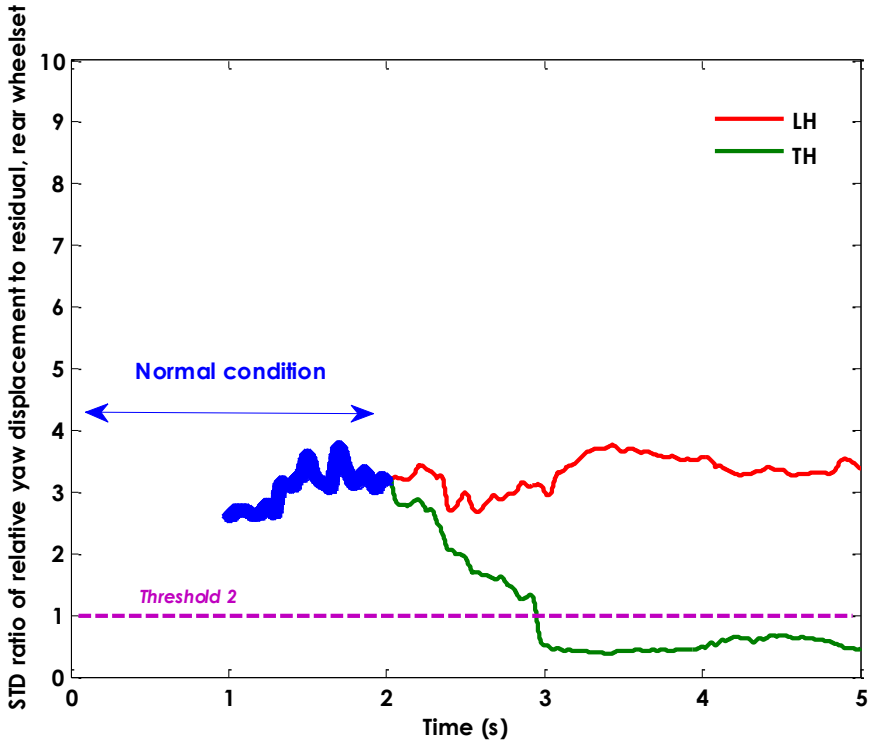

Figure 3-24: STD ratio of relative yaw displacement–rear wheelset fail-hard (time=2s)

For the fail-soft conditions, the location of the actuator fail-soft can be identified through the evaluation of the measurement of the lateral acceleration of the leading wheelset and its correspondent residual. In the event of the leading actuator failing soft, the measured lateral accelerometer of the leading wheelset significantly increases compared to its residual, whereas in the case of the fail-soft condition at the trailing wheelset the measured lateral accelerometer of the front wheelset (associated with the healthy actuator) remains almost identical to its residual. Therefore, the standard deviation ratio of the measurement to the corresponding residual can be considered to extract the feature for the actuator fail-soft, as expressed in Equations (3.4) and (3.5):

Leading actuator fail-soft:

$$\ddot{y}_{w_1} > (\ddot{y}_{w_1} - \hat{\ddot{y}}_{w_1}) \Rightarrow \frac{STD(\ddot{y}_{w_1})}{STD(\ddot{y}_{w_1} - \hat{\ddot{y}}_{w_1})} > Threshold_3 \qquad \textbf{Eq. 3-4}$$

Trailing actuator fail-soft:

$$\ddot{y}_{w_1} \cong (\ddot{y}_{w_1} - \hat{\ddot{y}}_{w_1}) \Rightarrow \frac{STD(\ddot{y}_{w_1})}{STD(\ddot{y}_{w_1} - \hat{\ddot{y}}_{w_1})} < Threshold_3 \qquad \textbf{Eq. 3-5}$$

Figure 3.25 shows the standard deviation of the ratio of the front lateral acceleration to its residual in the incident of short and open circuit in one of the actuators, respectively. In the figure, LOC and LSC represent the leading open circuit and leading short circuit; and TOC and TSC indicate the trailing open circuit and trailing short circuit, respectively. It clearly indicates that the rear actuator is in a fail-soft condition (i.e. open and short circuits) if the monitored variable is below a certain threshold. Exceedance of the threshold depicts the incident of the fail-soft for the front actuator.

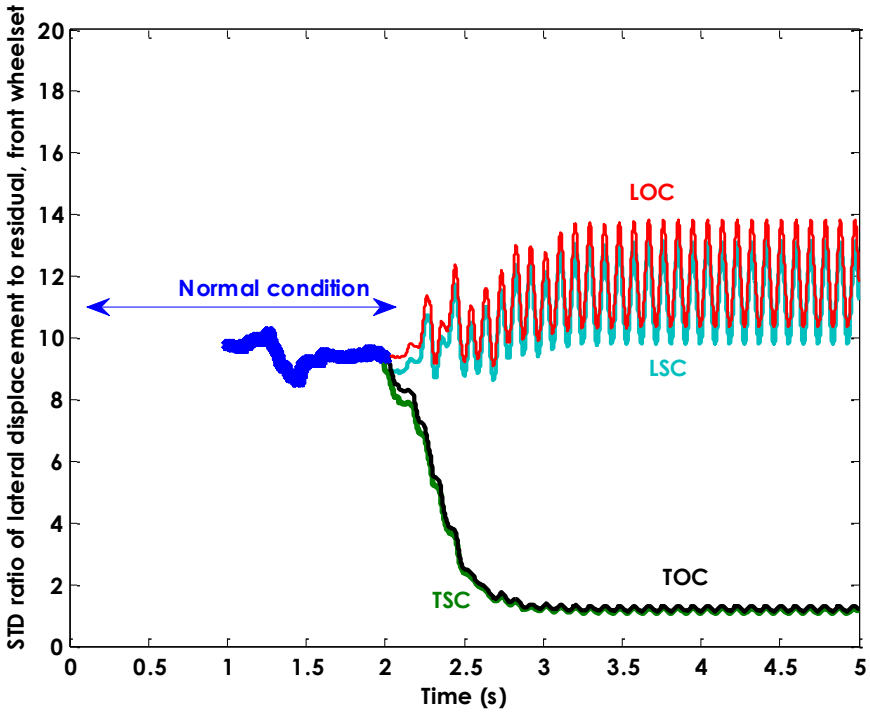

Figure 3-25: STD ratio of lateral acceleration–front wheelset fail-soft (time=2s)

Figure 3.26 illustrates the steps for the actuator fault detection and isolation for the proposed approach. In summary, a fail-soft condition can be isolated from the normal condition and the fail-hard through the evaluation of the residual of the lateral acceleration on the leading wheelset—this latter being used as it has already been considered to identify the location of the fail-soft condition. A fail-hard mode can be isolated through the ratio in standard deviation between the measured actuator displacement and its corresponding residuals generated from the state estimator.

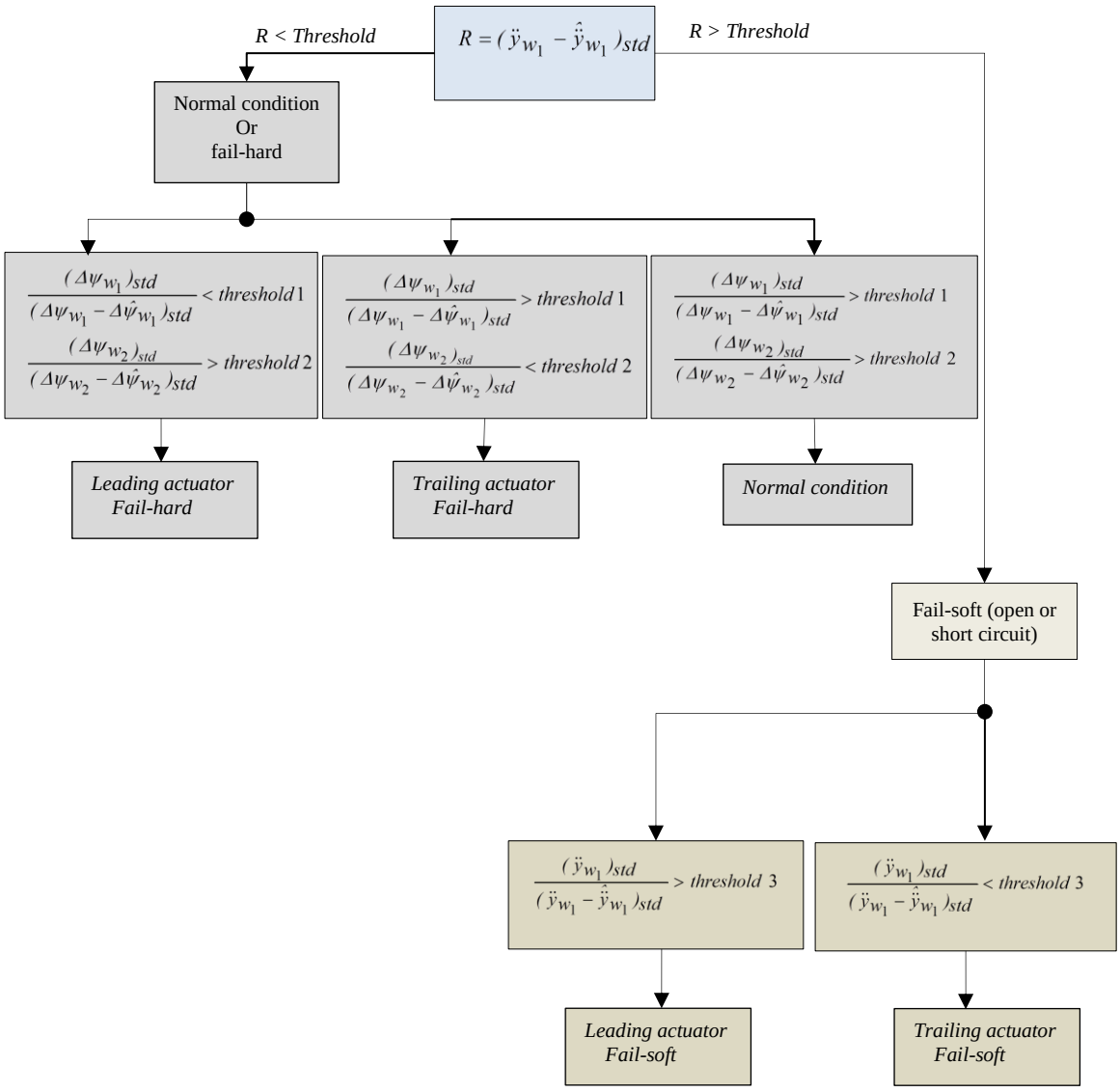

Figure 3-26: A block diagram for fault detection and isolation (Approach 1)

3.4 Assessment of the Fault Detection and Isolation Scheme

The proposed fault detection and isolation scheme is required to have the potential to provide robust fault detection and isolation in the incident of actuator failure. As the proposed strategy has been developed through a vehicle model-based approach, it must be able to diagnose the actuator failure in the presence of parameter variations, especially those related to the wheel-rail contact which is subject to large variations (Pearson, Goodall, Mei, &

Himmelstein, 2004). Also, the dynamic response of a vehicle is highly dependent on their input (Mei & Goodall, 2001) and therefore it is necessary to evaluate the features for fault detection and isolation on different track inputs. Furthermore, fault detection and isolation at different failure conditions will also depend on the reliability and availability of the sensors. Therefore, it is also necessary to establish that sensor failures do not compromise the effectiveness of the proposed fault detection and isolation in the presence of a faulty actuator. The assessment of the fault detection and isolation scheme with a parameter variation will be discussed in subsection 3.4.1, while the assessment of the fault detection and isolation on the different track inputs is given in section 3.4.2. Finally, the fault detection and isolation will be assessed in the event of sensor failure(s).

3.4.1 Assessment with parameter variation

The results of fault detection and isolation have so far been assessed using the nominal values of the vehicle model (with the conicity of 0.2 and creep coefficient of 10MN). However, it is necessary to evaluate the effectiveness of the proposed fault detection and isolation scheme when the dynamics of the vehicle change due to the deviation of those parameters at the wheel–rail interface. Therefore, in this study the conicity of 0.1 and 0.35 and creep coefficient of 5MN will be considered to analyse the proposed fault detection and isolation. Figure 3.27 shows the standard deviation ratio of the measurement of the relative yaw displacement of the front wheelset to its residual in the event of leading actuator with the hard failure at different conicities, where the front actuator fail-hard at a time of 2 (s) at the conicities of 0.2, 0.1 and 0.35, respectively. It clearly indicates the fault detection and isolation is still valid when the conicity is deviated from its nominal value, as the ratio of the measured signal to its residual in the event of actuator fail-hard is always below the threshold, whereas the standard deviation of the measured signal to its residual from the wheelset with the healthy actuator (rear wheelset) does not show a significant change to the normal

condition, as shown in Figure 3.28. Similar results are obtained if the rear actuator fails hard, as shown in Figures 3.29 and 3.30.

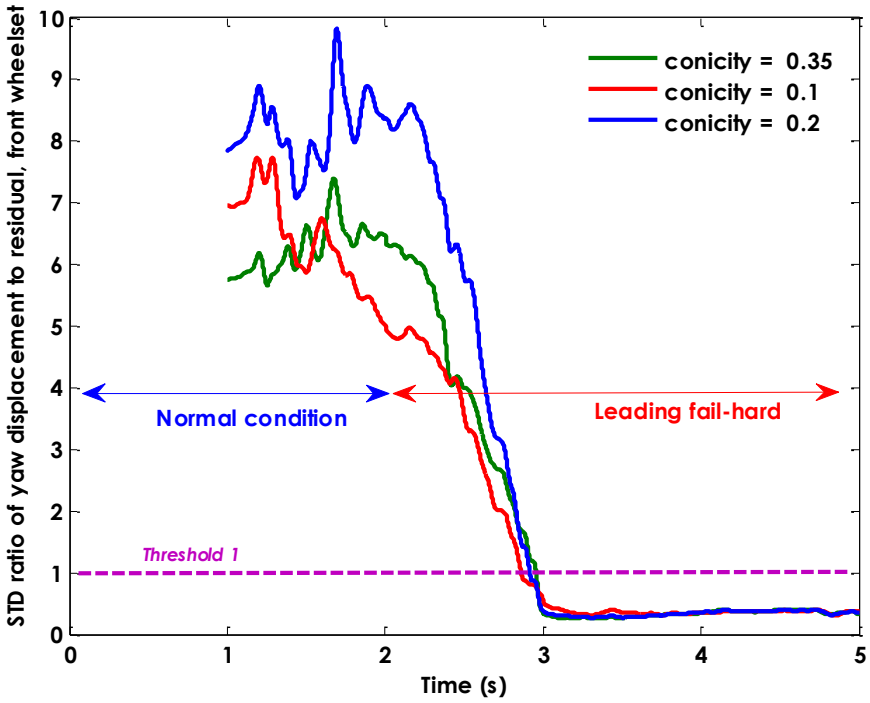

Figure 3-27: STD ratio of yaw displacement–front wheelset (front actuator fail-hard at time=2s) at different conicities

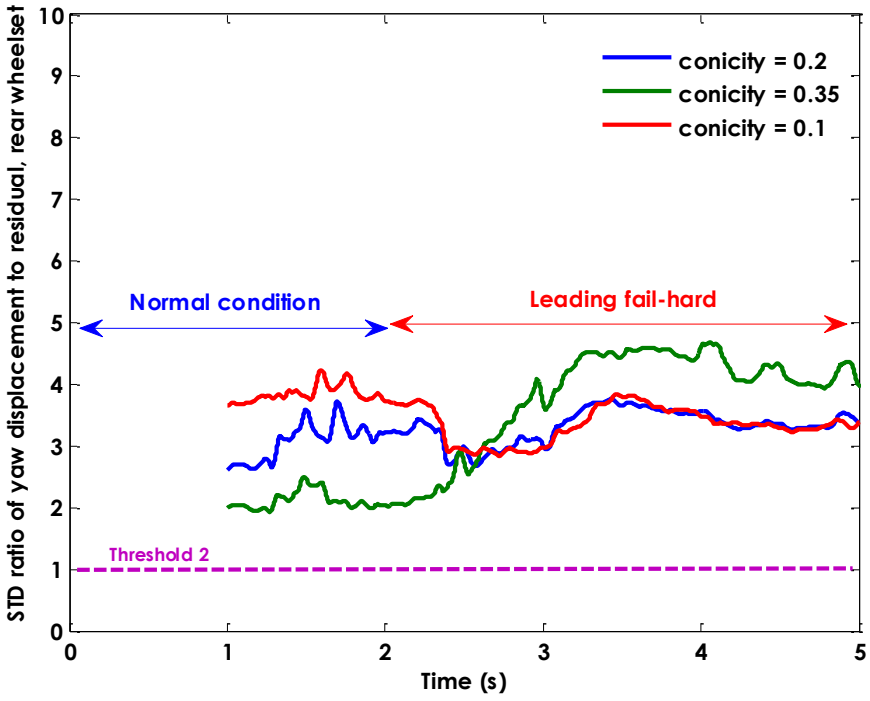

Figure 3-28: STD ratio of yaw displacement–rear wheelset (front actuator fail-hard at time=2s) at different conicities

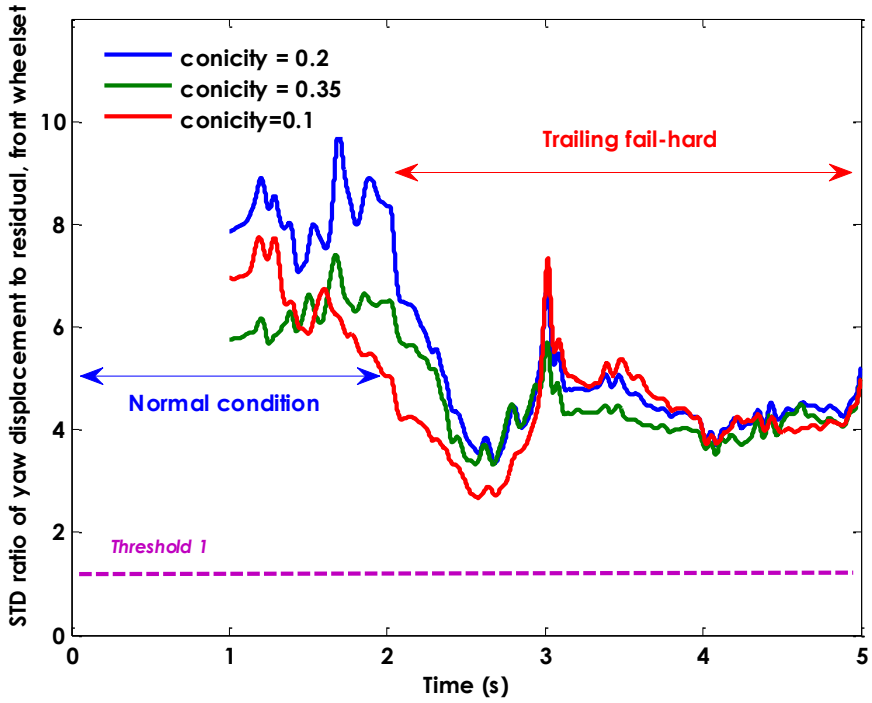

Figure 3-29: STD ratio of yaw displacement–front wheelset (rear actuator fail-hard at time=2s) at different conicities

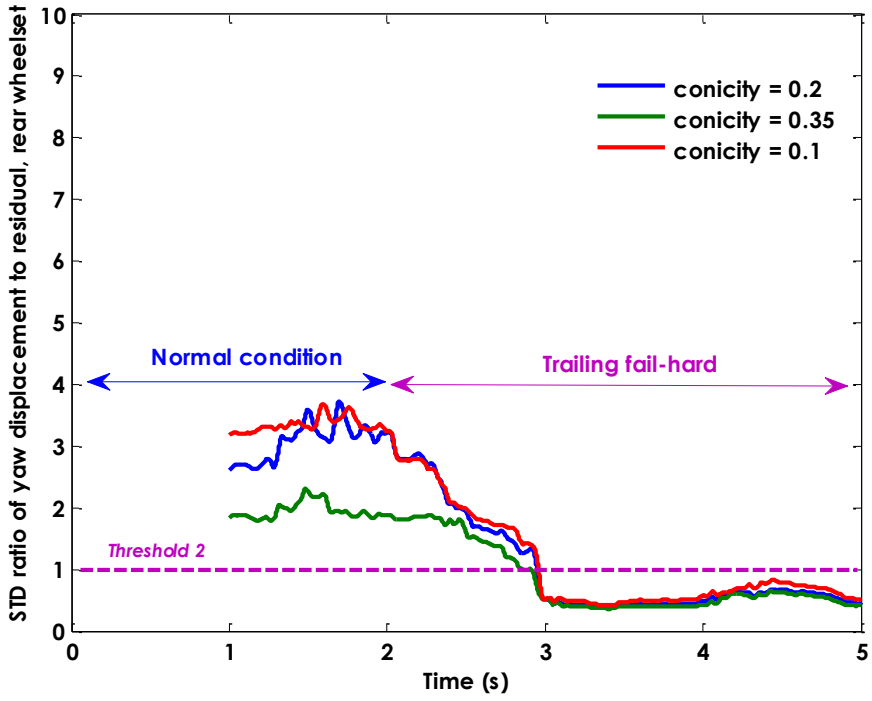

Figure 3-30: STD ratio of yaw displacement–front wheelset (front actuator fail-hard at time=2s) at different conicities

The study shows that the proposed fault detection and isolation strategy is also robust against the deviation of the creep coefficient. Figure 3.31 shows the standard deviation ratio of the

measurement of the relative yaw displacement of the leading wheelset to its residual in the event of leading actuator in the fail-hard condition at different creep coefficients, where the front actuator fail-hard at a time of 2 (s) at the creep coefficients of 10MN and 5MN, respectively. It is clear that the fault detection and isolation is again valid when the creep coefficient is changed from its nominal value, as the ratio of the measured signal to its residual in the event of actuator fail-hard is always below the threshold. In contrast, the standard deviation of the measured signal to its residual from the wheelset with the healthy actuator (rear wheelset) does not show a significant change to the normal condition, as shown in Figure 3.32. Similar results are obtained if the rear actuator fails hard.

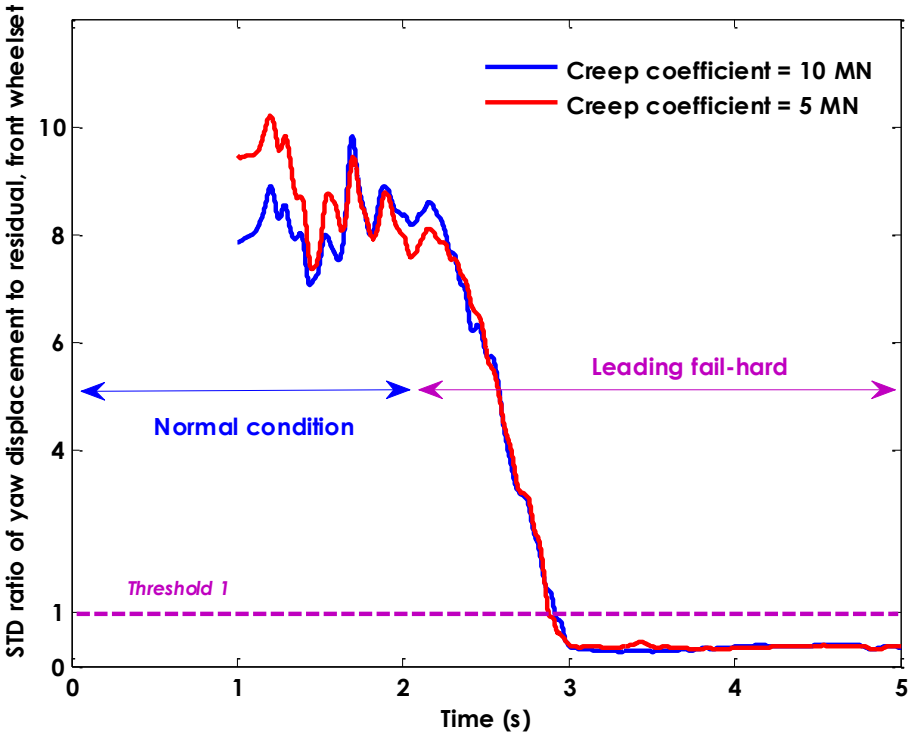

Figure 3-31: STD ratio of yaw displacement–front wheelset (front actuator fail-hard at time=2s) at different creep coefficients

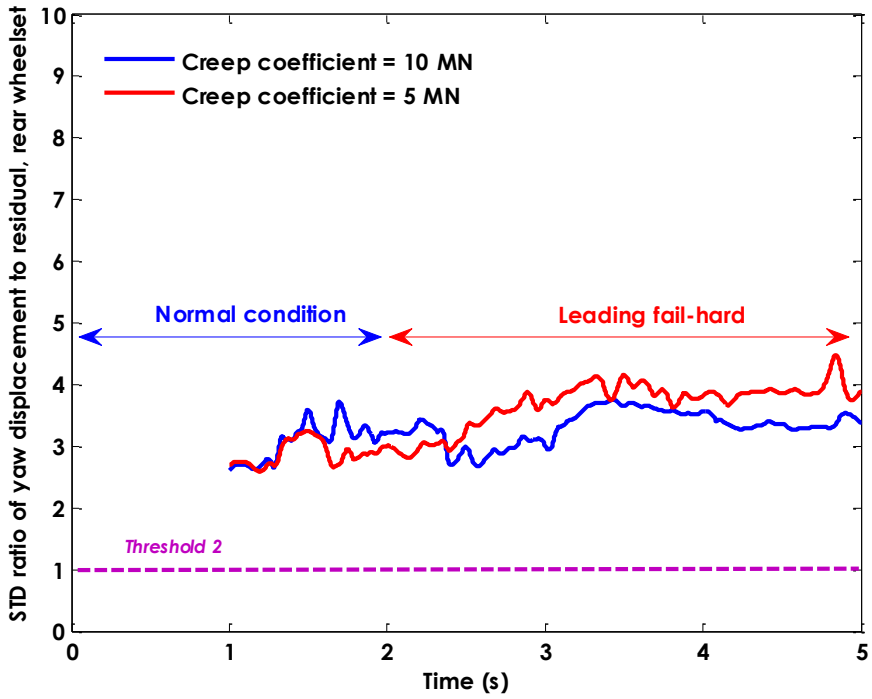

Figure 3-32: STD ratio of yaw displacement–rear wheelset (front actuator fail-hard) at different creep coefficients

The analysis of the simulation results indicates a similar level of robustness again the parameter variations in the event of actuator fail-soft (open and short circuits). Figure 3.33 and Figure 3.34 shows the standard deviation ratio of the measured lateral acceleration to its residual from the leading accelerometer on the leading wheelset when the incident of short circuit at the leading and trailing actuator occurs at time of 2(s) at different conicities respectively. Again, the standard deviation ratio is always above a threshold when the front actuator fails with short circuit (Figure 3.33) , whereas it is below the threshold in the incident of short circuit for the rear actuator (Figure 3.34). Similar results can be obtained in the incident of the open circuit.

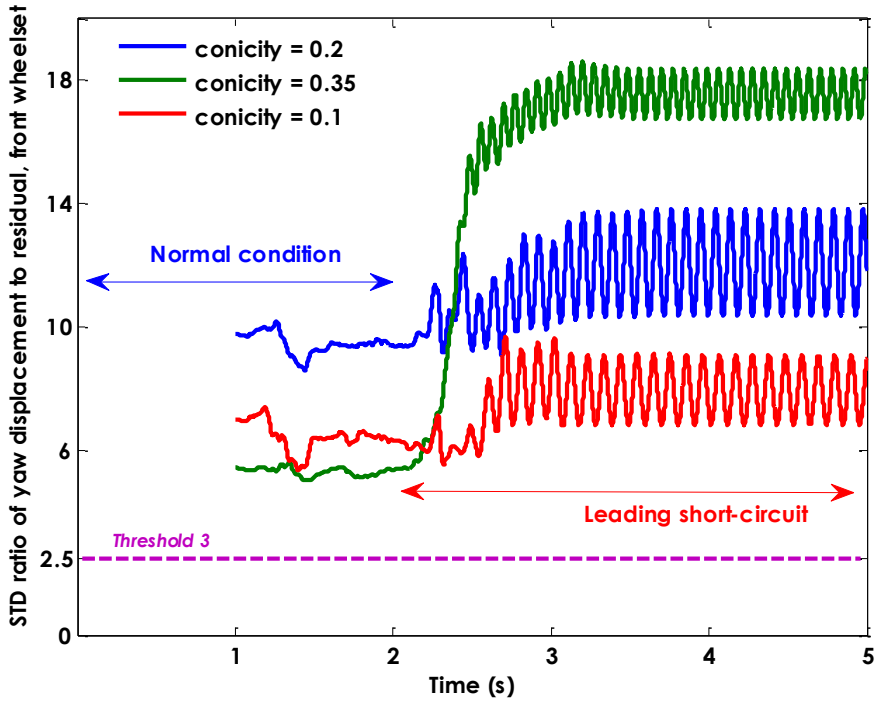

Figure 3-33: STD ratio of lateral acceleration–front wheelset (actuator open-circuit at time=2s) at different conicities

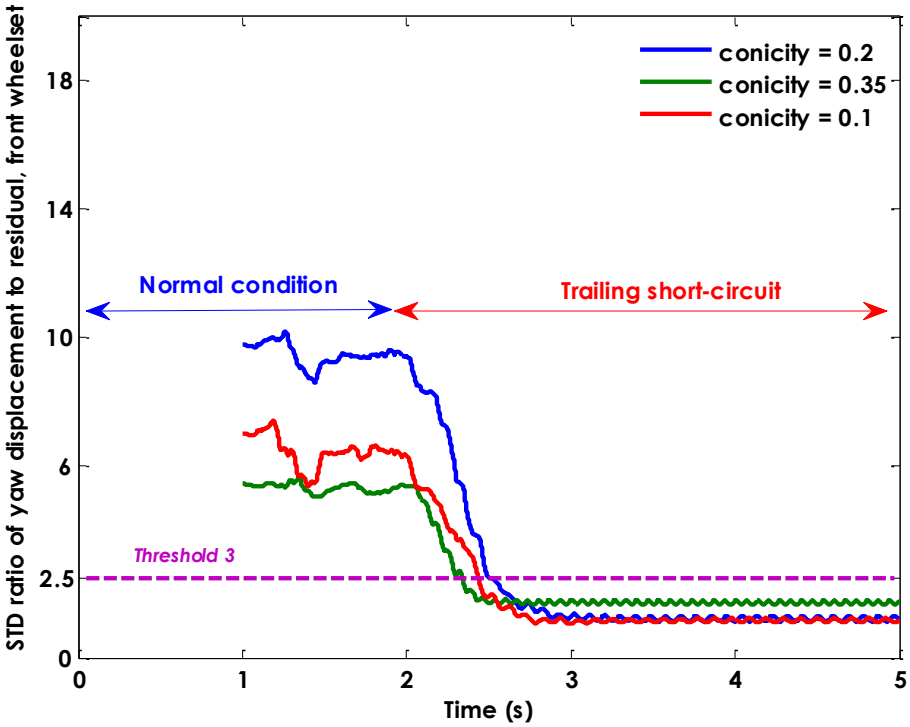

Figure 3-34: STD ratio of lateral acceleration–front wheelset (actuator short-circuit at time=2s) at different conicities

Figure 3.35 and Figure 3.36 show the standard deviation ratio of the measured lateral acceleration of the leading wheelset to its residual in the event of leading and trailing actuator with open circuit (failure occurs at a time of 2 (s)) at different creep coefficients. It clearly shows that the standard deviation ratio is always above a threshold when the front actuator fails with open circuit (Figure 3.35), whereas it is below the threshold in the incidence of open circuit for the rear actuator (Figure 3.36). Similar results can be seen in the incidence of the short circuit.

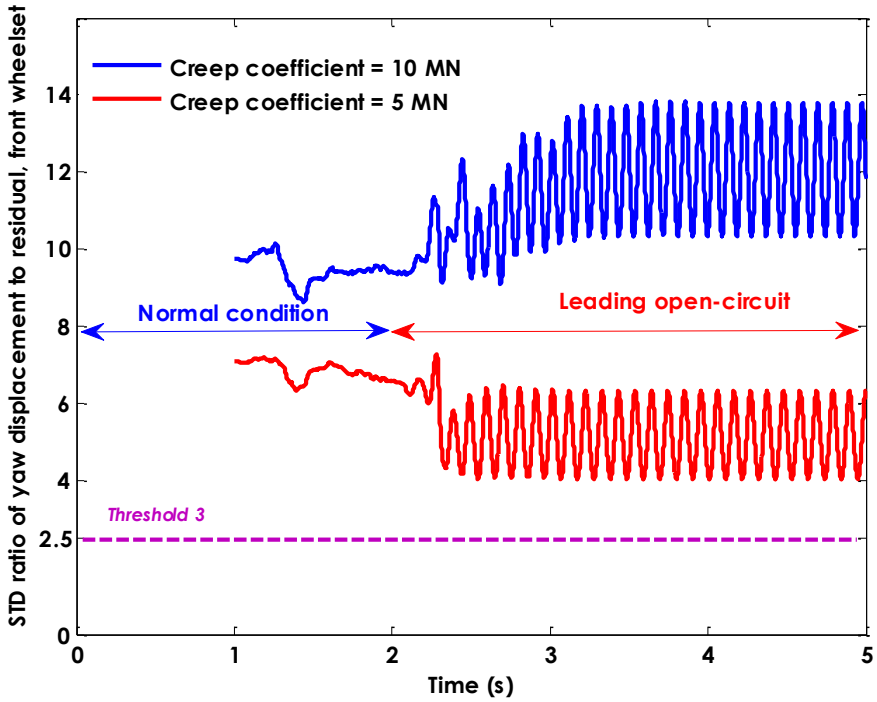

Figure 3-35: STD ratio of lateral acceleration–front wheelset (leading actuator open-circuit at time=2s) at different creep coefficient

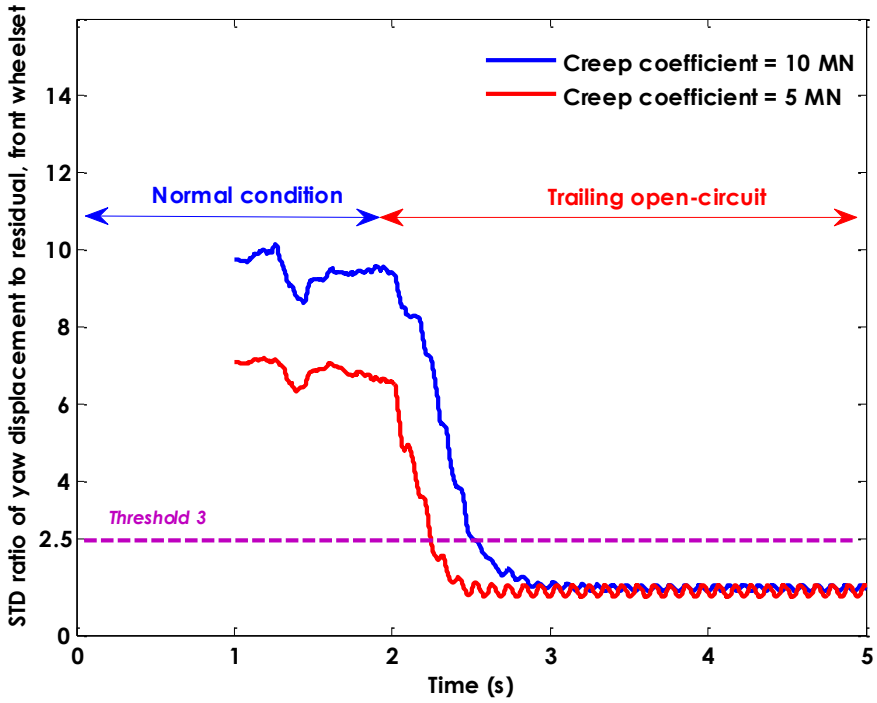

Figure 3-36: STD ratio of lateral acceleration–front wheelset (trailing actuator open-circuit at time=2s) different creep coefficient

3.4.2 Assessment with different track input

In order to assess the effectiveness of the fault detection and isolation, both deterministic and real track inputs are used in the simulation. The considered deterministic track input consists of a curve of the radius of 1250 (m) and cant angle of 6 degrees connected to a straight track via a transition of 2 (s) at the vehicle speed of 50 (m/s) (with no track irregularities). Although the measured data from a real track is less representative, nevertheless the real track data measured from a railway line between Paddington and Bristol in the U.K. are also used in the simulation, in addition to the computer generated random track input (Mei & Goodall, 2001).

The simulation results reveal that the proposed actuator fault detection and isolation is similarly effective on the real track measured data in terms of both detecting and identifying the type and location of the actuator failures. Figure 3.37 shows the standard deviation ratio of the measured relative yaw displacement from the leading wheelset to its residual when the

leading actuator fails-hard at the initial time of the simulation. In the figure, there is a clear reduction in the ratio for the immovable actuator compared to the normal condition, whereas the level of ratio remains almost identical to the normal condition for the healthy actuator at the rear wheelset, as indicated in Figure 3.38.

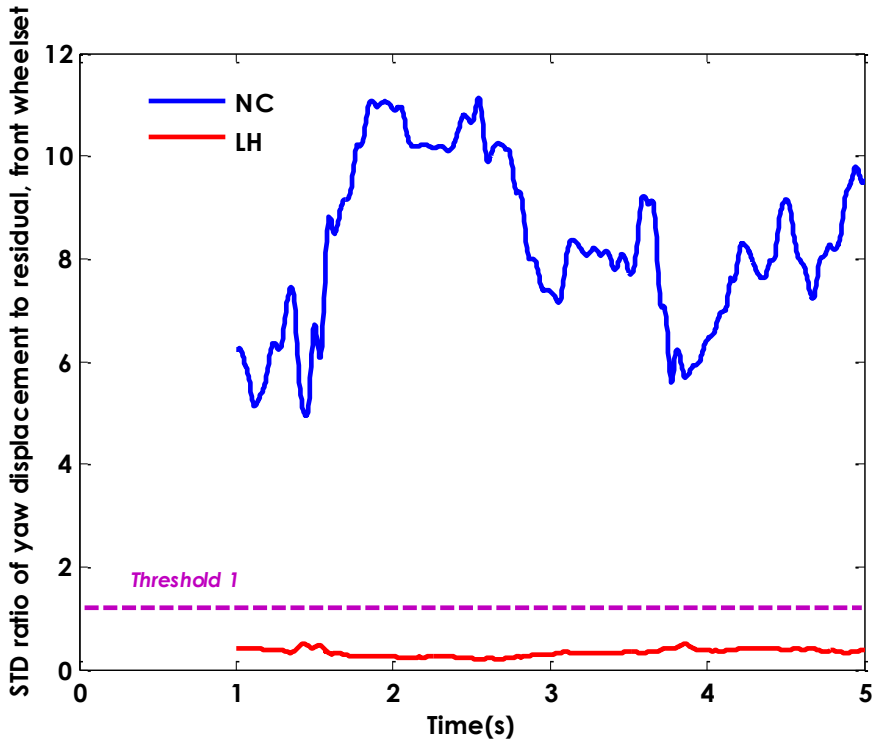

Figure 3-37: STD ratio of yaw displacement–front wheelset (front actuator fail-hard at time=0)

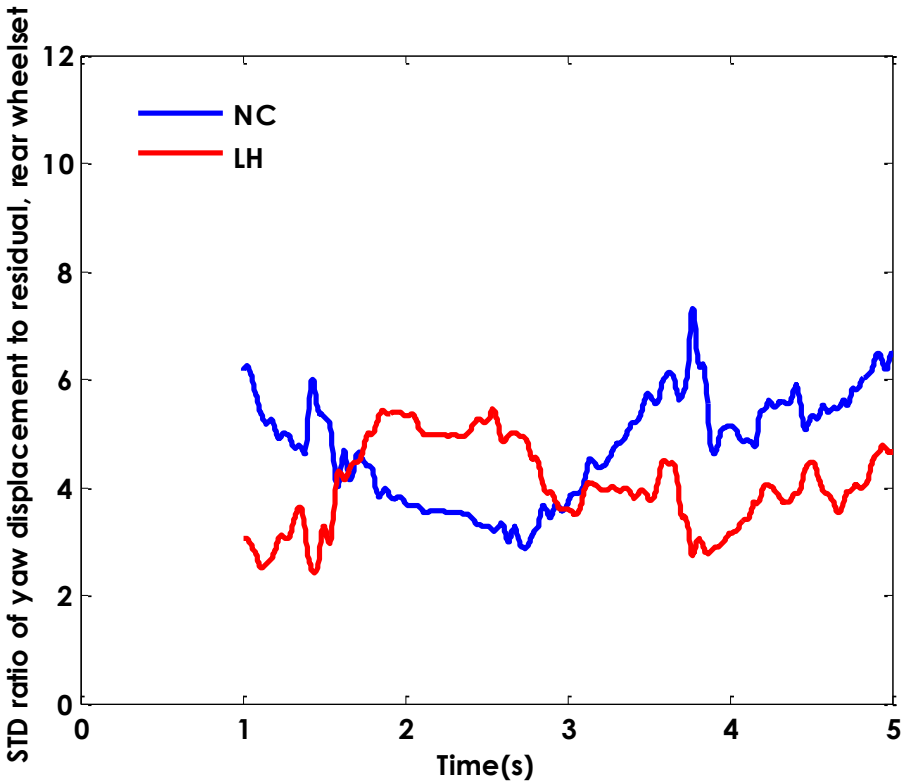

Figure 3-38: STD ratio of yaw displacement–rear wheelset (front actuator fail-hard at time=0)

For identifying which actuator fails soft, Figure 3.39 indicates the standard deviation ratio of the lateral acceleration of the leading wheelset to its residual in the incident of fail-soft. It confirms that the amount of ratio increases in the event of leading soft failure, and will decrease in the event of trailing actuator soft failure.

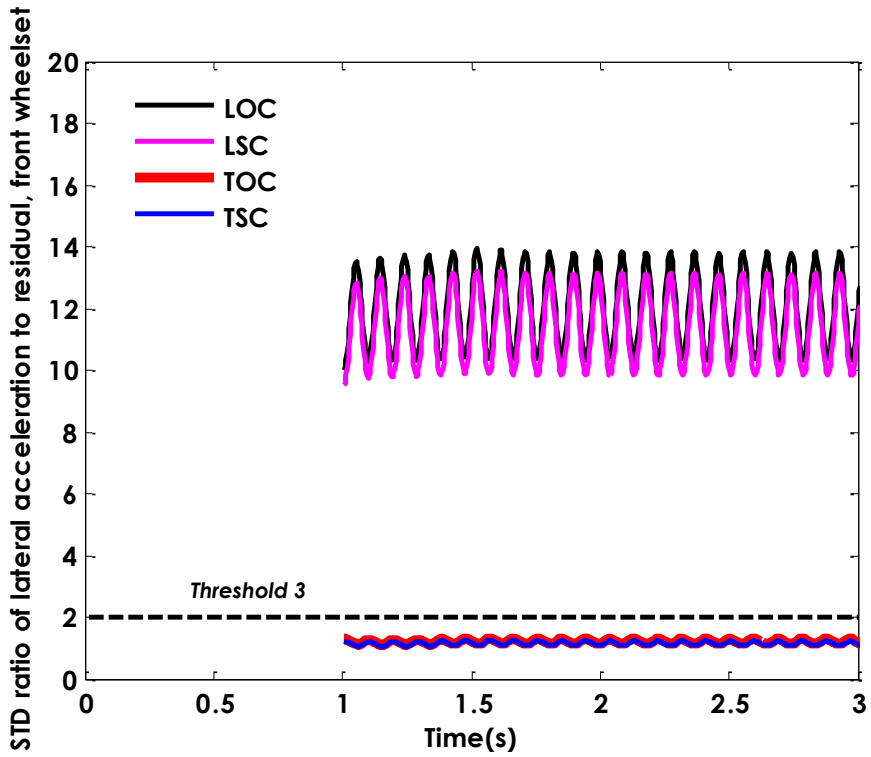

Figure 3-39: STD ratio of lateral acceleration–front wheelset (actuator fail-soft at time=0)

Furthermore, when the vehicle runs along a curved track, the proposed fault detection and isolation method is also shown to be able to identify the actuator failures. Figure 3.40 shows the standard deviation ratio of the relative yaw displacement to its residual when the leading actuator fails on the deterministic track. It clearly shows that the level of the ratio for the actuator with the hard failure is significantly reduced on the curved track compared to the vehicle with operational actuators.

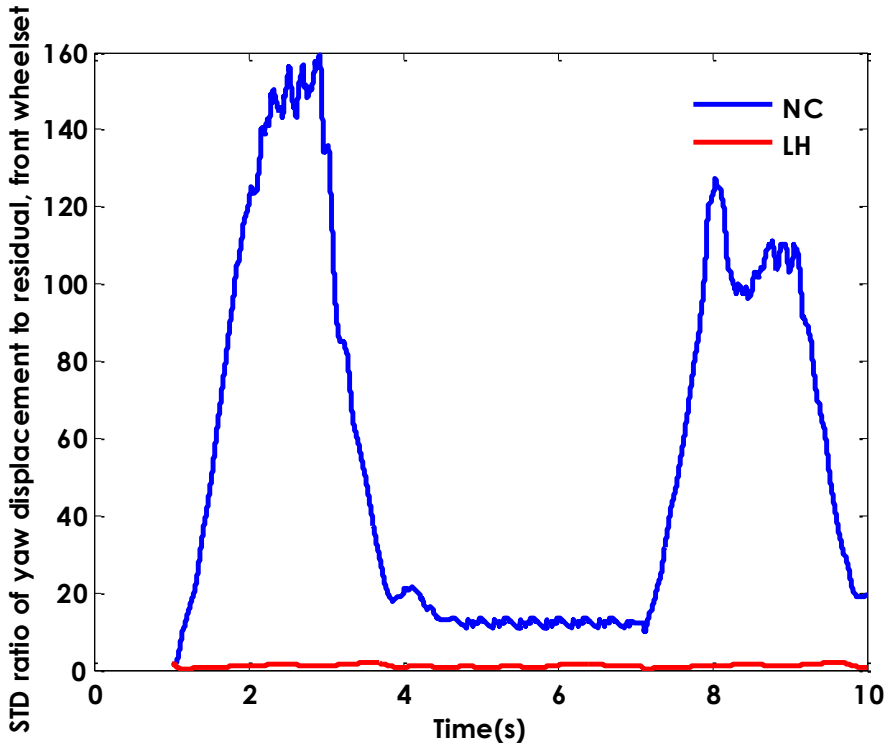

Figure 3-40: STD ratio of yaw displacement–front wheelset (front actuator fail-hard at time=0)

Figure 3.41 indicates the standard deviation ratio of the lateral acceleration of the leading wheelset to its residual in the incident of fail-soft. The obtained result on a deterministic track is almost identical compared to either the random or real track data. This can be expected due to the fact that the fail-soft failure leads to system instability – a condition where the internal dynamic properties play a far more significant role than the differences in input incitation.

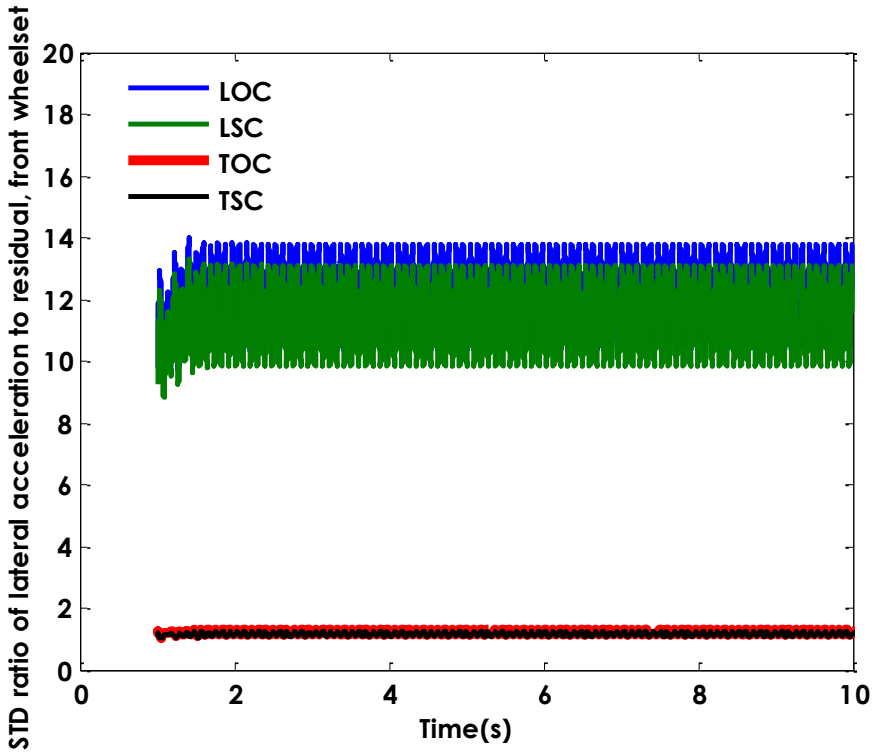

Figure 3-41: STD ratio of lateral acceleration–front wheelset (actuator fail soft at time=0)

Table 3-2 summarises the different track inputs and vehicle parameters that have been used in the simulation in order to evaluate the robustness of the proposed fault detection and isolation strategy. In the table "v" means the definition of the fault detection and isolation can provide reliable information in order to exclude the actuator malfunction among the healthy actuator without making any changes to the suggested fault detection and isolation definitions.

Table 3-2: Summarise the robustness of FDI at different track inputs and vehicle parameters; (v) means fault detection and isolation is valid

Actuator failure types	Fault detection and isolation	Robustness checks							
		Parameter variations					Track inputs		
		Creep coefficient values		Conicity values			Curved track (1250 m)	Random	Real track
		5 MN	10MN	0.1	0.2	0.35			
Leading actuator fail-hard	$(\ddot{y}_{w_1} - \hat{\ddot{y}}_{w_1})_{std} < threshold$ AND $\frac{(\Delta\psi_{w_1})_{std}}{(\Delta\psi_{w_1} - \Delta\hat{\psi}_{w_1})_{std}} < threshold1$ AND $\frac{(\Delta\psi_{w_2})_{std}}{(\Delta\psi_{w_2} - \Delta\hat{\psi}_{w_2})_{std}} > threshold2$	v	v	v	v	v	v	v	v
Trailing actuator fail-hard	$(\ddot{y}_{w_1} - \hat{\ddot{y}}_{w_1})_{std} < threshold$ AND $\frac{(\Delta\psi_{w_1})_{std}}{(\Delta\psi_{w_1} - \Delta\hat{\psi}_{w_1})_{std}} > threshold1$ AND $\frac{(\Delta\psi_{w_2})_{std}}{(\Delta\psi_{w_2} - \Delta\hat{\psi}_{w_2})_{std}} < threshold2$	v	v	v	v	v	v	v	v
Leading actuator fail-soft	$(\ddot{y}_{w_1} - \hat{\ddot{y}}_{w_1})_{std} > threshold$ AND $\frac{(\ddot{y}_{w_1})_{std}}{(\ddot{y}_{w_1} - \hat{\ddot{y}}_{w_1})_{std}} > threshold3$	v	v	v	v	v	v	v	v
Trailing actuator fail-soft	$(\ddot{y}_{w_1} - \hat{\ddot{y}}_{w_1})_{std} > threshold$ AND $\frac{(\ddot{y}_{w_1})_{std}}{(\ddot{y}_{w_1} - \hat{\ddot{y}}_{w_1})_{std}} > threshold3$	v	v	v	v	v	v	v	v

3.4.3 Sensors Failure

The failure of sensors may have different impacts on the overall system performance due to the fact that a faulty sensor gives incorrect information about the current state of the system, which could cause severe problems as it may lead to poor performance and also affect the

fault detection and isolation of the actuators (Kwan & Xu, 2004). It is therefore essential to detect sensor failures and isolate the faults from those of actuators.

The sensor faults may occur due to an abnormal change in the different parts of the sensor. Studies in (Sharma, Golubchik, & Govindan, 2010; Xu, Hines, & Uhrig, 1998) suggested the typical hardware faults that have been observed to cause sensor faults include damaged sensors, short-circuit connection, low battery and calibration errors. However, this study considers only a simple failure mode of zero output to demonstrate the possibility of detecting and isolating the sensor fault(s), as it is not the main objective of the study. In this case, the sensor under consideration will output a zero value for a large number of successive samples resulting in an increased estimation error from the Kalman Filter.

The effects of different sensor faults on the residuals are summarised in Table 3-3. The deviation is relative to the fault-free condition (normal condition) where all the sensors are functional. Although the use of residuals may detect a possible fault in one of the sensors, the table also reveals that it is difficult to use the residuals to isolate the sensor failure as the majority of the residuals increase for different sensor failures

Table 3-3: The deviation of residuals in the event of sensors failure

Sensors	Location	Symptoms							
		Residuals							
		r_1	r_2	r_3	r_4	r_5	r_6	r_7	r_8
Normal condition		0	0	0	0	0	0	0	0
Lateral accelerometer	Front wheelset	+	+	+	+	+	+	+	+
	Rear wheelset	+	+	+	+	+	+	+	+
	Bogie	+	0	+	0	+	+	+	+
Yaw accelerometer	Front wheelset	+	+	0	-	+	+	+	0
	Rear wheelset	0	+	+	+	+	+	+	0
	Bogie	+	0	+	+	+	+	+	+
Yaw displacement	Front wheelset	0	+	0	0	+	+	+	0
	Rear wheelset	0	0	0	+	+	+	0	+

Evidently, in the incident of sensor(s) failure the standard deviation ratio of the measured signal from a faulty sensor to its correspondent residual would drop to nearly zero, as the damaged sensor fails to zero value. This calculation has already been employed for the

actuator fault detection and isolation, and is extended here to detect and isolate the sensor failure of the yaw accelerometers mounted on the wheelsets, lateral and yaw accelerometers on the bogie frame without compromising actuator fault detection and identification as those sensors are not used directly for the purpose of actuator fault detection and isolation. On the other hand, the lateral accelerometer on the leading wheelset and relative yaw displacement on both the leading and trailing wheelsets are directly involved in the actuator fault detection and isolation and therefore alternative measures are needed to identify the fault(s) of those sensors.

It has been shown that in the event of actuator fail-soft (open and short circuits), the standard deviation ratio of the measurement of lateral accelerometer of the leading wheelset to its residual exceeds the threshold if the leading actuator fails, whereas it will fall below the threshold if the trailing actuator fails. Also, the level of the ratio will also fall below the threshold if the lateral accelerometer sensor fails, as shown in Figure 3.42. In the presented figure, S1 denotes the failure of the lateral accelerometer sensor on the front wheelset. It clearly shows that the ratio is at similar level in the lateral accelerometer failure and trailing actuator fail-soft.

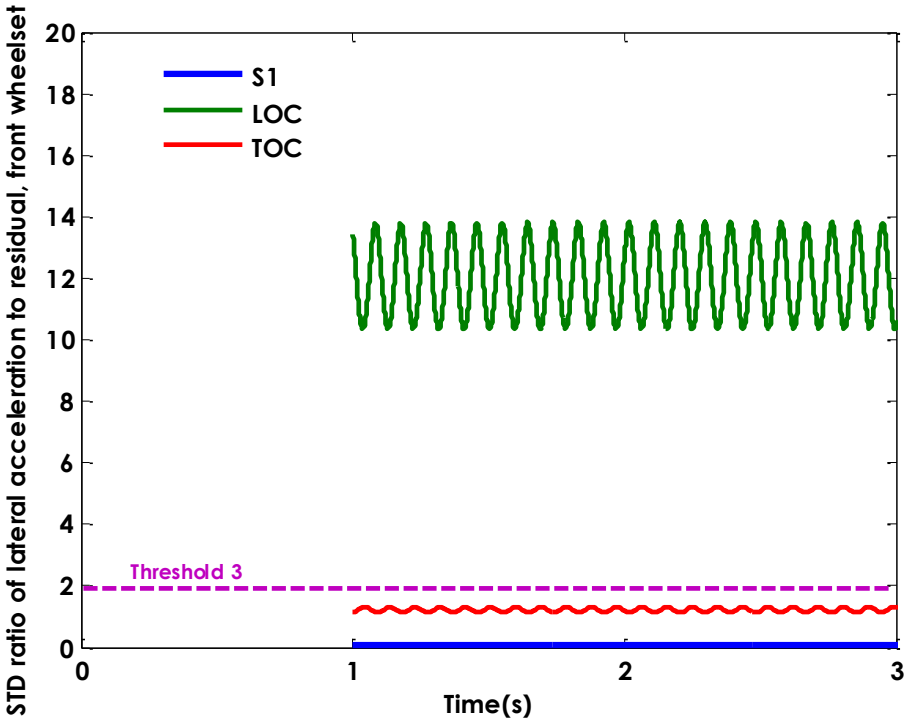

Figure 3-42: STD ratio of lateral acceleration–front wheelset (failures occur at time=0)

However, in the event of the sensor failure, the measured signal is zero (apart from sensor noises) and the estimated signal from the observer is not zero, as shown in Figure 3.43. Therefore, the difference between the measured signal and the estimated signal always tends to be negative (Figure 3.44). On the other hand, it has been highlighted that in the event of the trailing actuator fail-soft, the measured acceleration of the leading wheelset changes slower than its corresponding estimation data and consequently the difference between the measured signal and the estimated signal is expected to be positive in the incident of the trailing actuator failing soft (Figure 3.45). Therefore, in order to avoid the conflict between the actuator fail-soft and the failure of the lateral accelerometer on the wheelsets, the difference between the standard deviation of the lateral acceleration measurement and the standard deviation of the estimated wheelset lateral acceleration are included to enable the isolation of sensor and actuator faults, as expressed in Equations (3.6) and (3.7).

Trailing actuator fail-soft:

$$\left(\ddot{y}_{w_1}\right)_{std} - \left(\hat{\ddot{y}}_{w_1}\right)_{std} > 0 \qquad \textbf{Eq. 3-6}$$

Lateral accelerometer sensor failure:

$$\left(\ddot{y}_{w_1}\right)_{std} - \left(\hat{\ddot{y}}_{w_1}\right)_{std} < 0 \qquad \textbf{Eq. 3-7}$$

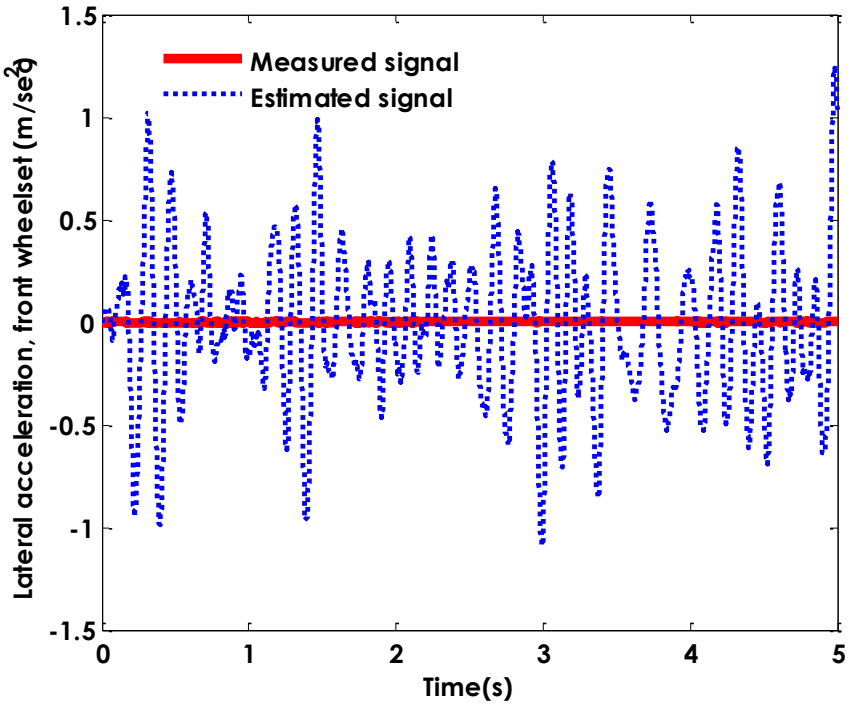

Figure 3-43: Measured and estimated lateral acceleration–front wheelset (front lateral accelerometer fails at time=0)

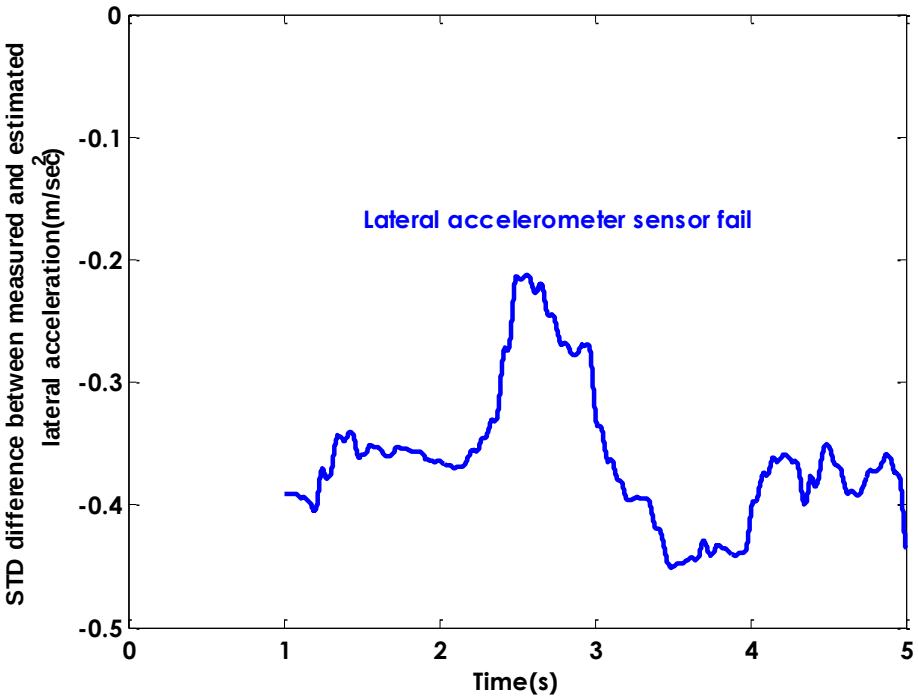

Figure 3-44: STD difference between the measured and estimated lateral acceleration–sensor failure at time=0

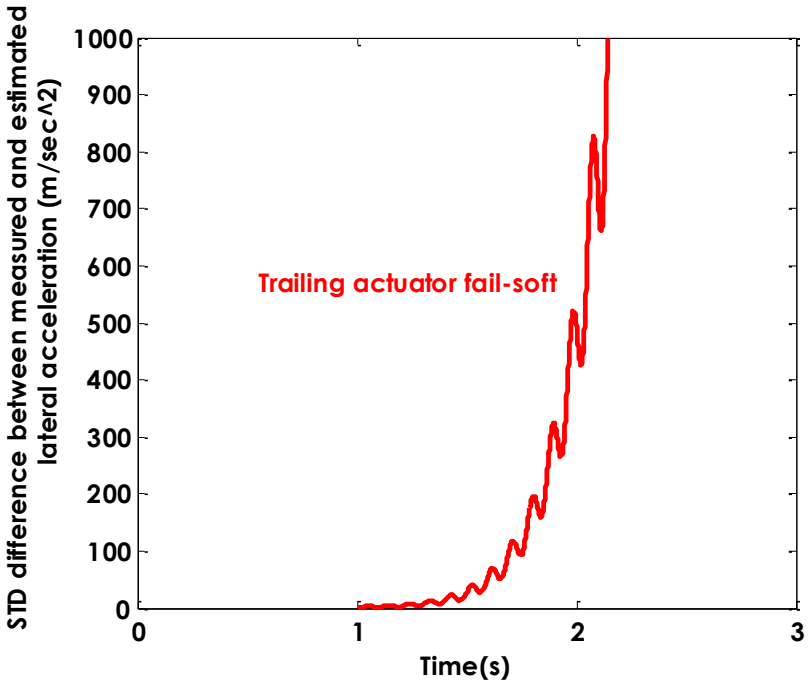

Figure 3-45: STD difference between the measured and estimated lateral acceleration–trailing actuator (fail-soft at time=0)

Similarly, other measures (in addition to the standard deviation ratio of the relative yaw displacement to its residual) are needed to separate the actuator fail-hard and the failure of the relative yaw displacement sensors, as shown in Figure 3.46, where S7 indicates the failure of the relative yaw displacement sensor on the front wheelset. A similar result will be obtained if the yaw displacement sensor failure and actuator fail-hard present at the trailing wheelset, as given in Figure 3.47, where S8 indicates the failure of the yaw displacement.

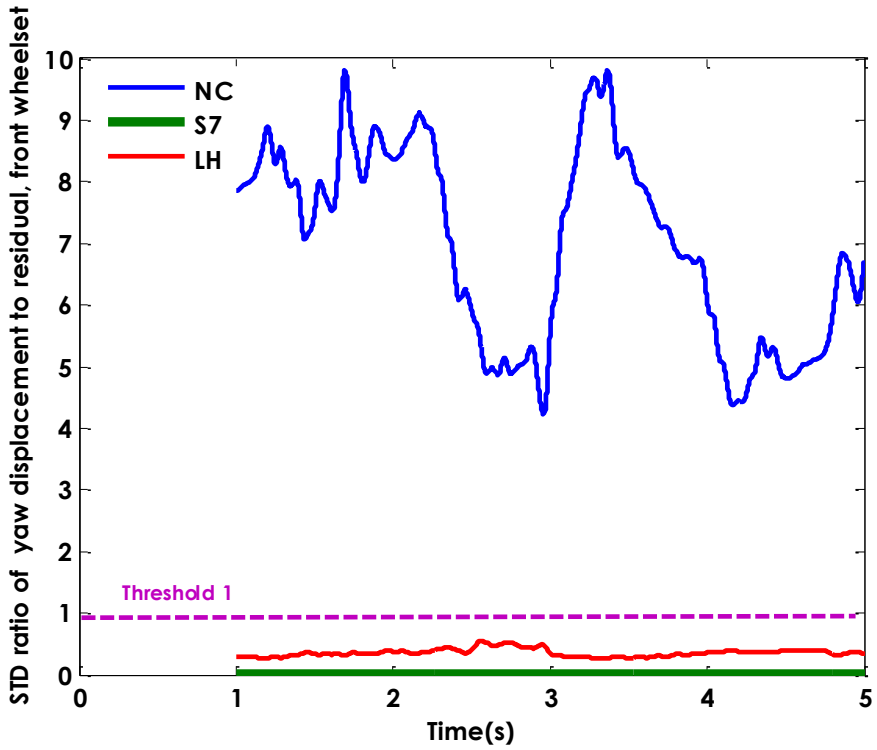

Figure 3-46: STD ratio of the yaw displacement–front wheelset, fails at time=0

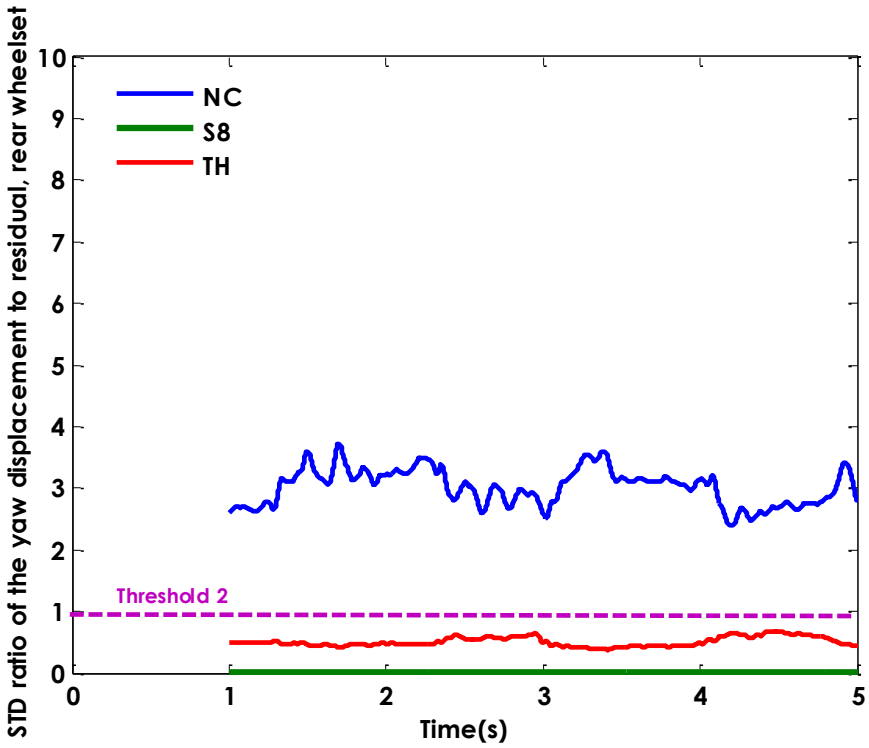

Figure 3-47: STD ratio of the yaw displacement–rear wheelset fails at time=0

However, this study shows that the generated residuals are significantly increased in the event of sensor failure compared to the normal condition or actuator fail-hard. Therefore, the use of the residual as an additional feature can overcome the apparent conflict between fault detection and isolation of the actuator fail-hard and the failure of the relative yaw displacement sensors. Figures 3.48 and Figure 3.49 show the standard deviation of the generated residual from the relative yaw displacement in the event of sensor and actuator fail-hard conditions. They clearly indicate that the generated residual in the event of sensor failure significantly increases compared to the actuator fail-hard and normal conditions. Therefore, the failure of the relative yaw displacement's sensor can be isolated from the actuator fail-hard through an evaluation of its residual.

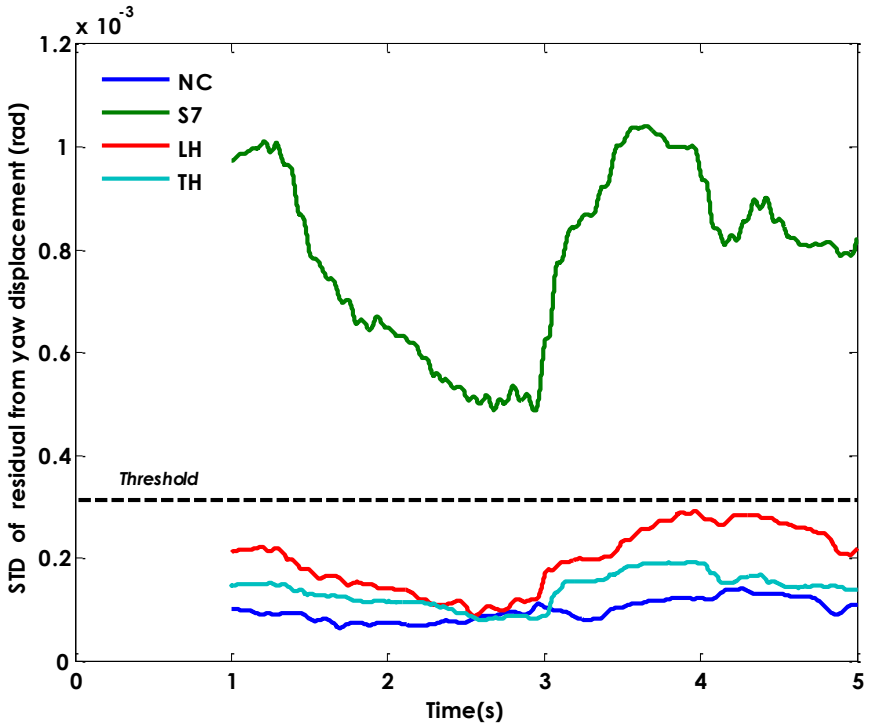

Figure 3-48: STD of residual from yaw displacement–front wheelset (faults occur at time = 0)

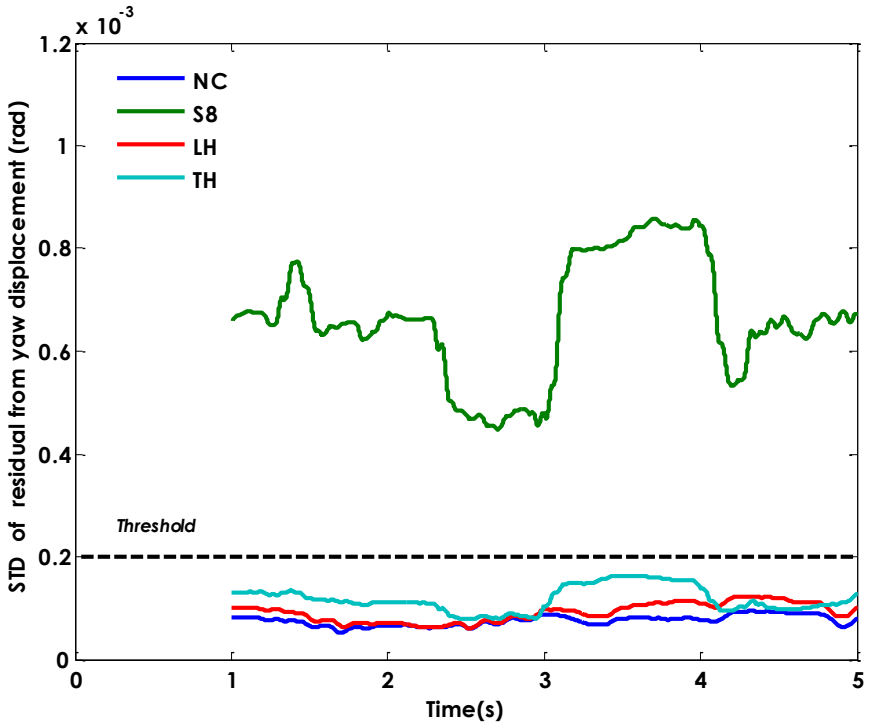

Figure 3-49: STD of residual from yaw displacement–rear wheelset (faults occur time=0)

Table 3.4 summarises the proposed strategy for fault detection and isolation in the event of actuator and sensor failures.

Table 3-4: Strategy for fault detection and isolation in the event of the actuator and sensor failures

Mode types			**Fault detection and defection**
Normal condition			$(\ddot{y}_{w_1} - \hat{\ddot{y}}_{w_1})_{std} < threshold$ AND $\frac{(\Delta\psi_{w_1})_{std}}{(\Delta\psi_{w_1} - \Delta\hat{\psi}_{w_1})_{std}} < threshold_1$ AND $\frac{(\Delta\psi_{w_2})_{std}}{(\Delta\psi_{w_2} - \Delta\hat{\psi}_{w_2})_{std}} < threshold_2$
Actuator failures	Fail-hard	**Front actuator**	$(\ddot{y}_{w_1} - \hat{\ddot{y}}_{w_1})_{std} < threshold$ AND $\frac{(\Delta\psi_{w_1})_{std}}{(\Delta\psi_{w_1} - \Delta\hat{\psi}_{w_1})_{std}} < threshold_1$ AND $\frac{(\Delta\psi_{w_2})_{std}}{(\Delta\psi_{w_2} - \Delta\hat{\psi}_{w_2})_{std}} > threshold_2$
		Rear actuator	$(\ddot{y}_{w_1} - \hat{\ddot{y}}_{w_1})_{std} < threshold$ AND $\frac{(\Delta\psi_{w_1})_{std}}{(\Delta\psi_{w_1} - \Delta\hat{\psi}_{w_1})_{std}} > threshold_1$ AND $\frac{(\Delta\psi_{w_2})_{std}}{(\Delta\psi_{w_2} - \Delta\hat{\psi}_{w_2})_{std}} < threshold_2$
	Fail-soft	**Front actuator**	$(\ddot{y}_{w_1} - \hat{\ddot{y}}_{w_1})_{std} > threshold$ AND $\frac{(\ddot{y}_{w_1})_{std}}{(\ddot{y}_{w_1} - \hat{\ddot{y}}_{w_1})_{std}} > threshold_3$
		Rear actuator	$(\ddot{y}_{w_1} - \hat{\ddot{y}}_{w_1})_{std} > threshold$ AND $\frac{(\ddot{y}_{w_1})_{std}}{(\ddot{y}_{w_1} - \hat{\ddot{y}}_{w_1})_{std}} > threshold_3$
Sensor failures	Leading lateral accelerometer		$\frac{(\ddot{y}_{w_1})_{std}}{(\ddot{y}_{w_1} - \hat{\ddot{y}}_{w_1})_{std}} < threshold_3$ AND $(\ddot{y}_{w_1})_{std} - (\hat{\ddot{y}}_{w_1})_{std}$
	Leading yaw accelerometer		$\frac{(\ddot{\psi}_{w_1})_{std}}{(\ddot{\psi}_{w_1} - \hat{\ddot{\psi}}_{w_1})_{std}} < threshold_4$

	Trailing lateral accelerometer	$\frac{(\ddot{y}_{w_2})_{std}}{(\ddot{y}_{w_2} - \hat{\ddot{y}}_{w_2})_{std}} > threshold_5$ AND $\left(\ddot{y}_{w_2}\right)_{std} - \left(\hat{\ddot{y}}_{w_2}\right)_{std} < 0$
	Trailing yaw accelerometer	$\frac{(\ddot{\psi}_{w_2})_{std}}{(\ddot{\psi}_{w_2} - \hat{\ddot{\psi}}_{w_2})_{std}} < threshold_6$
	Bogie lateral accelerometer	$\frac{(\ddot{y}_{w_g})_{std}}{(\ddot{y}_{w_g} - \hat{\ddot{y}}_{w_g})_{std}} > threshold_7$
	Bogie yaw accelerometer	$\frac{(\ddot{\psi}_{w_8})_{std}}{(\ddot{\psi}_{w_8} - \hat{\ddot{\psi}}_{w_8})_{std}} < threshold_8$
	Leading relative yaw displacement	$(\ddot{y}_{w_1} - \hat{\ddot{y}}_{w_1})_{std} < threshold$ AND $\frac{(\Delta\psi_{w_1})_{std}}{(\Delta\psi_{w_1} - \Delta\hat{\psi}_{w_1})_{std}} < threshold_1$ AND $\frac{(\Delta\psi_{w_2})_{std}}{(\Delta\psi_{w_2} - \Delta\hat{\psi}_{w_2})_{std}} > threshold_2$
	Trailing relative yaw displacement	$(\ddot{y}_{w_1} - \hat{\ddot{y}}_{w_1})_{std} < threshold$ AND $\frac{(\Delta\psi_{w_1})_{std}}{(\Delta\psi_{w_1} - \Delta\hat{\psi}_{w_1})_{std}} > threshold_1$ AND $\frac{(\Delta\psi_{w_2})_{std}}{(\Delta\psi_{w_2} - \Delta\hat{\psi}_{w_2})_{std}} < threshold_2$

3.5 Summary

This chapter presents a fault detection and isolation strategy for actively controlled railway vehicles for actuator failures as well as some cases of sensor faults. In this methodology, a vehicle-based approach through the use of a state estimator has been developed to identify the actuator failure by evaluating the residuals in the time domain. It has been proposed that the actuator in a hard mode can be isolated through evaluating the standard deviation ratio of measurement of the relative yaw displacement to their residuals. The actuator with the soft failure (open and short circuits) can be diagnosed by computing the standard deviation ratio of the measurement of the lateral accelerometer of the front wheelset to its residual. The proposed features for the actuator fault detection and isolation have been assessed in the

presence of parameter variations at the wheel–rail interface and different track inputs. It has been shown that the features for the actuator fault detection and isolation can provide robust information in order to diagnose the actuator failure. One of the critical design aspects is that the features for fault detection rely on the reliability of the sensors; therefore, the effectiveness of the actuator fault detection and isolation in the incident of the sensor failure has also been thoroughly studied. It has been shown that the failure of the wheelset yaw accelerometers, the wheelset leading lateral accelerometer, and mounted sensors on the bogie frame can be readily identified through evaluation of the residuals and standard deviation ratio of the measurement of that sensor failure to its residual, due to the fact that those measurement signals have not been used for the actuator fault detection and isolation. It has been demonstrated that there is a conflict between lateral accelerometer failure and trailing actuator fail-soft, as the amount of ratio for both events is below the threshold. In order to overcome the conflict between the actuator fail-soft and the lateral accelerometer sensor failure on the wheelsets, the difference between the standard deviation of lateral acceleration measurement and the standard deviation of the estimated wheelset lateral acceleration are included to remove such disagreement. Furthermore, the standard deviation ratio of the yaw displacement to its residual will be significantly reduced in the incident of actuator fail-hard and sensor failure of the yaw displacement. This study showed that the generated residuals significantly magnified in the event of yaw displacement failure compared to the normal condition and actuator fail-hard. Therefore, the use of residual as an additional feature can overcome the conflict between fault detection and isolation of the actuator fail-hard and the failure of the yaw displacement sensors.

Chapter 4 FAULT DETECTION AND ISOLATION (APPROACH 2)

4.1 Introduction

It has been shown in chapter 3 that the detection and isolation of actuator failure(s) can be achieved through the use of a vehicle-model based approach. The drawback is that this strategy will be reliant on the high order of the vehicle model, which can be problematic for practical implementation due to the increased complexity and the scheme is more dependent on the dynamic behaviour of the vehicle rather than that of the actuator itself.

This chapter aims to provide an alternative fault detection and isolation strategy by introducing an actuator model-based approach that detects actuator fault(s) from changes in actuator dynamics, where sensor fault(s) are also considered as the reliability of the FDI scheme is highly reliant on the information provided by the sensors. This approach will be based on the use of a Local Kalman Filter (LKF) for each of the two actuators for the fault detection and isolation for the actuators and sensors (Mirzapour & Mei, 2014). Figure 4.1 illustrates the overall fault detection and isolation strategy for the active wheelset control system. The output measurements from sensors of each actuator are fed to a local Kalman Filter (LKF) that generates individual residuals which are then analysed in order to provide information for monitoring the status of the actuator as well as that of the sensors.

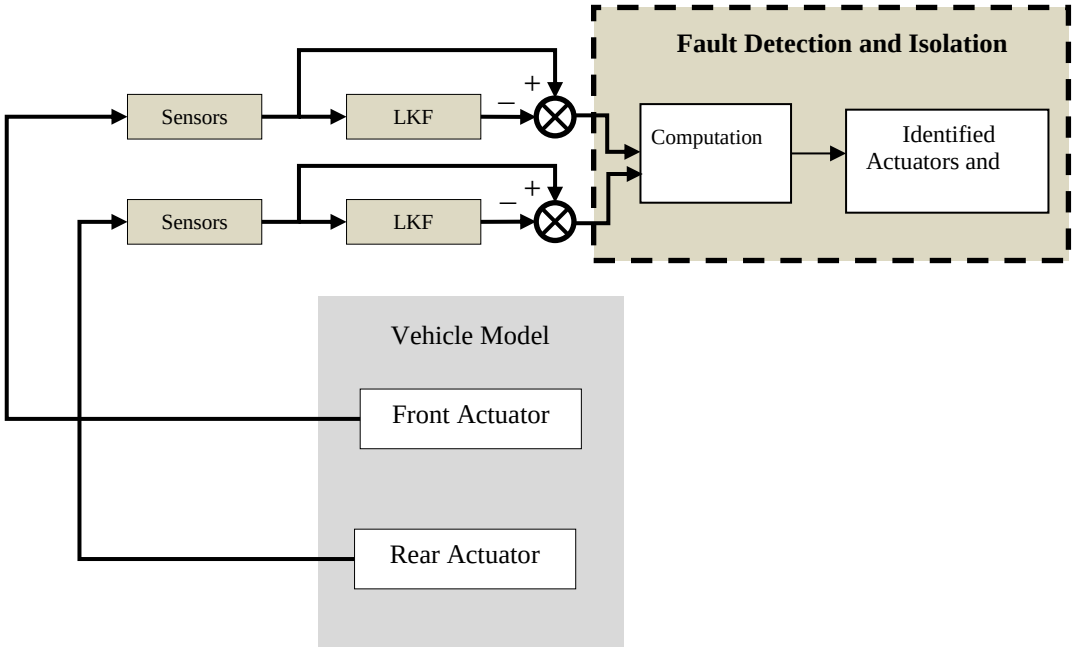

Figure 4-1: Overall fault detection and isolation strategy (Approach 2)

This chapter is organised as follows. Section 4.1 presents the formulation and basic design of the actuator model-based approach for the proposed fault detection and isolation scheme. Section 4.2 establishes a fault detection and isolation methodology for both actuator and sensor malfunctions, Details to extract the features for fault detection and isolation are provided in section 4.3. Section 4.4 assesses the robustness of the proposed FDI on different track inputs. Finally, a summary will be provided.

4.2 Local Kalman Filter Design for Actuators

Although the detection and isolation of actuator malfunctions may be realised directly by using sensor measurement signals from the actuators, additional safeguards would be needed if sensor failures are also considered. Therefore, the actuator model-based approach is developed through the use of a Local Kalman Filter (LKF) as the actuator dynamics are well known. The generated errors between estimated data and measured data will be used to detect

and isolate both actuator and sensor failure(s). The term of 'local' is used as the employed Kalman-Bucy Filter only represents the dynamics of each actuator at the local level. Equation (4.1) defines a state–space representation of the actuator model (from the actuator dynamics in chapter 2) for each wheelset for the LKF design, where x_{ac} is a vector of state variables; u_{ac} is the actuator's control input vector. The output torque of the actuator and the motor voltage are considered as control inputs to the Kalman filter and they can be readily made available from the sensor measurement and the local torque controller respectively.

$$\dot{x}_{ac} = A_{ac}.x_{ac} + B_{ac}.u_{ac} + G_{ac}.w_{ac}; \qquad \textbf{Eq. 4-1}$$

Where;

$$A_{ac} = \begin{bmatrix} \frac{-C_m}{I_m} & \frac{K_t}{I_m} & \frac{1}{I_m} \\ \frac{-K_b}{L_a} & \frac{-R_a}{L_a} & 0 \\ 0 & 0 & 10^{-3} \end{bmatrix};$$

$$B_{ac} = \begin{bmatrix} 0 & \frac{1}{L_a} & 0 \end{bmatrix}^T;$$

$$G_{ac} = \begin{bmatrix} 0 & 0 & 1 \end{bmatrix}^T;$$

$$x_{ac} = \begin{bmatrix} \dot{\theta}_m & i_a & \tau_g \end{bmatrix}^T;$$

$$u_{ac} = V_a;$$

$$w_{ac} = \tau_g;$$

In the equation, the state-space representation of the actuator is re-formulated to include the output torque (τ_g) as one of the state variables so that the effect of the vehicle dynamics on the actuator behaviours can be taken into account without the need to include the more complex models. In the design, a small value of 10^{-3} is used in the state matrix for the torque

variable (τ_g) in order to have a full rank of matrix A_{ac} and the derivative of ($\dot{\tau}_g$) is treated as a source of random disturbance – both are technical measures in the model based design approaches. Each actuator is equipped with three sensors for the measurement of the actuator speed (motor rotational velocity), the motor current and the output torque to be applied to the wheelsets from the actuator gearbox (Mirzapour & Mei, 2014). The output equation for the measurements is given in Equation (4.2). The measurement noises (v_{ac}) are set to 2% of their maximum absolute values of the corresponding sensors, which are considered typical for the sensors of this kind.

$$y_{ac} = C_{ac} x_{ac} + H_{ac} v_{ac} \quad \textbf{Eq. 4-2}$$

Where;

$$y_{ac} = \begin{bmatrix} \dot{\theta}_m & i_a & \tau_g \end{bmatrix}^T;$$

$$C_{ac} = \begin{bmatrix} 1 & 0 & 0 \\ 0 & 1 & 0 \\ 0 & 0 & 1 \end{bmatrix};$$

The state-space representation of the actuator in Equation (4.1) and (4.2) enable the necessary matrices and vectors to determine the gain for the local Kalman Filter as given in Equation (4.3). However, in order to obtain the Kalman gain the states from the Riccati equation as given in Equation (4.3) should be calculated at the first step (Maybeck, 1979).

$$K_{ac} = P_{ac} C_{ac}^{\ T} R_{ac}^{\ -1} \quad \textbf{Eq. 4-3}$$

$$\dot{P}_{ac}(t) = A_{ac} P_{ac}(t) + P_{ac}(t) A_{ac}^{\ T} - K_{ac} . C_{ac} . P_{ac}(t) + Q_{ac} \quad \textbf{Eq. 4-4}$$

where K_{ac} is the Kalman gain and P_{ac} the covariance matrix. By tuning the covariance matrices for the process noise Q_{ac} and measurement noise R_{ac}, the above Riccati equation can provide the desired tracking performance and robustness of the LKF in both the normal conditions and in the event of either actuator or sensor failures. The measurement noise

matrix (R_{ac}) for each actuator can be calculated from measurement noise (v_{ac}) as given in Equation (4.5).

$$R_{ac} = \sum_{i=1}^{n} \frac{(v_{ac_i} . v^T{}_{ac_i})}{n} \quad \textbf{Eq. 4-5}$$

Where
n = 3; due to the number of sensors for each actuator

However, the process noise covariance has been tuned manually and a value of 7.4×10^3 for the process noise is found to deliver a desirable performance. The calculated covariance matrix (P_{ac}) and the Kalman gain (K_{ac}) generate the state estimate as given in Equation (4.6).

$$\dot{\hat{x}}_{ac} = A_{ac}\hat{x}_{ac} + B_{ac}u_{ac} + K_{ac}(y_{ac} - C_{ac}.\hat{x}_{ac} - D_{ac}.u_{ac}) \quad \textbf{Eq. 4-6}$$

For example, Figure 4.2 gives the measured and estimated motor rotational velocity of the front actuator in the normal no fault condition, where the estimation error is also shown - a close match between the measurement and estimation is self-evident. The generated residuals (estimated errors) of the LKF are then used to detect actuator and sensor faults (Mirzapour & Mei, 2014) as described in the next section

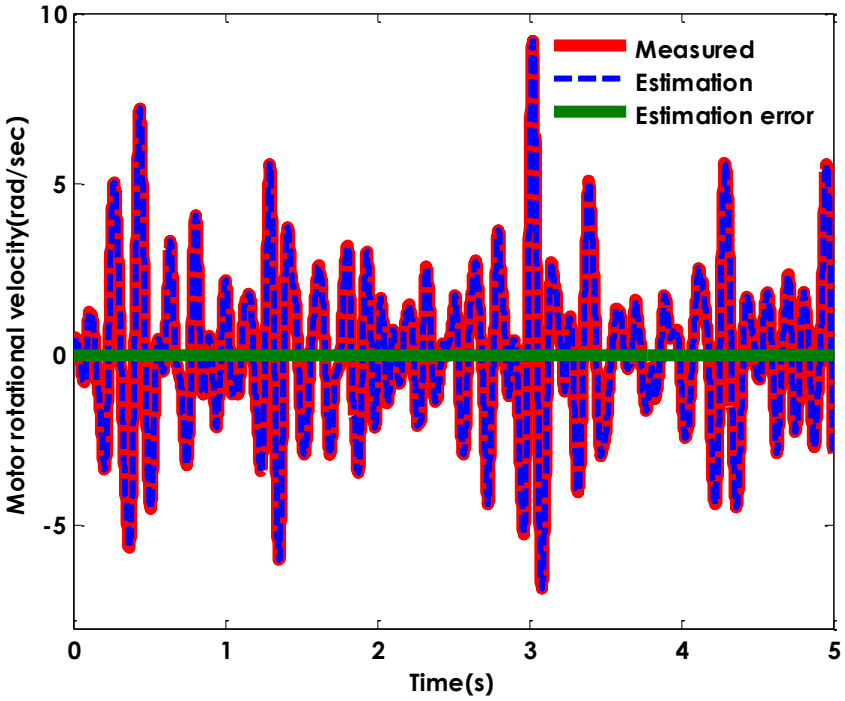

Figure 4-2: Motor rotational velocity under normal condition

4.3 Fault Detection and Isolation for Actuators and Sensors

Different failure modes of the actuators (i.e. fail-hard and fail-soft) and the sensor faults can be detected and isolated by evaluating the estimation errors generated by the local Kalman filter(s).

4.3.1 Actuator fail-hard

In the incident of actuator fail-hard, the rate of change of the motor rotation displacement of the actuator is reduced to zero and the relative movement between the wheelset and the bogie frame would be severely restricted – the latter is only possible due to elasticity in the connections (Mirzapour & Mei, 2014). On the other hand, the actuator dynamics in the normal condition is used in the design of the local Kalman filter and therefore differences between the measurements and the estimations will be expected.

From figure 4.3, it is apparent that the motor current in the event of fail-hard significantly increases compared to the normal condition where the fault occurs at a time of 2 (s). This is

because the wheelset control associated with the faulty actuator is demanding more torque as a consequence of the lack of controlled motion or controlled torque output at the wheelset.

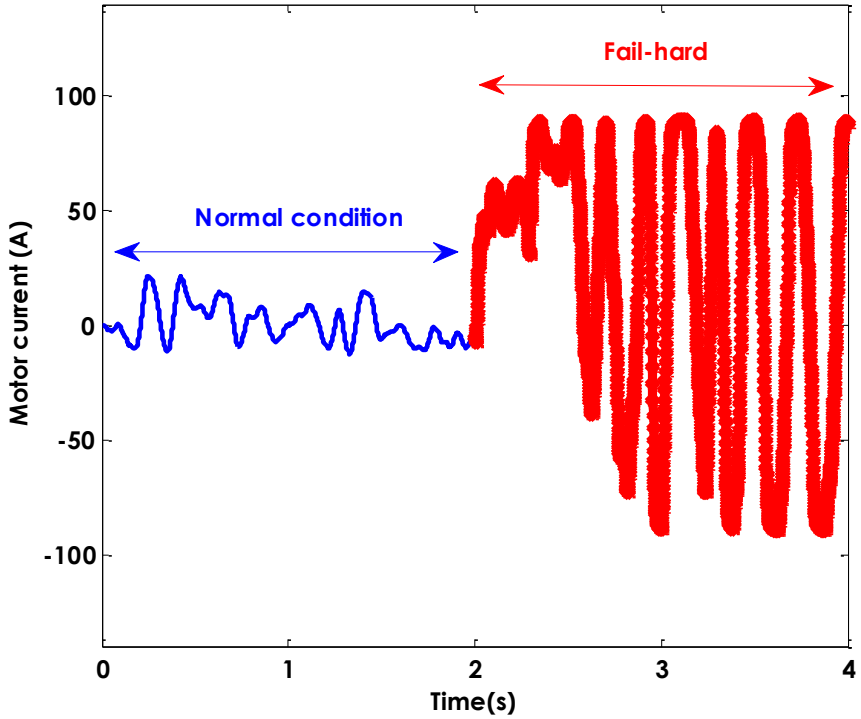

Figure 4-3: Motor current–actuator (fail-hard at time=2s)

On the other hand, the measured torque from the actuator (at the point of the output to the wheelset) is only a consequence of the high stiffness in the connection between the actuator and wheelset in response to track inputs, and this torque would be expected to increase as the actuator is locked in the fail hard condition as shown in Figure 4.4.

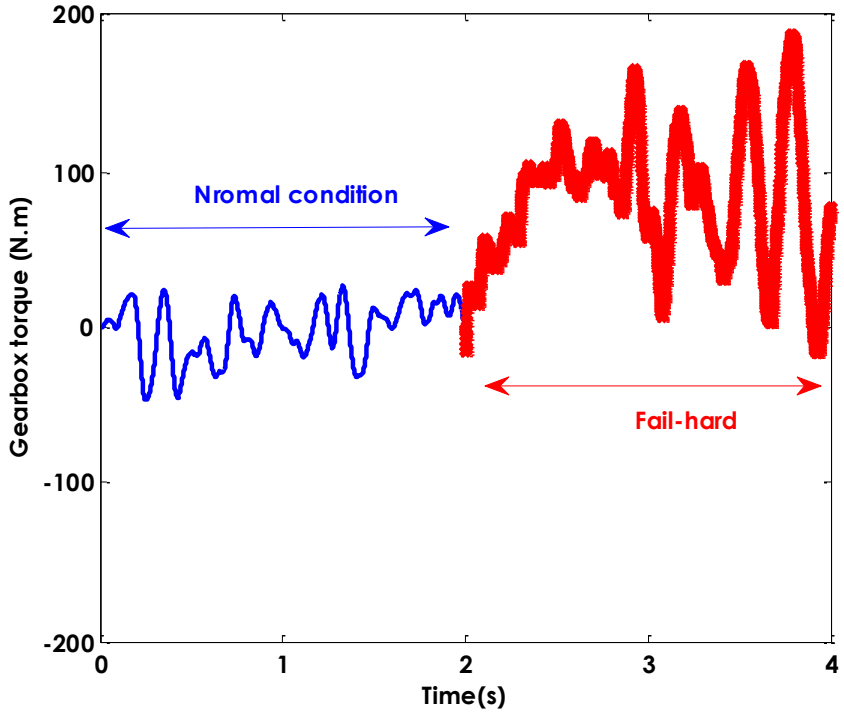

Figure 4-4: Gearbox torque –actuator (fail-hard at tim=2s)

Therefore, the estimation errors associated with the faulty actuator are also expected to increase in comparison to the normal condition. Figures 4.5, 4.6 and 4.7 compare the generated residuals for the leading actuator between the normal conditions and when the leading actuator is in the fail-to-hard mode —the fault occurs at time of 2(s) in the simulation. They clearly show that the level of the error signals is significantly increased for the faulty actuator, whereas the generated residuals for the healthy (rear) actuator should remain almost identical to those in the normal condition. Further on, in the case of trailing actuator fail-hard, the generated residuals for the leading actuator are approximately equal to the normal condition, while the faulty actuator for the trailing wheelset generates much increased residuals compared to the normal condition (Mirzapour & Mei, 2014).

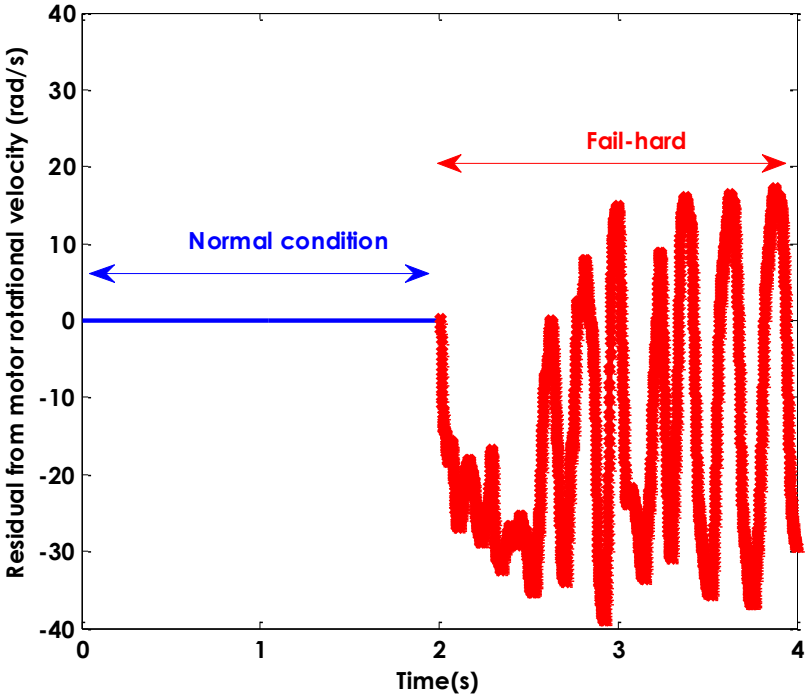

Figure 4-5: Residual from motor rotational velocity–actuator (fail-hard at time=2s)

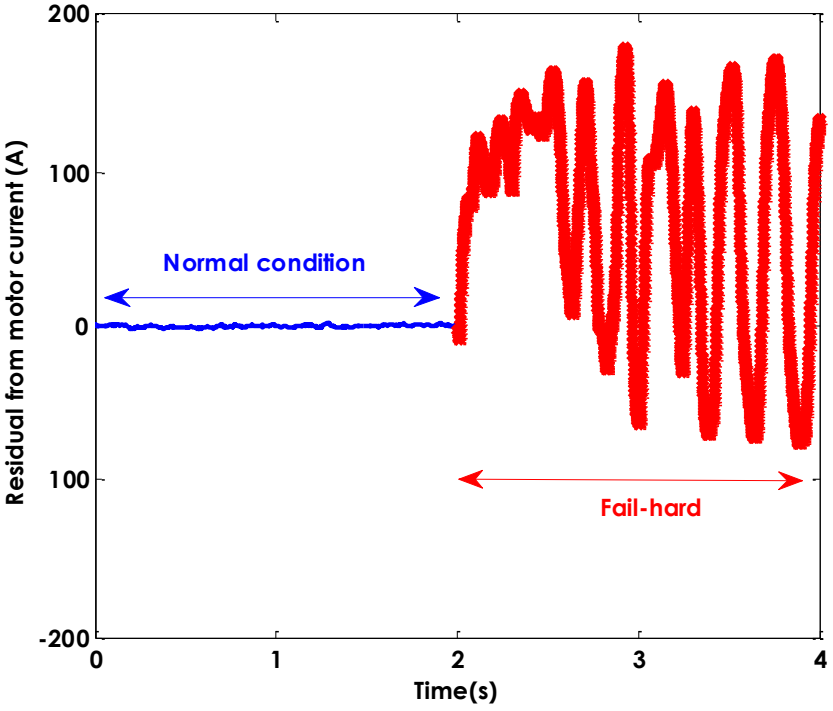

Figure 4-6: Residual from motor current–actuator (fail-hard at time=2s)

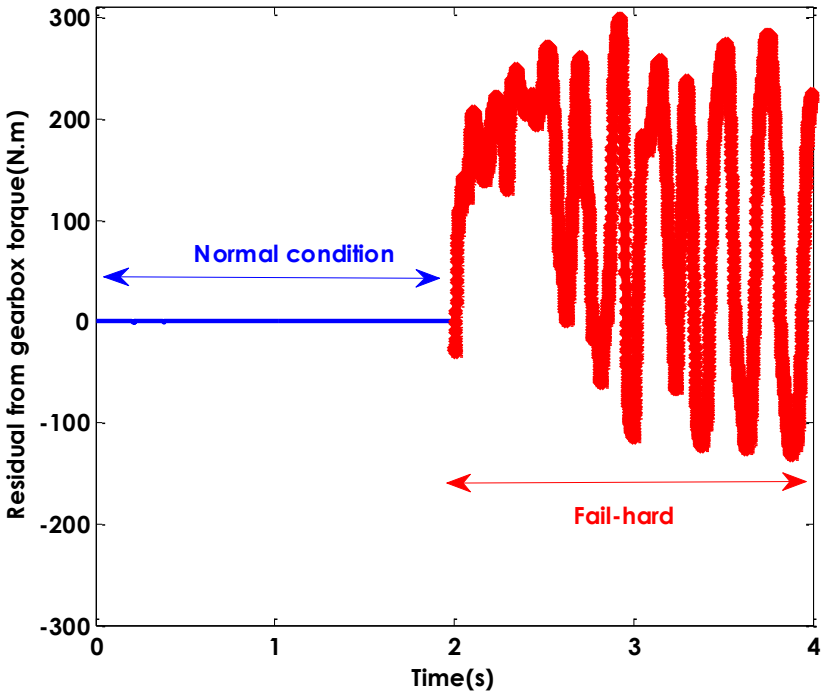

Figure 4-7: Residual from output torque–actuator (fail-hard at time=2s)

4.3.2 Actuator fail-soft

The actuator fail-soft leads to the system instability and therefore the estimation errors generated by the observer will be expected to show an oscillation (Mirzapour, Mei, & Xuesong, 2014). Figures 4.8, 4.9 and 4.10 compare the generated residuals of motor rotational speed, motor current and gearbox torque from the actuator in the incident of fail-soft (open & short circuit) in the normal condition and when the leading actuator fails in the soft mode at the initial time of the simulation. They clearly indicate that the generated residuals associated with the damaged actuator tends to increase significantly compared to the normal condition (Mirzapour & Mei, 2014).

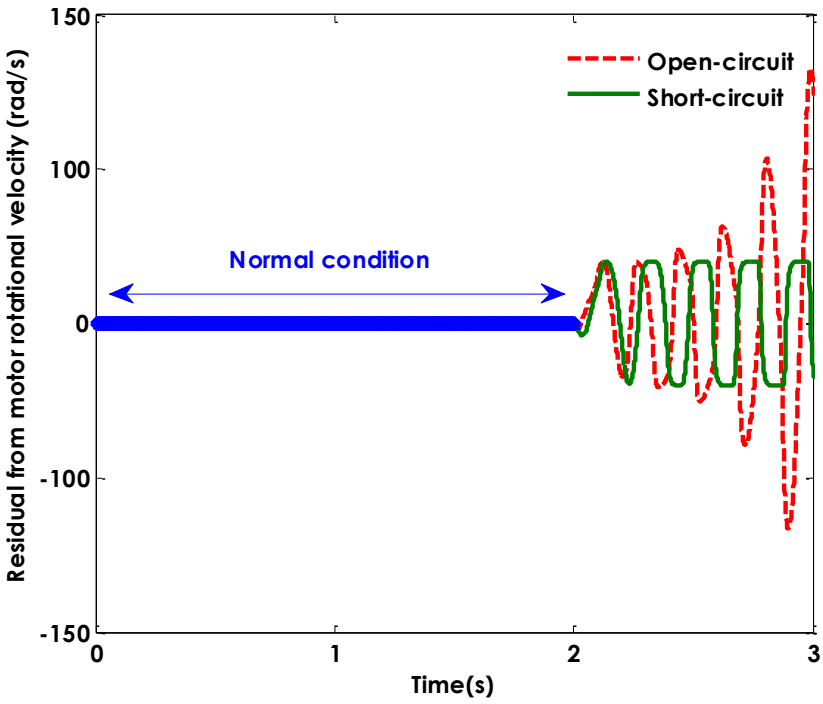

Figure 4-8: Residual from motor rotational velocity–actuator (fail-soft at time=2s)

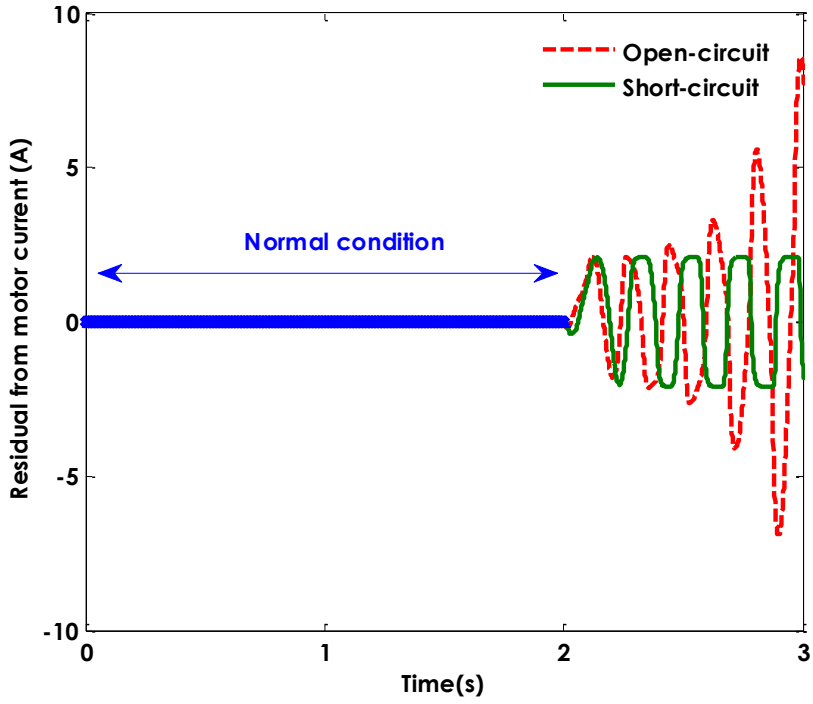

Figure 4-9: Residual from motor current–actuator (fail-soft at time=2s)

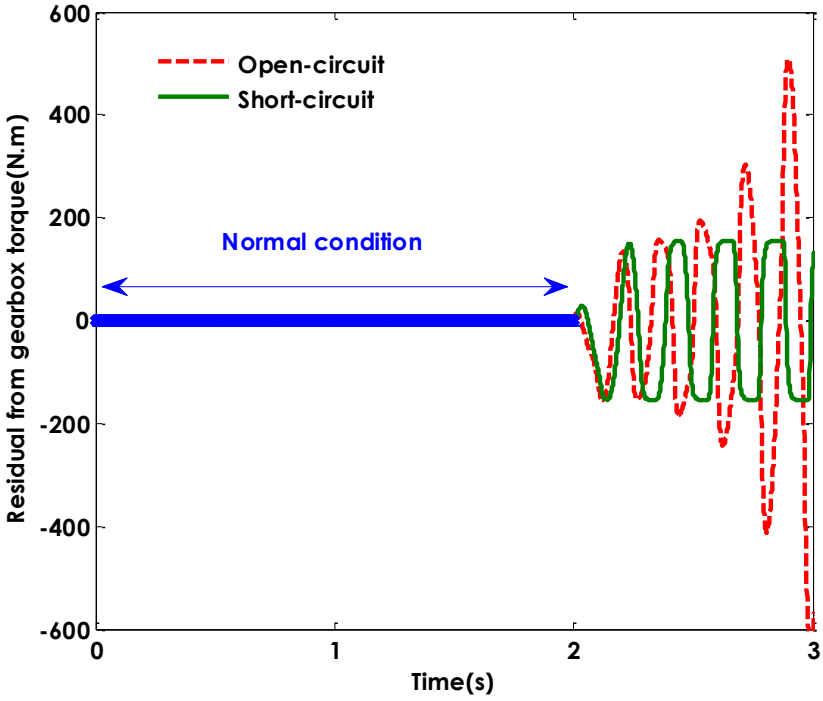

Figure 4-10: Residual from gearbox torque–actuator (fail-soft at time=2s)

However, it is necessary to identify the actuator fail-hard from the fail soft (open or short circuit) condition, as the two failure modes lead to different consequences for the vehicle dynamic behaviour and hence require different control re-configurations. From the results above, it is evident that the all generated residuals associated with the faulty actuator (either fail-hard or fail-soft) tend to increase and the use of residuals alone is not sufficient to provide adequate information in order to separate the actuator fail hard from the fail soft. Hence, it is essential to include extra measures in order to isolate the type of actuator fault and in this case that the measurement of the motor rotational velocity (which is already used by the local Kalman filter) can be added as an indicator for isolating fail hard for the incident of short and open circuit (Mirzapour & Mei, 2014).

4.3.3 Sensor failure

The proposed strategy for the actuator fault detection and isolation is highly dependent on the reliability of the information that is provided by the sensors (Mirzapour, Mei, & Xuesong, 2014). Each actuator employs three sensors to measure the rotational velocity, current and output torque. Therefore, it is necessary to ensure that an abnormal change in one of those sensors does not affect the reliability of the fault detection and isolation for the actuators. In this study, only a relative simple (but common) failure mode of sensor output failing to zero is considered - investigations for other failure modes are possible, but are recommended for further studies due to the time constraint.

It is reasonable to expect that, in the case of any of the sensor failures, only generated residuals associated with the faulty sensor will increase in any substantial way (Patton, Chen, & Nielsen, 1995), whereas the residuals of other measurements are not (or at least much less) affected – unlike in the case of actuator faults where all residuals are affected. This is because in the presence of the sensor failure, the observer (LKF) cannot provide good tracking performance for the sensor concerned and therefore the estimation error increases compared to the normal condition. For example, Figure 4.11 shows the generated residual from the motor rotational velocity in the incident of the speed sensor failure. The estimation error in the presence of the sensor failure is significantly increased in comparison to the normal condition.

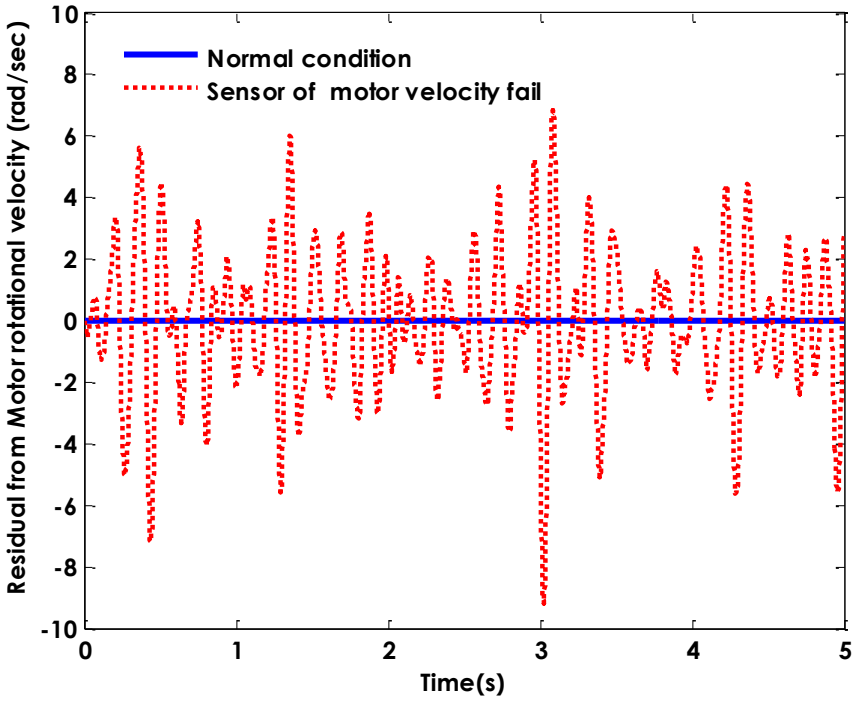

Figure 4-11: Residual from motor rotational velocity–sensor failure at time=0

4.4 Fault Detection and Isolation Scheme

In order to compute and extract the feature(s) to detect and isolate different faults of the actuators and sensors, the calculation of standard deviation moving window is used.

In order to choose a suitable window size a compromise has to be made between limiting the motor current, especially in the event of fail-hard, and the ability to detect any abnormal changes quickly enough. In the case of the actuator fail-hard the motor current increases rapidly as the faulty actuator requests more torque. The simulation analysis shows that a window size of 300 (m.s) can provide a reliable fault detection and isolation without letting the faulty actuator draw further high current as a consequence of the lack of controlled motion at the wheelset. For example, Figure 4.12 shows the magnitude of the motor current increased quickly to nearly 80 (A) after 300 (m.s) of the actuator failure. It seems that tuning the window size of 300 (m.s) excludes the fault actuator from the system in order to avoid a further damage to the motor.

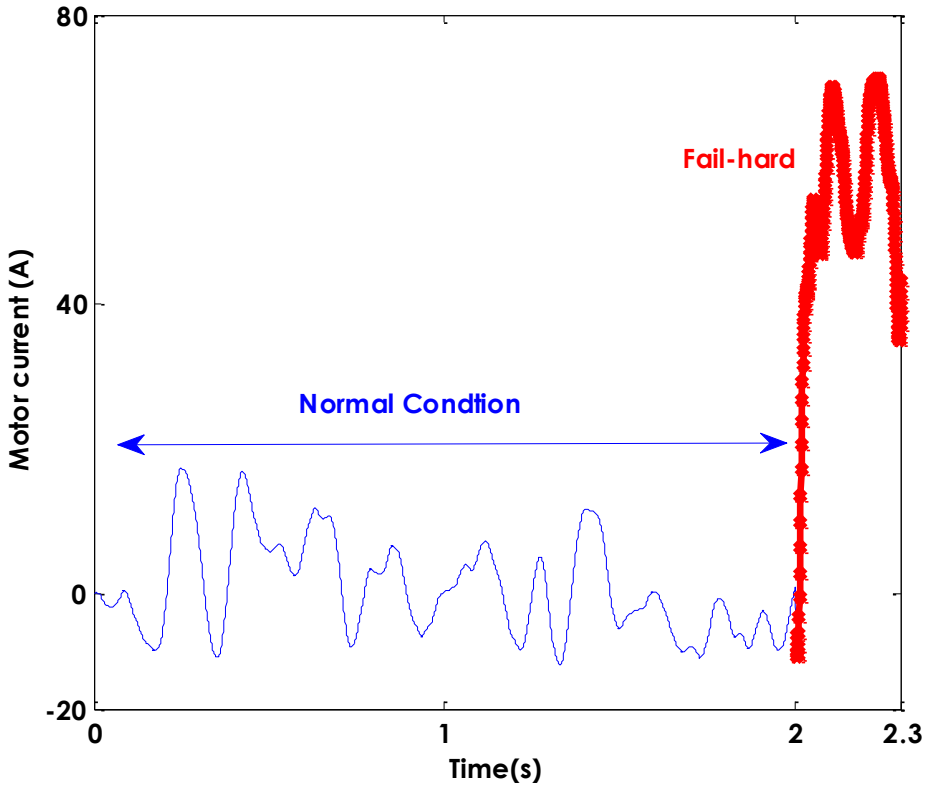

Figure 4-12: Motor current- fail hard at time=2s

Figures 4.13, 4.14 and 4.15 show the standard deviations of the motor velocity, motor current and the output torque using the moving window of 300 (m.s) in the case of the actuator failure, where the different actuator faults are introduced at the time of 1 (s). They clearly indicated that the all generated residuals are significantly increased after the time of 1 (s) where a failure is present in the actuator.

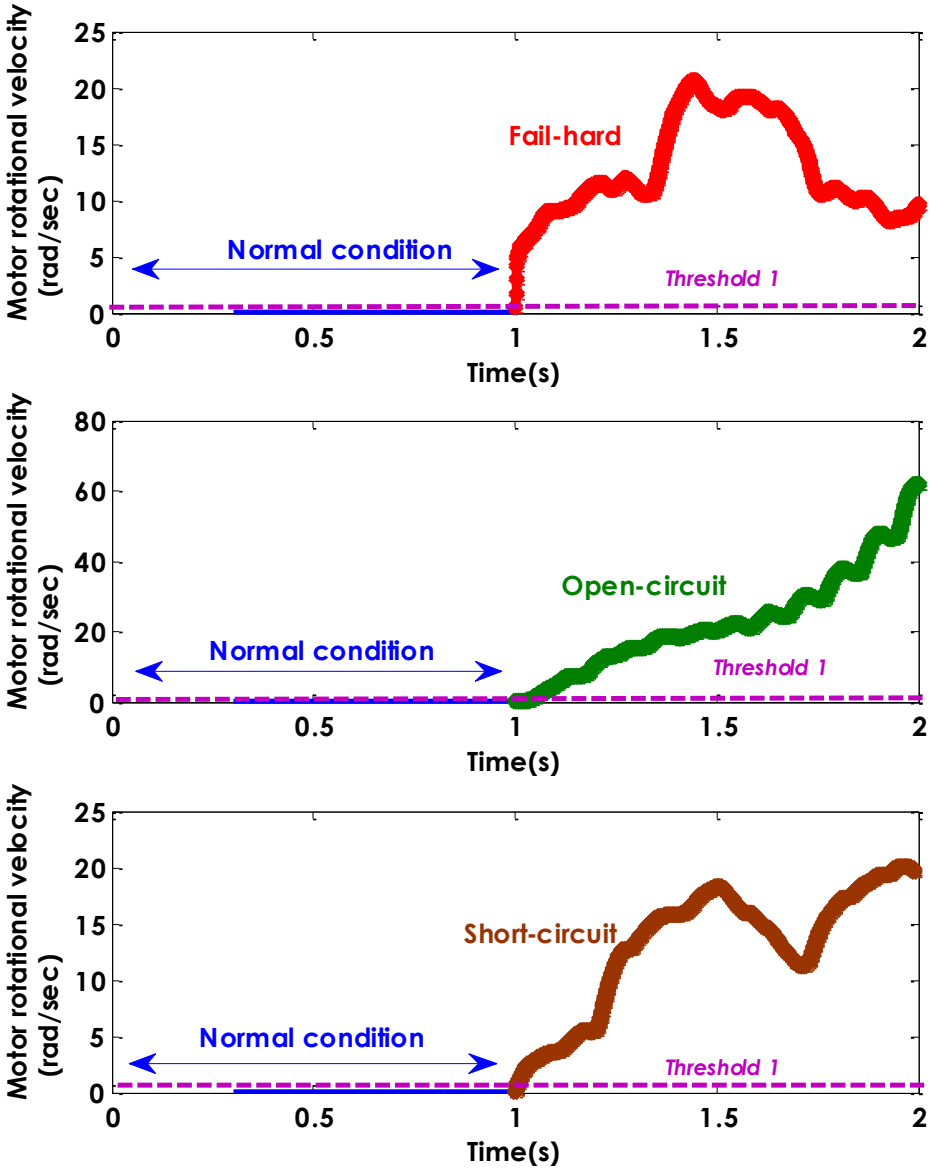

Figure 4-13: Residual from motor rotational velocity–actuator failures at time=1s

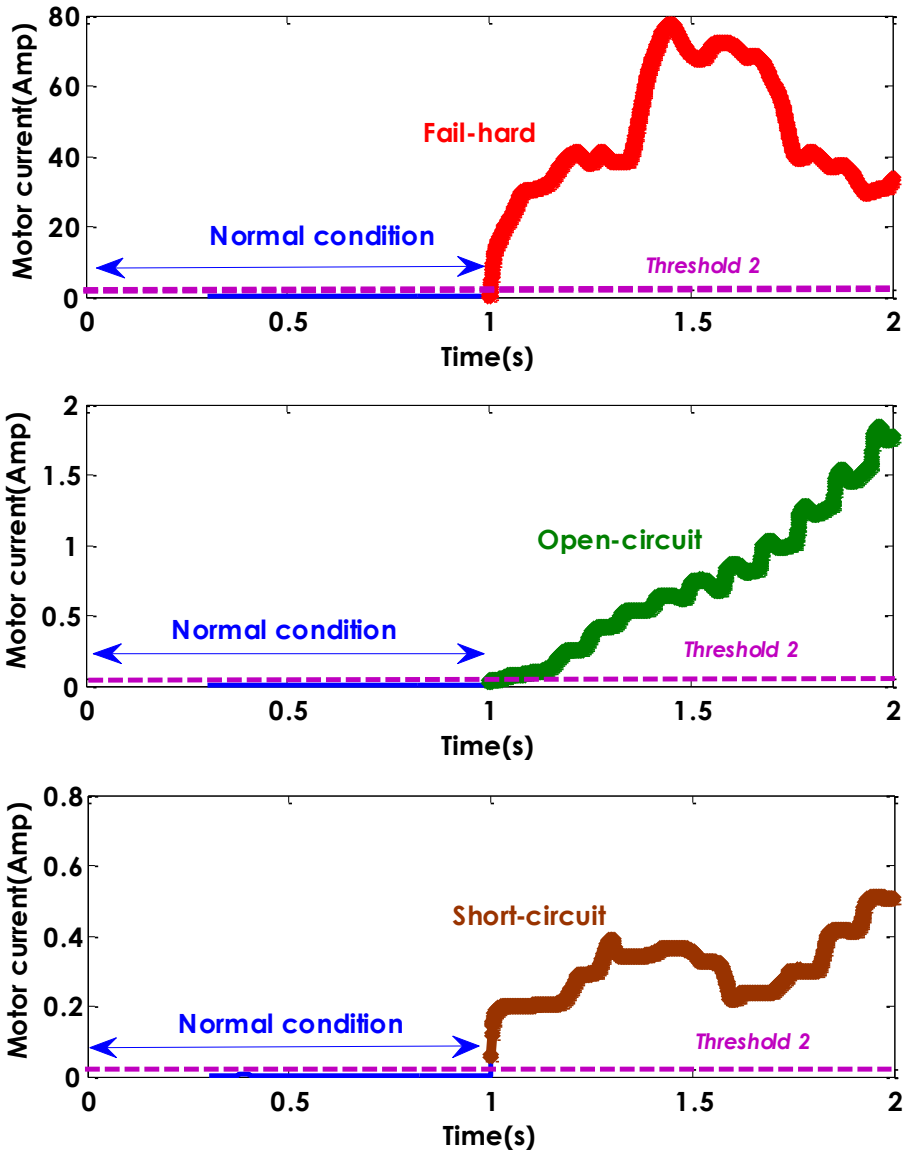

Figure 4-14: Residual of motor current–actuator failures at time=1s

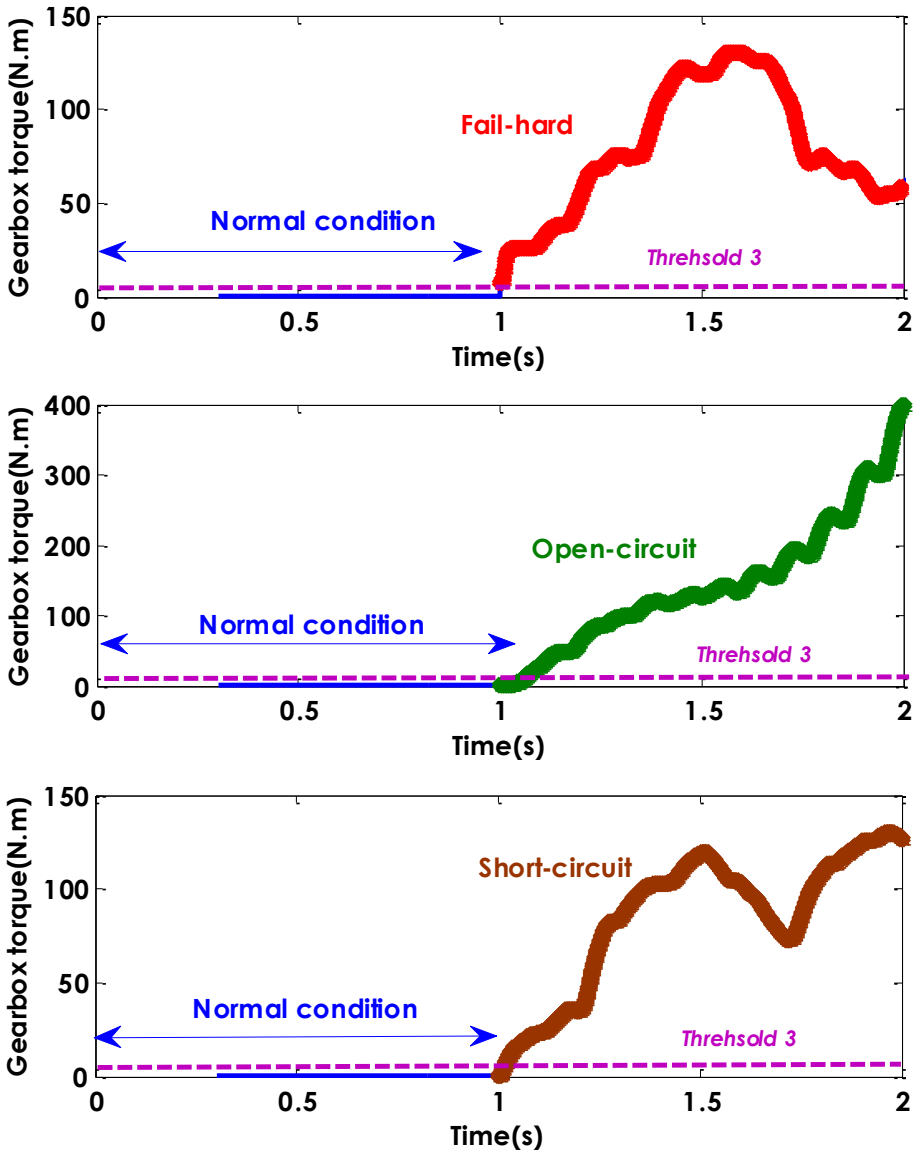

Figure 4-15: Residual of output torque (gearbox torque)–actuator failures at time=1s

On the other hand, the sensor failure can be detected and isolated through the use of residuals as there is a clear increase in the residual from the sensor concerned. For example, Figure 4.16 presents the standard deviation of the residuals for the motor rotational velocity, motor current and output torque respectively using a moving window of 300(m.s), where the torque sensor of the motor fails at the time of 1 (s). It clearly reveals how the estimation errors are starting to increase when torque sensor faults occurs whereas the generated residuals from

motor rotational velocity and motor current remain at the similar level as those in the normal condition.

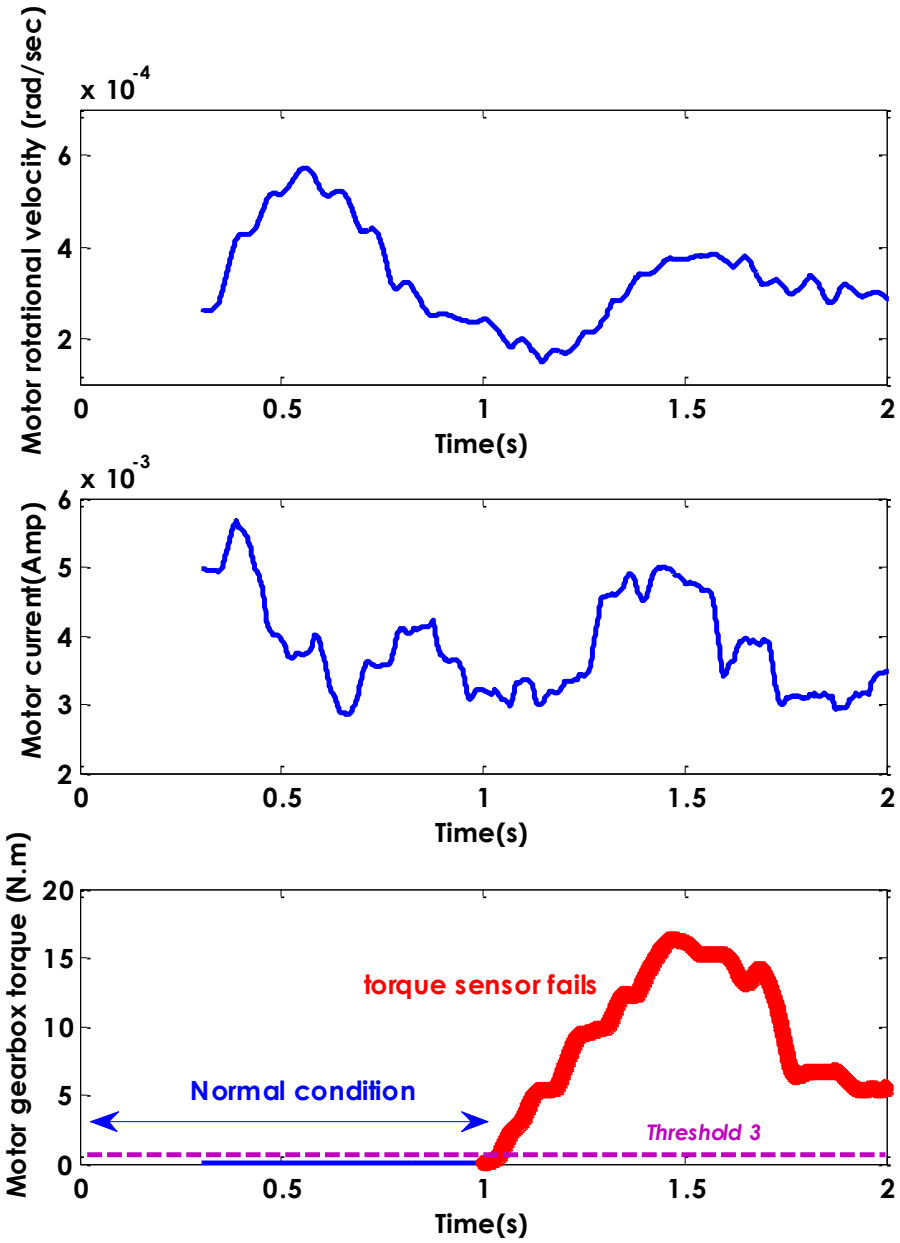

Figure 4-16: STD of residuals–torque sensor failure at time=1s

Table 4-1 summarises the different faults and how the detection and isolation may be achieved, where (+) and (—) indicate an increase and decrease, respectively, of the residuals or measurements relative to the normal condition and (0) indicates that there is no significant change from the normal condition. It appears from Table 4-1, in the case of the actuator

failure, the increases in all generated residuals from the motor velocity, motor current and gearbox torque are observed. In addition, the type of actuator failure can be identified through the use of the measurement of the motor rotational velocity as its measurement is reduced to zero in the event of fail hard. Furthermore, the location of the faulty actuator can be easily diagnosed through the evaluation of their residuals as the errors associated with damaged actuator are subject to increase whereas the estimation errors from the healthy actuator do not show substantial changes. Also Table 4-1 demonstrates that the sensors' failure can be identified through evaluation of the residual associated with damaged sensor. Further on, Figure 4.17 illustrates how the concluded results that have been obtained in Table 4-1 can be used in order to implement fault detection and isolation concept for different failure modes; where R_1, R_2 and R_3 represent the generated residuals from motor rotational velocity, motor current and gear-box torque of the front actuator and R_4, R_5 and R_6 denote the generated residuals from motor rotational velocity, motor current and gear-box torque of the rear actuator.

Table 4-1: The symptoms for FDI

Fault		**Symptoms**							
		Residual						*Measured*	
		$\dot{\theta}_{m_1} - \hat{\dot{\theta}}_{m_1}$	$i_{a_1} - \hat{i}_{a_1}$	$\tau_{g_1} - \hat{\tau}_{g_1}$	$\dot{\theta}_{m_2} - \hat{\dot{\theta}}_{m_2}$	$i_{a_2} - \hat{i}_{a_2}$	$\tau_{g_2} - \hat{\tau}_{g_2}$	$\dot{\theta}_{m_1}$	$\dot{\theta}_{m_2}$
Normal Condition		0	0	0	0	0	0	0	0
Leading Actuator	*Hard*	+	+	+	0	0	0	—	0
	Open circuit	+	+	+	0	0	0	+	+
	Short circuit	+	+	+	0	0	0	+	+
Trailing Actuator	*Hard*	0	0	0	+	+	+	0	—
	Open circuit	0	0	0	+	+	+	+	+
	Short circuit	0	0	0	+	+	+	+	+
Sensors of front Actuator	*Motor velocity*	+	0	0	0	0	0	—	0
	Motor current	0	+	0	0	0	0	0	0
	Gearbox torque	0	0	+	0	0	0	0	0
Sensors of rear Actuator	*Motor velocity*	0	0	0	+	0	0	0	—
	Motor current	0	0	0	0	+	0	0	0
	Gearbox torque	0	0	0	0	0	0	0	0

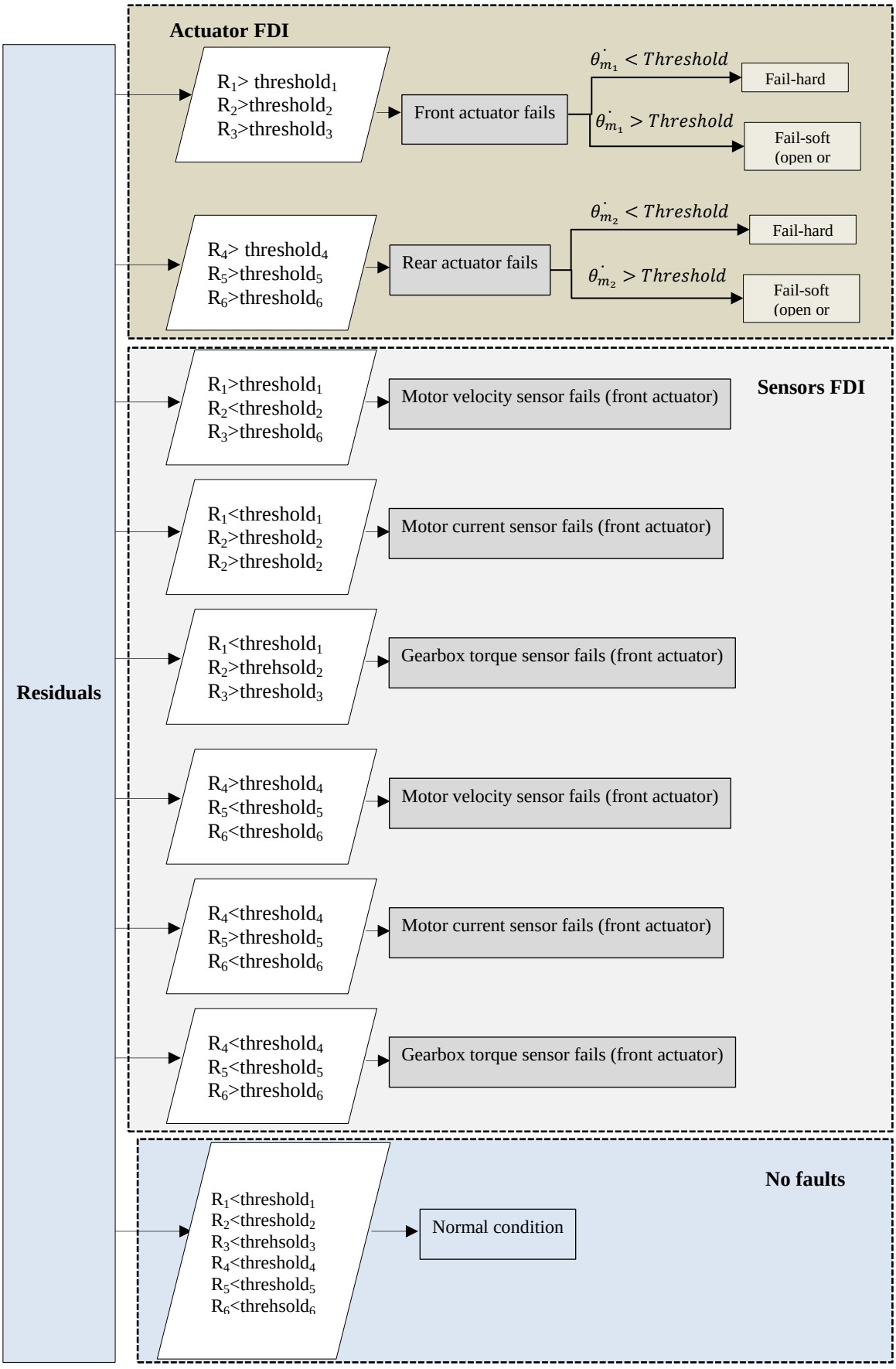

Figure 4-17: A block diagram for fault detection and isolation (Approach 2)

4.5 Assessment of Fault Detection and Isolation

This approach uses the local Kalman filter and, unlike the vehicle model based approach as presented in the previous chapter, it is not affected by the condition changes in the vehicles or at the wheel-rail interface as the model does not use the vehicle model. For example, Figure 4.18 shows the standard deviation moving window of the residuals from the motor velocity of the actuator in the hard failure condition at different conicity values when the incident occurs at the initial time of the simulation. In the figure, NC2, NC1 and NC3 represent the normal condition at the conicities of 0.2, 0.1 and 0.35, respectively; LH2, LH1 and LH3 denote the leading actuator failing in the hard mode at the conicities of 0.2, 0.1 and 0.35, respectively.

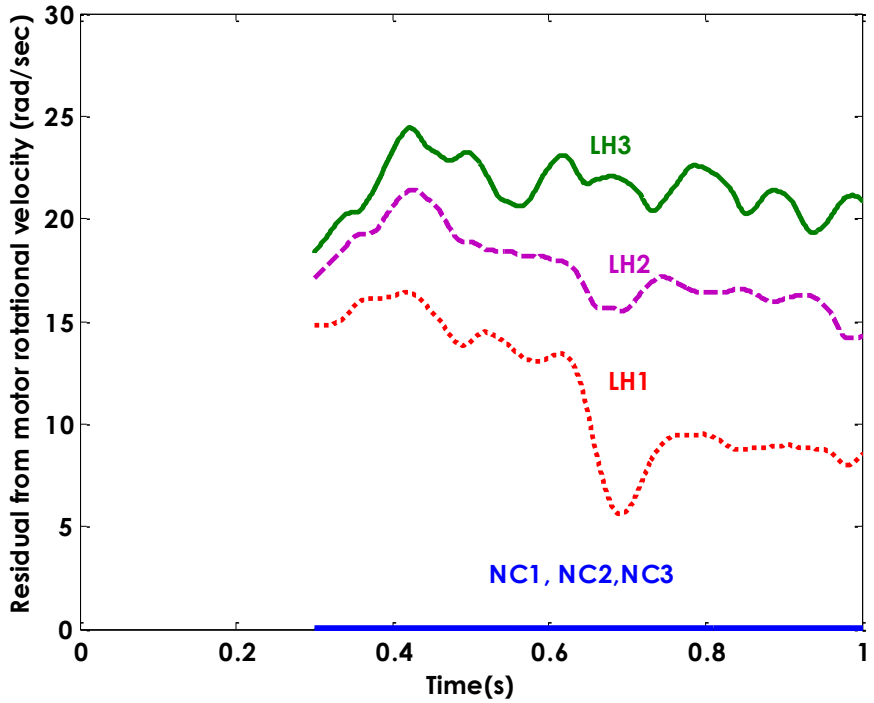

Figure 4-18: STD of residual from motor rotational velocity–actuator (fail-hard at time=0) vs conicity

The difference between different conicity values in the case of actuator fault is caused by the different control demand from the active controller in response to the condition change at the wheel-rail interface, but it is clear that there is no difficulty to detect and isolate the fault from the normal condition.

4.5.1 Deterministic track inputs

The assessment of the proposed fault detection and isolation strategy above is carried out using a straight track with irregularities. A deterministic track section (with no track irregularities) is included here to evaluate the performance, using a curved track with a radius of 1250 (m) radius and a cant angle of 6° having transition sections of 2 (s) at both ends. The simulation analysis shows that the proposed strategy for FDI can provide reliable information to identify any abnormal changes of either actuators or sensors. Figures 4.19 and 4.20 show the standard deviation in the incident of the fail hard at time 0. As figures show the estimation errors on the transition times are significantly increased compared to the normal condition. The level of changes of the estimation errors are reduced on a constant curve, nevertheless they are still clearly higher compared to the normal condition for the purpose of fault detection and isolation.

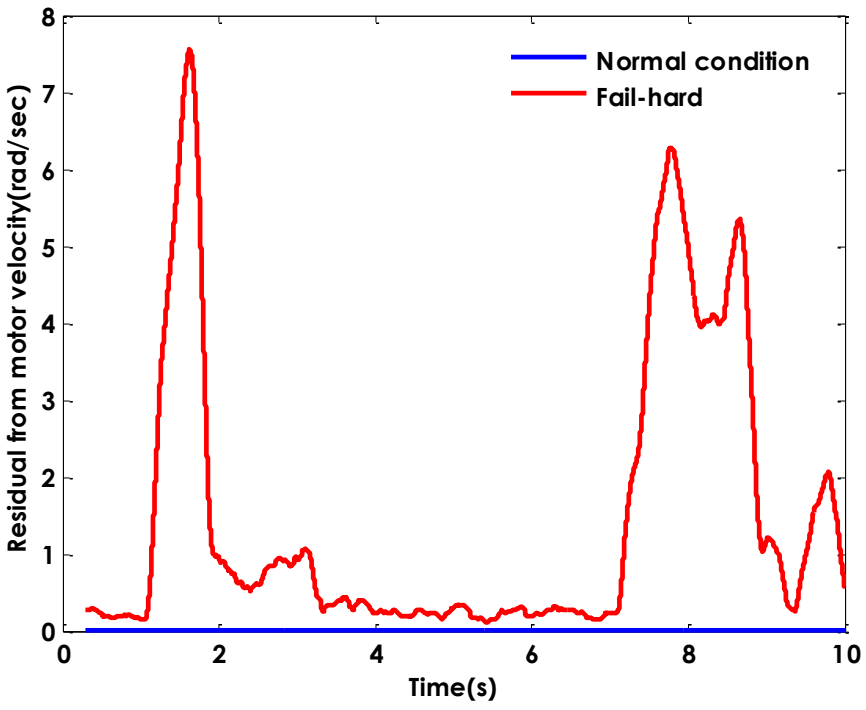

Figure 4-19: STD of residual from motor velocity–actuator (fail hard at time=0) on curved track

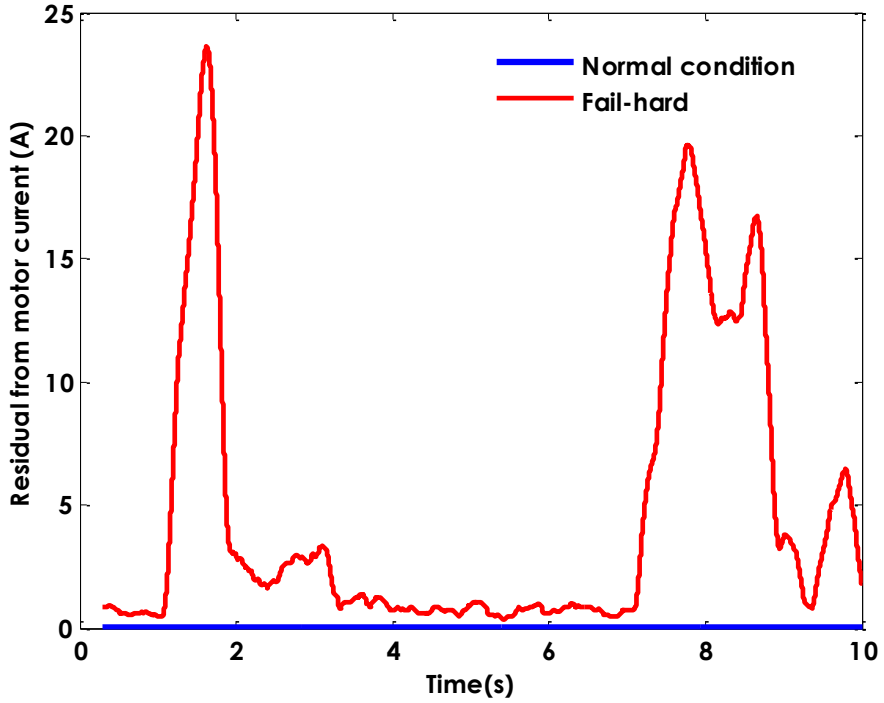

Figure 4-20: STD of residual from motor current–actuator (fail hard at time=0) on curved track

In the case of the actuator fail soft, the generated residuals are significantly increased on either constant curve or transition times as shown in Figures 4.21 and 4.22. The generated residuals for the actuator fail soft are shown for the first 2 seconds only due to the fact the system is unstable and the generated residuals from the faulty actuator increase exponentially with time.

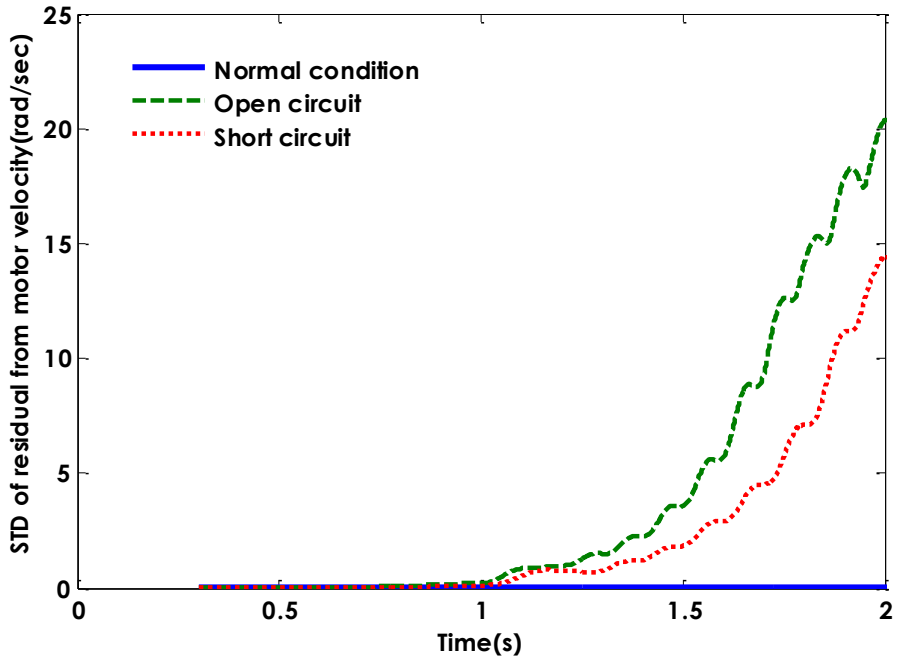

Figure 4-21: STD of residual from motor current–actuator (fail-soft at time=0) on curved track

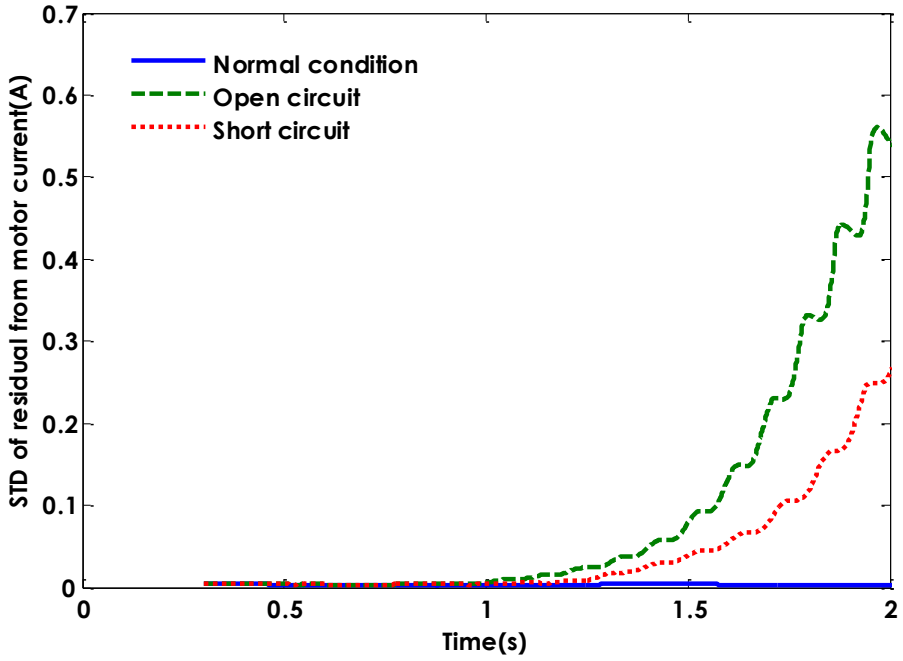

Figure 4-22: STD of residual from motor current–actuator (fail-soft at time=0) on curved track

Figures 4.23, 4.24 and 4.25 show the standard deviation of the residuals in the incident of motor velocity sensor failure, motor current failure and gearbox torque sensor failure respectively. The simulation analysis shows that in the case of any of the sensor failures the generated error of the damaged sensors are higher on the transition times compared to the

constant curve. However, a threshold can be readily set on the generated residuals in all cases of the sensor failures for the purpose of diagnosing any abnormal changes in the sensors.

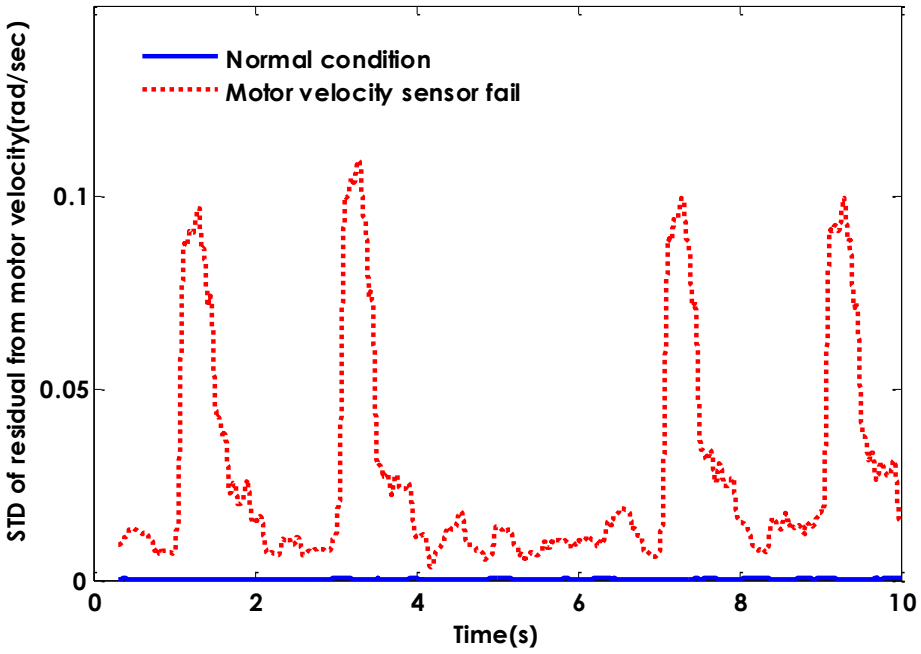

Figure 4-23: STD of residual from motor velocity–motor velocity sensor failure at time=0 on curved track

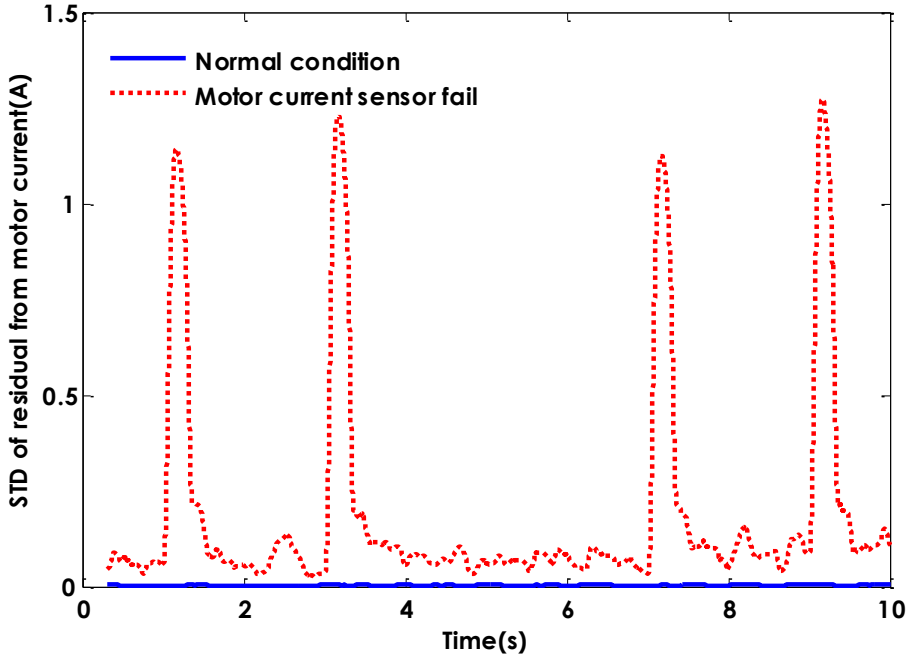

Figure 4-24: STD of residual from motor current–motor current sensor failure at time=0 on curved track

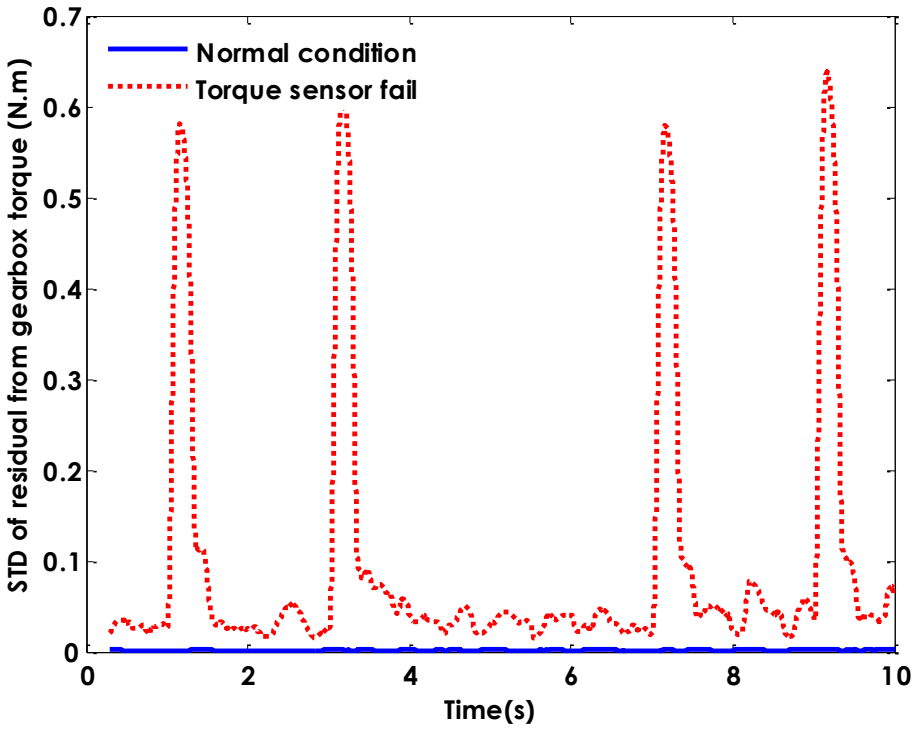

Figure 4-25: STD of residual from gearbox torque–torque sensor failure at time=0 on curved track

4.5.2 Measure track data

Figures 4.26 and 4.27 show the standard deviations, using a moving widow with the size of 300(m.s), of the generated residuals in the incident of the actuator failures. It shows that when the vehicle is operated under a normal condition of up to 1 (s) the genereted residuals are very low; whereas when fault occurs at time of 1(s) the error in the actuator subject to a significant increases compared to the normal condition.

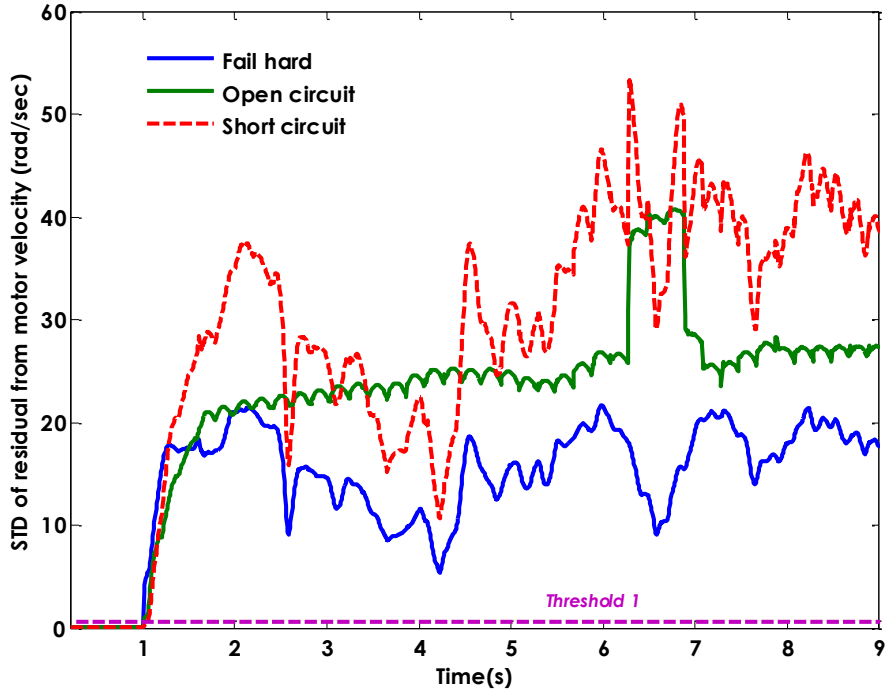

Figure 4-26: STD of residual from motor velocity–actuator failures at time=0 on real track data

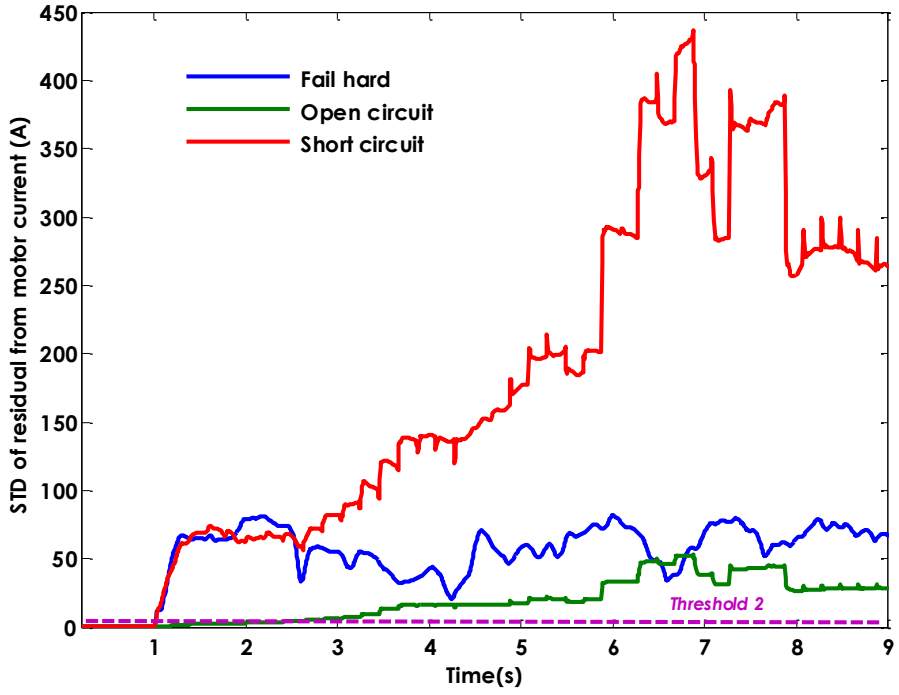

Figure 4-27: STD of residual from motor current–actuator failures at time=0 on real track data

Figure 4.28 shows the generated residuals in the incident of the sensor failures, where SF1, SF2 and SF3 denote the failures of the motor sensor, motor current and motor toque

respectively. It shows that when the vehicle is operated under a normal condition of up to 1 (s) the genereted residuals are very low; whereas when fault occurs in the sensors at time of 1(s) the error of sensor failures tends to increase.

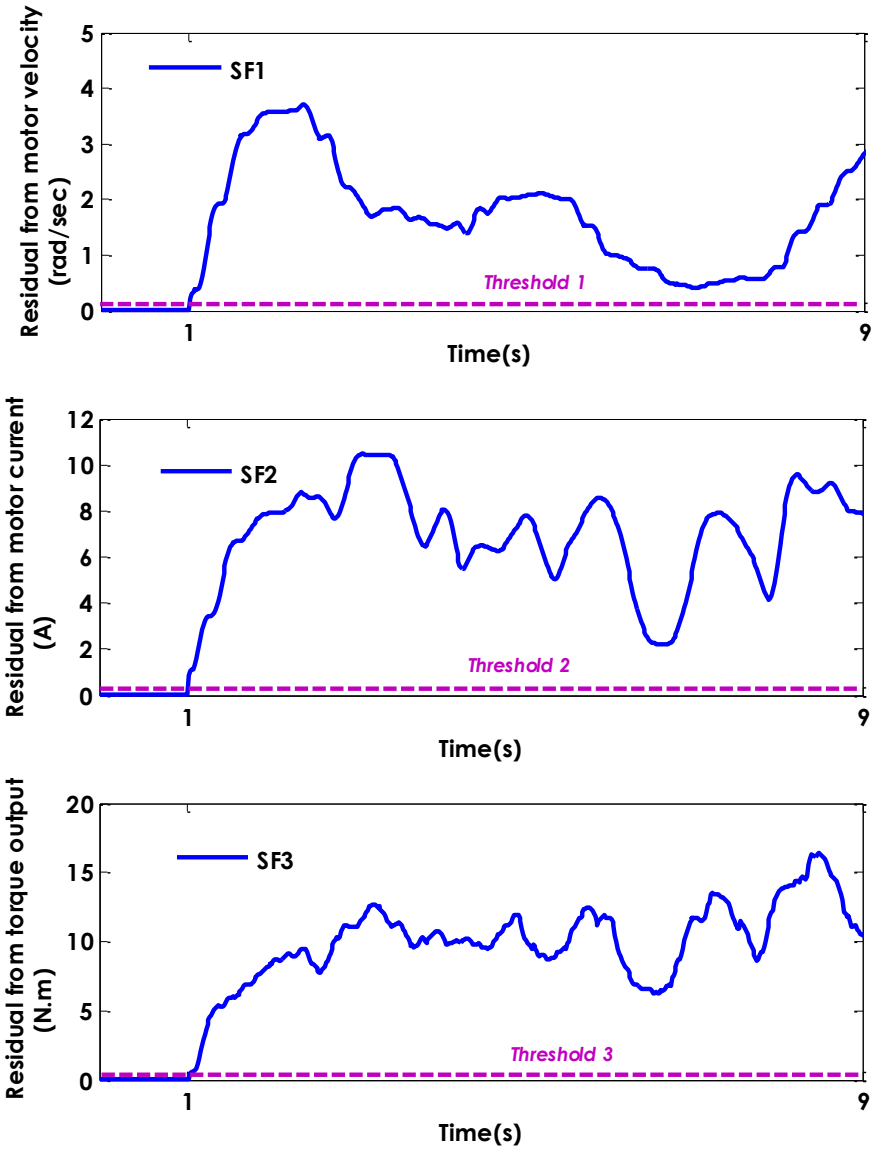

Figure 4-28: STD of residuals–sensor failures at time=0 on real track data

Table 4-2 summaries the type of the different track input that has been used in order to evaluate the robustness of the proposed fault detection and isolation strategy. The simulation analysis showed that the suggested fault detection and isolation in Figure 4.17 can provide

reliable information about any abnormal changes in actuator or sensor without the need of making any changes to the definition of the fault detection and isolation.

Table 4-2: Type of different track inputs to test the robustness of the FDI (approach 2)

Track inputs		
Curved track	Random	Real track data
Curve radius 1250 (m) Cant angle 6°	The random track input represents the roughness of a typical high speed main Line—generated from filtered white-noise in order to provide a broad frequency spectrum with a relatively high level of irregularities	Measured real track data between Paddington and Bristol in UK

4.6 Summary

This chapter has presented the development of a fault detection and isolation strategy for the detection of actuator and sensor faults using local Kalman filters based on the actuator dynamics. It has been shown that the fault(s) in the actuators can be diagnosed by a combination of the estimation errors from the KF based-actuator and measurement signals; whereas the fault(s) in the sensor can be identified through an evaluation of the estimation error from the sensor concerned. The standard deviation with a moving window has been suggested to extract the features for the FDI. It was shown that in the case of either of the sensors failures, there is a clear increase in the residual from the sensor concerned. On the other hand, in the case of the actuator failure, although the increase in generated residuals from the motor rotational velocity, the motor current and output torque of the motor is perceived, but only the generated residuals from the motor velocity and motor current were considered for the purpose of FDI. Further on, in order to separate the fail-hard from the fail-soft (either short or open circuit) conditions, the use of residuals alone was not sufficient as all generated residuals associated with the faulty actuator are largely increased. Therefore

the sensor output for the motor velocity was used as a supplement measure to provide information for isolating actuator fail hard from the cases of short and open circuits. In addition, both real track data and deterministic track were used as inputs in the simulation in order to ensure that the proposed strategy can provide valid information when the vehicle runs along different track inputs.

Chapter 5 CONTROL RE-CONFIGURATION & INTEGRATION

5.1 Introduction

The previous chapters have studied two approaches for detecting and isolating faults of the actuators, which can be used to enable a change of control strategies (through control re-configuration) that will cope with the identified fault(s) in order to guarantee the vehicle's stability and curving performance. This must be achieved only through the remaining actuator. The level of control input, i.e. the number of operational actuators, is reduced and consequently increased control effort for the remaining actuator may be expected. Hence, there is a design trade-off for the control reconfiguration between the stability and curving performance of the vehicle and the actuation requirements. Furthermore, railway vehicles are subject to parameter variations especially at the wheel-rail interface such as conicity (Pearson, Goodall, Mei, & Himmelstein, 2004), and therefore the robustness of the re-configuration strategies must be ensured (Zhang & Jiang, 2008). This chapter is organised as follows. Section 5.2 studies the control-reconfiguration strategies for the different fault conditions (i.e. fail hard and fail soft). Section 5.3 presents the integration of the proposed control reconfiguration strategies with the fault detection and isolation schemes as developed in the previous chapters to demonstrate how the two parts of the entire fault tolerant strategy work together in a simulated 'real situation' environment. Section 5.4 assesses the robustness of the fault tolerant strategy against parameter variations.

5.2 Control Re-configuration Strategy

After a fault is detected and isolated, the controller will need to be re-configured (Patton, Chen, & Nielsen, 1995; Frank, 1990) in order to deliver the desired torque demand to the wheelsets through the remaining actuator in order to maintain stability and curving performance. The re-configuration for performance is concerned with the minimisation or

elimination of all unnecessary creep forces at the wheel–rail interfaces along the curved track (Bruni, Goodall, Mei, & Tsunashima, 2007) in order to minimise the contact forces at the wheel–rail interface in order to reduce the wear and rolling contact fatigue (Perez, Stow, & Iwnicki, 2006), especially during curving (Mei & Goodall, 2003a). In the longitudinal direction it is desirable to eliminate the creep force to reduce unwanted yaw motion, whereas in the lateral direction some creep forces are required to provide the force necessary to compensate for any cant deficiency when the wheelset negotiates the curved track (Monk-Steel, Thompson, de Beer, & Janssen, 2006). This is achievable or partially achievable through the re-design and tuning of the gains of the optimal control with the input reduced from two to one (Mirzapour, et al., 2012).

5.2.1 Control re-configuration for actuator fail-hard

In the event of the actuator failing hard, the objective of the re-configuration is to re-configure the controller with the remaining (operational) actuator with the main aim to maintain as much as possible the vehicle's performance (Mirzapour, Mei, & Xuesong, 2014). It should be noted that the fail-hard condition means that one of the wheelsets is locked in a fixed position of yaw displacement relative to the bogie frame such that it cannot take the desired position on the curved tracks or straight track depending on the exact position it is locked to. Therefore some level of performance degradation (Zhang & Jiang, 2008) for the wheelset affected will be inevitable and the control re-configuration will aim to provide a performance at least not worse than that of the vehicle with passive suspensions.

The re-configuration of the controller can be achieved by re-tuning the control gain (Blanke, Staroswieck, & Wu, 2001) for the remaining actuator in order to compensate for the degraded performance as a consequence of the actuator hard failure. In the re-design of the optimal controller with a single input from the remaining functional actuator, the effect of the failed actuator will need to be considered and is modelled in the form of high level stiffness

between the wheelset and the bogie frame to represent the material stiffness in the connections of the actuators to the bogie frame and wheelset. Equations (5.1) and (5.2) show the mathematical representations of the torque input for actuator failing hard at the leading and trailing wheelsets respectively; K_f represents the effective yaw stiffness from the material stiffness in the connections of the actuator to the bogie frame and wheelset. In the equations (α_1) and (α_2) also represent the radial angular positions of the locked actuators in the non-zero positions of the leading and trailing wheelsets respectively and ($\frac{L_v}{R}$) represents the impact of the track curvature.

Leading actuator fail- hard:

$$\tau_{f1} = -K_f(\psi_{w1} - \psi_g + \frac{L_v}{R_1} + \alpha_1) \quad \textbf{Eq. 5-1}$$

Trailing actuator fail- hard:

$$\tau_{f2} = -K_f(\psi_{w2} - \psi_g - \frac{L_v}{R_2} - \alpha_2) \quad \textbf{Eq. 5-2}$$

By Substituting the Equations (5.1) or (5.2) in the vehicle dynamics model that are provided in chapter 2 gives the revised model of the vehicle in the incidence of hard failure. Equations (5.3)–(5.8) represent the dynamics of the wheelsets and bogie frame in the yaw direction in the presence of hard failure for the leading and trailing wheelsets.

For leading actuator fail-hard:

$$\ddot{\psi}_{w1} = {}^{1}\!/_{I_w}[{}^{2f_{11}L_g^2}\!/_{V_s}\dot{\psi}_{w1} - {}^{2f_{11}\lambda L_g}\!/_{r_0}y_{w1} + {}^{2f_{11}L_g^2}\!/_{R_1} + {}^{2f_{11}\lambda L_g}\!/_{r_0}y_{t1} - K_f(\psi_{w1} - \psi_g + \frac{L_b}{R_1})], \quad \textbf{Eq. 5-3}$$

$$\ddot{\psi}_{w2} = {}^{1}\!/_{I_w}[{}^{2f_{11}L_g^2}\!/_{V_s}\dot{\psi}_{w2} - {}^{2f_{11}\lambda L_g}\!/_{r_0}y_{w2} + {}^{2f_{11}L_g^2}\!/_{R_2} + {}^{2f_{11}\lambda L_g}\!/_{r_0}y_{t2} + \tau_{w2}], \quad \textbf{Eq. 5-4}$$

$$\ddot{\psi}_g = {}^{1}\!/_{I_g}[-2L_v^2C_s\dot{\psi}_g - 2L_v^2K_s\psi_g + L_vC_s\dot{y}_{w1} - L_vC_s\dot{y}_{w2} + L_vK_sy_{w1} - L_vK_sy_{w2} + K_f(\psi_{w1} - \psi_g + \frac{L_b}{R_1}) - \tau_{w2})], \quad \textbf{Eq. 5-5}$$

For trailing actuator fail-hard:

$$\ddot{\psi}_{w_1} = {}^{1}\!/_{I_w}[{}^{2f_{11}L_g^2}\!/_{V_s}\dot{\psi}_{w_1} - {}^{2f_{11}\lambda L_g}\!/_{r_0}y_{w_1} + {}^{2f_{11}L_g^2}\!/_{R_1} + {}^{2f_{11}\lambda L_g}\!/_{r_0}y_{t_1} + \tau_{w_1}], \quad \textbf{Eq. 5-6}$$

$$\ddot{\psi}_{w2} = {}^{1}\!/_{I_w}[{}^{2f_{11}L_g^2}\!/_{V_s}\dot{\psi}_{w2} - {}^{2f_{11}\lambda L_g}\!/_{r_0}y_{w2} + {}^{2f_{11}L_g^2}\!/_{R_2} + {}^{2f_{11}\lambda L_g}\!/_{r_0}y_{t2} - K_f(\psi_{w2} - \psi_g + \frac{L_b}{R_2})], \quad \textbf{Eq. 5-7}$$

$$\ddot{\psi}_g = {}^{1}\!/_{I_g}[-2L_v^2C_s\dot{\psi}_g - 2L_v^2K_s\psi_g + L_vC_s\dot{y}_{w1} - L_vC_s\dot{y}_{w2} + L_vK_sy_{w1} - L_vK_sy_{w2} - \tau_{w1} + K_f(\psi_{w2} - \psi_g + \frac{L_b}{R_2})], \quad \textbf{Eq. 5-8}$$

To re-design the controller for the fault conditions, the number of control inputs will be reduced to one input (Mirzapour, Mei, & Hussain, 2012) and the control input (τ_{w_1}, τ_{w_2}) represents the torque in the yaw direction at either wheelset produced by the remaining operational actuator. Equations (5.9) and (5.10) define a state–space representation of the vehicle model suitable for the optimal control design (with reduced control input), where *x* is a vector of state variables, *u* is the control input vector, *w* is a vector of track inputs, and *y* is a vector of outputs or measurements.

$$\dot{x} = A \cdot x + B \cdot u + \mu \cdot w, \qquad \textbf{Eq. 5-9}$$

Where;

$$\mathrm{x} = \left[\dot{y}_{w_1} \quad y_{w_1} - y_{t_1} \quad \dot{\psi}_{w_1} \quad \psi_{w_1} \quad \dot{y}_{w_2} \quad y_{w_2} - y_{t_2} \quad \dot{\psi}_{w_2} \quad \psi_{w_2} \quad \dot{y}_g \quad y_g - \left(\frac{y_{t_1} + y_{t_2}}{2} \right) \quad \dot{\psi}_g \quad \psi_g \quad \dot{y}_v \quad y_v - \left(\frac{y_{t_1} + y_{t_2}}{2} \right) \right]^T;$$

Leading actuator fail-hard: $u = \tau_{w_2}$;

Trailing actuator fail-hard: $u = \tau_{w1}$;

$$y = C \cdot x + D \cdot u; \qquad \textbf{Eq. 5-10}$$

where;

$$y = \left[y_{w_1} \quad \psi_{w_1} \quad y_{w_2} \quad \psi_{w_2} \right]^T$$

A general diagram of the re-design control structure is shown in Figure 5.1 where a dotted box indicates the weighting factor for tuning the re-design controller. A control gain matrix for the re-configured control with the single control input can be tuned to ensure a good design by optimising the weighting matrices of *Q* and *R*. In this study the values of the weighting matrices have been chosen manually to gives the best results by achieving the following forces on curves tracks:

- Zero longitudinal creep force on steady curve.
- Equal lateral creep force.

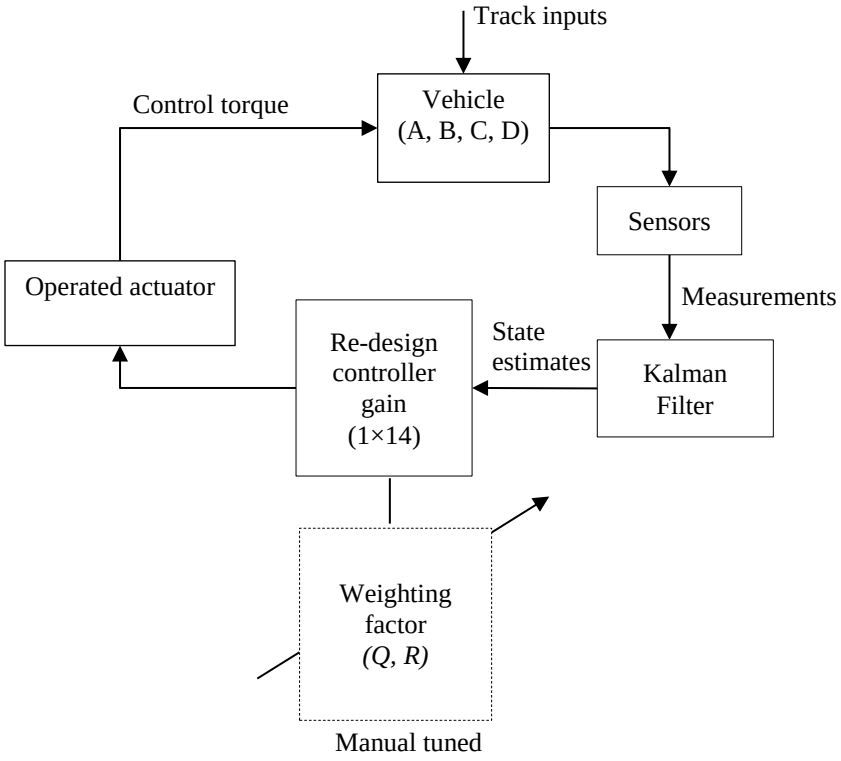

Figure 5-1: Re-design control strategy scheme

Equations (5.11) and (5.12) represent the selected value for Q and R for the leading and trailing fail-hard, respectively.

Leading actuator fail-hard:

$$Q = diag(1.78,0.01,7,0.01); \quad R = 10^{-12} \qquad \textbf{Eq. 5-11}$$

Trailing actuator fail-hard:

$$Q = diag(60.5,0.01,60,0.01); \quad R = 10^{-12} \qquad \textbf{Eq. 5-12}$$

In order to assess the vehicle curving performance, a deterministic track input is used in the simulation with a radius of 1250 (m) and a cant angle of 6°, connected to a straight track via a transition time of 2 (s). The vehicle speed of 50 (m/s) is used. Figure 5.2 reveals that the

control re-configuration in the incident of leading actuator fail-hard can help to reduce the contact forces in the longitudinal direction for the rear wheelset compared to the original controller without re-configuration, but there is only a small reduction in the contact force at the front wheelset where the actuator fault occurs as the actuator in a fail-hard condition locks the wheelset and there is little scope for improvement. A similar performance improvement is obtained for the rear actuator failure, as shown in Figure 5.3.

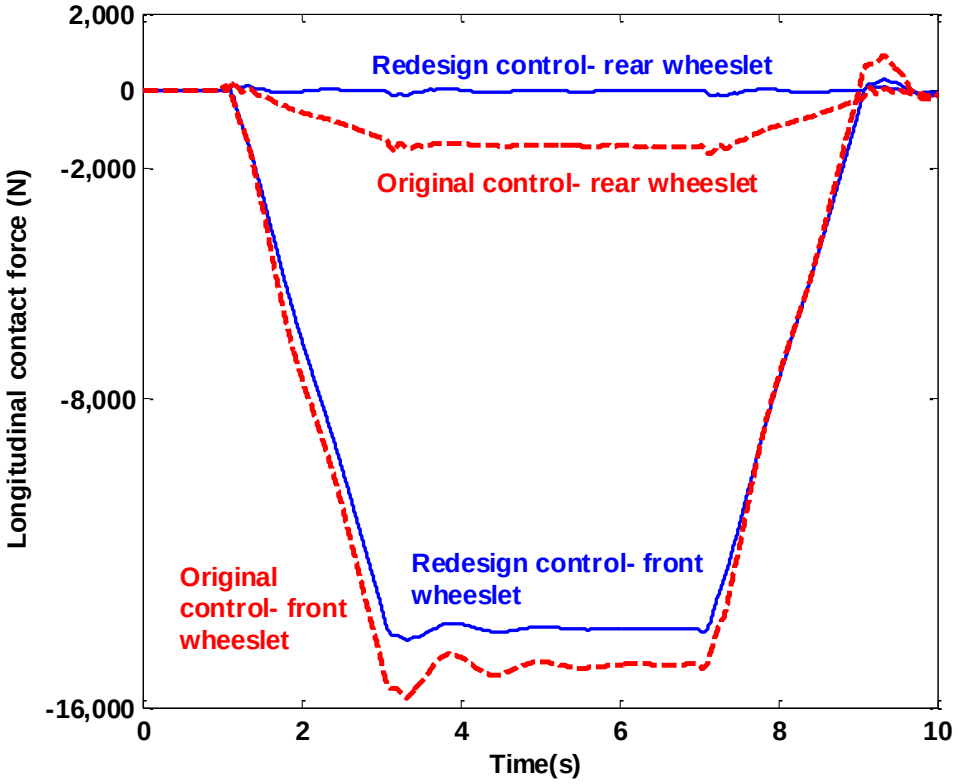

Figure 5-2: Longitudinal contact force in incident of leading fail hard–original vs re-configuration control

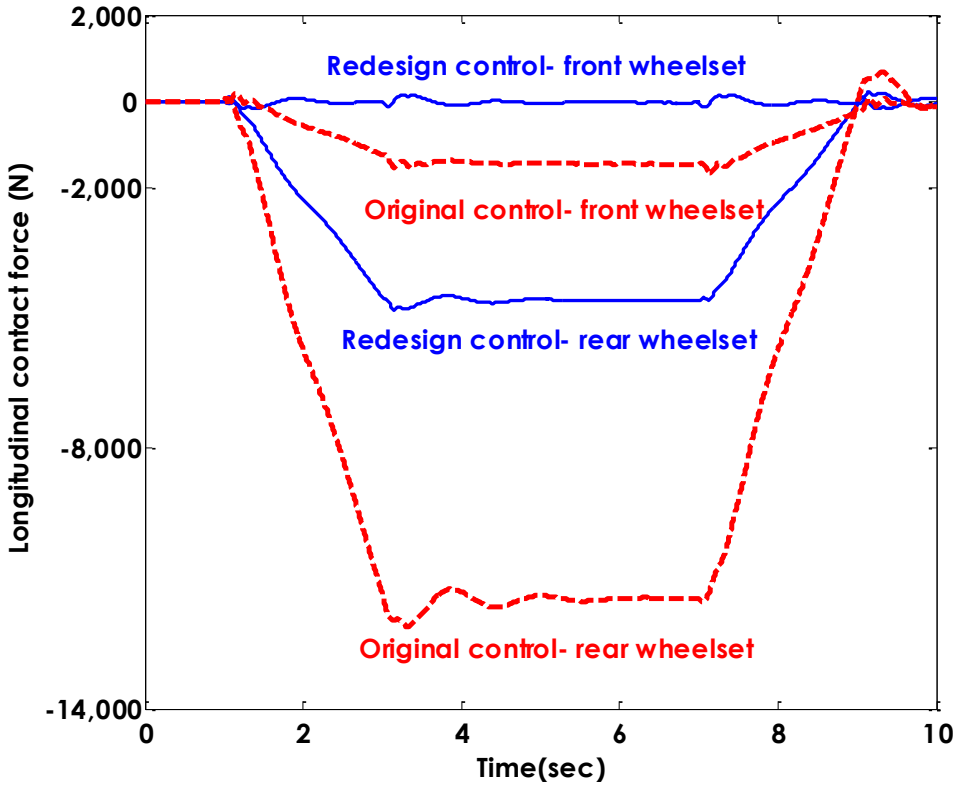

Figure 5-3: Longitudinal contact force in incident of trailing fail hard–original vs re-configuration control

The tuning of the re-configured controller is carried out also to ensure that the demanded control effort for control re-configuration is not significantly increased compared to the normal condition. As shown in Figure 5.4, the maximum control torque on the transition curve is nearly 180 (N.m) for the normal condition and it is at a similar level for the actuator fail-hard conditions.

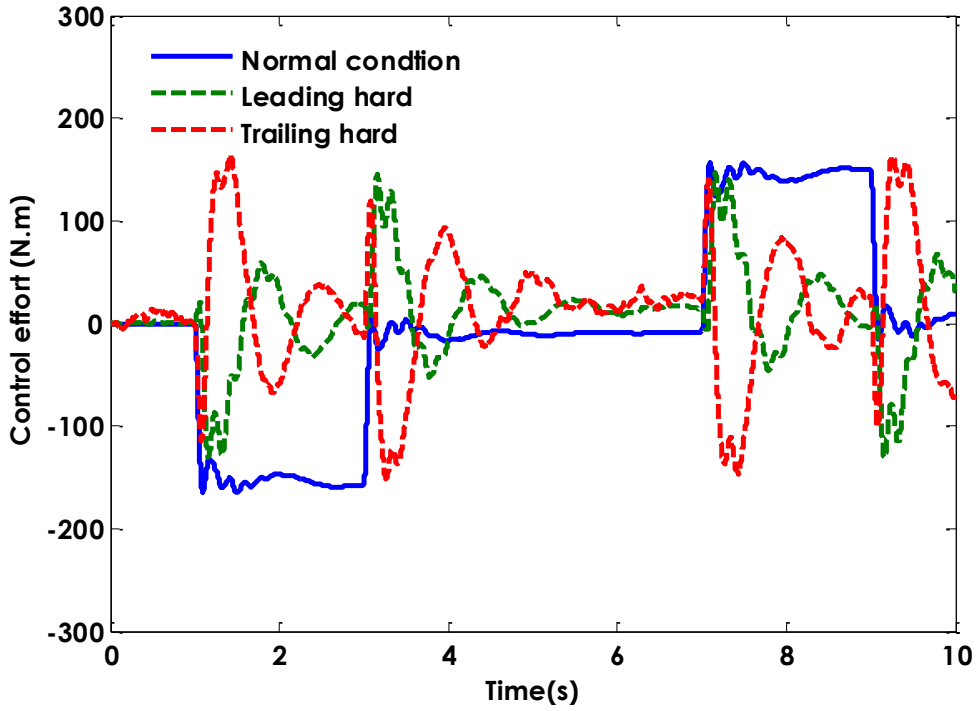

Figure 5-4: Control effort–normal condition vs re-configuration control (fail-hard)

The results in Table 5-1 compare the root mean square values of the control effort between the normal condition and fail-hard on the curve with the radius of 1250 (m) and the straight track with irregularities. They suggest that the demand for control effort is dominated by the requirements on a random track, which are much higher than that on the curved track. This is particularly the case for high-speed vehicles, as the effect of the track roughness becomes worse when the vehicle travelling speed increases. As indicated in Table 5-1, the required control effort for the actuator fail-hard can be smaller compared to the normal condition on a curved track; especially for the leading actuator fail-hard. However, on a random track the required control effort for the actuator fail-hard shows an increase compared to the normal condition.

Table 5-1: The requirements of the control effort between normal condition and fail-hard

Actuator condition/ failures		Actuator control effort (r.m.s)	
		Random track	***Curved track***
Normal condition		*2.4 (k.N.m)*	*78.5 (N.m)*
Fail-hard	***Front actuator***	*3.1 (k.N.m)*	*45.8 (N.m)*
	Rear actuator	*2.9 (k.N.m)*	*62.7 (N.m)*

5.2.2 Control re-configuration for actuator fail-soft

In the event of the fail-soft condition, the original active controller would not be able to stabilise the vehicle and the priority of the control re-configuration for the active control systems is then to restore stability, with the curving performance a secondary design issue (Mirzapour, Mei, & Xuesong, 2014). Equations (5.13)–(5.18) represent the dynamics of the wheelsets and bogie frame in the yaw direction in the presence of the fail-soft actuator for the leading and trailing wheelsets.

For leading actuator fail-soft:

$$\ddot{\psi}_{w1} = {}^{1}\!/_{I_w}\left[{}^{2f_{11}L_g^2}\!/_{V_s}\dot{\psi}_{w1} - {}^{2f_{11}\lambda L_g}\!/_{r_0}y_{w1} + {}^{2f_{11}L_g^2}\!/_{R_1} + {}^{2f_{11}\lambda L_g}\!/_{r_0}y_{t1}\right], \quad \textbf{Eq. 5-13}$$

$$\ddot{\psi}_{w2} = {}^{1}\!/_{I_w}\left[{}^{2f_{11}L_g^2}\!/_{V_s}\dot{\psi}_{w2} - {}^{2f_{11}\lambda L_g}\!/_{r_0}y_{w2} + {}^{2f_{11}L_g^2}\!/_{R_2} + {}^{2f_{11}\lambda L_g}\!/_{r_0}y_{t2} + \tau_{w2}\right], \quad \textbf{Eq. 5-14}$$

$$\ddot{\psi}_g = {}^{1}\!/_{I_g}\left[-2L_v^2C_s\dot{\psi}_g - 2L_v^2K_s\psi_g + L_vC_s\dot{y}_{w1} - L_vC_s\dot{y}_{w2} + L_vK_sy_{w1} - L_vK_sy_{w2} + \tau_{w2}\right)\right], \quad \textbf{Eq. 5-15}$$

For trailing actuator fail-soft:

$$\ddot{\psi}_{w1} = {}^{1}\!/_{I_w}[{}^{2f_{11}L_g^2}\!/_{V_s}\dot{\psi}_{w1} - {}^{2f_{11}\lambda L_g}\!/_{r_0}y_{w1} + {}^{2f_{11}L_g^2}\!/_{R_1} + {}^{2f_{11}\lambda L_g}\!/_{r_0}y_{t1} + \tau_{w1}],$$ **Eq. 5-16**

$$\ddot{\psi}_{w2} = {}^{1}\!/_{I_w}[{}^{2f_{11}L_g^2}\!/_{V_s}\dot{\psi}_{w2} - {}^{2f_{11}\lambda L_g}\!/_{r_0}y_{w2} + {}^{2f_{11}L_g^2}\!/_{R_2} + {}^{2f_{11}\lambda L_g}\!/_{r_0}y_{t2}],$$ **Eq. 5-17**

$$\ddot{\psi}_g = {}^{1}\!/_{I_g}[-2L_v^2C_s\dot{\psi}_g - 2L_v^2K_s\psi_g + L_vC_s\dot{y}_{w1} - L_vC_s\dot{y}_{w2} + L_vK_sy_{w1} - L_vK_sy_{w2} - \tau_{w1}],$$ **Eq. 5-18**

The control input of either τ_{w1} or τ_{w2} represents the torque in the yaw direction produced by the remaining operational actuator, where the input from the failed actuator is set to zero to represent the fail-soft condition. The other aspects of the state-space model for the vehicle dynamics are the same as in the fail-hard condition as defined in Equations (5.9) and (5.10) and the values of the weighting matrices given in Equations (5-19) and (5-20) have been chosen manually to minimise the control effort and the contact forces (Mirzapour, Mei, & Hussain, 2012).

Leading actuator fail-soft:

$$Q = diag(40,0.01,900,0.01,8\times10^4);$$
$$R = 10^{-12}$$ **Eq. 5-19**

Trailing actuator fail-soft:

$$Q = diag(900,0.01,40,0.01,5.9\times10^4);$$
$$R = 10^{-12}$$ **Eq. 5-20**

The vehicle stability is guaranteed as the design formulation for the full state feedback and optimal control takes into account the reduction of control input from two to one (Mirzapour, Mei, & Hussain, 2012). Note that both the open circuit and short circuit will be stabilised with the same control gains as the difference in the effect of the two types of faults is trivial

due to the low velocity operation of the actuators and hence relatively low level of the back e.m.f produced in the case of short circuit. Table 5-2 shows that the eigenvalues of the vehicle dynamics in the event of the leading actuator fail-soft (open-circuit) are well damped by the re-designed control (for re-configuration), where the parameter values given in Appendix B are used. Similar results for the short circuit and the trailing actuator fail soft are also obtained.

Table 5-2: Eigenvalue analysis of the vehicle dynamic modes for re-configuration control

Eigenvalues	Speed of 50 (m/sec)	
	Damping (%)	Frequency (Hz)
Wheelset high frequency	93	106.71
	93	106.71
	98	113.7
	98	113.7
Bogie	28	48.4
	28	48.4
	33	10.8
	33	10.8
Kinematic mode 1	18	7
	18	7
Kinematic mode 2	14	5.8
	14	5.8
Body of vehicle	20	0.91
	20	0.91

Figure 5.5 gives the longitudinal forces at the wheel–rail contact patches for the front and rear wheelsets in the event of open circuit and short circuit at the leading actuator, where RCO1 and RCO2 show the performances of the leading and trailing wheelsets of the re-configured controller in the event of open circuit; RCS1 and RCS2 show the performance of the leading

and trailing wheelsets of the re-configured controller in the event of short circuit; and NC1 and NC2 denote the front and rear wheelsets in the normal condition where both actuators are functioning. The simulation results reveal that, when the controller is re-configured with one control input, good steering performance can be achieved on the curved track. The contact forces at the leading wheelset are almost zero and very similar to that in the normal condition which is also almost zero. Interestingly, however, the tuning of the controller for a balance between the control effort and the curving appear to lead to some increase of the contact forces at the rear wheelset (with the healthy actuator) in comparison with the normal condition.

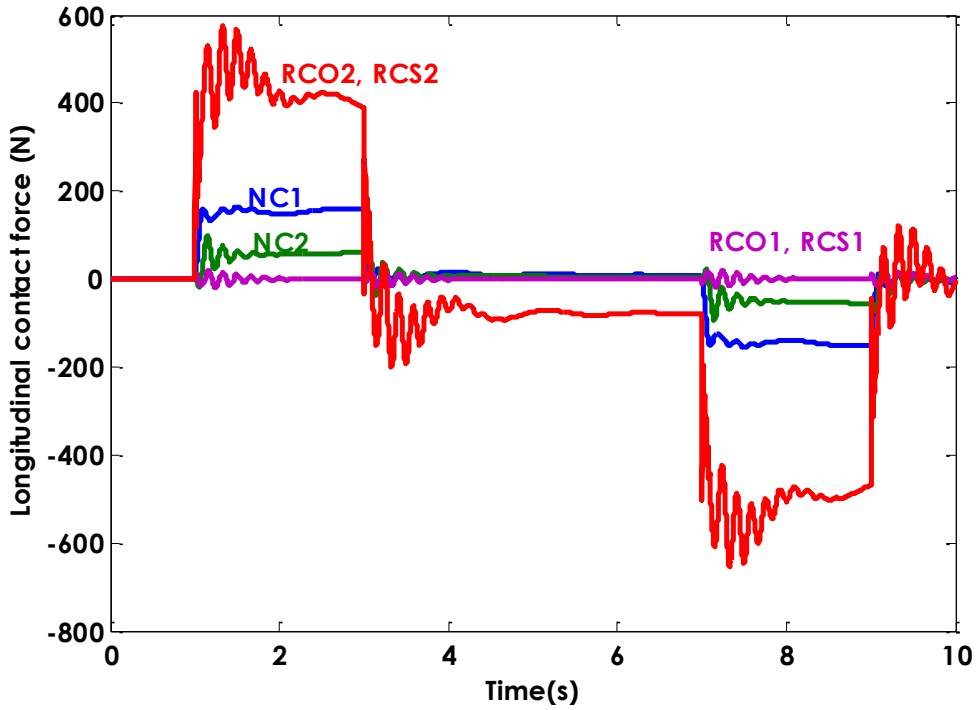

Figure 5-5: Longitudinal contact force of leading fail soft–normal condition vs re-configuration control

However, the simulation analysis shows that when the trailing actuator fails in soft mode, the increase of the longitudinal contact force which occurred to the leading wheelset (operated actuator) is approximately two times higher compared to the contact force of the trailing wheelset when the soft failure is apparent at the leading actuator (Figure 5.6).

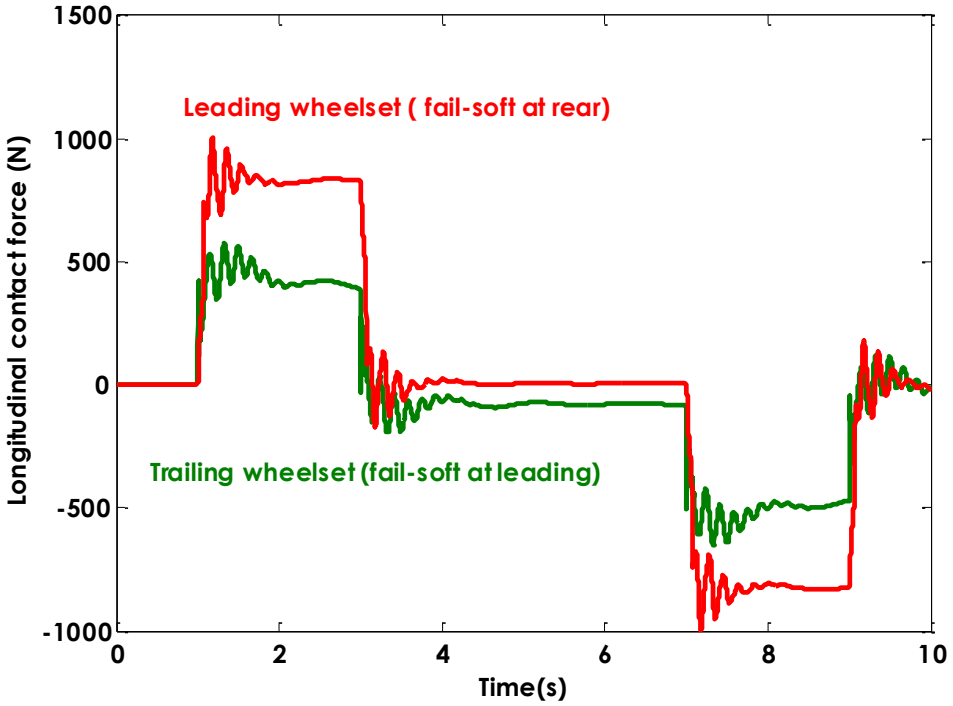

Figure 5-6: Longitudinal contact force–actuator (fail-soft) with re-configuration control

Further investigation reveals that the lateral contact forces of the two wheelsets are not affected once the stability is restored by the reconfigured control, and they remain almost identical in either the normal condition or actuator fail-soft as shown in Figure 5.7.

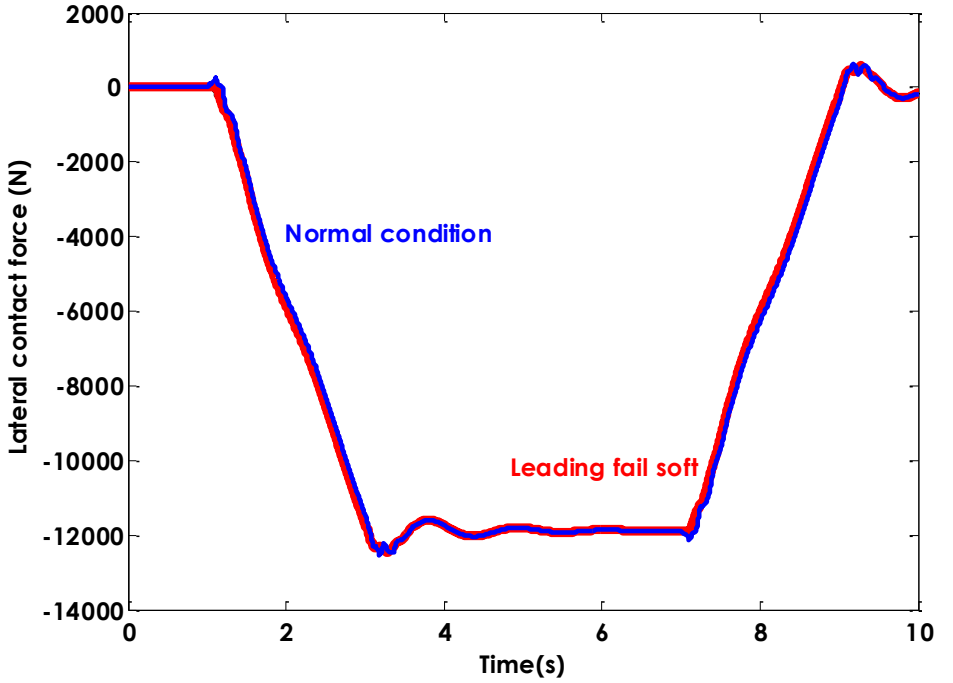

Figure 5-7: Lateral contact force–leading actuator (fail-soft) vs normal condition

The control torque required to maintain stability and good curving performance with a single actuator in the event of the other actuator failing soft is expected to be higher in comparison to the normal condition. Figure 5.8 compares the actuator torque demand between the normal condition (NC) and when one of the actuators fails in the soft mode (i.e. open and short ciruites) on the curved track, which suggests that the required torque demand in the event of trailing fail-soft (TFS) may be two times higher than the normal condition and leading fail-soft (LFS).

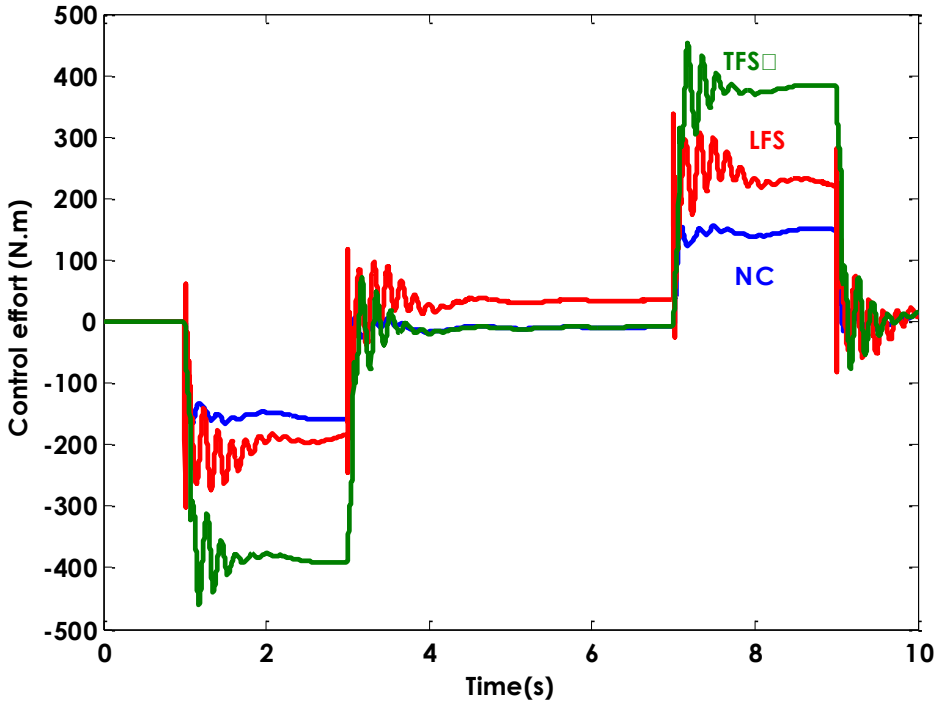

Figure 5-8: Actuator torque demand–normal condition vs re-configuration control (fail-soft)

The results in Table 5-3 compare the requirements of the control effort between the normal condition and actuator fail-soft on both the curve with the radius of 1250 (m) and the straight track with random roughness. It is clear that the demand for control effort is dominated by the requirements on the random track, which is consistent with the case of fail-hard condition but at a much higher level (at 13 k.N.m and 8.6 k.N.m for the leading and trailing actuator fail-soft). An important observation drawn from this is that the fail-soft (i.e., short circuit and open circuit) condition is the most demanding to provide the stability control in term of

actuator output because the need to provide stability and cope with the high frequency components of the track irregularities especially when the vehicle travelling speed increases.

Table 5-3: The requirements of the control effort between normal condition and fail-soft

Actuator condition/ failures		**Actuator control effort (r.m.s)**	
		Random track	***Curved track***
Normal condition		*2.4 (k.N.m)*	*78.5 (N.m)*
Open and short circuits	***Front actuator***	*13 (k.N.m)*	*141 (N.m)*
	Rear actuator	*8.6 (k.N.m)*	*240 (N.m)*

5.3 Robustness of the Control Re-configuration

The developed control re-configuration is required to be robust against vehicle parameter variations in the system such as changes due to the non-linearity profile at wheel–rail interface in particular the conicity of the wheelsets at the contact point with the rail surface (Mei & Goodall, 2001). It has been shown previously that the proposed FDI schemes can provide robust detection and isolation of the actuator malfunction. Therefore, the robustness of the re-configured controllers should also be thoroughly investigated in order to ensure that the fault tolerant strategy for the active wheelset control will also work reliably when the vehicle parameters deviate from their nominal values (Pearson, Goodall, Mei, & Himmelstein, 2004). The robustness of the re-configuration control is assessed against the variation of the wheelset conicity in the typical range of 0.15 and 0.35. Figure 5.9 shows the level of the damping for the re-configured controllers (for fail-hard) over a range of conicities between 0.1 and 0.4, where a minimum damping of 8% and 5.65% at the worst case of the conicity of 0.4 is achieved for the leading and trailing actuator fail-hard (LH, TH)

respectively. This confirms the previous observation that the stability is not a primary concern for the fail-hard conditions.

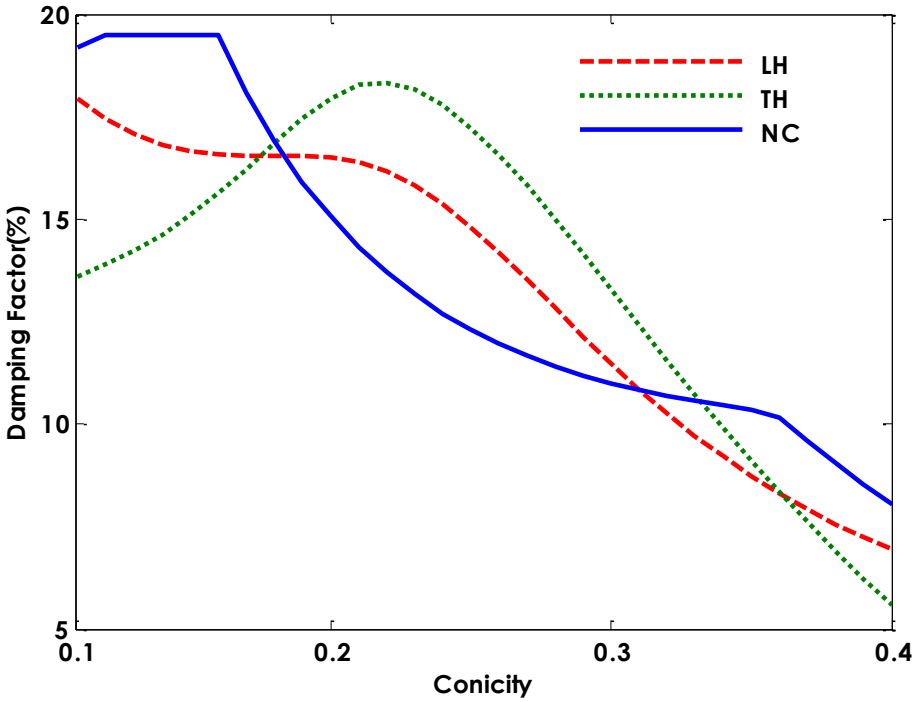

Figure 5-9: Fail-hard minimum damping vs conicity

However, this is a more serious concern in the event of fail-soft (i.e., open and short circuit) as this type of failure leads to vehicle instability. Figure 5.10 shows the minimum damping with the re-configured controller when the leading actuator fails in the open-circuit mode. It reveals that the re-configured control (tuned manually) is only able to stabilise the vehicle for the conicity range between 0.18 and 0.25.

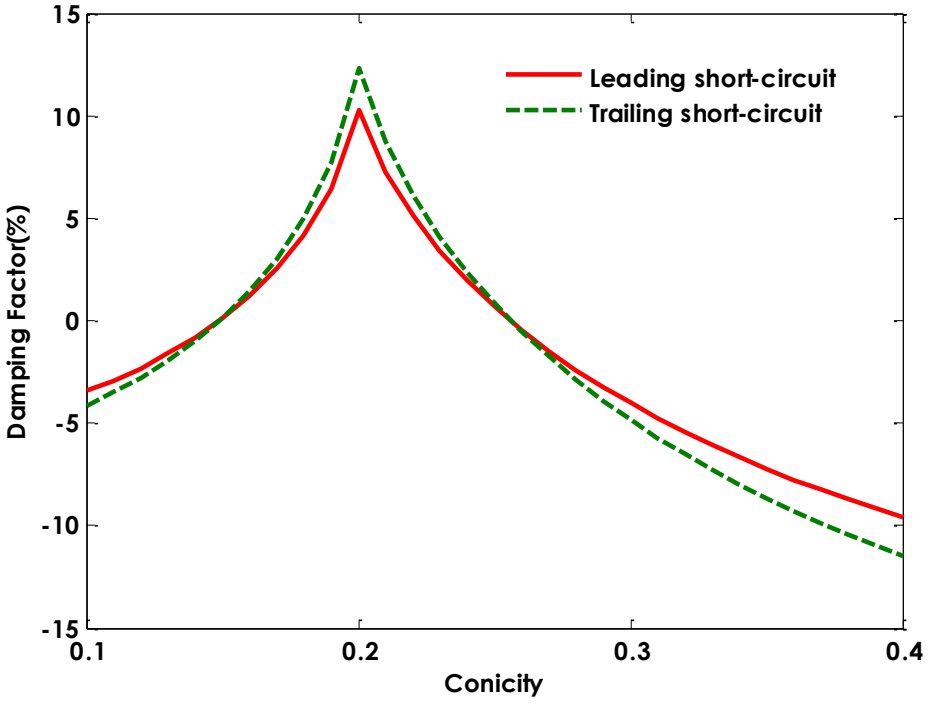

Figure 5-10: Short-circuit minimum damping vs conicity

In this study, the genetic algorithms (GA) are also considered for the purpose of optimisation in order to search for the best control gains to ensure that the re-configured controller can provide good stability over a range of conicities. The GA is an optimisation technique that searches globally based on the principle of biological evolution, and operates on a population which is built up with many individuals to evolve under specified selection rules that minimise the cost function and satisfying constraint simultaneously (Haupt & Haupt, 2004, p. 36). One of the most important issues in the use of GA is the definition of the objective functions (Mei & Goodall, 2000b). The objective in this study is to minimise the largest root mean square (RMS) value of the control effort of the healthy actuator within the constraint of the minimum damping above 5% at three different levels of conicity, as shown in Equation (5.21).

$$Obj = \min\left(\sqrt{\sum_{1}^{N}\frac{\tau^2{}_w}{N}}\right) \quad \textbf{Eq. 5-21}$$

Subject to;

$$Sub = max\left(\lambda_{0.1} \geq 5\%;\quad \lambda_{0.2} \geq 5\%;\quad \lambda_{0.4} \geq 5\%\right)$$

Where ($\lambda_{0.1}$, $\lambda_{0.2}$, $\lambda_{0.4}$) represent the conicity at 0.1, 0.2 and 0.4, respectively, and *N* is the index of the variable's time response vectors over the period of the simulation. Although a real wheelset has significant conicity variations between 0.1 and 0.6 especially if flange contact occurs. But, the study used the linearised models of the wheel-rail contact mechanism due to the fact the nonlinearities are fairly small unless there is flange contact, a condition which actively controlled wheelset avoids. Therefore, the choice of conicity between 0.1 and 0.4 (worst case) can ensure that the re-designed controllers are robust against the parameter variations at wheel-rail interface especially during negotiation of curves. The simulation analysis shows that the GA tuned control gains can improve the robustness of the re-configuration controller at different conicities. Figure 5.11 compares the minimum damping of the two re-configuration controllers when the leading actuator fails soft in open circuit. It clearly reveals that the GA tuned controller for reconfiguration can provide stability for the vehicle at different conicities.

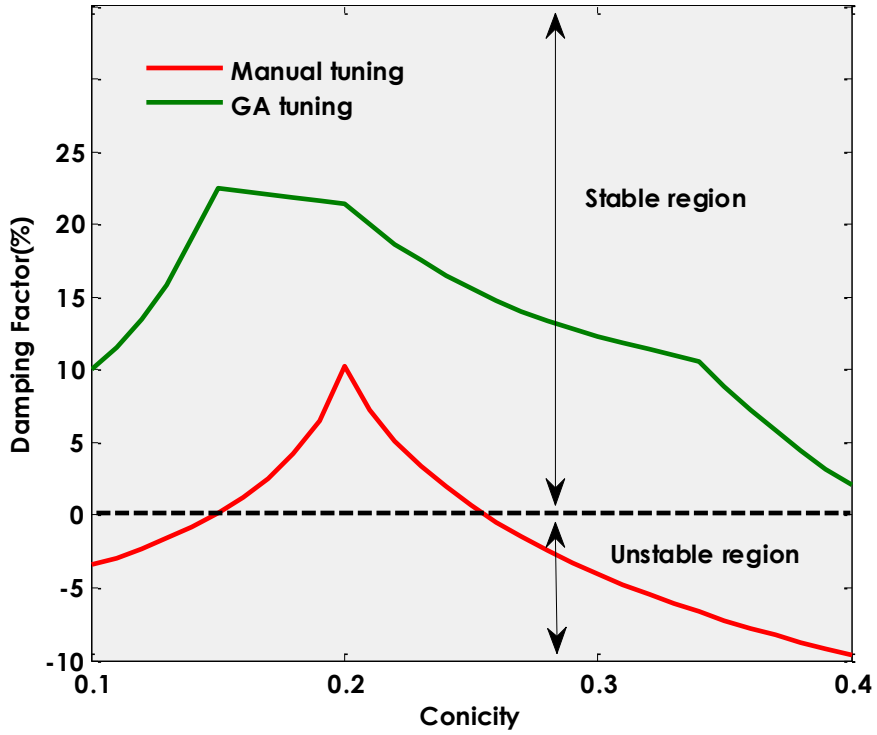

Figure 5-11: Minimum damping with two different re-tunings

Although stabilisation becomes a possibility through the GA optimisation, the control effort significantly increases compared with the optimal approach that is designed with the nominal value. Table 5-4 indicates the required control effort with GA approaches to maintain stability over a range of conicities. It demonstrates that the maximum control effort with the GA approach that can guarantee the stability reaches nearly 80 (k.N.m) on the curved track, whereas it is increased to nearly 300 (k.N.m) on the random track.

Table 5-4: The required control effort with GA

Location of fail soft (open & shot circuits)	Track input	Actuator control effort (k.N.m)
	Random	*300.1*
Front actuator		
	Deterministic	*80*
	Random	*300.4*

Rear actuator			
	Deterministic	*80.8*	

Therefore, one of the critical design challenges is that the actuation requirement significantly increases in order to guarantee the robustness of the re-configuration controller. This is because the effects of the conicity on the dynamic properties of a rail vehicle in the scenarios of short-circuit and open-circuit actuator can be significant. Future research should attempt to ensure that the re-configuration controller meets the robust requirement without having substantial adverse impact on the actuator size. Previous research in (Charles, Goodall , & Dixon , 2008) presented an approach based around an Extended-Kalman Filter (EKF) method that includes conicity as an extra estimation parameter, although the drawback of this approach is that it would increase the complexity due to the complex wheel–rail geometry. The other approach that might be considered is to include extra measurements as part of the feedback to improve robustness (Mirzapour, Mei, & Xuesong, 2014). However, both approaches need to be investigated for future development in order to implement the fault tolerance technique for actively controlled wheelsets to justify the safety and reliability of this new technology in the railway industry.

5.4 Integrated FDI and Control Re-configuration

It has been shown that the proposed re-configuration control can maintain stability and good curving performance. However, it is necessary to integrate the re-configured controllers with the FDI schemes in order to evaluate fully the effectiveness of the overall fault tolerant strategy in the different actuator failure modes. Both the vehicle model based schemes and local actuator model based schemes for the fault detection and isolation are considered for the

integration with the control reconfiguration strategies to assess the advantages and disadvantages of each fault detection scheme.

5.4.1 Fail-hard

In the fail-hard conditions, the two different FDI schemes (i.e., the vehicle-based approach and actuator-based approach) provide similar results when integrated with re-configured control. Figures 5.12 and 5.13 compare the generated longitudinal contact forces at the leading and trailing wheelsets and Figures 5.14 and 5.15 show the generated lateral contact forces with two different FDI schemes; where the front actuator fails hard at the time of 5 (s) on a curved track (without track irregularities). In each figure FDI 1 denotes the fault detection and isolation scheme through vehicle model based approach (chapter 3) and FDI 2 represents the fault detection and isolation through actuator model-based approach (chapter 4). It is evident that either FDI approach detects the fault quickly to allow the re-configuration in the system for the re-designed controller to take corrective actions. It is apparent from Figures 5.12 and 5.13 that the longitudinal forces at the trailing wheelset can be significantly reduced compared to the leading wheelset where the failure occurs (locked actuator). Meanwhile, the lateral contact forces for the trailing wheelset are increased compared to the leading wheelset in order to compensate the centrifugal forces around the curved track.

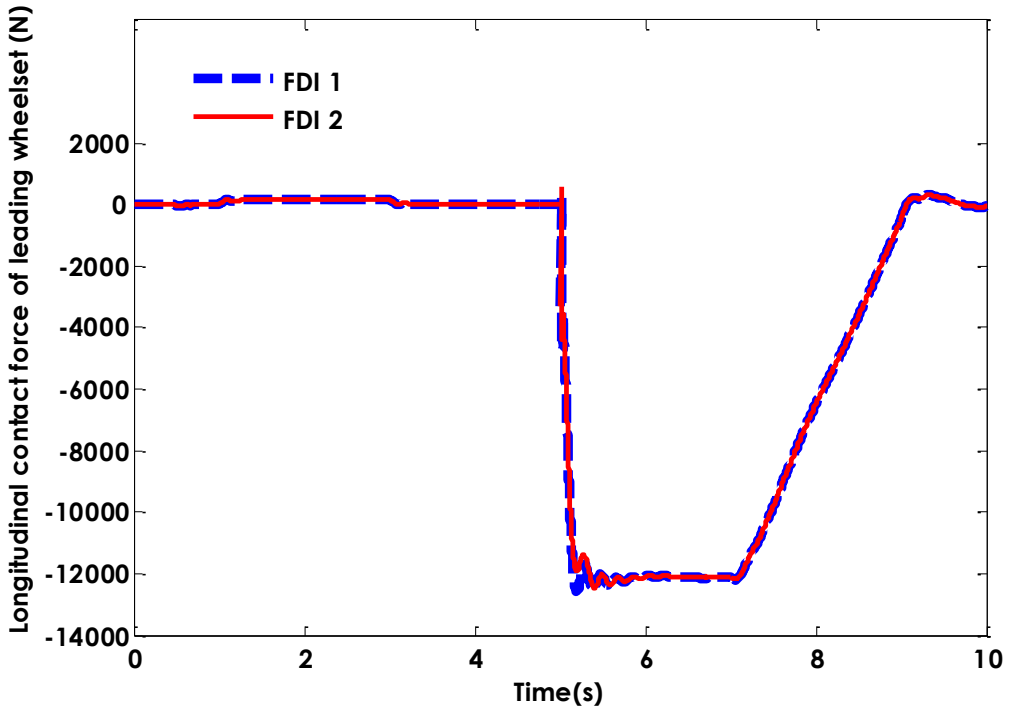

Figure 5-12: Longitudinal contact forces leading wheelset (curved track) –FDI approaches 1 & 2 (fail-hard)

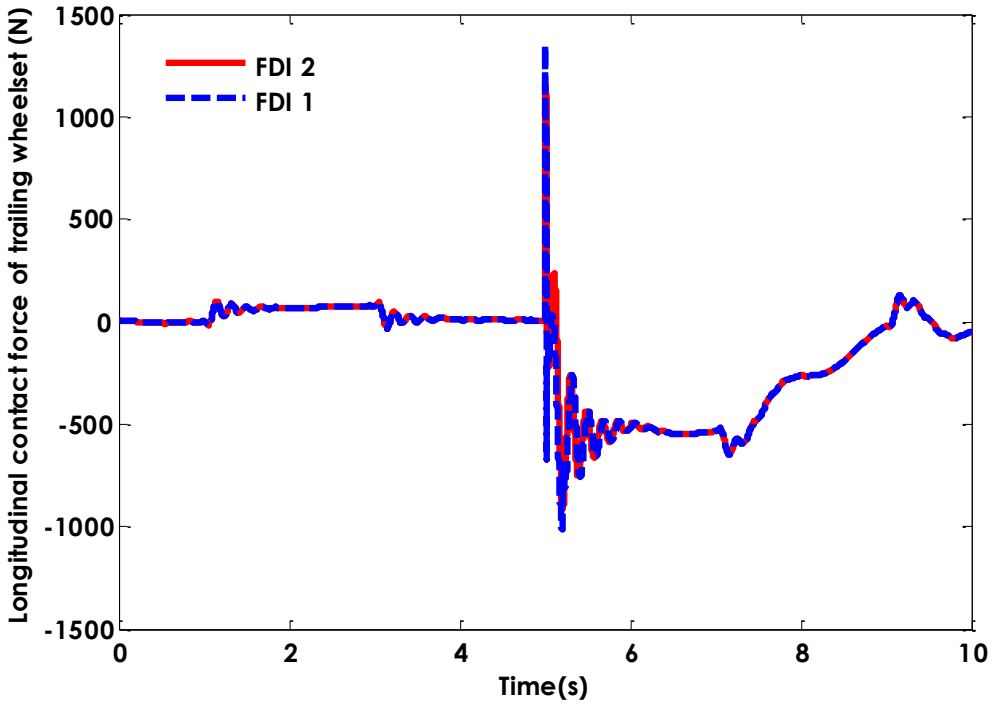

Figure 5-13: Longitudinal contact forces trailing wheelset (curved track) –FDI approaches 1 & 2 (fail-hard)

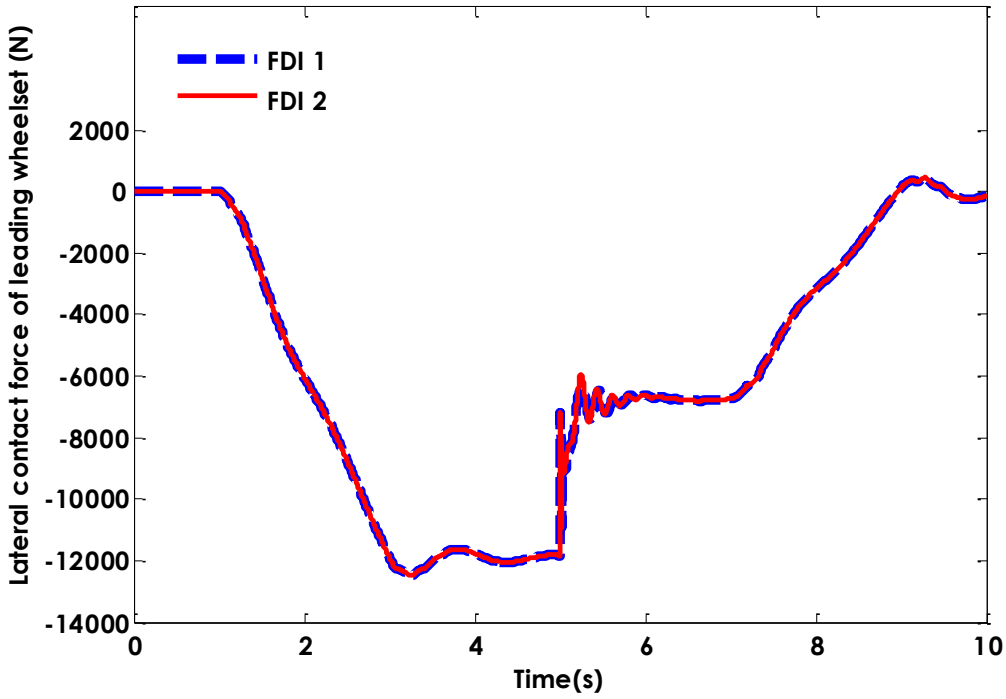

Figure 5-14: Lateral contact forces leading wheelset (curved track) –FDI approaches 1 & 2 (fail-hard)

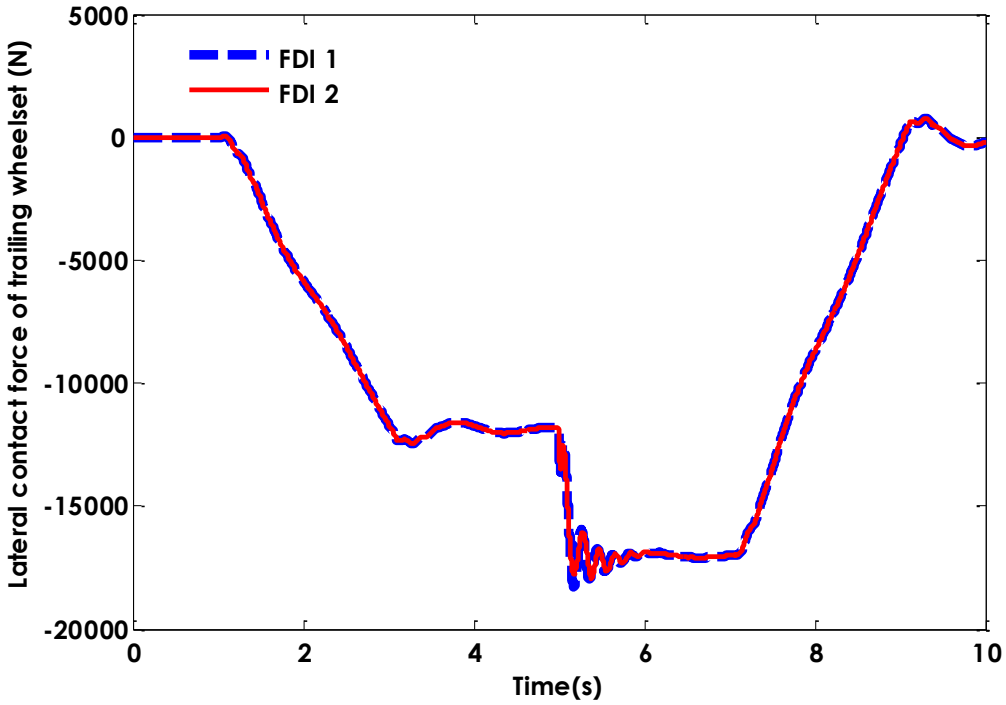

Figure 5-15: Lateral contact forces trailing wheelset (curved track) –FDI approaches 1 & 2 (fail-hard)

Figures 5.16 and 5.17 compare the generated longitudinal contact forces at the leading and trailing wheelsets and Figures 5.18 and 5.19 reveal the generated lateral contact forces with

two different FDI schemes, when the front actuator is locked at the time of 1 (s) on a straight random track. Figures show that the performance of the fault tolerant strategy with the two different FDI schemes is almost identical. It can be seen from the figures that the longitudinal contact forces at the rear wheelst (Figure 5.17) are approximately half of those at the leading wheelset (Figure 5.16). This is due to the fact that the re-configured controller takes action at the trailing wheelset and therefore reduces the contact forces in the longitudinal direction compared to the leading wheelet where the wheelset is locked due to the actuator failure. On the other hand, the lateral contact force at the trailing wheelset is higher in comparison to the leading wheelset.

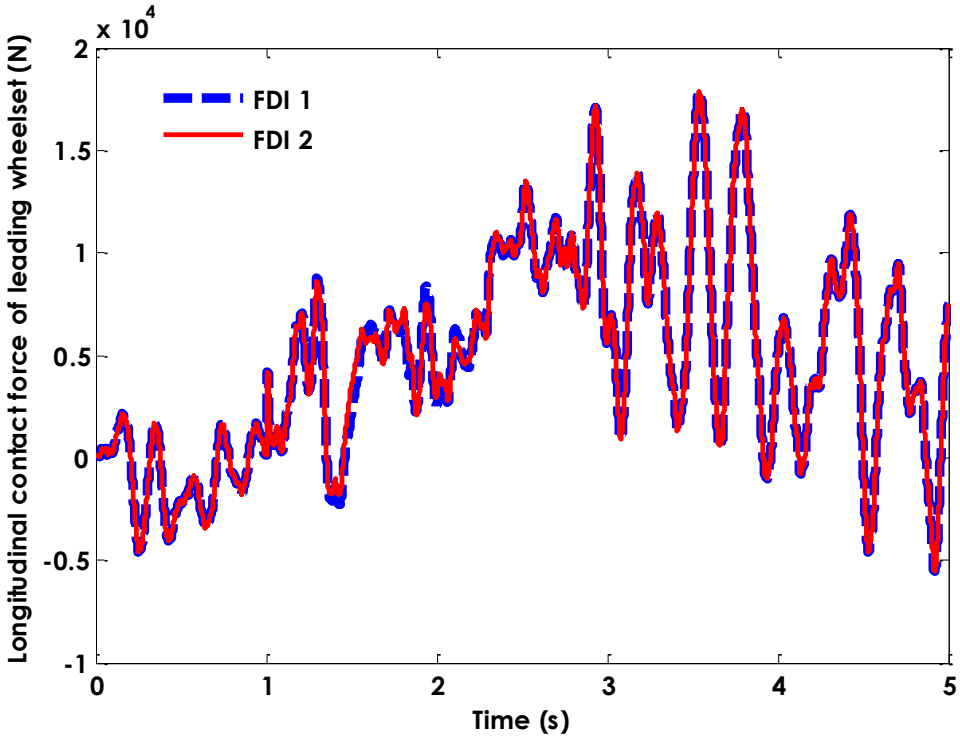

Figure 5-16: Longitudinal contact forces leading wheelset (random track) –FDI approaches 1&2(fail-hard)

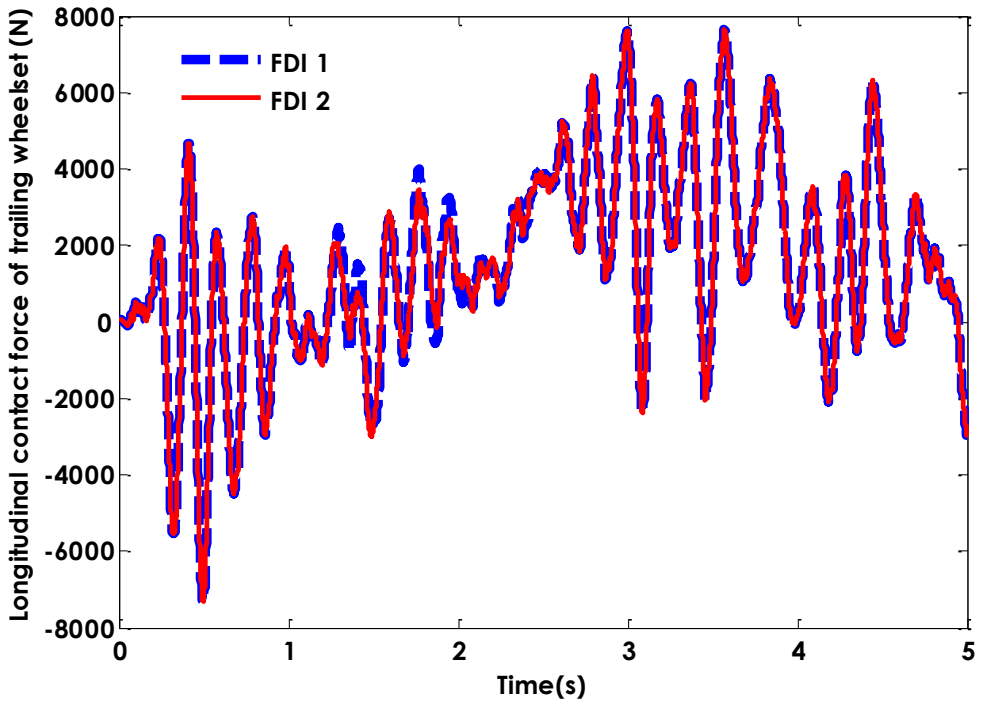

Figure 5-17: Longitudinal contact forces trailing wheelset (random track) –FDI approaches 1&2(fail-hard)

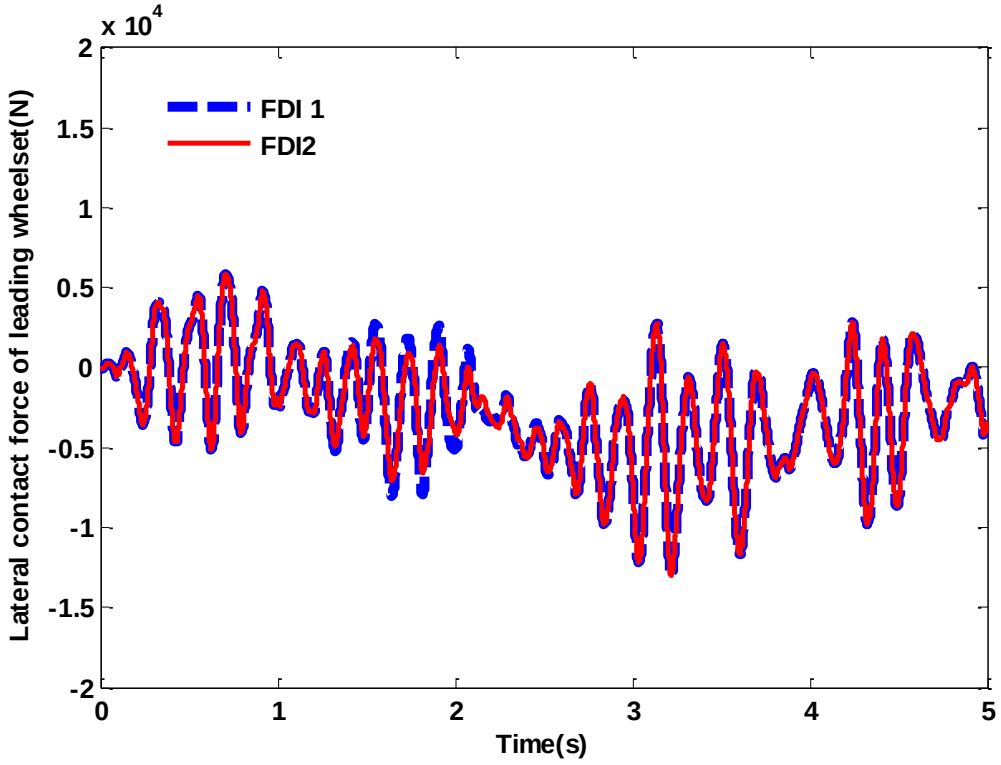

Figure 5-18: Lateral contact forces leading wheelset (random track) –FDI approaches 1 & 2 (fail-hard)

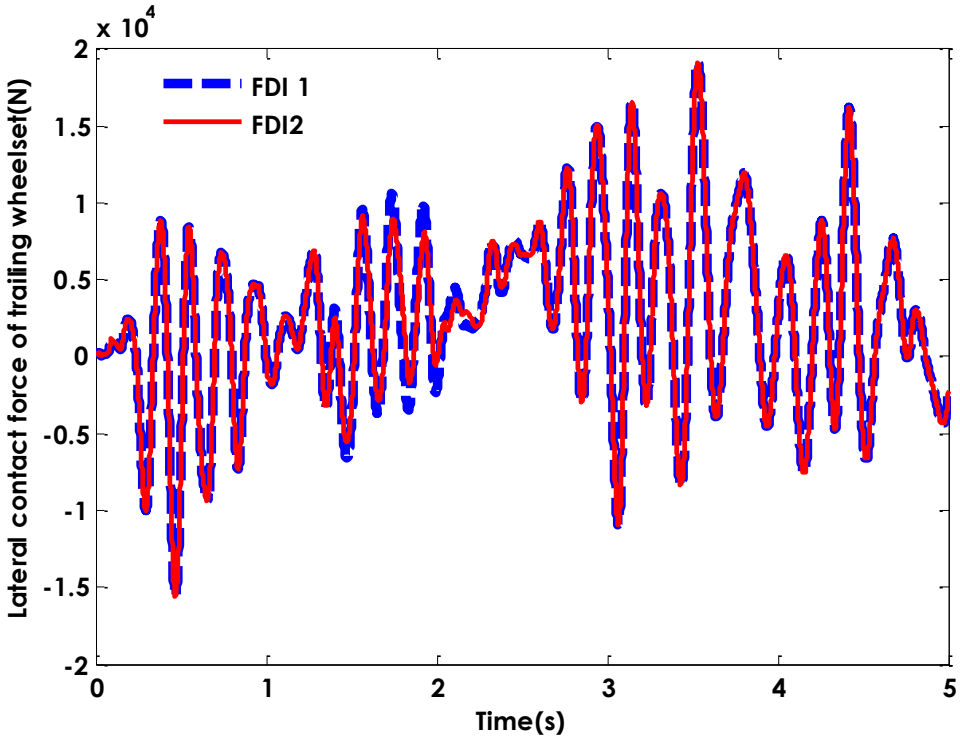

Figure 5-19: Lateral contact forces trailing wheelset (random track) –FDI approaches 1 & 2 (fail-hard)

5.4.2 Fail-soft

However, the two FDI approaches have a significantly different effect on the performance of the fault tolerant strategy in the event of actuator open and short circuit. Figure 5.20 shows the longitudinal contact force of the rear wheelset when the short circuit occurs at the front actuator at the time of 5 (s) on a curved track. The vehicle model based FDI scheme (FDI 1) shows that it takes about 1.5 (s) for the control re-configuration to take place and there is a large increase in the contact force to cope with the identified fault.

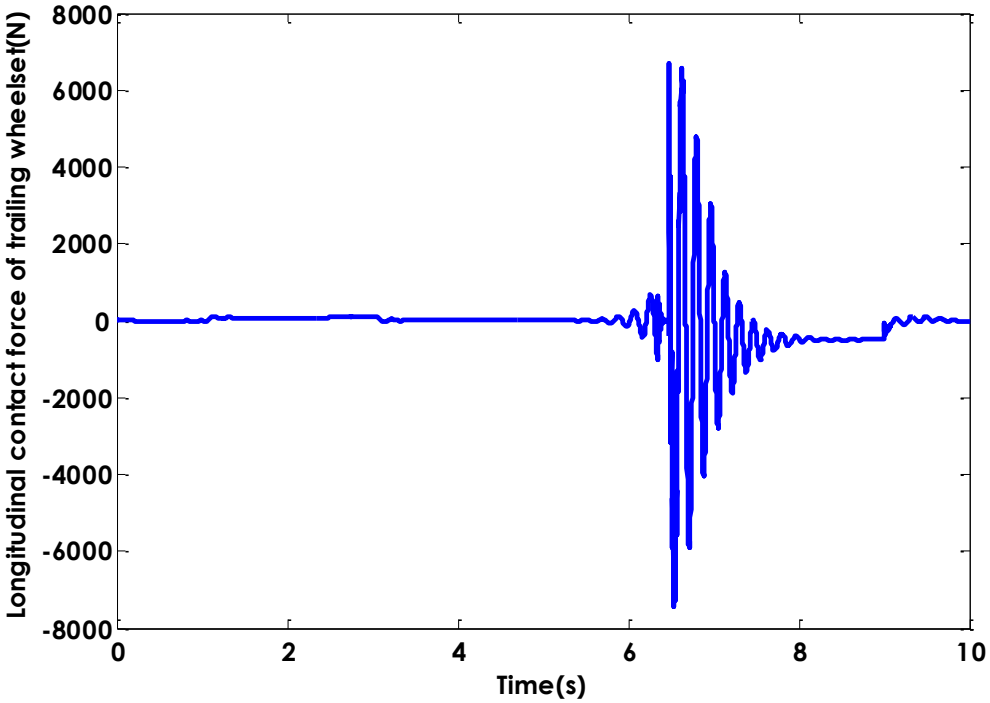

Figure 5-20: Longitudinal contact force trailing wheelset (curved track) –FDI approach 1 (short-circuit)

The actuator model-based approach (FDI 2) appears to provide a much better performance for a fault tolerant strategy due to its faster fault detection. Figure 5.21 shows that the reaction time of the fault tolerant control is much shorter (less than 0.5s) and the contact force for the transition time is significantly lower. Figure 5.22 compares the lateral contact forces at the trailing wheelsets with the two different fault detection approaches, and clearly reveals that the lateral contact force is also significantly lower when the fault tolerant strategy is implemented than with FDI 2 (actuator model-based).

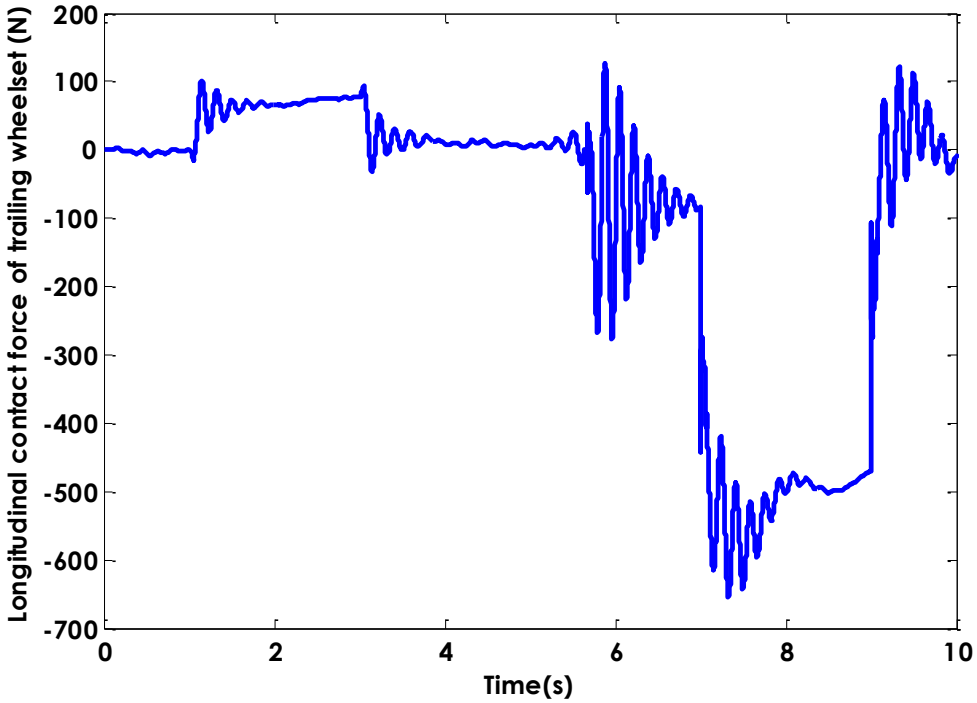

Figure 5-21: Longitudinal contact force trailing wheelset (curved track) –FDI approach 2 (short-circuit)

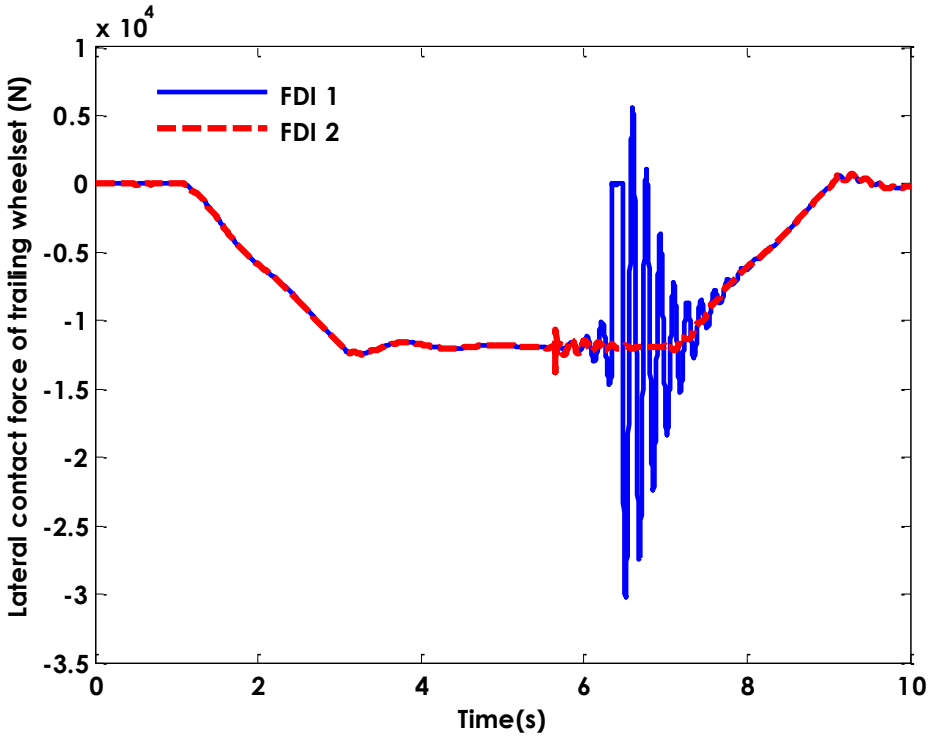

Figure 5-22: Lateral contact forces trailing wheelset (curved track) –FDI approaches 1&2 (short-circuit)

Figure 5.23 indicates how the different FDI schemes would affect the control effort. As the figure shows, the control effort for FDI approach 1 (FDI 1) is significantly higher compared

to the FDI approach 2 (FDI 2) due to the fact that the former required more time to cope with identified fault compared to the latter as already shown in Figure 5.20.

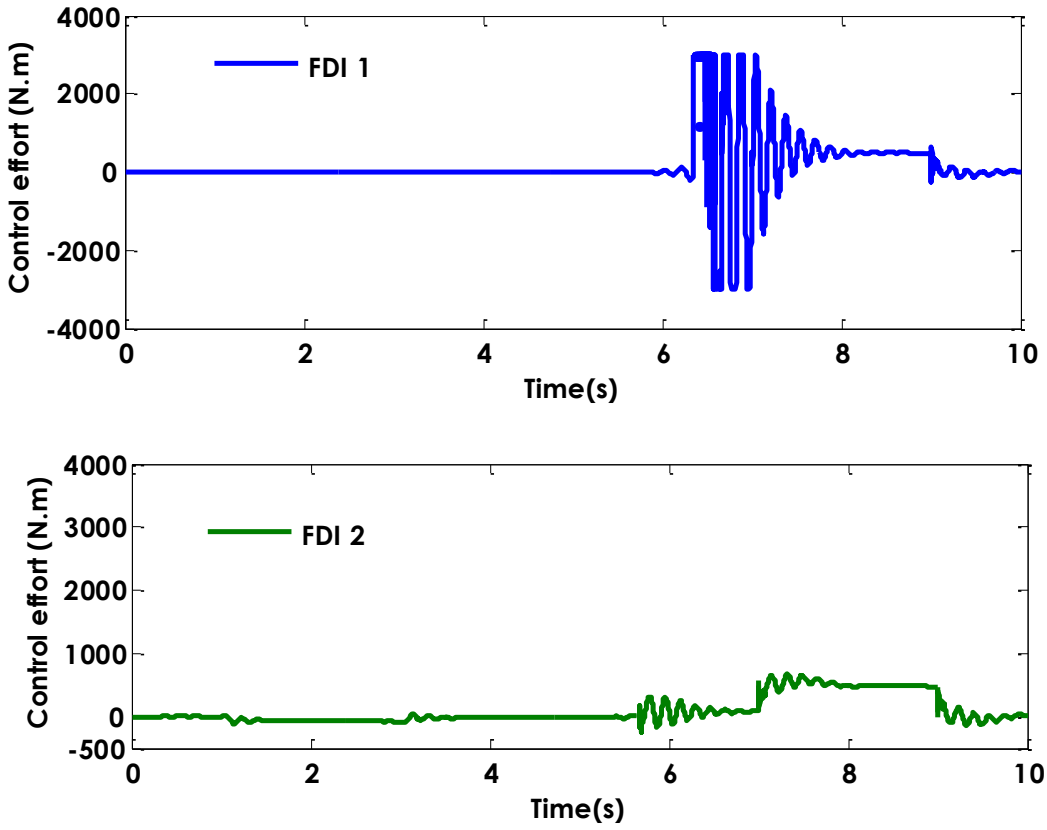

Figure 5-23: Control effort (curved track) –FDI approaches 1 & 2 (short-circuit)

Figures 5.24 and 5.25 show the generated contact forces in the longitudinal and lateral directions when the short circuit occurs in the front actuator at the time of 1 (s) on a random track. They clearly show that the generated contact forces when the fault tolerant strategy is implemented with the actuator model-based approach (FDI 2) are significantly lower when compared to FDI 1 (vehicle model-based), as the fault detection scheme through FDI 2 provides a faster fault detection compared to FDI 1. Similar results are obtained in the event of open circuit and actuator failure at the rear wheelset.

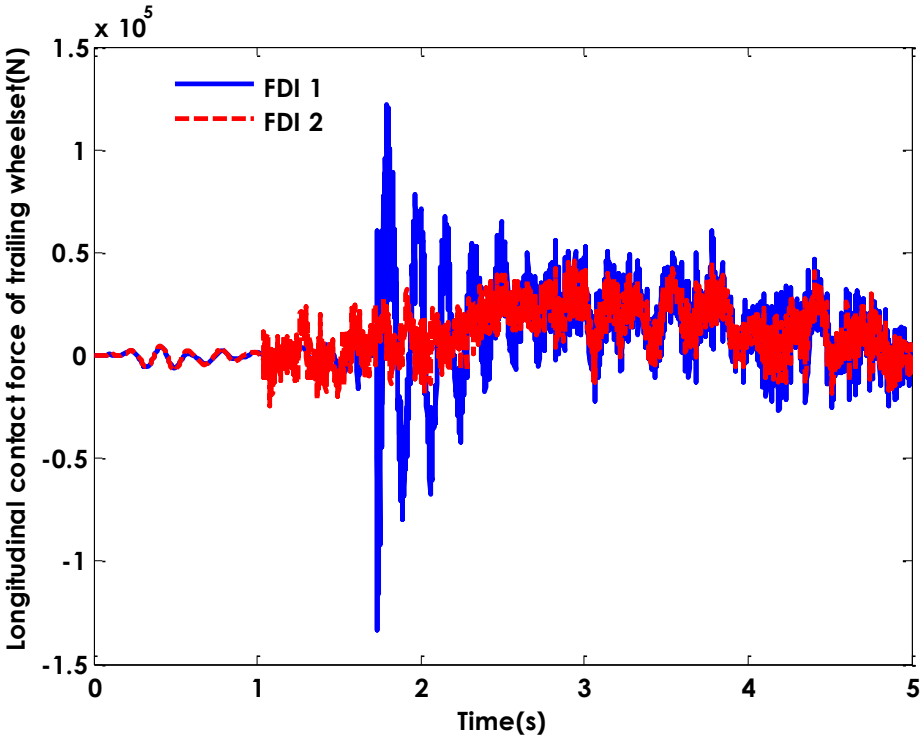

Figure 5-24: Longitudinal contact force (random track) –FDI approaches 1& 2 (short-circuit)

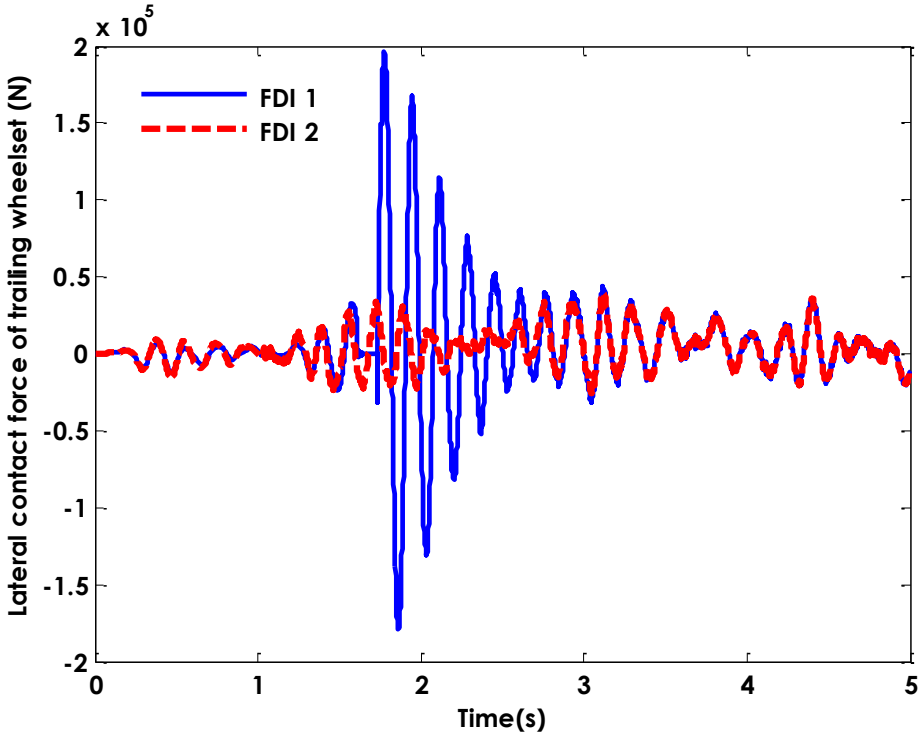

Figure 5-25: lateral contact force (random track) –FDI approaches 1 & 2 (short-circuit)

The difference in the detection time between the two FDI schemes which will have an effect on the wheelset movement in the lateral and yaw directions. Figure 5.26 shows the lateral

displacement of the front and rear wheelsets when the trailing actuator fails in open circuit at the time of 5 (s), where approach 1 is used. It clearly reveals that the slow fault detection would increase the oscillation; whereas the fault tolerant strategy through approach 2 would substantially reduce such oscillation as it can cope quickly with the faulty actuator, as shown in Figure 5.27.

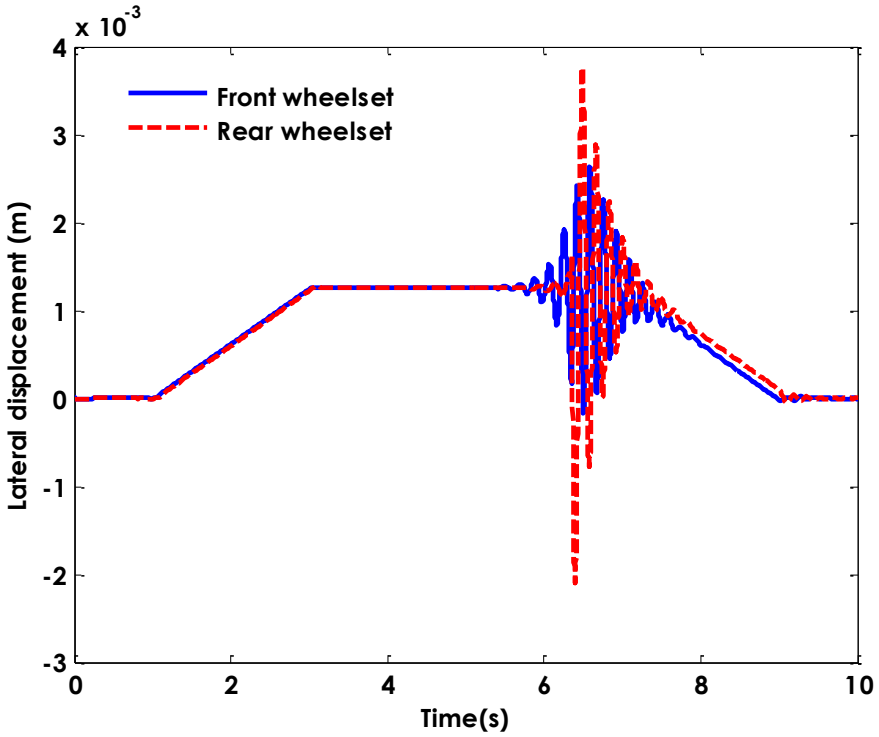

Figure 5-26: Lateral displacement–FDI approach 1 (open-circuit)

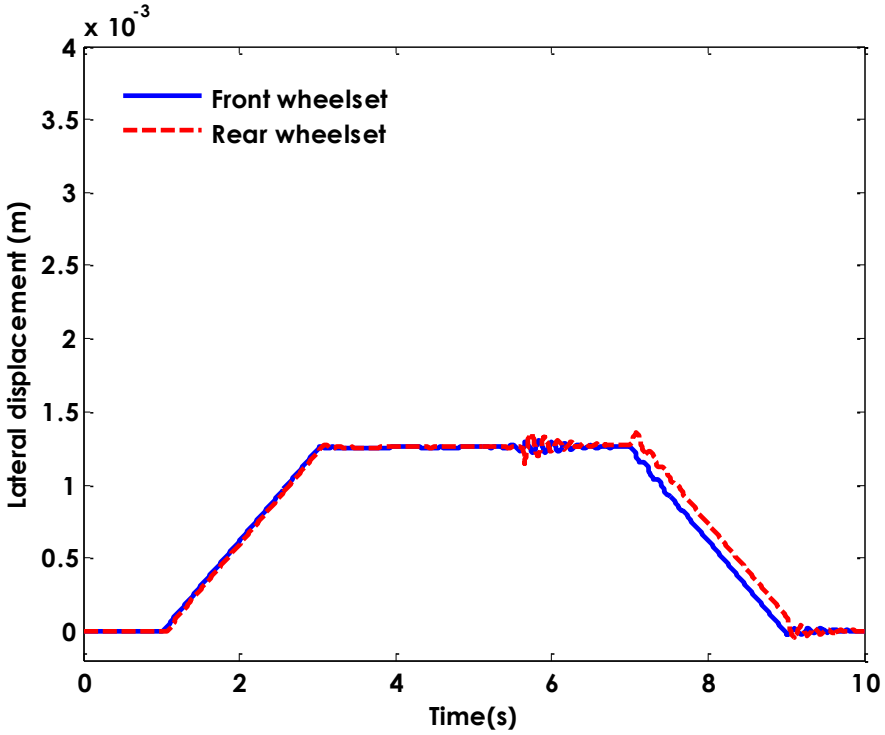

Figure 5-27: Lateral displacement–FDI approach 2 (open-circuit)

5.5 Summary

It has been demonstrated that in the scenario of fail-hard the stability is not the main concern, and a primary objective for the control re-configuration is to minimise the contact forces at the wheel–rail interface in order to reduce the wear and rolling contact fatigue, especially during curving. Furthermore, in the event of fail-soft (i.e., short circuit or open circuit), the main objective of the re-configuration control is to maintain the vehicle stability. It has been shown that in the event of actuator failure, the number of control inputs is reduced from two to one (as the number of actuators reduces); however, the feedback signals provided by the stated observer remain the same. Therefore, the control re-configuration can be achieved by re-tuning the control gains of the proposed optimal controller through weighting matrices for different failure modes. In addition, the actuator requirements for the re-configuration control have been demonstrated. This shows that the requirements of control effort for the actuator fail-hard do not show a significant increase compared to the normal condition, whereas the

demand of control effort significantly increases in the event of open and short circuits compared to the normal condition. Furthermore, the robustness of the re-configuration controller has been assessed at the variation of the wheelset conicity in a typical range of 0.1 and 0.4. This was a particular concern in the case of fail-soft (in either open circuit or short circuit mode), whereas it is less of a problem for the fail-hard case. This reveals that in the event of fail-soft, the re-configuration control is only able to stabilise the vehicle for the conicity between 0.18 and 0.25. Moreover, the GA was considered to search for the best control gain in order to ensure that the re-configuration control can provide good damping over a range of conicities. It was highlighted that although the stabilisation can be achieved through the use of GA, the required control effort would significantly increase. Further research is required to ensure that the re-configuration controller meets the robust requirements. The re-configuration controller also has been integrated with two different FDI schemes in order to ensure that the fault tolerant strategy can work effectively to maintain stability and curving performance. Further on, it has been shown that the fault tolerant strategy provides better performance with an FDI that has been developed through the actuator-based approach, particularly in the presence of actuator open and short circuits.

Chapter 6 CONCLUSION AND FUTURE WORK

6.1 Conclusion

This research has been focussed on the development of a fault-tolerant strategy for active wheelset control in the presence of actuator failure(s) in order to maintain stability and good curving performance. In this study, the fault tolerance has been developed through an analytical redundancy without the need for redundant actuators, in order to keep the overall cost down. The proposed fault tolerant strategy consists of two main parts: Fault Detection and Isolation (FDI) and Re-configuration Control (RC).

This research has considered three of the most common types of actuator failure for the electro-mechanical actuators used in the study for the active wheelset control: fail-hard (FH), short circuit (SC) and open circuit (OC). The fail-hard is a failure condition when the motor shaft of the actuator becomes immovable; whereas the short circuit and open circuit are failures that occur in the electrical parts of the actuator which correspond to zero voltage and zero current in the motor respectively.

Two different FDI schemes for the actuators have been developed: the vehicle model-based approach and actuator mode-based approach. In the first method, a vehicle model-based approach using a Kalman Filter (KF) has been used to detect and identify the actuator failure in the time domain. The proposed Kalman Filter was also implemented in the control scheme to estimate the full state's feedback for the controller. It has been demonstrated that the actuator fail-hard can be detected through the evaluation of the standard deviation ratio of the measured signal from the relative yaw motion to its residual. The actuator fail-soft (i.e., open and short circuits) can be isolated by the standard deviation ratio of the measurement of the lateral accelerometer of the front wheelset to its residual. The drawback of this approach was slower fault detection, particularly for the actuator fail-soft as a minimum window size of 1

(s) for computing the standard derivations is required to extract the feature for the fault detection purpose.

The second FDI scheme has been developed based on the dynamic model for each of the two actuators through a Local Kalman Filter (LKF) to identify any abnormal changes in the actuator. The investigation has shown that a fault could be detected and isolated through the evaluation of the residual in the time domain by using the standard deviation with a moving window that is much less that the first approach.

The robustness of the FDI schemes with the two different approaches has been assessed when the parameters at the wheel–rail interface such as conicity and creep coefficient are deviated from their nominal values. In addition, both straight track with irregularities and deterministic track have been used as inputs in the simulation in order to ensure that the proposed strategy can provide reliable and consistent information when the vehicle runs along different track inputs. The robustness of the FDI has also been assessed in the event of the sensor failure(s), as the detection and isolation of the actuator fault(s) are highly reliant on the reliability of the sensors.

Furthermore, the control re-configuration to cope with different actuator faults and failure modes have been investigated in details. It has been demonstrated that, in the scenario of fail-hard, a main objective for the control re-configuration is to minimise the contact forces at the wheel–rail interface in order to reduce the wear and rolling contact fatigue, especially during curving. In the event of fail-soft (i.e., short circuit or open circuit), the main objective of the control re-configuration is to maintain the vehicle stability, and the curving performance becomes a secondary issue.

It has been demonstrated that the control re-configuration could be achieved by re-tuning the original controller to maintain stability and good curving performance. In order to improve

the robustness of the controller for the actuator fail-soft when the conicity deviates from its nominal value, Genetic Algorithms (GA) have been applied to search for the control gains. Finally, the re-configuration controllers have been integrated with the two different FDI schemes in order to ensure that the fault tolerant strategy can work effectively to maintain stability and curving performance. It has been illustrated that the fault tolerant strategy provides better performance with the FDI that has been developed through the actuator-based approach, particularly in the presence of actuator open and short circuits due to the faster fault detection and isolation.

The key contributions of this research can be summarised as follows:

- Proposing and developing a fault tolerant control system through an analytical redundancy in the incident of actuator failures in order to address the gap in the research field as fault tolerance for actuator failures has largely been achieved through hardware redundancies in reported applications.
- Investigating and developing a thorough understanding of the effect of actuator faults and failure modes on the vehicle behaviours/properties that provide the necessary foundation for the development of the proposed fault-tolerant control scheme for the rail wheelsets.
- Developing effective fault detection and isolation methods for actuator faults, but also taking into account of the reliability and robustness of the FDI schemes in the presence of sensor failures and parameter uncertainties in the system.

6.2 Future Work

Future research would be required to ensure that the re-configuration controller meets the robust requirement, e.g., by considering the use of additional measurements to increase the

robustness or Extend Kalman Filter where the conicity can be included as an extra estimation parameter.

In the case of the actuator failure(s), this study only investigates a situation where the actuator is physically stuck or loses all its control effectiveness. However, the actuator failure(s) may be preceded by a slowing of actuator response and/or a greater current demand than normal for the required output torque. Therefore, it will be suggested that a condition where the actuator loses only part of its control effectiveness could be investigated for future study.

In addition, this research has used a simplified model of the actuator and the vehicle for developing the fault tolerant strategy. In future, it is suggested that the concept is extended onto the whole vehicle model.

Furthermore, the fault tolerant strategy concentrates only on the actuator failure, but there is also the possibility of other abnormal changes in the sensor and microcontroller. It seems that might the best solution be to use hardware redundancy for the sensors and analytical redundancy for the actuators. It is suggested that the concept of the fault tolerant strategy be developed for those hardware failures in the future in order to ensure the basic functionality of the whole system.

Further on, this research has only considered the optimal controller with full-state; however, it is suggested that the concept of the fault tolerant strategy can be extended to use different controllers that have been developed for the actively controlled wheelset. Finally, while this research has considered the conventional solid-axle wheelset with bogie for developing the fault tolerant strategy, there is further scope in the future to extend the concept on different vehicle configuration such as the independently rotating wheelset, the directly independently rotating wheelset, the directly steered wheelset and the secondary yaw control.

APPENDIX A CALCULATION OF CREEPAGE

I. This Appendix demonstrates the procedure for the calculation of the creepage in longitudinal, lateral and spin directions.

Figure 1 shows a side view perspective of both the right and left wheelsets, with the two wheels fixed at the same axle. As the wheelset is travelling forward at a constant speed of V_s , the rotational speed of the individual wheel is determined by:

$$\omega = \frac{V_s}{r_0}$$

When the wheelset is moving along a track in the longitudinal direction, both the track curvature *1/R* and the wheelset yaw motion ψ can affect the forward speed of the wheelset, and therefore the longitudinal creepage.

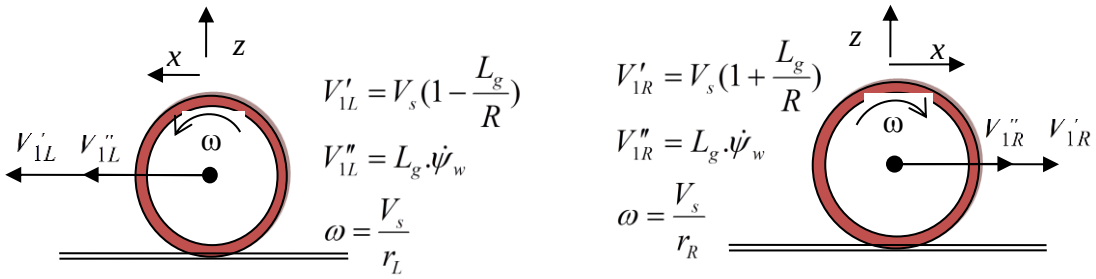

Figure 1: Side view of the left and right wheel

In the case of the wheelset moving during curve negotiation, the effect of the longitudinal velocity for both the left wheel V'_{1L} and right wheel V'_{1R} are diverse due to the impact of the track curvature *1/R* , which is given as follows:

$$V'_{1L} = V_s(1 - \frac{L_g}{R})$$

$$V'_{1R} = V_s(1 + \frac{L_g}{R})$$

The effect of yaw motion ψ on the longitudinal velocity for both the left wheel V_{1L}'' and right wheel V_{1R}'' can be expressed as:

$$V_{1L}'' = L_g.\cos(\dot{\psi}_w) \xrightarrow{\psi \approx \varepsilon} V_{1L}'' = L_g.\dot{\psi}_w$$
$$V_{1R}'' = L_g.\cos(-\dot{\psi}_w) \xrightarrow{\psi \approx \varepsilon} V_{1R}'' = -L_g.\dot{\psi}_w$$

Where ε is a small value

The combination of equations can express the total longitudinal velocity for both the left and right wheels denoted as V_{1R} and V_{1L} , respectively.

$$V_{1L} = V_{1L}' + V_{1L}'' = V_s(1 - \frac{L_g}{R}) + L_g\dot{\psi}_w$$
$$V_{1R} = V_{1R}' + V_{1R}'' = V_s(1 + \frac{L_g}{R}) - L_g\dot{\psi}_w$$

According to the definition of creepage:

$$\gamma_{1L} = \frac{V_{1L} - V_{1L}}{V_s}$$

Where ν_1 is the actual velocity when the creep exists and ν_1 is the pure rolling velocity when no creep exists. Therefore, creepage in the longitudinal direction can be expressed as:

$$\gamma_{1L} = 1 - \frac{L_g}{R} + \frac{L_g\dot{\psi}_w}{V_s} - \frac{\omega.r_L}{V_s}$$

$$\gamma_{1R} = 1 + \frac{L_g}{R} - \frac{L_g\dot{\psi}_w}{V_s} - \frac{\omega.r_R}{V_s}$$

The results from the creepage in the longitudinal direction clearly indicate that the creepage in the longitudinal direction is dependent upon the track curvature (*1/R*), yaw speed and relative displacement between the wheelset and track, as the rolling radii for the left and right wheel are determined by *(y-y$_t$)*, as explained in Equation (2.8). The creepage in the lateral

direction is determined by a combination of the component of travelling speed and the speed of lateral displacement of the wheels, as shown in Figure 2.

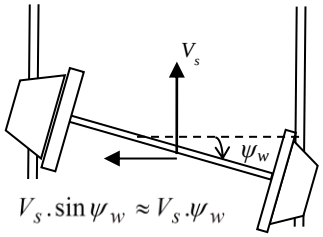

Figure 2: Creepage in the lateral direction

The velocities in the lateral direction of the two wheels on the left/right side can be stated as follows:

$$V_{2L} = \dot{y}_w - V_s \cdot \sin\psi_w \cong \dot{y}_w - V_s \cdot \psi_w$$
$$V_{2R} = \dot{y}_w + V_s \cdot \sin\psi_w \cong \dot{y}_w - V_s \cdot \psi_w$$

According to the definition of creepage.

$$\gamma_2 = \frac{\nu_2' - \nu_2}{V_s}$$

Where ν_2 is the actual velocity when the creep exists and ν_2' is the pure rolling velocity when no creep exists. Therefore, creepage in the lateral direction can be express as:

$$\gamma_{2L} = \frac{\dot{y}_w}{V_s} - \psi_w$$
$$\gamma_{2R} = \frac{\dot{y}_w}{V_s} - \psi_w$$

This clearly indicates that the creepage in the lateral direction is related to the speed of lateral displacement and yaw motion of the wheelset. The creepage in the spin direction is

determined by the relative angular velocity (about the normal axis to the contact patch) which is provided by both the rotation and yaw motion of the wheelset. The combination of the spin velocities of left and right wheels can be expressed as:

$$\Omega_{3L} = \dot{\psi}_w + \omega.\sin\lambda_L \cong \dot{\psi}_w + \omega.\lambda_L \xrightarrow{\omega=\frac{V_s}{r_0}} \Omega_{3L} = \dot{\psi}_w + \frac{V_s\lambda_L}{r_0}$$

$$\Omega_{3R} = \dot{\psi}_w - \omega.\sin\lambda_R \cong \dot{\psi}_w - \omega.\lambda_R \xrightarrow{\omega=\frac{V_s}{r_0}} \Omega_{3R} = \dot{\psi}_w - \frac{V_s\lambda_R}{r_0}$$

According to the definition of creepage:

$$\gamma_3 = \frac{\Omega_3' - \Omega_3}{V_s}$$

Where Ω_3 is the actual velocity when the creep exists and Ω_3' is the pure rolling velocity when no creep exists. Therefore, creepage in the lateral direction can be express as:

$$\gamma_{3L} = \frac{\dot{\psi}_w}{V_s} + \frac{\lambda_L}{r_0}$$

$$\gamma_{3R} = \frac{\dot{\psi}_w}{V_s} - \frac{\lambda_R}{r_0}$$

As such, it can be deduced that the creepage in the spin direction is dependent upon the yaw velocity and relative lateral displacement between the wheelset and track.

APPENDIX B VEHICLE NUMERICAL PARAMETERS

Vehicle symbol and parameter in the simulation	
Symbols	***Parameters***
V_s, g	Vehicle forward speed (50m/s), Gravity (9.8 $m.s^{-2}$)
m_w, I_w	wheelset mass (1250 kg) and yaw inertia (700 kgm^2)
l_g, l_v	Half gauge of wheelset(0.75m), half spacing of axle(1.225m)
r_0, λ	wheel radius(0.45m), and conicity (0.2)
m_g, I_g	Bogie mass(6945 kg), and Yaw inertia (3153 kgm^2)
K_{sc}, C_{sc}	Secondary Lateral and longitudinal stiffness (511 kNm^{-1}), and damping(37 $kNsm^{-1}$)
K_s, C_s	primary Lateral stiffness (4750 kNm^{-1}), and damping (7705 N sm^{-1})
K_f	Material stiffenss (10^8 kNm^{-1})
m_v	Half vehicle mass (15000kg)
f_{11}, f_{22}	Longitudinal/ lateral creepage coefficient (10MN).
R_1, R_2	Radius of the curved track at the leading and trailing Wheeslet(1250 m).
$\theta_{c_1}, \theta_{c_2}$	cant angle of the curved track at the leading and trailing wheelset (6°)
I_m	Motor's rotor moment of inertia (0.00115 $kg.m^2$)
I_{ma}	Motor's stator moment of inertia (0.00345 $kg.m^2$)
R_a	Motor armature resistance (0.112Ω)
L_a	Motor armature inductance (9.04e-4 H)
K_t	Motor torque constants (2.685 $N.m.A^{-1}$)
K_b	Motor back e.m.f constant (0.435)
n	Gear ratio (1/87)
K_g	Gearbox drive stiffness(1.131102e9 $N.m.rad^{-1}$)
C_g	gearbox drive damping (7540.7 N.m $s.rads^{-1}$)
C_m	motor gearbox shaft damping (0.0084 $N.m.rads^{-1}$)

APPENDIX C LIST OF PUBLICATIONS

I. Mirzapour, M., Mei, T. X., & Hussain, I. (2012). Assessment of fault tolerance for actively controlled railway wheelset. UKACC International Conference (pp. 631 - 636). Cardiff, UK: IEEE.

II. Mirzapour, M., Mei, T. X., & Xuesong, J. (2014). Fault detection and isolation for an active wheelset control system. *Vehicle System Dynamics, 52*(1), 157-171.

III. Mirzapour, M., & Mei, T. X. (2014). Detection and isolation of actuator failure for actively controlled railway wheelsets. *UKACC International Conference* (pp. 561 - 566). Loughborough, UK: IEEE.

APPENDIX D COPY OF UKACC' 2012 PAPER

Assessment of fault tolerance for actively controlled railway wheelset

Mirzapour, M., Mei, T.X. & Hussain

UKACC International conference on control, 3-5 Sep 2012

University of Cardiff, UK

Publisher IEEE

Assessment of Fault Tolerance for Actively Controlled Railway Wheelset

Mohammad Mirzapour
School of Computing, Science Engineering
The University of Salford
Great Manchester, M5 4WT, UK
m.mirzapour@edu.salford.ac.uk

T.X Mei
School of Computing Science Engineering
The University of Salford
Great Manchester, M5 4WT, UK
t.x.mei@salford.ac.uk

I Hussain
School of Electronic Engineering
Mehran University
Jamshoro, Pakistan
imtiaz.hussain@faculty.muet.edu.pk

Abstract— **this paper studies the key issue of fault tolerance for actively controlled railway wheelsets. It assesses failure modes in such systems, with a focus on actuator failures, and consequence of those hardware failures. It seeks to establish the necessary basis for control reconfiguration to ensure system stability and performance in the event of a faulty, without the need for hardware redundancies. A number of control schemes (with and without faults) are included in the study. Both analytical and simulation results are presented.**

Keywords-Railway; Wheelset; Active control; Stability; Actuator; Fault tolerance.

INTRODUCTION

Conventional wheelset for the railway vehicle is composed of the two coned (or profiled) wheels rigidly fixed to a common axle to rotate at the same angular velocity. When an unconstraint wheelset rolling along the track it is displaced laterally due to track irregularities, the rolling radii therefore are different because of the profiles of these two wheelset. Consequently, different forward speeds obtained for each wheelset due to the difference rolling radii to provide a natural centering/curving action. However, an unconstrained wheelset also presents a problem of kinematic instability known as the "Kinematic Oscillation" or wheelset "hunting" [1,2].

Traditionally the wheelset is stabilized by using passive suspensions on conventional rail vehicle, but such additional stiffness affects the pure rolling action of the wheelset around the curve. It has been theoretically proven that to this design conflict between stability and curving performance can be solved by applying active control instead of conventional passive components within the primary suspension of railway vehicle [2].

Passive components in the primary suspensions can be designed in such a way not to fail in order to maintain the stability and steering performance of railway vehicle and they are generally accepted as "safe" in railway industry. However, any new technology must prove that it can cope with any failures to demonstrate that any component faults would not lead to the system failure such that passenger safety is not compromised under such conditions. From a practical point of view, any active control scheme must be also able to maintain an effective operation of a rail system in order to meet the necessary standard of reliability [3]. Hardware redundancy technique may be used in the system to guarantee safety operation of such a system. Whilst it may be acceptable to apply the above technique in sensors due to their relatively low cost, it is far more difficult to justify the use of multiple actuators in a cost effective manner for redundancy or accommodate those within the limited space of railway bogie [3]. There are two main approaches for fault tolerant control systems. The first philosophy relies on the existing system redundancies to achieve acceptable performance in the event of component failures. In this type of systems, once the controllers designed, it will remain stable. It should be noted that the redundancies in such a system are usually in hardware forms. The second methodology takes a completely different approach to achieve fault tolerance. It involves such procedures as real-time fault detection, isolation, and control system reconfiguration. The redundancy in such a system may be an analytical form [4] and help to minimize the use of the hardware redundancies in order to keep the overall cost down [5].

The object of this study is to develop the fault tolerance approaches without using redundant actuators to provide stability across a range of operation conditions with different failure modes. It investigates the possibilities/feasibilities of re-configuring the controller based on the use of remaining actuator(s) in the system. For this study, the paper will review first a number of different control methods for railway wheelsets in the normal condition to understand how control for stability and/or curving performance is achieved. A thorough assessment of failure modes and adverse effect of the

faults on the system stability and performance is then carried out, followed by an investigation into control re-tuning/re-configuration for fault tolerance. The paper is organized as following. The mathematical dynamic model of railway vehicle is presented in Section II. Consideration of basic control scheme is given in section III. Section V demonstrates the different fail modes of railway vehicle with the actuator faults and re-configuration of the controller based on the remaining actuator Finally, conclusion and future work will be discussed.

MATHEMATICAL MODEL OF THE RAILWAY VEHICLE

A railway vehicle mainly consists of a vehicle body and two bogie frames, and each bogie frame consists of a bogie frame and the two wheelsets. The wheelsets are connected to the bogie frame with springs and dampers in the longitudinal and lateral directions. For this study, only the plan-view dynamics of a half vehicle is used to analysis stability and steering performance of the vehicle, which is the accepted practice in railway industry [6]. Fig.1 gives a plan-view diagram of the half body vehicle model used for this study. The equations of motion for a railway vehicle when running along a track are mainly determined by the creep forces between wheel and rail contact patches. In this paper, a linear model has been considered, which is justified as the active control tends to reduce the effect of non-linearity in the wheelsets [7]. The linear model of the motion contains seven degrees of freedom, i.e. the lateral and yaw motions for each wheelset and for the bogie frame, and a lateral displacement for the vehicle body defined by (1) to (7). The model is therefore 14th order in total, and can be represented in the state space model by (8) [6].

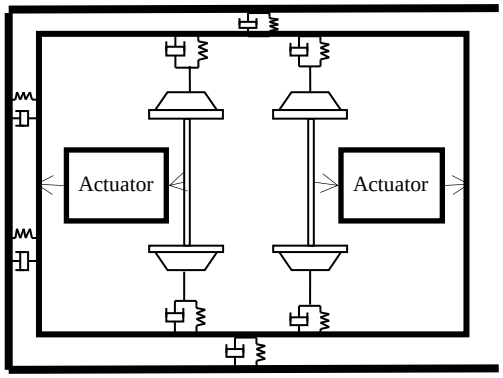

Figure 1: Plane-view of the vehicle

The input vector u represents the control inputs to the wheelsets, and the vector μ is used to represent the inputs from the railway track, including the lateral displacement, cant, and curvature. The lateral track displacement is a random input, which represents track irregularities along the path track, whereas the track curvature and cant are the deterministic inputs [6]. More details of the vehicle parameters in the equations are provided in the Appendix A.

$$\ddot{y}_{w_1} = -\frac{1}{m_w}[(\frac{2f_{11}}{V_s} + C_s)\dot{y}_{w_1} - K_s y_{w_1} + 2f_{22}\Psi_{w_1} + C_s\dot{y}_g + K_s y_g + C_s L_v\dot{\Psi}_g + K_s L_v\Psi_g + m_w(\frac{V_s^2}{R_1} - g\cdot\theta_{c_1})], \quad (1)$$

$$\ddot{\Psi}_{w_1} = -\frac{1}{I_w}[\frac{-2f_{11}L_g^2}{I_w V_s}\dot{\Psi}_{w_1} - \frac{-2f_{11}\lambda L_g}{I_w r_0}y_{w_1} + \frac{2f_{11}L_g^2}{I_w R_1} - \frac{-2f_{11}\lambda L_g}{I_w r_0}y_{t_1} + \frac{\tau_{w_1}}{I_w}], \quad (2)$$

$$\ddot{y}_{w_2} = -\frac{1}{m_w}[(\frac{2f_{11}}{V_s} + C_s)\dot{y}_{w_2} - K_s y_{w_2} + 2f_{22}\Psi_{w_2} + C_s\dot{y}_g + K_s y_g - C_s L_v\dot{\Psi}_g - K_s L_v\Psi_g + m_w(\frac{V_s^2}{R_2} - g\cdot\theta_{c_2})], \quad (3)$$

$$\ddot{\Psi}_{w_2} = -\frac{1}{I_w}[\frac{-2f_{11}L_g^2}{I_w V_s}\dot{\Psi}_{w_2} - \frac{-2f_{11}\lambda L_g}{I_w r_0}y_{w_2} + \frac{2f_{11}L_g^2}{I_w R_2} - \frac{-2f_{11}\lambda L_g}{I_w r_0}y_{t_2} + \frac{\tau_{w_2}}{I_w}], \quad (4)$$

$$\ddot{y}_g = \frac{1}{m_g}[-(2\cdot C_s + C_{sc})\cdot\dot{y}_g - (2\cdot K_s + K_{sc})y_g + C_s\dot{y}_{w_1} + K_s y_{w_1} + C_s\dot{y}_{w_2} + K_s y_{w_2} + C_{sc}\dot{y}_v + K_{sc}y_v + m_g V_s^2(\frac{1}{R_1} + \frac{1}{R_2}) - m_g g(\frac{\theta_{c_1}}{2} + \frac{\theta_{c_2}}{2})], \quad (5)$$

$$\ddot{\Psi}_g = \frac{1}{I_g}[-2L_v^2 C_s\dot{\Psi}_g - 2L_v^2 K_s\Psi_g + L_v C_s\dot{y}_{w_1} - L_v C_s\dot{y}_{w_2} + L_v K_s y_{w_1} - L_v K_s y_{w_2} - (\tau_{w_1} + \tau_{w_2})] \quad (6)$$

$$\ddot{y}_v = \frac{1}{m_v}[-C_{sc}\dot{y}_v - K_{sc}y_v + C_{sc}\dot{y}_g + K_{sc}y_g + m_v V_s^2(\frac{1}{2R_1} + \frac{1}{2R_2}) - m_V g(\frac{\theta_{c_1}}{2} + \frac{\theta_{c_2}}{2})], \quad (7)$$

$$\dot{x} = A\cdot x + B\cdot u + \mu\cdot w, \quad (8)$$

$$x = \begin{bmatrix}\dot{y}_{w_1} & y_{w_1} & \dot{\Psi}_{w_1} & \Psi_{w_1} & \dot{y}_{w_2} & y_{w_2} & \dot{\Psi}_{w_2} & \Psi_{w_2} & \dot{y}_g & y_g & \dot{\Psi}_g & \Psi_g & \dot{y}_v & y_v\end{bmatrix}$$

$$u = \begin{bmatrix}\tau_{w_1} & \tau_{w_2}\end{bmatrix},$$

$$\mu = \begin{bmatrix} y_{t_1} & \theta_{c_1} & \frac{1}{R_1} & y_{t_2} & \theta_{c_2} & \frac{1}{R_2}\end{bmatrix},$$

BASIC WHEELSET CONTROL SCHEMES

The railway wheelset can be stabilized by using either passive suspension or through the use of active control. For active approaches, it is possible to achieve this by applying either a yaw torque or lateral force between the bogie and the wheelset, but the yaw control is preferred as it also tends to improve the ride quality experienced by passengers [8].

Therefore, this study only discusses approaches that apply control in the yaw direction to provide desired damping to stabilize the system. The review of the control strategies is to provide a background for the study of fault tolerant control issues and more detail of the controls can be found in the references provided [9,6,10]. The suspension/control schemes are considered in the study are:

- Passive Suspension that uses conventional passive yaw stiffness in the primary suspensions.
- Active Yaw Damping where the two wheelset of the bogie are controlled by applying a yaw torque proportional to the lateral velocity of the wheelset.
- Sky-hook Yaw Stiffness where the control output of each actuator is set to be proportional to the absolute yaw motion of each wheelset
- Optimal Control where the controllers for the two inputs (actuators) are designed with the use of full state feedback (from either direct measurements or through the use of an estimator).

The track input used in the simulation, to study the control performance on curves for both active controllers and passive suspension, represents a curved track with radius of 1250m connected to straight track via a transition of 2sec. The curved track is canted inward by 6 degrees to reduce the lateral acceleration experienced by the passengers (a normal features of railway track). The vehicle speed of 50m/s is used – parameters of the vehicle are provided is Appendix A. The simulation result in Fig.2 and Fig.3 clearly illustrates that active control can provide good curving performances to reduce the longitudinal and lateral creep forces, compared with passive suspension, when both leading and trailing actuator functioning normally.

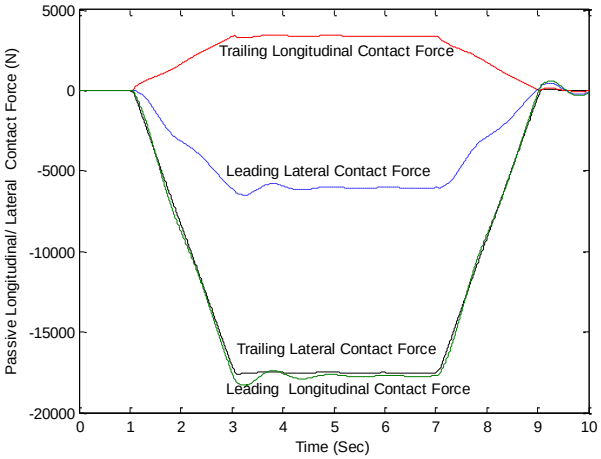

Figure 2: Passive Longitudinal/ Lateral creep forces

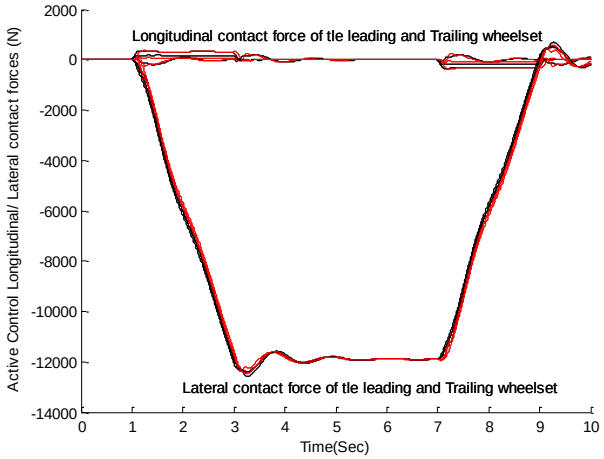

Figure 3: Active control Longitudinal/ Lateral contact forces

However, the active controllers are designed based on the assumption that both actuators function as expected and extra measures (possibly through the use of fault tolerance) will be needed in order to maintain the stability and if possible curving performance if one of the control channels fails to deliver. Therefore, it is essential to establish first a full understanding how the fault(s) affect the bogie dynamics in the system and then define what corrective actions can be taken [3].

CONTROL ANLYSIS IN FAULT CONDITIONS

In the normal condition with both actuators functioning, the bogie is designed to be stable. Fig.4 shows the minimum damping ratio of the wheelset modes with the different controllers where the stability is achieved across a wide range of speed with a critical speed of over 100m/s in the three of controllers except active yaw damper [3].

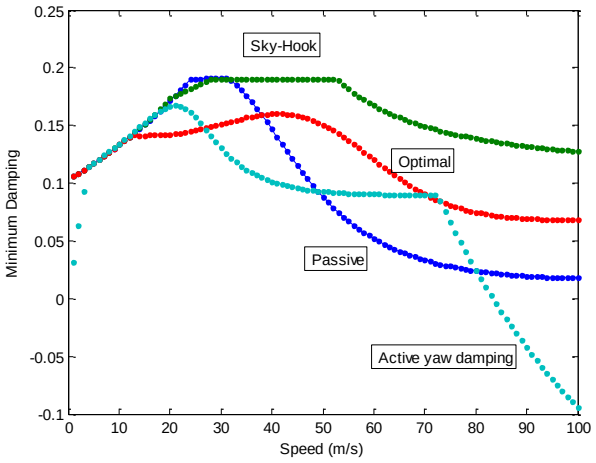

Figure 4: Comparison of different control scheme

However, this is expected to change dramatically, when one of the actuators fails. In this study, two failure modes are

considered – one is fail-hard and the other fail-soft, representing an actuator jam and free-motion respectively.

The aim of fault tolerance for actively control system is to preserve stability conditions and maintain the current curving performance close to desired ones (or at least not worse than the passive system in the normal condition) in the presence of actuator faults. In this study, the full state feedback is considered as a start point and a control gain matrix is designed to control the remaining actuator in order to explore the fault tolerant control possibilities.

Fail-Hard

In the fail hard mode, one of the actuators is assumed to be blocked and can be simulated as a spring with very high stiffness between the bogie frame and the axle. The bogie stability at different speed for the selected active control schemes are compared in Figs.5a and 5b, where the fail hard occurs in the leading and trailing wheelset respectively. In Figs.5a and 5b, the critical speed is reduced to 62m/s for the active sky-hook control scheme with the malfunction of the leading actuator and around 75m/s if the trailing actuator fails-hard respectively. A fault in the trailing actuator would result in an even lower critical speed for all three active control schemes. However the fail-hard condition poses a more problem for the curving performance of the bogie.

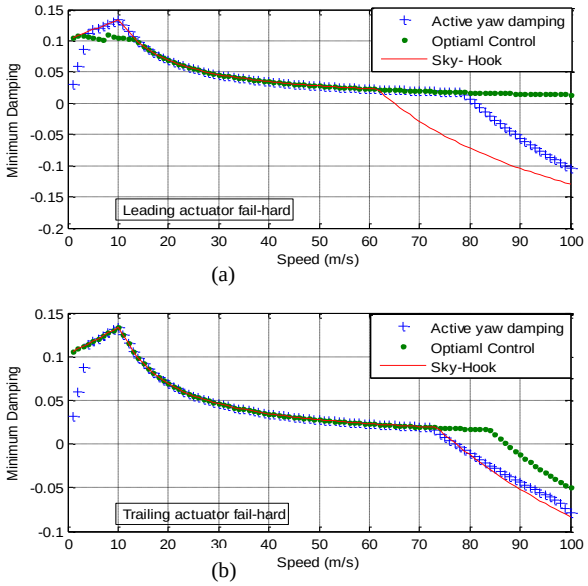

Figure 5: Stability of different control schemes with leading/trailing fault

The simulation result in Fig.6 and Fig.7 indicate clearly that when fail hard occurs in the leading and trailing control input respectively, the original controller will not be able to provide the 'right' control effort as the contact creep forces at the both leading and trailing wheelset increase significantly on the curved track, delivering a poor steering condition. The objective of the fault tolerance in the fail-hard case is therefore is to try and minimize the adverse impact of the actuator failure on the curving performance. It can be seen that the curving performance is more under risk when fail-hard occurs for the leading actuator. The simulation results in Fig. 6 and 7 suggest that the contact forces with the original controller are even worse than that with the passive suspension (Fig.2). However, retuning of the control gains for the remaining actuator does seem to provide a solution to improve curving performance of the bogie in the event of fail-hard in the leading or trailing actuator as evidenced by results in Fig.8 and Fig.9 respectively. The simulation results in Fig.8 and 9 in comparison with Fig.6 and 7 of the original controller indicate that the re-tuned optimal controller for the remaining actuator can reduce the contact forces and maintain curving performance close to that of the passive suspension. In this approach optimal controllers are tuned manually by choosing different values for weighting factor. Although the stability is guaranteed with the optimal control design, the re-design of the other active control schemes is less straight-forward and the research is ongoing to ensure such designs will meet both stability and performance requirements, e.g. by applying optimization technique to search for the best control structures and control gains.

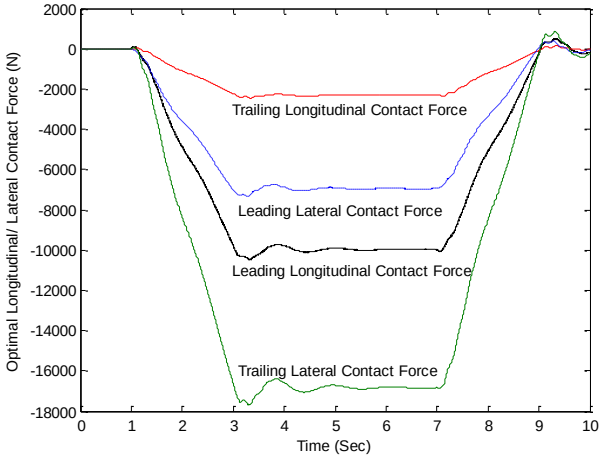

Figure 6: Original controller optimal controller /Leading Fail Hard

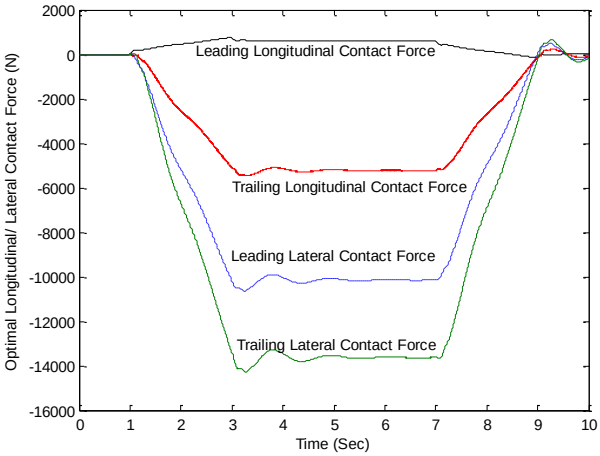

Figure 7: original optimal controller/Trailing Fail Hard

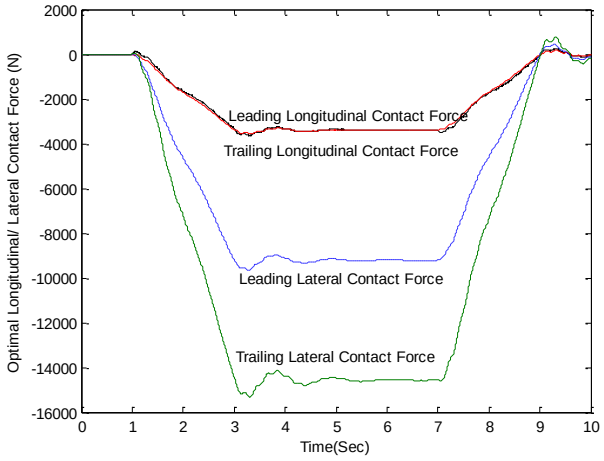

Figure 8: Retune manually optimal controller/ Leading fail Hard

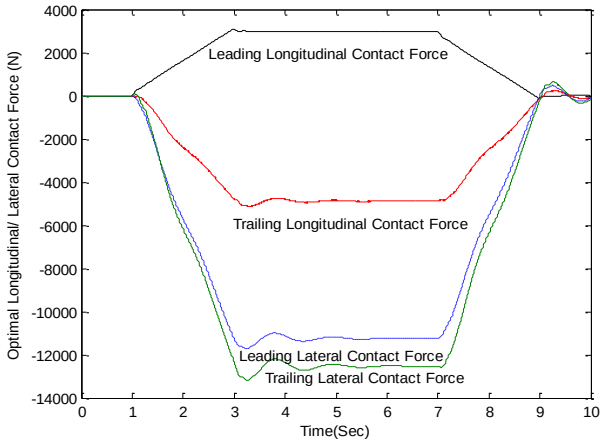

Figure 9: Retune manually Optimal Controller/ Trailing Fail Hard

Fail-Soft

The second type of the actuator malfunction is known as fail-soft, which is when one of the actuator is unconstraint from its control input. Control torque for the failed actuator in this scenario is zero and therefore not able to stabilize the kinematic mode of the wheelset. Figs.10a and 10b compares with the stability of the bogie with different active control schemes when one of the actuators fail-soft [3]. In Figs.10a and 10b, the critical speed is reduced to approximately 10m/s for all three active control schemes in the event of an actuator fault. Clearly, in the event of fail-soft condition the active controller would not able to stabilize the system and the operation speed of the system will have to be reduced very quickly to a very low level to avoid potentially dangerous situation if no other corrective actions are taken [3].

Therefore, in this scenario, the priority of fault tolerance for the active control systems is to preserve stability control in the presence of actuator fail-soft, with the curving performance a secondary design issue.

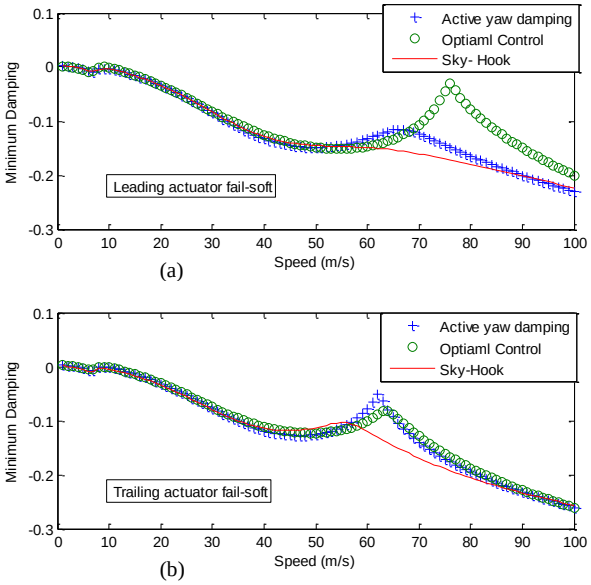

Figure 10: Stability of the different controller with leading/trailing actuator

In the event of fail-soft, the bogie stability is guaranteed if the number of control input is reduced from two actuators to one, and therefore more feedbacks are available for more sophisticated control design to provide desired control torque through the remaining actuator [3]. Fig.11 clearly reveals the bogie stability across a wide range of speed through re-designing of the optimal controller with one control input. It is also necessary to assess performance of redesign controller around the curve. Fig.12 gives the lateral and longitudinal contact forces at the wheel-rail contact points for the leading and trailing wheelset in the event of fail soft at the trailing actuator. The simulation result indicates clearly when the controller is re-designed with one control input (representing the remaining actuator), the perfect steering condition is achieved on the curved track, where the longitudinal contact forces at both leading and trailing wheelset are zero and the lateral contact forces of the two wheelsets are equal [13].

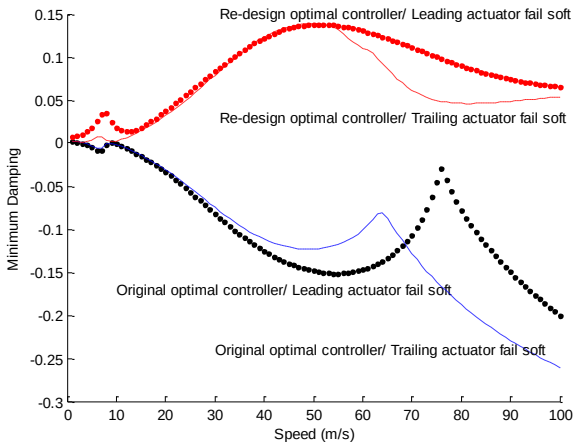

Figure 11: Stability of original / re-design optimal controller with leading/trailing fail soft in actuator

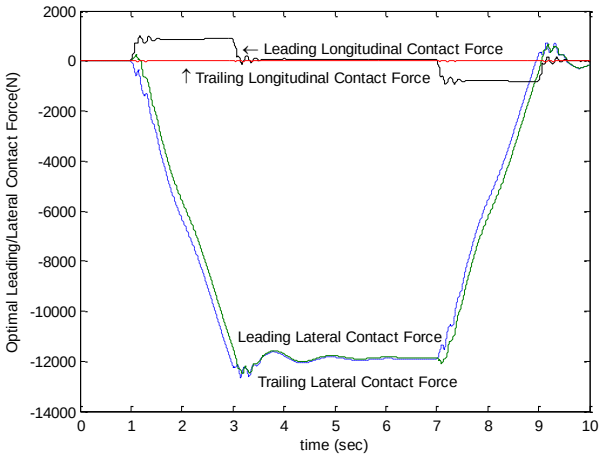

Figure 12: Curving performance of re-design optimal controller with trailing fail-soft

CONCLUTION AND FUTURE WORK

This paper has studied the fundamental fault tolerant control issues for actively controlled railway vehicles through analytical redundancy to guarantee controllability of the system in the event of actuator fault. A reconfiguration based strategy for managing both soft and hard faults has been investigated, focusing on solving instability and curving performance issues respectively. The design reconfiguration controller has been evaluated by their performance capability as evidenced in simulation results.

Research is ongoing to develop optimization technique to search for the best control gain and control structure in the event of fail-hard in such a way that ensure both stability and curving performance. However, there is clearly scope for extending the work other failure modes with different actuator configurations.

REFERENCES

[1] C. Esveld, Modern Railway Track, Delf University of Technology: BV Amesterdam, 2001.

[2] R. Goodall and H. Li, "Modelling and analysis of a railway wheelset for active control," in UK Control, Swansea, 1998,September.

[3] T.X. Mei, "A Study of Fault Tolerance For Active Wheelset Control," in 22 nd IAVSD, Manchester,UK, 2011.

[4] Q. Zhao and J. Jin, "Realiable Tracking Control System Design Against Actuator Failures," in SICE 97, Tokushima,Japan, 1997.

[5] H. G. Guo, Automative Informaticand communicative system, London, UK: IGI Global, 2009.

[6] J. Pearson, R. Goodall, T.X. Mei and G. Himmelstein, "Active Stability Control Stategies For A High Speed Bogie," Science Direct, vol. 12, no. Control Engineering Practice, pp. 1381-1391, 2004.

[7] T.X. Mei and H. Li, "Control Design for the Active Stabilization of Rail Wheelset," Dynamic, System, Measurement and Control, vol. 130, no. 1, pp. 011002 - 011011, Jan 2008.

[8] T.X. Mei and R. Goodall, "Wheelset control strategies for a 2-axle railway vehicle," Vehicle System Dynamics, vol. 33, pp. 653-664, 2000.

[9] S. Bruni, R. Goodall and T.X. Mei, "Control and monitoring for railway vehicle dynamics," International Journal of Vehicle Mechanics and, vol. 45, p. 743–779, 2007.

[10] P. Aknin, J. Ayasse and A. Devallez, "Active Steering of Railway Wheelsets," in 12th IAVSD Conference, Lyon, France., 1991.

[11] R. Iserman, "Model_Based Fault Detection and And Diagnosis Satus and Applications," in 16th IFAC Symposium on Automatic Control in Aerospace, Osaka, Japan, 2004.

[12] R. Goodall and T.X. Mei, "LQG and GA solutions for Active Steering of Railway Vehicles," IEE Proceedings-Control Theory and Applications, vol. 147, no. 1, pp. 111-116, 2000.

[13] S. Shen, T. Mei, R. Goodall, J. Pearson and G. Himmelstein, "A syudy of active steering strategies for a railway bogie," in IAVSD, Kanagawa, Japan, 2003.

APPENDIX A

Vehicle symbol and parameter in the simulation

Symbols	***Parameters***
$y_{w_1}, y_{w_2}, y_g, y_v$	Lateral diplacement of leading, trailing wheelset, bogie frame and vehicle body
$\psi_{w_1}, \psi_{w_2}, \psi_g$	yaw diplacemet of leading, trailing and bogie fram
V_s	Vehicle forward speed (50m/s)
m_w, I_w	wheelset mass (1250 kg) and yaw inertia (700 kgm^2), respectively
I_g, I_v	Half guage of wheelset(0.7 m), half spacing of axle(1.225 m)
r_0, λ	wheel radius(0.45 m), and conicity (0.2)
m_g, I_g	Bogie frame mass(6945 kg), and Yaw inertia (3153 kgm^2) respectively.
K_{sc}, C_{sc}	Secondary Lateral and longitudinal stiffness (511 kNm^{-1}), and damping(37 kNsm^{-1}) respectively.
K_s, C_s	primary Lateral stiffness (4750 kNm^{-1}), and damping (7705 N sm^{-1}) respectively.
m_v	Half vehicle mass (15000kg)
f_{11}, f_{22}	Longitudinal and lateral creepage coefficient (10MN).
R_1, R_2	Radius of the curved track at the leading and trailing Wheeslet(1250 m).
$\theta_{c_1}, \theta_{c_2}$	cant angle of the curved track at the leading and trailing wheelset (6°)
y_{t_1}, y_{t_2}	Track lateral diplacement for leading and trailing wheelsets, respectively
τ_{w_1}, τ_{w_2}	Controlled torque for leading and trailing weelset respectively.
g	Gravity (9.8 m/s^2)

APPENDIX E COPY OF "VEHICLE SYSTEM DYNAMICS" PAPER

FAULT DETECTION AND ISOLATION FOR AN ACTIVE WHEELSET CONTROL SYSTEM

Mirzapour M, Mei T.X, Xuesong J

Published in Vehicle System Dynamics, Vol 52, Supplement 1, p.p 157-171, 2014

Abstract

Active control for railway wheelsets in the primary suspension has been shown to offer a number of performance gains, and especially it can be used to stabilise the wheelsets without compromising the vehicle's performance on curves. However, the use of actuators, sensors and data processors to replace the traditional passive suspension raises the issue of system safety in the event of a failure of the active control, which could result in the loss of stability (i.e., wheelset hunting), and in more severe cases, derailment. This paper studies the key issue of condition monitoring for an actively controlled railway system, with a focus on actuator failures to detect and isolate failure modes in such a system. It seeks to establish the necessary basis for fault detection to ensure system reliability in the event of malfunction in one of the two actuators. Computer simulations are used to demonstrate the effectiveness of the method.

Keywords: railway; active control; condition monitoring; fault tolerance; actuators; sensors

1. Introduction

Active control for railway wheelsets in primary suspensions has been shown to offer a number of performance gains, especially that it can be used to stabilise the wheelsets without compromising the vehicle's performance on curves, to reduce the wear of the wheels and track, and to minimise the track shifting forces [1]. Recently, a number of different wheelset configurations and active control methodologies have been proposed [2], including Actuated solid-axle wheelset (ASW), Actuated independently rotating wheelset (AIRW), Driven independently rotating wheelset (DIRW), Directly steered wheel (DSW) and Secondary yaw control (SYC). Although the control requirements as well as control possibilities are largely reliant on the vehicle and wheelset configurations that have been outlined, the most important challenge relates to strategies for the safety and reliability of the active control [3].

In the active approach, the use of actuators, sensors and data processors to replace traditional passive suspensions raises the issue of system safety in the event of a failure of the active control, which could result in the loss of stability (i.e., wheelset hunting) and in more severe cases, derailment. Traditionally, mechanical components are used for the wheelset stabilisation and are generally accepted as "safe" which is largely achieved through mechanical overdesign [4]. However, the practical implementation for active (electronic) control systems can only be made possible if the safety and reliability requirements can be met [5].

Effective condition monitoring of safety-critical control systems through fault detection and isolation (FDI) is essential to ensure that the overall safety of such systems is not compromised [6], and such condition monitoring must be able to estimate or detect incipient faults in real time and in a reliable manner [3] and it should not be affected by other parameter changes and/or uncertainties in the system [7].

A research project at Salford University (UK) is being carried out to study an analytical redundancy-based fault tolerance approach for the active wheelset control, where the issue of fault detection and isolation for the active control system is one of the key research objectives. The focus of the research is on actuator failures, although the issue of sensor faults would also be considered. Some initial studies by the authors to establish a critical understanding of instability problems and re-configuration possibilities/feasibilities in the event of actuator fault(s) were reported in [4] and [8]. This study, however, is concerned with the development of a fault detection and isolation method to detect actuator failure(s), in order to enable the controller in the system to be re-configured to cope with the identified fault in the proposed fault tolerant system. The actuators (as well as the active control as a whole) are an integral part of the vehicle dynamics, and therefore cannot be treated in

isolation in the development of an effective Fault detection and Isolation (FDI) method. Previous studies [4] [8]have suggested that the dynamic properties of a railway vehicle/bogie can be severely affected by an actuator failure in the system, and that the changes also occur in different ways depending on the failure modes (e.g., fail-hard or soft) and location (e.g., at the leading or trailing wheelset) of the failed actuator. In order to identify abnormal changes a model-based approach is studied in this paper to exploit the dynamic changes in a railway vehicle (caused by an actuator fault) for fault detection and isolation in the event of hard and soft failures, respectively.

The paper is organised as follows. The mathematical dynamic model and control design of the railway vehicle is presented in the next section. Section 3 deals with the approach to developing a model-based estimator to provide the controllers with the required feedback variables, where also the estimated data from the proposed estimator will be used to diagnose the faulty actuator. Section 4 demonstrates the performances of the railway vehicle with the actuator faults, while Section 5 addresses the key issues of fault detection and isolation in the event of actuator malfunction. Finally, a conclusion will be offered and future work will be discussed.

2. Modelling of railway dynamics and control design

The first step is to develop the appropriate models for describing the dynamic behaviour of a railway vehicle system. This study uses a conventional two-axle bogie with a half body frame [9]. Because the active steering action only affects the lateral and yaw motions of the vehicle, only the plan view dynamic of a half vehicle needs to be considered [10]. Figure 1 gives a simplified plan view diagram of the half vehicle [9], where the wheelsets are connected to the bogie frame via springs and dampers in the lateral direction. In practice, some form of longitudinal connection is needed to transmit traction and braking forces from the wheelsets

to the vehicle body frame, but this is not a concern of the current study [11]. There are also actuators placed between the wheelsets and the bogie frame in the yaw direction for the implementation of active controls [7]. The equations of motion for a railway vehicle when travelling along a track are principally determined by the creep forces that are generated between the wheel and rail contact patches [12]. In this paper, a linear model has been considered, which is justified as the active control tends to reduce the effect of non-linearity in the wheelsets [11].

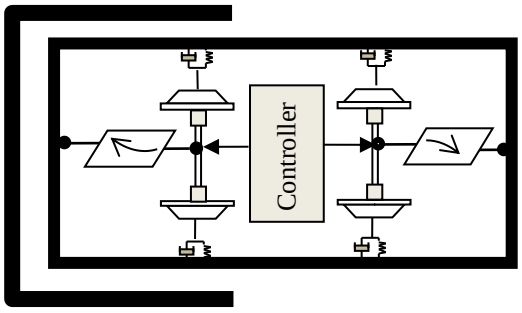

Figure1: Actuated solid-axle wheelset (ASW)

The linear model of the motion contains seven degrees of freedom, i.e., the lateral and yaw motions for each wheelset and for the bogie frame, and a lateral displacement for the vehicle body defined by equations (1) to(7). The model is therefore the 14th order in total [6].

$$\ddot{y}_{w_1} = -\frac{1}{m_w}[(\frac{2f_{22}}{V_s} + C_s)\dot{y}_{w_1} - K_s y_{w_1} + 2f_{22}\psi_{w_1} + C_s\dot{y}_g + K_s y_g + C_s L_v\dot{\psi}_g + K_s L_v\psi_g + m_w(\frac{V_s^2}{R_1} - g\cdot\theta_{c_1})], \quad (1)$$

$$\ddot{\psi}_{w_1} = \frac{1}{I_w}[\frac{2f_{11}L_g^2}{V_s}\dot{\psi}_{w_1} - \frac{2f_{11}\lambda L_g}{r_0}y_{w_1} + \frac{2f_{11}L_g^2}{R_1} + \frac{2f_{11}\lambda L_g}{r_0}y_{t_1} + \tau_{w_1}], \quad (2)$$

$$\ddot{y}_{w_2} = -\frac{1}{m_w}[(\frac{2f_{22}}{V_s} + C_s)\dot{y}_{w_2} - K_s y_{w_2} + 2f_{22}\psi_{w_2} + C_s\dot{y}_g + K_s y_g - C_s L_v\dot{\psi}_g - K_s L_v\psi_g + m_w(\frac{V_s^2}{R_2} - g\cdot\theta_{c_2})], \quad (3)$$

$$\ddot{\psi}_{w_2} = \frac{1}{I_w}[\frac{2f_{11}L_g^2}{V_s}\dot{\psi}_{w_2} - \frac{2f_{11}\lambda L_g}{r_0}y_{w_2} + \frac{2f_{11}L_g^2}{R_2} + \frac{2f_{11}\lambda L_g}{r_0}y_{t_2} + \tau_{w_2}], \quad (4)$$

$$\ddot{y}_g = \frac{1}{m_g}[-(2\cdot C_s + C_{sc})\cdot\dot{y}_g - (2\cdot K_s + K_{sc})y_g + C_s\dot{y}_{w_1} + K_s y_{w_1} + C_s\dot{y}_{w_2} + K_s y_{w_2}$$
$$+ C_{sc}\dot{y}_v + K_{sc}y_v + m_g V_s^2(\frac{1}{R_1} + \frac{1}{R_2}) - m_g g(\frac{\theta_{c_1}}{2} + \frac{\theta_{c_2}}{2})], \quad (5)$$

$$\ddot{\psi}_g = {}^{1}\!/_{I_g}\,[-2L_v^2 C_s \dot{\psi}_g - 2L_v^2 K_s \psi_g + L_v C_s \dot{y}_{w_1} - L_v C_s \dot{y}_{w_2} + L_v K_s y_{w_1} - L_v K_s y_{w_2} - (\tau_{w_1} + \tau_{w_2})], \quad (6)$$

$$\ddot{y}_v = {}^{1}\!/_{m_v}\,[-C_{sc}\dot{y}_v - K_{sc} y_v + C_{sc}\dot{y}_g + K_{sc} y_g + m_g V_s^2 ({}^{1}\!/_{R_1} + {}^{1}\!/_{R_2}) \quad (7)$$
$$- m_g g ({}^{\theta_{c_1}}\!/_{2} + {}^{\theta_{c_2}}\!/_{2})],$$

The control input at the either wheelset (τ_{w_1}, τ_{w_2}) represents the torque in the yaw direction produced by the corresponding actuator, where a model of electric-mechanical actuator is also developed for the study. The lateral track displacement is a random input, which represents track irregularities along the path track; whereas the track curvature and cant are the deterministic inputs [13]- more details of the vehicle parameters in the equations are provided in Appendix A. Conventional solid axle wheelset can be stabilised by using either passive suspension or through the use of active control. For active approaches, it is possible to achieve this by applying either a yaw torque or lateral force between the bogie and the wheelset, but the yaw control is preferred as it also tends to improve the ride quality experienced by passengers [10].

A number of control strategies are possible [2] [14], but in this study, optimal control approach is used for designing active control as the full state feedback required for the controller can be provided by the state observer used also for the fault detection and isolation scheme. The design of the optimal controller is fairly standard and for the wheelset control it has been found that the minimisation of the lateral wheel-rail deflection and control of the angle of attack for the provision of curving force results in a controller that provides the desired degree of stability and performance [14]. Equations (8) and (9) define a state-space representation of the vehicle model suitable for optimal control design, where ***x*** is a vector of state variables, ***u*** is the control input vector, ***w*** is a vector of track inputs, and ***y*** is a vector of outputs or measurements [9].

$$\dot{\boldsymbol{x}} = \mathbf{A} \cdot \boldsymbol{x} + \mathbf{B} \cdot \boldsymbol{u} + \boldsymbol{\mu} \cdot \boldsymbol{w}; \tag{8}$$

Where;

$$\boldsymbol{x} = \left[\dot{y}_{w1} \quad y_{w1} \quad \dot{\psi}_{w1} \quad \psi_{w1} \quad \dot{y}_{w2} \quad y_{w2} \quad \dot{\psi}_{w2} \quad \psi_{w2} \quad \dot{y}_g \quad y_g \quad \dot{\psi}_g \quad \psi_g \quad \dot{y}_v \quad y_v\right]^T;$$

$$\boldsymbol{u} = \left[\tau_{w1} \quad \tau_{w2}\right]^T;$$

$$\boldsymbol{y} = \mathbf{C} \cdot \boldsymbol{x} + \mathbf{D} \cdot \boldsymbol{u}; \tag{9}$$

Where;

$$\boldsymbol{y} = \left[y_{w1} \quad \psi_{w1} \quad y_{w2} \quad \psi_{w2}\right]^T;$$

The cost function is given in Equation (10), where the first term reflects the expected performance of the controller and the second term reflects the control effort requirement [13]. By tuning the weighting matrices $\mathbf{Q}$ and $\mathbf{R}$ to ensure a good design of the optimal controller [9], a control gain matrix $\mathbf{K}$ is obtained and the control input vector consisting of the two actuator torque signals is defined by Equation (11).

$$J = \int \left(\boldsymbol{y}^{\boldsymbol{T}} . \mathbf{Q} . \boldsymbol{y} + \boldsymbol{u}^{\boldsymbol{T}} . \mathbf{R} . \boldsymbol{u}\right) dt; \tag{10}$$

Where;

$$\mathbf{Q} = diag(45.5, 0.01, 3.5, 0.01); \qquad \mathbf{R} = diag(10^{-12}, 10^{-12});$$

$$\boldsymbol{u} = -\mathbf{K} . \boldsymbol{x}; \tag{11}$$

3. Estimator design

The optimal controllers for the two inputs (actuators) are designed with the use of full state variables, and a majority of the feedback such as wheel-rail deflection and wheelset angle of attack is not readily measureable [15]. Therefore, some form of state estimation is required to

provide state estimates to the controller in order for the controller to calculate the torque demands.

The approach adopted in this research study is to use a Kalman-Bucy Filter (KF) to provide the required feedback variables. More importantly, this KF can also be used for the purpose of fault diagnosis and condition monitoring tasks, where the fault detection and isolation scheme for actuators can be developed [13]. In addition, the use of the KF can also guarantee that the correct feedback information is available to ensure the system integrity in the case of sensor failure(s) [14]. The Kalman filter is designed based on Equation (12), where the estimated signals would be used to detect fault(s) in the actuators [12].

$$\dot{\boldsymbol{x}}_{\boldsymbol{k}} = \mathbf{A}_{\mathbf{k}} \cdot \boldsymbol{x}_{\boldsymbol{k}} + \mathbf{B}_{\mathbf{k}} \cdot \boldsymbol{u}_{\boldsymbol{k}} + \boldsymbol{\mu}_{\mathbf{k}} \cdot \boldsymbol{w}_{\boldsymbol{k}}, \tag{12}$$

$$\boldsymbol{x}_{\boldsymbol{k}} = \left[\dot{y}_{w_1} \quad y_{w_1} - y_{t_1} \quad \dot{\psi}_{w_1} \quad \psi_{w_1} \quad \dot{y}_{w_2} \quad y_{w_2} - y_{t_2} \quad \dot{\psi}_{w_2} \quad \psi_{w_2} \quad \dot{y}_g \quad y_g - \left(y_{t_1} + y_{t_2} \middle/ 2 \right) \quad \dot{\psi}_g \quad \psi_g \quad \dot{y}_v \quad y_v - \left(y_{t_1} + y_{t_2} \middle/ 2 \right) \right]^T$$

Where;

$$\boldsymbol{u}_{\boldsymbol{k}} = \left[\tau_{w1} \quad \tau_{w2} \quad 1/R_1 \quad \theta_{c1} \quad 1/R_2 \quad \theta_{c2} \right]^T ; \boldsymbol{w}_{\boldsymbol{k}} = \left[\dot{y}_{t_1} \quad \dot{y}_{t_2} \right]^T,$$

In the equation, the lateral displacements of the wheelsets, bogie and vehicle body are replaced by their lateral displacements relative to the track in order to control the vehicle to follow the track; the derivatives of the track irregularities are considered as the input white noise for the design [10].

The vehicle is equipped with eight sensors (six accelerometers and two displacements). The accelerometers are used to measure the lateral and yaw acceleration of the leading and trailing wheelsets and the bogie frame, while the two displacement sensors are used to measure the yaw motion of each wheelset relative to the bogie – the latter is used to provide information of the wheelset, but to avoid the need for axle mounted sensors which

would be problematic in practice due to the hostile working environment. The output equation for the measurements is given in Equation (13).

$$\boldsymbol{y_k} = \mathbf{C_k}.\boldsymbol{x_k} + \mathbf{D_k}.\boldsymbol{u_k} + \boldsymbol{v_k}; \tag{13}$$

Where;

$$\boldsymbol{y_k} = \left[\ddot{y}_{w1} \quad \ddot{\psi}_{w1} \quad \ddot{y}_{w2} \quad \ddot{\psi}_{w2} \quad \ddot{y}_{g} \quad \ddot{\psi}_{g} \quad \Delta\psi_{w1} \quad \Delta\psi_{w2}\right]^T;$$

$$\Delta\psi_{w1} = \psi_{w1} - \psi_g;$$

$$\Delta\psi_{w2} = \psi_{w2} - \psi_g$$

$\boldsymbol{v_k}$ represents the measurement noise vector, and the measurement matrix $\boldsymbol{C_k}$ is obtained readily from the system matrix $\boldsymbol{A_k}$. In this study, all measurement noises are set to 2% of their maximum value at the vehicle speed of 50 (m.sec^{-1}). The covariance matrix **Q** for the process noise (track) is given in Equation (14), while tuning **Q** is important to minimise the estimation error.

$$\mathbf{Q} = \begin{bmatrix} 1\times10^{-6} & 0 \\ 0 & 1\times10^{-6} \end{bmatrix} \tag{14}$$

4. Control analysis in fault conditions

In active control, good performance during curve negotiation can be achieved if both actuators remain fully functional. In order to be able to develop a fault detection and isolation scheme, it is first necessary to define different failure modes that are likely to occur for the actuator and to understand the consequence of those hardware failures. Two of the most regular actuator failures are considered in this research – one is a fail-hard and the other fail soft [8].

4.1 Fail-hard

In the case of electro-mechanical actuators as used in this study, a fail-hard is a failure

condition when an actuator becomes stuck or immovable [18]; this might be caused by a mechanical jam, due to lack of lubrication. Figure 2 and 3 show the relative yaw angle between the bogie frame and the wheelset, where the actuator at the leading or trailing wheelset fails in hard mode at the time of 5(sec). The relative yaw angle for the wheelset with the hard failure is severely restricted as expected – the small movements are due to the flexibility included in the study for the connection of the actuators to the bogie frame.

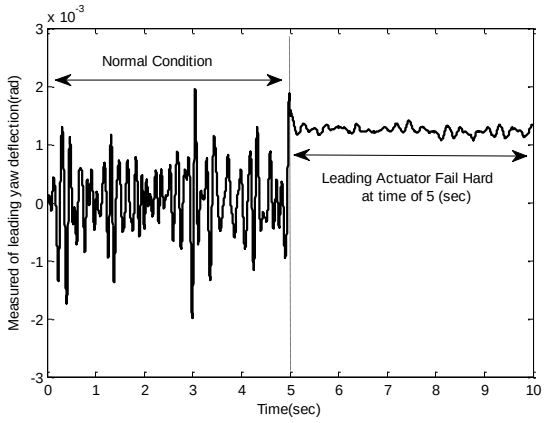

Figure 2: Measured relative yaw deflection of leading wheelset

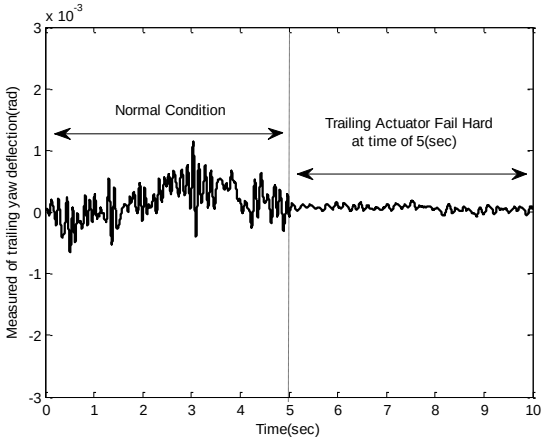

Figure 3: Measured relative yaw deflection of trailing wheelset

Figure 4 compares the minimum damping ratio of the wheelset modes between normal condition, and when one of the actuator fail-hard [8]. In the normal condition with both actuators functioning, the bogie is designed to be stable. An actuator hard failure would

reduce the stability margins, but does not present a major concern for stability - even in the case of trailing actuator failure, the critical speed is still around 85 ($m.sec^{-1}$) or 306 ($km.h^{-1}$). However, the fail-hard condition poses a more problem for the curving performance of the bogie.

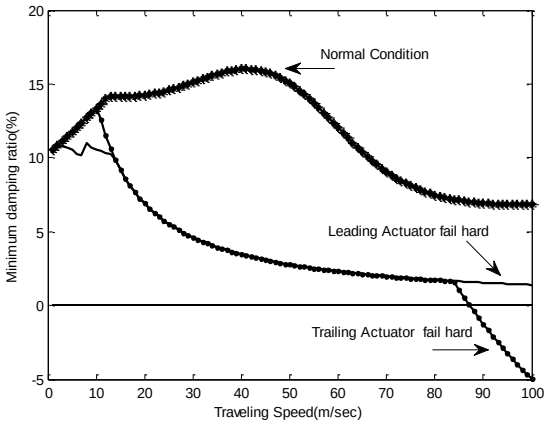

Figure 4: Minimum damping ratio

The simulation results in Figure 5 and 6 indicate clearly that when fail hard occurs in the leading and trailing control input respectively, the original controller will not be able to provide the 'right' control effort as the contact creep forces at the both leading and trailing wheelset increase significantly on the curved track, delivering a poor steering condition. Therefore, the objective of the fault tolerance in the fail-hard scenario is to minimize the adverse impact of the actuator failure on the curving performance. It can be seen that the curving performance is more under risk when fail-hard occurs for the leading actuator.

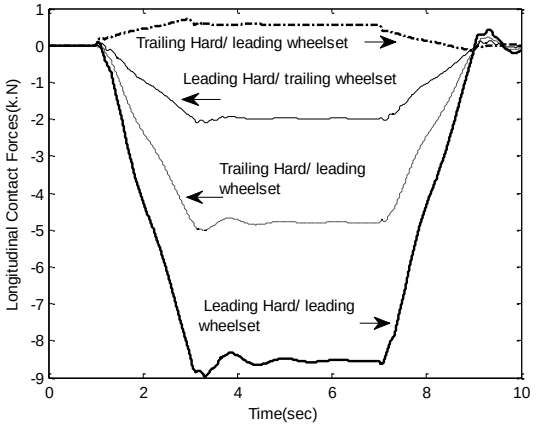

Figure 5: Longitudinal contact forces

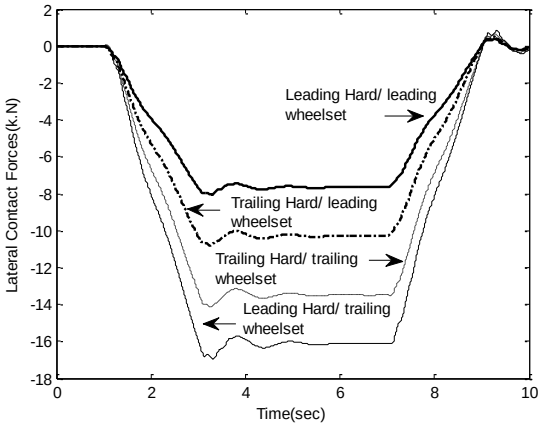

Figure 6: Lateral contact forces

4.2 Fail-soft

A fail-soft is a failure condition whereby the control surface moves freely without providing any moment to the vehicle, which may be caused by a failure of the electric motor to deliver any output torque [18]. The control torque for the failed actuator in this scenario is zero and therefore not able to stabilise the kinematic mode of the wheelset. Figure7 and 8 show the lateral deflections of both the leading and trailing wheelsets in the event of fail-soft for front and rear actuators, respectively, at the time of 5 (sec). This wheelset lateral deflection is larger enough to cause flange contact and possible derailment, if timely detection and corrective measures are not taken.

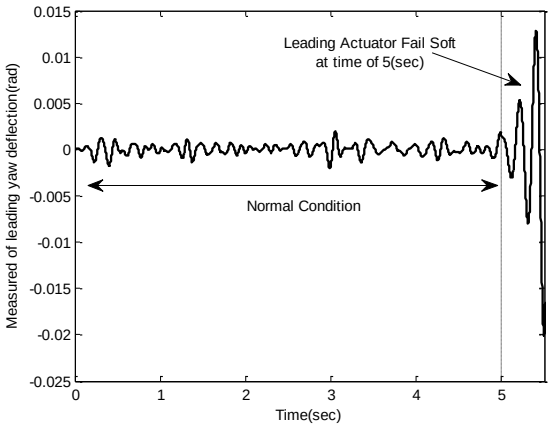

Figure 7: Leading yaw deflection

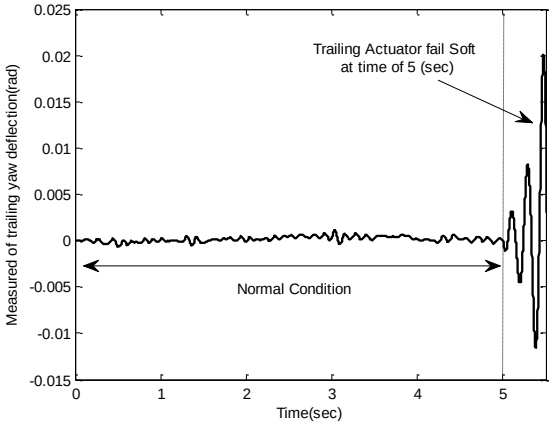

Figure 8: Trailing yaw deflection

Clearly, in the event of fail-soft condition, the active controller would not able to stabilize the system and therefore the priority of fault tolerance for the active control systems is to preserve stability control in the presence of actuator fail-soft, with the curving performance a secondary design issue.

5. Fault detection and isolation

In the event of actuator malfunction, the fault detection is possible using the model-based fault detection method, by the mean of the evaluation of the residuals. In this study, the Kalman filter based method is preferred for fault detection because it is already implemented in the control scheme to estimate the full-states' feedback for the controller. Therefore, the

residuals can be generated capture between the estimated data $\hat{y}_k$ and measured data y_k indicated by the sensors.

5.1 Fail-hard detection

Figure 9 (a) and 9(b) compare the generated residuals of relative yaw angle for both wheelsets between normal condition, and when the leading actuator is locked-up (i.e. fail-to hard mode) at the time of zero. They clearly show that the level of the error signals is significantly increased, as the wheelset will be locked by the faulty actuator. In the scenario of trailing actuator fail-hard, the generated residuals of the yaw deflection for both wheelsets are increased compared to the normal condition, as shown in Figure 10 (a) and 10(b) respectively.

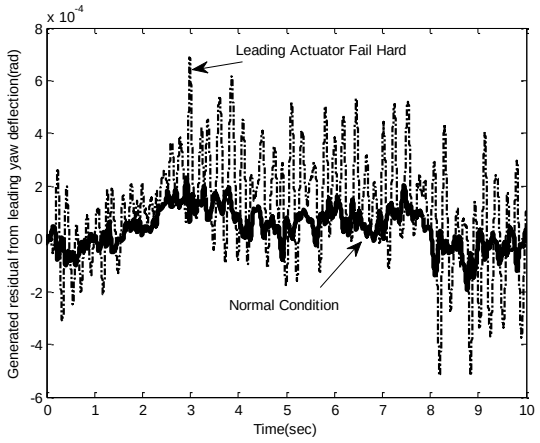

Figure 9(a). Generated residual of leading yaw deflection when leading fail-hard

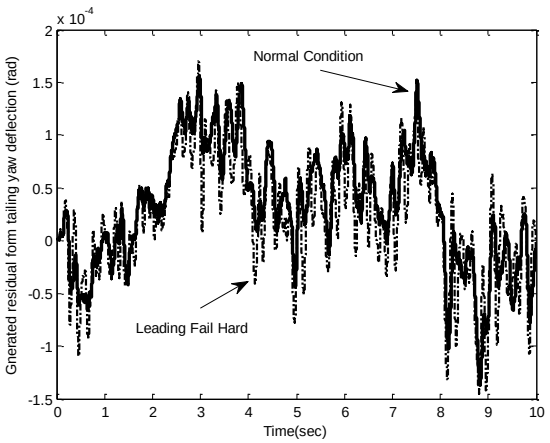

Figure 9(b). Generated residual of trailing yaw deflection when leading fail-hard

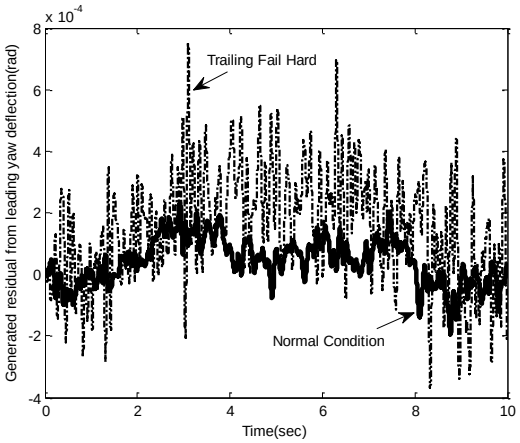

Figure 10(a). Generated residual of leading yaw deflection when trailing fail-hard

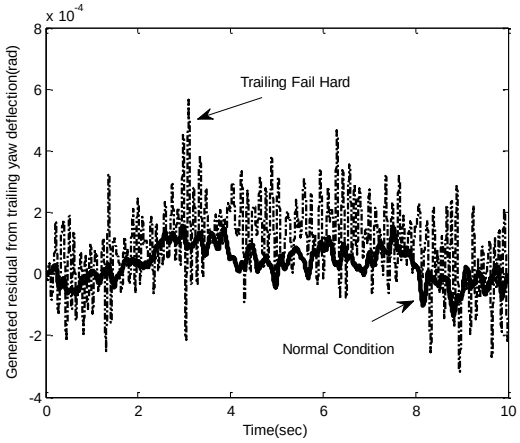

Figure 10(b). Generated residual of trailing yaw deflection when trailing fail-hard

In order to extract features for fault detection and isolation, the root mean square or standard deviation can be considered, but in this study the latter is used as in the fail-hard mode as an actuator may lock-up at different positions rather than just at zero position. Therefore, the

standard deviation moving window has been used to analyse the data. Figure 11 and 12 compare the standard deviation moving window with the size of 1 (sec) of the residuals of the relative yaw angle for both wheelsets when one of the actuators is fail-hard and in the normal condition.

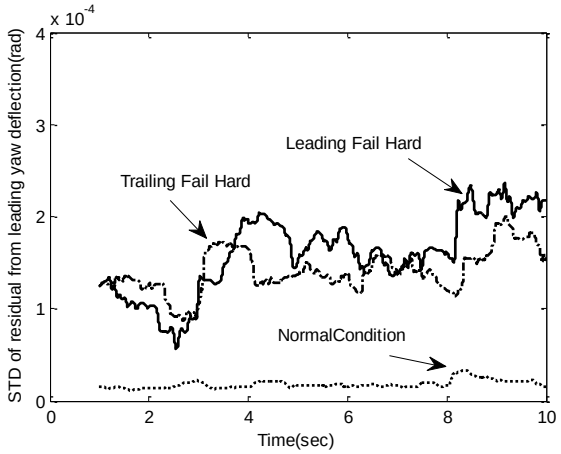

Figure 11: STD of residual from leading yaw deflection

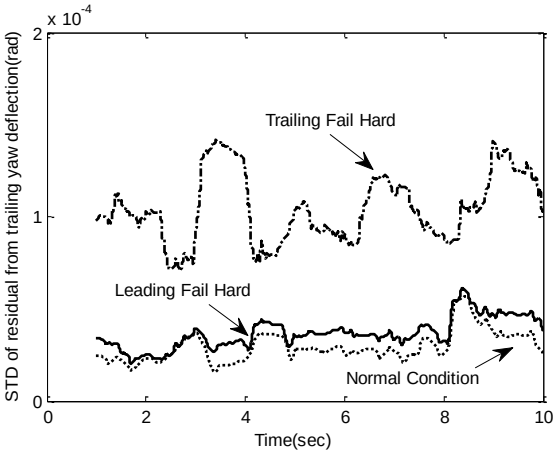

Figure 12: STD of residual from trailing yaw deflection

It can clearly be seen that the actuator fail-hard can be detected and isolated if the residuals of the yaw deflections are above a certain threshold. The leading actuator with the hard failure can be detected when the standard deviation of the generated residual from the leading yaw deflection exceeds a certain point (Figure 11), while the standard deviation moving window of the generated residual from the trailing yaw deflection does not show a significant change (Figure 12). The event of trailing hard failure can be identified when the

standard deviation running window of generated residual from the relative yaw displacement at the trailing wheelset exceeds a certain point (Figure 12).

Further analysis shows that the generated residuals from the yaw accelerometers of the two wheelsets do not show significant changes in fail-hard conditions compared to the normal condition. For example, Figure 13 reveals that the standard deviation moving window of generated residual from the leading yaw accelerometer is always below a certain point. The latter pattern can be considered to separate the hard failure from the soft mode.

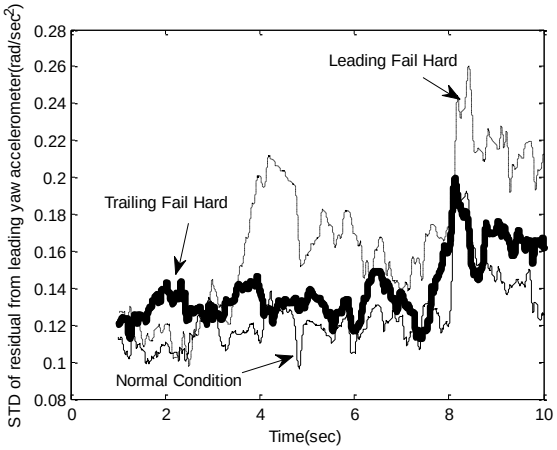

Figure 13: STD of residual from leading yaw accelerometer

5.2 Fail-soft detection

The actuator in the event of fail-soft can lead to system instability, and therefore the residuals generated by the observer will be expected to show an oscillation (or a limit cycle if the non-linearity of the wheel-rail profiles is considered) as demonstrated in Figure 14 where one of the actuators fails in the soft mode at the time of zero.

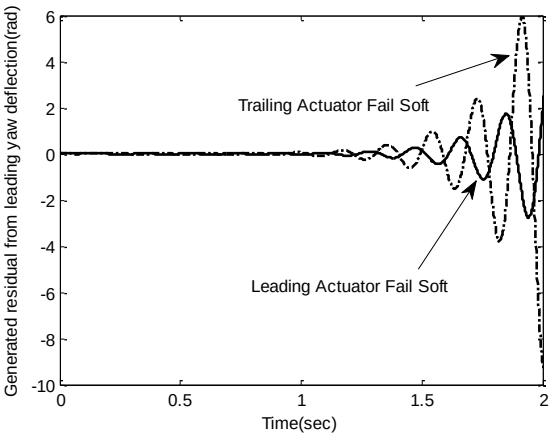

Figure 14: residual of trailing yaw deflection

However, it seems that the use of residuals alone is not sufficient to identify whether the fail-soft occurs at either front or rear actuators as all generated residuals from sensors are largely increased. Therefore, it is necessary to include extra patterns in order to isolate the location of the soft failure.

Study shows that the standard deviation ratio of measurement of the lateral accelerometer of the front and rear wheelsets to its residual can be used to determine the location of the soft mode respectively. Figure 15 and 16 show the standard deviation running window with the size of 1 (sec) of the ratio of the front and rear lateral acceleration to their residuals when one of the actuator fail-soft at the time of zero respectively. It clearly indicates that the ratios for the wheelsets with the faulty actuator are higher.

This is due to the fact that when the actuator fail-soft occurs either in the leading or trailing wheelset, the faulty actuator is not able to deliver any torque to the wheelset and therefore the lateral oscillation of that wheelset without actuator torque significantly increase. Based on the simulation results, the ratio of the leading accelerometer to its residual for the leading wheelset in the event of leading actuator fail-soft is above 8 and in the event of trailing actuator fail-soft is below 2 (Figure 15), whereas, the ratio of the trailing accelerometer to its residual for the trailing wheelset in the event of the trailing actuator fail-soft is above 3 and in the event of leading actuator fail-soft is below 3 (Figure 16).

It can be seen that the standard deviation of the measurement of the lateral accelerometers of the wheelset to their residuals can provide a proper threshold to identify the actuator fail-soft. Therefore, the location of the actuator fail-soft can be diagnosed if the ratios exceed a certain point.

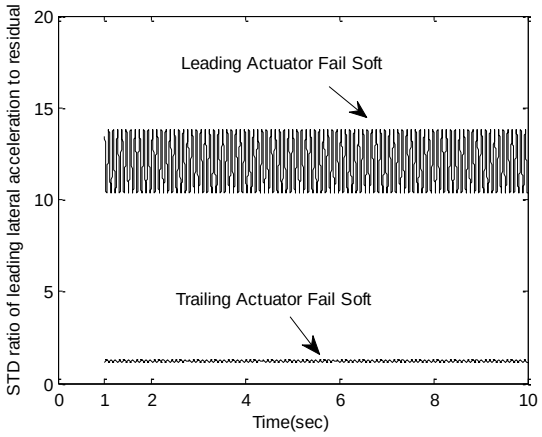

Figure 15: STD ratio of leading lateral accelerometer to residual

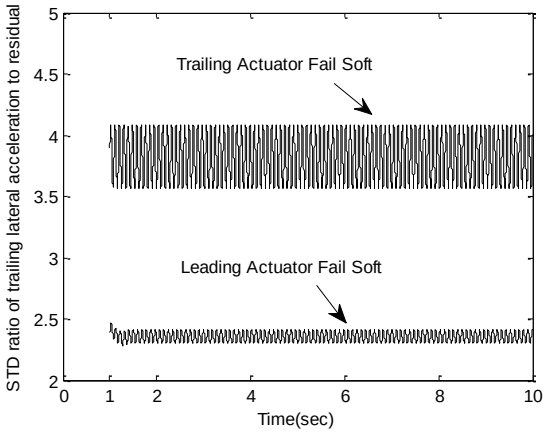

Figure 16: STD ratio of trailing lateral accelerometer to residual

In order to detect the actuator in the hard failure from the soft failure, the generated residual from the wheelset yaw accelerometer can be considered due to the fact that the magnitude of those generated residuals does not show significant changes in the fail hard condition compared to the normal condition (Figure 13). Table-1 summarises the change of the residuals in the event of actuator failure(s), where R_1, R_2, R_3, R_4, R_5, R_6, R_7 and R_8

represent the generated residuals from leading lateral accelerometer, leading yaw accelerometer, trailing lateral accelerometer, trailing yaw accelerometer, bogie lateral accelerometer, bogie yaw accelerometer, leading and trailing yaw deflection respectively.

Table 1: The generated residuals from measured signals; ++ large increase; +ε relatively small increase; 0 no significant change; + increase.

Fault	location	*Residuals*							
		R_1	R_2	R_3	R_4	R_5	R_6	R_7	R_8
Soft	Leading wheelset	+ +	+ +	+ +	+ +	+ +	+ +	+ +	+ +
	Trailing wheelset	+ +	+ +	+ +	+ +	+ +	+ +	+ +	+ +
Hard	Leading wheelset	+	0	0	0	+ε	0	+	0
	Trailing wheelset	+	0	+ε	0	+	+	+	+

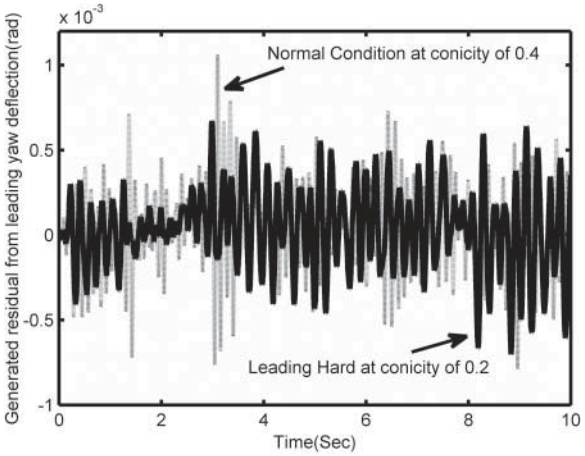

Figure 17. Generated residual from leading yaw deflection at conicity of 0.2 and 0.4

One of the critical design challenges is that the features for fault detection must be robust against uncertainties, such as parameter variations at the wheel-rail interface. For example, Figure 17 indicates that the generated residual from leading yaw deflection in the

event of leading actuator fail-hard at the conicity of 0.2 can give similar output as that in the normal condition at constant conicity of 0.4. This is because the effect of the parameters such as conicity on the dynamic properties of a rail vehicle can be significant, and deviations from the nominal values used in the model changes could lead to estimation inaccuracies in the similar way as the fault conditions. Research is on-going to ensure the FDI scheme will meet the robust requirements of diagnosing the actuator failure, e.g. by considering the use of additional measurements to improve the robustness and/or extended Kalman filter where the conicity can be included as an extra estimation parameter.

6. Conclusion

This report presents a novel fault detection and isolation strategy for actively controlled railway vehicles in the event of actuator failure, in order to ensure the system safety and maximise the vehicle performance under the fault conditions.

In this methodology, a model-based approach using the Kalman-Bucy Filter has been used to detect and identify the actuator failures by residuals' evaluation in the time domain. It is suggested that the actuator in a hard mode can be readily isolated through evaluating the generated residuals from the yaw deflection sensors. The actuator with the soft failure can be isolated by computing the standard deviation ratio of measurement of the lateral accelerometer of the front wheelset to its residual.

One of the critical design aspects is that the features for fault detection depend on the reliability of the sensors, and also must be robust against structured uncertainties, such as the parameter variations at the wheel-rail interface and nonlinearities of the vehicle dynamics. Therefore, the robustness of the proposed FDI will need to be considered in the further work

in order to ensure the reliability of the proposed new technology against uncertainties in the system and in the event of other faults in the control system.

Acknowledgement

Authors wish to acknowledge the support of the EPSRC, Rail Research UK Association (RRUKA) and Southwest Jiaotong University (State Key Laboratory of Traction Power) for funding/supporting the project, which made this study possible.

Appendix A

Vehicle symbol and parameter in the simulation

Symbols	Parameters
$y_{w_1}, y_{w_2}, y_g, y_v$	Lateral diplacement of leading, trailing wheelset, bogie frame and vehicle body
$\psi_{w_1}, \psi_{w_2}, \psi_g$	yaw diplacemet of leading, trailing and bogie fram.
V_s	Vehicle forward speed (50m/s)
m_w, I_w	wheelset mass (1250 kg) and yaw inertia (700 kgm^2), respectively
I_g, I_v	Half guage of wheelset(0.7 m), half spacing of axle(1.225 m)
r_0, λ	wheel radius(0.45 m), and conicity (0.2)
m_g, I_g	Bogie frame mass(6945 kg), and Yaw inertia (3153 kgm^2) respectively.
K_{sc}, C_{sc}	Secondary Lateral and longitudinal stiffness (511 kNm^{-1}), and damping(37 $kNsm^{-1}$) respectively.
K_s, C_s	primary Lateral stiffness (4750 kNm^{-1}), and damping (7705 N sm^{-1}) respectively.
m_v	Half vehicle mass (15000kg)
f_{11}, f_{22}	Longitudinal and lateral creepage coefficient (10MN).
R_1, R_2	Radius of the curved track at the leading and trailing Wheeslet(1250 m).
$\theta_{c_1}, \theta_{c_2}$	cant angle of the curved track at the leading and trailing wheelset (6°)
y_{t_1}, y_{t_2}	Track lateral diplacement for leading and trailing wheelsets, respectively
τ_{w_1}, τ_{w_2}	Controlled torque for leading and trailing weelset respectively.
g	Gravity (9.8 m/s^2)

References

[1] T. Mei and H. Li, “Control Design for the Active Stabilization of Rail Wheelset,” Dynamic, System, Measurement and Control, vol. 130, no. 1, pp. 011002 - 011011, Jan 2008.

[2] S. Bruni, R. Goodall, T. Mei and H. Tsunashima, “Control and monitoring for railway vehicle dynamics,” International Journal of Vehicle Mechanics and Mobility, pp. 743 - 779, 01 July 2007.

[3] R. Goodall and T. Mei, “Advanced Control and Monitoring for Railway Vehicle Suspensions,” In STECH'06, Proceedings of International Symposium on Speed-up and Service Technology for Railway and Maglev Systems, Chengdu Sichuan P.R.China,, pp. 0-16, 2006.

[4] T. Mei, “A Study of Fault Tolerance For Active Wheelset Control,” in 22 nd IAVSD, Manchester,UK, 2011.

[5] D. Fischer, M. Borner, J. Schmitt and R. Isermann, “Fault detection for lateral and vertical vehicle dynamics,” Control Engineering Practice, vol. 15, no. 3, pp. 315-324, 2007.

[6] Y. Hayashi, H. Tsunashima and Y. Muramo, “Fault detection of railway vehicle suspension system using multiple-model approach,” Jornal of Mechanical systems for transportation nad logistics, vol. 1, no. 1, pp. 88-99, 2008.

[7] R. Patton, “FAULT-TOLERANT CONTROL SYSTEMS: THE 1997 SITUATION,” in IFAC SAFEPROCESS'1997, Hull,UK, 1997.

[8] M. Mirzapour and T. Mei, “Assessment of Fault Tolerance for Actively Controlled Railway Wheelset,” in IEEE,UKACC, Cardiff, 2012.

[9] J. Pearson, R. Goodall, T. Mei and G. Himmelstein, “Active stability control strategies for a high,” Control Engineering Practice, vol. 41, pp. 1381-1391, 2004.

[10] T. Mei and R. Goodall, “Wheelset control strategies for a 2-axle railway vehicle,” Vehicle System Dynamics, vol. 33, pp. 653-664, 2000.

[11] T. Mei and R. Goodall, “Robust Control for Independently Rotating Wheelsets on a Railway Vehicle Using Practical Sensors,” vol. 9, no. 4, JULY 2001.

[12] V. Garg and R. Dukkipati, Dynamic of Railway Vehicle Systems, CANADA: ACADEMIC PRESS, 1984.

[13] T. Mei and R. Goodall, “LQG and GA solutions for active steering of railway vehicles,” Control Theory and Applications, IEE Proceedings - (Volume:147 , Issue: 1), pp. 111 - 117, 2000.

[14] T. Mei and R. Goodall, “Recent development in active steering of railway vehicles.,” Vehicle System, vol. 39, no. 6, p. 415–436, 2003.

[15] T. Mei, H. Li and R. Goodall, “Kalman Filters applied to actively controlled railway vehicle,” ransactions of the Institute of Measurement and Control 23, pp. 163-181, 2001.

[16] R. Iserman, “Model_Based Fault Detection and And Diagnosis Satus and Applications,” in 16th IFAC Symposium on Automatic Control in Aerospace, Osaka, Japan, 2004.

[17] Y. Zhanga and J. Jiang, “Bibliographical review on reconfigurable fault-tolerant control systems,” vol. 32, no. 2, 2008.

[18] H. Alwi, E. Christopher, P. Tan and Chee, Fault Detection and Fault-Tolerant Control Using Sliding Modes, London: Springer, 2011,page 7-27.

[19] R. Isermann, “Mechatronic systems—Innovative products with embedded control,” Control Engineerin Practice, vol. 16, pp. 14-29, 2008.

[20] R. Ngigi, C. Pislaru, A. Ball and F. Gu, “Modern techniques for condition monitoring of railway vehicle dynamics,” Journal of Physics: Conference Series364, 2012.

[21] T. Mei and R. Goodall, “Practical strategies for controlling railway wheelsets with independently rotating wheels,” vol. 125, 2003.

[22] R. Isermann, Fault-Diagnosis Applications, Verlag Berlin Heidelberg, Germany: Springer, 2011.

APPENDIX F COPY OF UKACC' 2014 PAPER

Detection and isolation of actuator failure for actively controlled railway wheelsets

Mirzapour M, Mei T.X

UKACC International conference on control, 9-11 July 2014

University of Loughborough, UK

Publisher IEEE

Detection and isolation of actuator failure for actively controlled railway wheelsets

Mohammad Mirzapour
School of Computing, Science Engineering
The University of Salford
Greater Manchester, M5 4WT, UK
m.mirzapour@edu.salford.ac.uk

T.X Mei
School of Computing, Science Engineering
The University of Salford
Greater Manchester, M5 4WT, UK
t.x.mei@salford.ac.uk

Abstract—**This paper studies a model-based approach for the condition monitoring of an actively controlled railway system, with a focus on actuator failures to detect and isolate failure modes in such a system. It seeks to establish the necessary basis for fault detection to ensure system reliability in the event of an abnormal change in one of the two actuators. Computer simulation is used to demonstrate the effectiveness of the method.**

Keywords—active control; railway system; condition monitoring; fault tolerance; fault detection and isolation

I. INTRODUCTION

A conventional railway wheelset for the railway vehicle is composed of two coned (or profiled) wheels rigidly fixed to a common axle. Although this arrangement has the advantages of natural curving, it exhibits a sustained oscillation when the wheelset is unconstrained. Traditionally, the wheelset is stabilized by using passive suspensions on conventional rail vehicles, but such additional stiffness affects the pure rolling action of the wheelset during curve negotiation. Therefore, if passive components are to be used then a compromise has to be made between steering and stability [1]. However, recent studies have demonstrated that this design conflict can be solved by applying active control for railway wheelsets in primary suspensions to stabilize the wheelset without compromising the vehicle's performance during curve negotiation, leading to a significant reduction in the wear of the wheelset and track and minimized track-shifting forces [2]. In this new approach, the improved dynamic performance is achieved through the use of actuators, sensors, and the software that implements the control algorithm to provide a link between the controller and vehicle system to be controlled. However, the use of actuators, sensors to replace the traditional passive suspensions raises the issue of system safety in the event of a failure of the active control, which could result in the loss of stability and in more severe cases, derailment [3]. Therefore, active systems for safety-critical applications have to achieve a high level of integrity through fault tolerance approaches that ensure the basic functionality of the overall system whilst allowing component fault(s) [2].

Although hardware redundancies may be used in the system to ensure the necessary functionality and safety of such a system, and sometimes it may be acceptable to use redundant sensors due to their relatively low costs, it is difficult to justify the likely high cost of using multiple actuators for redundancy and/or to accommodate these within the limited space of a railway bogie. On the other hand, an analytical redundancy method can help to minimize the use of the hardware redundancies in order to keep the overall cost down [4].

For the main components used in an active control system, the actuators tend to be cost intensive and require more space to be embedded than sensors and electronic control units; hence, developing an analytical redundancy-based fault tolerance approach for active wheelset control that does not increase the number of actuators is essential [5]. In order to develop a fault tolerant control (FTC) scheme for actively controlled wheelsets in the event of actuator failure, fault detection and isolation (FDI) performs a substantial task by providing information about actuator faults in the system that enables the controller in the system to be re-configured in order to cope with identified faults [6].

Fault detection and isolation techniques have been widely studied, some of which are concerned with the detection of actuator failures in different industrial applications. For example, a neural network has been used to detect and diagnose the malfunction of a pneumatic actuator of a train door [7]; Wolfram and Isermann [8] demonstrated the use of parameter estimation for detecting the electro-mechanical actuator of a textile machine when the electrical part of an ac motor breaks down; and study in [9] used the Extend Kalman Filter (EKF) to detect pump pressure faults in an electro-hydraulic actuation system. However, a literature review of the railway vehicle suggests that the majority of condition monitoring tasks are comprehensively considered as the fault identification in dynamic systems [10] such as conicity estimation [11], suspension failure [12], creep force [13] and creep coefficients [14]. The subject of the FDI of the actuator failure(s) with the use of active control within primary suspension has not been addressed for the railway vehicles.

In this paper, the objective of the study is to focus on the development of an FDI method with a model-based technique for the electromechanical actuators to identify actuator failure in order to enable the appropriate reconfiguration to take place to facilitate the development of a fault tolerant control scheme. Modelling techniques and specified models for railway vehicle dynamic systems are well developed, and therefore a model-

based approach is considered in this paper to exploit the dynamic changes (caused by an actuator fault) of a vehicle for FDI in different failure modes (e.g. hard and soft failures). In this study, a Kalman-Bucy Filter (KF) based method is used to develop a fault detection scheme where the residuals will be generated to capture differences between the output of the dynamic model and the measurements from sensors. Two different sensing options will be discussed in relation to condition monitoring tasks, and a thorough assessment of the FDI of the actuator faults with the two sensing options will then be carried out.

II. VEHICLE DYNAMIC AND CONTROL SCHEME

This study uses a conventional two-axle bogie with a half body frame, which is a standard practice in the study of rail vehicle dynamics. Figure 1 presents a simplified plan view diagram of the vehicle scheme which consists of two wheelsets, a bogie frame and a half vehicle body. The wheelsets are connected to the bogie via springs and dampers in the lateral direction. In practice, some form of longitudinal connection is needed to transmit traction and braking forces from the wheelsets to the vehicle body frame, but this is not a concern of the current study and hence not included [1]. On each wheelset, an actuator is also placed between the wheelset and the bogie in the yaw direction for implementation of the active control [15]. The equations of motion for a railway vehicle when travelling along a track are principally determined by the creep forces that are generated between the wheel and rail contact patches [16].

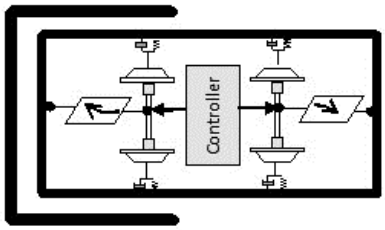

Figure 1: Simplified plan view diagram

The linear model of the motion contains seven degrees of freedom representing the lateral and yaw motion of the two wheelsets, lateral and yaw motion of the bogie frame and lateral motion of the half vehicle body [1]. The use of the linear model is justified as the active control tends to reduce the effect of non-linearity in the wheelsets [17] and it can be demonstrated by the equations given in [18]. The variable and parameters of the vehicle scheme are defined in the Appendix.

Figure 2 shows the overall fault tolerant control (FTC) scheme for the railway vehicle used in this study. The FTC scheme consists of two parts: the first part is a re-configuration active controller, and the other an FDI scheme for detecting and isolating potential component failure(s). The FDI will also be concerned with sensor faults [2], but this paper will deal with the issue of actuator failure(s) only. When the vehicle starts to run along a track, the output measurements from the vehicle model to the Kalman-Bucy Filter (KF) provide state estimates to the controller, while the controller calculates the torque demands which are sent to the actuators, and which then apply the required control torque to the vehicle's wheelsets. At the same time, the output measurements from each actuator to the a local Kalman filter generate its own residuals which are then analyzed in order to provide information for identification of the actuator's status. If an abnormal change is diagnosed based on information provided by the FDI filter, the controller re-configuration unit will adjust the structure and the tuning of the controller in order to maintain the desired performance.

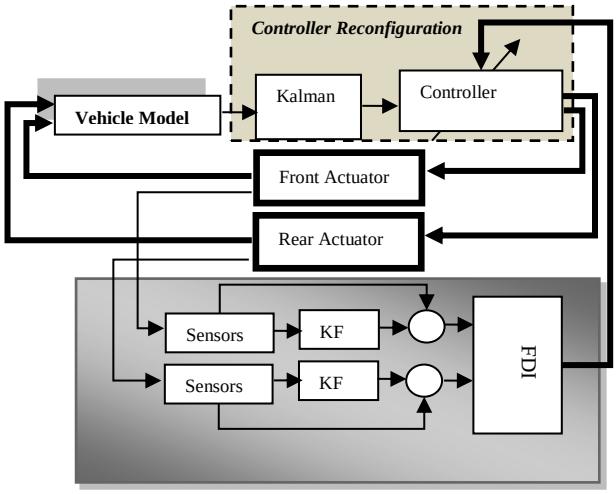

Figure 2: Fault tolerant control scheme

III. ACTUATOR DYNAMICS

Different technologies can be considered in order to realize the actuation system in active suspension, such as pneumatic actuation, electro-hydraulic actuation, electro-mechanical actuation and electro-magnetic actuation [19]. However, in this study, electro-mechanical actuation is selected to meet the main requirement for the active control: to stabilize the kinematic modes and curving performance. The actuator model consists of two sections: the first models the electrical dynamics of a dc motor, while the second models the mechanical parts of the motor inertia and gearbox ratio. The linear model for the actuator is given in Eq. (1) and Eq. (2), respectively.

$$I_m \ddot{\theta}_m = K_t \cdot i_a + \tau_g \tag{1}$$

$$di_a/dt = R_a/L_a \cdot i_a + V_a/L_a - K_b \cdot \dot{\theta}_m/L_a \tag{2}$$

Where:

$$\tau_g = (\psi_w - \dot{\theta}_m/n) . K_g/n$$

The nomenclatures for symbols used in the above equations are provided in the Appendix—together with the parameter values assumed for all calculations presented in this section. The use of a Proportional-integral (PI) controller for the actuator is found to satisfy the requirements for the control of torque output, as given in Eq. (3).

$$C(s) = e(G_p + G_i/s) \quad (3)$$

Where e represents an error value as the difference between the measured current (i_a) of the dc motor and the desired current set-point (i_{set}); this can be determined readily from the demand torque (τ_w) discussed in section 2, as the current is proportional to the gear ratio and motor constant as shown in Eq. (4).

$$i_{ref} = \tau_w / (n \cdot K_t) \quad (4)$$

If both actuators remain fully functional, vehicle stability and good curving performance on a curved track can be achieved. However, if one of the actuators fails, the vehicle, its stability and performance can be significantly affected [18]. This research considers the two most common actuator failures: fail-hard and fail-soft. The fail-hard is a failure condition when the motor shaft of an actuator becomes immovable (i.e. blocked); this could be caused by a mechanical jam due to a lack of lubrication [20]. The study in [18] demonstrated that an actuator with hard-failure does not have a major problem with stability, but the vehicle performance on curves can be significantly affected and hence the priority for the control reconfiguration will be to provide an improved steering action. A fail-soft condition is a failure whereby the control surface moves freely without providing any moment to the vehicle, which may result due to a failure of the electric motor to deliver any output torque [20]. In this scenario, the motor current for the failed actuator is zero, and as a result, the control torque for the failure actuator becomes zero; therefore, the actuator is unable to stabilize the kinematic mode of the wheelset and therefore the control reconfiguration will need to focus on the provision of stability control [5]. It is clear that the effective detection and isolation for potential actuator failures (as presented in the section below) will play a critical part in the overall fault tolerance scheme for the active control of railway vehicles.

IV. DESIGN OF THE FDI SCHEME

In this study, a KF-based method is used to monitor the actuator conditions. Therefore, the residuals can be generated to capture between the estimated data $\hat{y}_c$ and measured data y_c indicated by the sensors. The KF filter is implemented here to monitor the actuator status instead of estimating the actuator's states. Equation (5) defines a state-space representation of the actuator model for the KF design.

$$\dot{x}_c = A_c \cdot x_c + B_c \cdot u_c + G_c \cdot w_c; \quad (5)$$

Where;

$$\dot{x}_c = \left[\ddot{\theta}_m \quad di_a/dt \quad \dot{\tau}_g \right]^T$$
$$u_c = V_a;$$
$$w_c = \dot{\tau}_g$$

In the equation, the derivative of the torque ($\dot{\tau}_g$) between the wheelset and gearbox is considered as a noise source in the design; the inclusion of ($\dot{\tau}_g$) in the design will show that the resulting KF provides adequate information for the FDI function. In the design, a small value of 0.001 is used for the torque variable (τ_g) to have a full rank of matrix A_c. In this study, two sensing options will be discussed. In option 1, each actuator is equipped with two sensors–one to measure the actuator speed and the other to measure the motor current [21]. The output equation for the measurements is given in Eq. (6).

$$y_c = C_c \cdot x_c + H_c \cdot v_c \quad (6)$$

Where;

$$y_c = \left[\dot{\theta}_m \quad i_a \right]^T;$$

In option 2, an additional sensor is included, a strain gauge measuring the torque applied to the wheelset from the actuator gearbox. The output equation for the measurement is given in Eq. (7).

$$y_c = C_c \cdot x_c + H_c \cdot v_c \quad (7)$$

Where;

$$y_c = \left[\dot{\theta}_m \quad i_a \quad \tau_g \right]^T;$$

Where C_c can be obtained readily from the system matrix A_c, and v_c represents the measurement noise vector. In this study, all measurement noises are set to 2% of their absolute maximum values at the vehicle speed of 50(m.sec^{-1}). By tuning the covariance matrix for the process noise Q_c, the tracking performance and robustness of the KF can be thoroughly studied. The process noise is set to the covariance value of the derivative of the torque between the wheelset and gearbox, while the generated residuals of the KF will be used to provide information for the condition monitoring tasks.

A. Fail-hard detection and isolation

When an actuator fails in hard mode the actuator is immovable, i.e. the movement of the faulty actuator would be severely limited (due to elasticity in the connections). For example, Figure 3 indicates that the motor rotational velocity for the leading wheelset when the front actuator was locked significantly reduced. The study reveals that the generated residuals with the sensor option 1 alone are not sufficient to provide adequate information for fault identification in the event of actuator fail-hard, as all generated residual residuals are almost identical to the normal condition. This is due to the fact that the measurement signals used for the sensor option 1 do not provide information about the effect of the dynamic conditions of the wheelset (i.e. the load) on the actuator. Although the measured signal of the motor rotational velocity is reduced, it cannot be used alone for FDI as a benchmark is required to identify an abnormal change. The FDI may however be possible with some extra data processing.

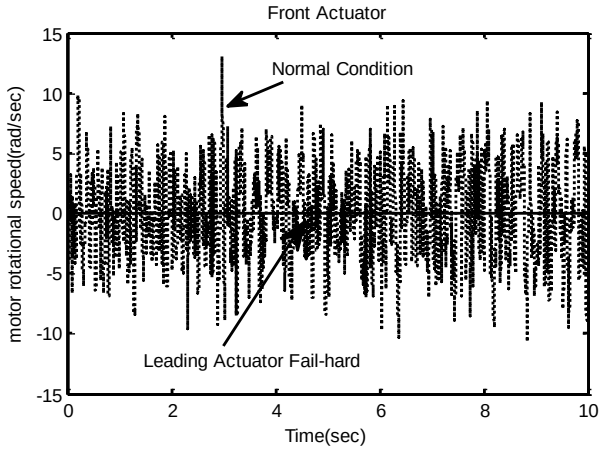

Figure 3: Measured motor rotational velocity

This study uses the standard deviation ratio of measurement of the rotational velocity of the motor to its residual to detect and isolate the actuator with the hard failure. This is because when the actuator fail-hard occurs either in the leading or trailing wheelset, the motor rotational velocity of the faulty actuator is potentially reduced, whereas the generated residuals remain unchanged; therefore, the amount ratio can provide a reliable indication of when the fault occurred. The standard deviation (STD) was preferred here as the actuator can be locked in different positions. Figure 4 shows the standard deviation running window with a size of 200(m.sec) of the ratio of the front motor rotational velocity to its residual, when the leading actuator fails hard. It clearly indicates that the ratios for the wheelsets with the faulty actuator are significantly lower. Similar results will be found when the trailing actuator fails hard.

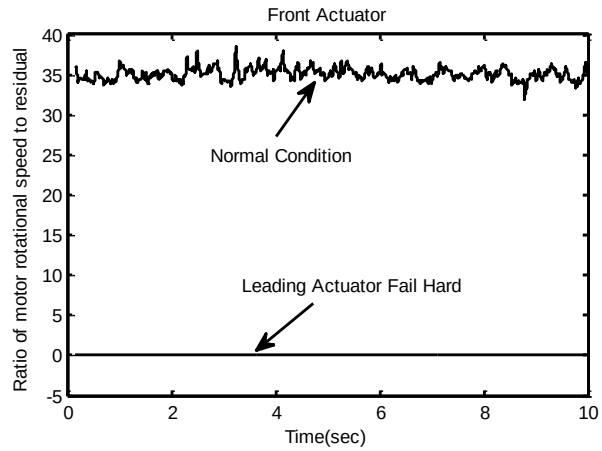

Figure 4: STD ratio of motor rotational velocity to residual – front actuator

In the sensor option 2, the fault detection can be possible simply by the evaluation of the residuals in the event of fail-hard, because the inclusion of an additional measurement provides extra information about the torque between the gearbox and the wheelset. Figures 5, 6 and 7 compare the generated residuals for the leading actuator between the normal condition, and when the leading actuator is in fail-to-hard mode. They clearly show that the level of the error signals is significantly increased for the faulty actuator, whereas the generated residuals for the healthy actuator do not show significant changes. In the scenario of trailing actuator fail-hard, the generated residuals for the leading actuator are approximately equal to the normal condition, while the faulty actuator for the trailing wheelset generates higher residuals compared to the normal condition.

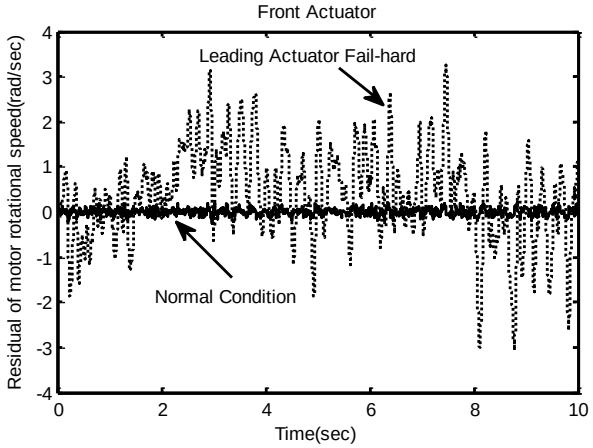

Figure 5: Residuals from motor rotational velocity – front actuator

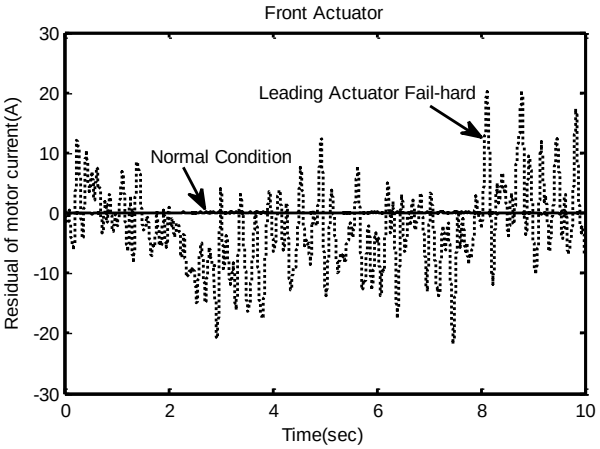

Figure 6: Residuals from motor current – front actuator

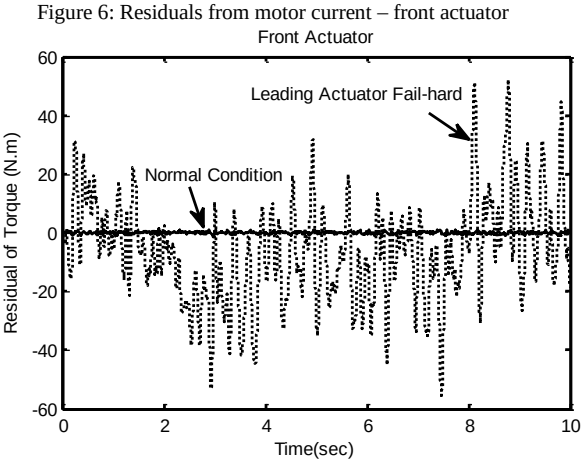

Figure 7: Residuals from gearbox torque – front actuator

In order to extract features for the FDI, the root mean square or standard deviation of the residuals can be considered; however in this study, the latter is preferred as an actuator may

lock-up at different positions rather than just at the zero position.

B. Fail-soft detection and isolation

The actuator in the event of fail-soft can lead to system instability, and therefore the residuals generated by the observer in either sensor option 1 or option 2 will be expected to show an oscillation—or a limit cycle if the non-linearity of the wheel-rail profiles is considered. Figures 8, 9 and 10 compare the generated residuals of the front actuator when options 1 and 2 are used for fault detection. They show the generated residuals of motor rotational speed, motor current and torque between the gearbox and wheelset in the normal condition, and when the leading actuator fails in soft mode. They noticeably indicate that the generated residual signals of the leading actuator are radically magnified, as the faulty actuator is not able to deliver any torque to the wheelset. Although the generated residuals of the rear actuator which functions properly increase, this gain is slow, and an abnormal change in actuator can be identified within 200(m.sec), as seen in Figure 11. Therefore, it is necessary to enable the controller to be re-scheduled to cope with the identified fault, before causing any further damage to the healthy actuator and to maintain vehicle safety. Similar results can be achieved when the trailing actuator fails soft. It seems that the use of residuals is sufficient to detect the actuator fail-soft and to identify whether the fail-soft occurs at either the front or rear actuator.

In order to detect the difference(s) between the actuator in the hard failure and the soft failure when option 2 is used, and as all the generated residuals of the faulty actuator increase, the generated residual from the motor rotational velocity can be considered due to the fact that the magnitude of those generated residuals does not exceed 4(rad.sec^{-1}) in the fail-hard condition (Figure 5), whereas it will increase drastically in the event of fail-soft (Figure 8).

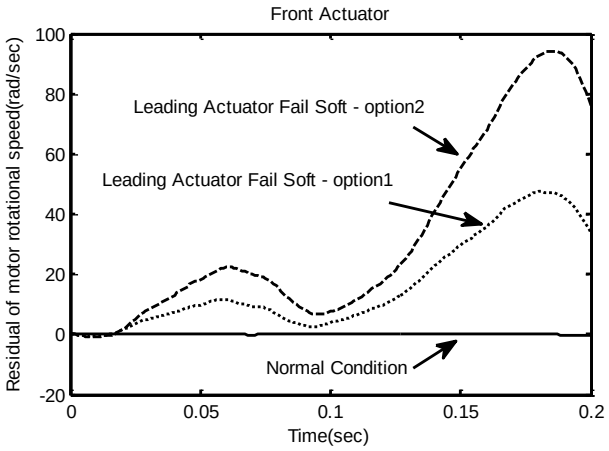

Figure 8: Residuals from motor rotational velocity – front actuator

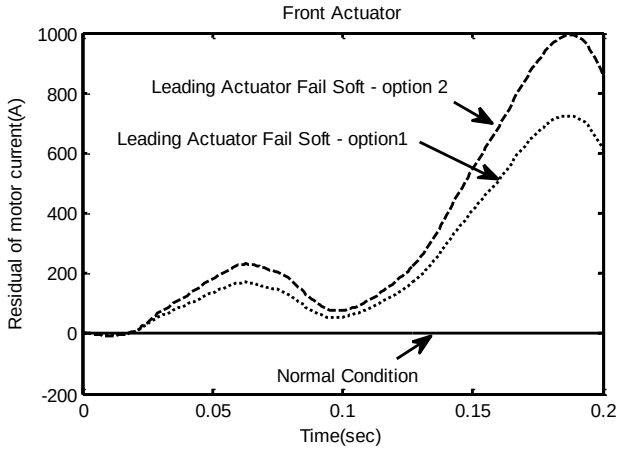

Figure 9: Residuals from motor current – front actuator

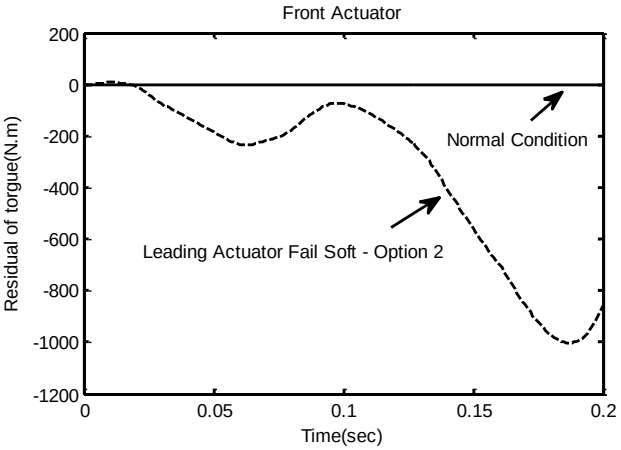

Figure 10: Residuals from torque – front actuator

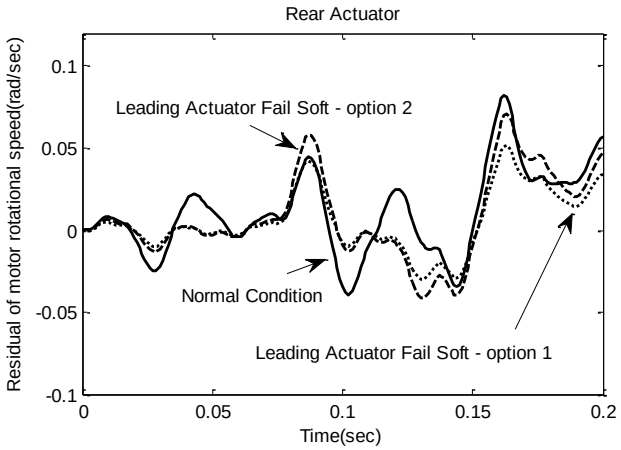

Figure 11: Residuals from motor rotational velocity – rear actuator

V. CONCLUSION

This paper presents a novel FDI strategy for actively controlled railway vehicles in the event of actuator failure, in order to ensure system safety and reliability under fault conditions. Two different options with different combinations of sensors have been suggested for developing fault detection in order to monitor the condition of the actuators. In the first

option, the actuator in the hard mode can be isolated by computing the standard deviation ratio of the measurements of the motor rotational velocity to its residual. In the scenario of the fail-soft, FDI can be achieved through the residuals' evaluation. In the second option, the type and location of the actuator failure can be identified readily through the residual evaluation.

Research is ongoing to integrate the rescheduling technique into the developed methods of FDI in order to implement a fault-tolerance technique for actively controlled wheelsets that will justify the safety and reliability of this new technology for use in the railway industry.

REFERENCES

[1] J. Pearson, R. Goodall, T. Mei and G. Himmelstein, "Active stability control strategies for a high," *Control Engineering Practice*, vol. 41, pp. 1381-1391, 2004.

[2] M. Mirzapour and T. Mei, "FAULT DETECTION AND ISOLATION FOR AN ACTIVE CONTROL WHEELSET," 23rd IAVSD International conference, Qingdao, August, 2013.

[3] R. Goodall and T. Mei, "Advanced Control and Monitoring for Railway Vehicle Suspensions," In STECH'06, Proceedings of International Symposium on Speed-up and Service Technology for Railway and Maglev Systems, Chengdu Sichuan P.R.China, pp. 1-16, 2006.

[4] T. Mei, "A Study of Fault Tolerance For Active Wheelset Control," in 22nd IAVSD, Manchester,UK, 2011.

[5] T. Mei, "A Study of Fault Tolerance For Active Wheelset Control," in 22nd IAVSD, Manchester,UK, 2011.

[6] R. Isermann, Fault-Diagnosis Applications, Verlag Berlin Heidelberg, Germany,Springer, 2011.

[7] N. Lehrasab, H. Dassanayake, C. Roberts, S. Fararooy and C. Goodman, "Industrial fault diagnosis: Pneumatic train door case study," Proceedings of the Institution of Mechanical Engineers, vol. 216, no. 3, pp. 175-183, May 2002.

[8] A. Wolfram and R. Isermann, "Component based tele-diagnosis approach to a textile machine," Control Engineering Practice, vol. 10, no. 11, pp. 1251-1257, 2002.

[9] L. An and N. Sepehri, "Hydraulic actuator circuit fault detection using extended Kalman filter," in American Control Conference, Colorado, USA, 2003.

[10] R. Ngigi, C. Pislaru, A. Ball and F. Gu, "Modern techniques for condition monitoring of railway vehicle dynamics," Journal of Physics: Conference Series364, 2012.

[11] G. Charles, R. Goodall and R. Dixon, "Model-based condition monitoring at the wheel–rail interface," International Journal of Vehicle Mechanics and Mobility, vol. 46, pp. 415-430, 2008.

[12] H. Tsunashima and H. Mori, "Condition monitoring of railway vehicle suspension using adaptive multiple model approach," in Control Automation and Systems (ICCAS), Gyeonggi-do, 2010.

[13] C. Ward, R. Goodall and R. Dixon, "Contact force estimation in the railway vehicle wheel-rail interface," in 18th IFAC World Congress, Milan, 2011.

[14] H. Imtiaz and T. Mei, "Multi kalman filtering approach for estimation of wheel-rail contact conditions," in UKACC International Conference, Coventry, UK, 2010.

[15] T. Mei and R. Goodall, "Recent development in active steering of railway vehicles.," Vehicle System, vol. 39, no. 6, p. 415–436, 2003.

[16] V. Garg and R. Dukkipati, Dynamic of Railway Vehicle Systems, CANADA: ACADEMIC PRESS, 1984.

[17] T. Mei and R. Goodall, "Robust Control for Independently Rotating Wheelsets on a Railway Vehicle Using Practical Sensors," vol. 9, no. 4, JULY 2001.

[18] M. Mirzapour and T. Mei, "Assessment of Fault Tolerance for Actively Controlled Railway Wheelset," in *IEEE,UKACC*, Cardiff, 2012.

[19] A. Pacchioni, R. Goodall and S. Bruni, "Active suspension for a two-axle railway vehicle," International Journal of Vehicle Mechanics and Mobility, vol. 48, no. 1, pp. 105-120, 2010.

[20] H. Alwi, E. Christopher, P. Tan and Chee, Fault Detection and Fault-Tolerant Control Using Sliding Modes, London: Springer, 2011,page 7-27.

[21] E. Koutroulis, J. Chatzakis, K. Kalaitzakis, S. Manias and N. Voulgaris, "A system for inverter protection and real-time monitoring," Microelectronics Journal, vol. 34, p. 823–832, 2003.

APPENDIX

Vehicle symbol and parameter in the simulation

Symbols	***Parameters***
$y_{w_1}, y_{w_2}, y_g, y_v$	Lateral diplacement of leading, trailing wheelset, bogie frame and vehicle body
$\psi_{w_1}, \psi_{w_2}, \psi_g$	Yaw displacement of leading, trailing wheelset and bogi frame
V_s, g	Vehicle forward speed (50m/s), Gravity (9.8 $m.s^{-2}$)
m_w, I_w	wheelset mass (1250 kg) and yaw inertia (700 kgm^2)
l_g, l_v	Half guage of wheelset(0.75 m), half spacing of axle(1.225 m)
r_0, λ	wheel radius(0.45 m), and conicity (0.2)
m_g, I_g	Bogie mass(6945 kg), and Yaw inertia (3153 kgm^2)
K_{sc}, C_{sc}	Secondary Lateral and longitudinal stiffness (511 kNm^{-1}), and damping(37 $kNsm^{-1}$)
K_s, C_s	primary Lateral stiffness (4750 kNm^{-1}), and damping (7705 $N\,sm^{-1}$)
m_v	Half vehicle mass (15000kg)
f_{11}, f_{22}	Longitudinal/ lateral creepage coefficient (10MN).
R_1, R_2	Radius of the curved track at the leading and trailing Wheeslet(1250 m).
$\theta_{c_1}, \theta_{c_2}$	cant angle of the curved track at the leading and trailing wheelset (6°)
y_{t_1}, y_{t_2}	Track lateral diplacement for leading and trailing wheelsets
τ_{w_1}, τ_{w_2}	Controlled torque for leading and trailing weelset
I_m	Motor moment of inertia (0.00115 $kg.m^2$)
R_a	Motor armature resistance (0.112Ω)
L_a	Motor armature inductance (9.04e-4 H)
K_t	Motor torque constants (1.611 $N.m.A^{-1}$)
K_b	Motor back e.m.f constant (1.305)
n	Gear ratio (1/87)
K_g	Gearbox drive stiffness(1.131102e6 $N.m.rad^{-1}$)

REFERENCES

(1973). *Aircraft Accident Report: American Airlines 1972.* Washington, US: National Transportation Safety Board.

(1979). *Aircraft Accident Report American Airlines.* Washington, US: National Transportation Safety Board.

Aknin, P., Ayasse, J. B., & Devallez, A. (1991). Active steering of railway wheelsets. *Proceedings of the 12th IAVSD Conference.* Lyon, France.

Albers, A., Meid, M., & Ott, S. (2010). Avoiding clutch excited judder by using an active clamping force control. *Proceedings of International Conference on Noise and Vibration Engineering (ISMA).* Leuven, Belgium.

Alwi, H., Christopher, E., Tan, P., & Chee. (2011). *Fault Detection and Fault-Tolerant Control Using Sliding Modes.* London, UK: Springer.

Anon, A. (1997). A powerful lightweight packed with innovative ideas-single-axle running gear. *research journal of Deutsche Bahn AG (BahnTech), 3*(97), pp. 4-9.

Ayasse, J. B., & Chollet, H. (2006). Chapter 4: Wheel – Rail Contact. In S. Iwnicki (Ed.), *Handbook of Railway Vehicle Dynamics* (pp. 85-120). New york: CRC Press.

Balaban, E., Bansal, P., Stoelting, P., & Saxena, A. (2009). A Diagnostic Approach for Electro-Mechanical Actuators in Aerospace Systems. *Aerospace conference* (pp. 1-13). Big Sky, Montana, US: IEEE.

Benıtez, Hector, García, N., & Fabián. (2005). *Reconfigurable distributed control.* London, UK: Springer.

Blanke, M., Izadi Zamanabadi, R., Bogh, R., & Lunau, Z. P. (1997). Fault tolerant control systems- a holistic view. *Journal of Control Engineering Practice, 5*(5), pp. 693–702.

Blanke, M., Staroswieck, M., & Wu, N. E. (2001). Concepts and Methods in -Fault-tolerant Control. *Proceedings of American Control Conference. 4*, pp. 2606 - 2620. Arlington, Virginia, US: IEEE.

Borner, M., Straky, H., Weispfenning, T., & Isermann, R. (2002). Model based fault detection of vehicle suspension and hydraulic brake systems. *Journal of Mechatronics, 12*(8), pp. 999–1010.

Brickle, B. V. (1986). Railway vehicle dynamics. *Journal of Physics in Technology, 17*(4), pp. 181-186.

Briere, D., Favre, C., & Traverse, P. (2001). Chapter 12: Electrical flight controls, from Airbus A320/330/340 to future military transport aircraft: A family of fault-tolerant system. In C. R. Spitzer (Ed.), *Digital Avionics Handbook* (2 ed., Vol. 2). Boca Raton, FA, US: CRC Press.

Bruccoleri, M., Amico, M., & Perrone, G. (2003). Distributed intelligent control of exceptions in reconfigurable manufacturing systems. *Journal of Production Research, 41*(7), pp. 1393–1412.

Bruni, S., Goodall, R., Mei, T. X., & Tsunashima, H. (2007). Control and monitoring for railway vehicle dynamics. *Journal of Vehicle System Dynamics, 45*(7–8), pp. 743–779.

Chandler, P. R. (1984). Self-repairing flight control system reliability and maintainability program—executive overview. *National Aerospace and Electronic Conference* (pp. 586–590). Dayton, US: IEEE.

Chapra, S. C., & Canale, R. P. (2009). *Numerical Methods for Engineers* (6th ed.). New York, US: McGraw Hill.

Charles, G., Goodall , R., & Dixon , R. (2008). Model-based condition monitoring at the wheel–rail interface. *Journal of Vehicle System Dynamics, 46*(1), pp. 415-430.

Chen, J. (1995). *Robust residual generation for model-based fault diagnosis of dynamic systems*. York, Uk: (PhD thesis), University of York, York. Retrieved from http://etheses.whiterose.ac.uk/2468/1/DX191764.pdf.

Chen, J., & Patton, R. J. (1999). *Robust Model-Based Fault Diagnosis for Dynamic Systems* (3 ed.). US: Springer.

Chen, J., Roberts, C., & Weston, P. (2008). Fault detection and diagnosis for railway track circuits using neuro-fuzzy systems. *Journal of Control Engineering Practice, 16*(5), pp. 585–596.

Chow, E. Y., & Willsky, A. S. (1980). Issue in the development of a general algorithm for reliable failure detection. *In Proceedings of 19th Conference on Decision and Control including the Symposium on Adaptive Processes* (pp. 1006-1012). Albuquerque, NM, USA: IEEE.

Clarke, D. W. (1995). Sensor, actuator, and loop validation. *Colloquium on Advances in Control Technology*. *15*, pp. 39-45. London: IET.

Crepin, P., & Kress, R. (2000). Model based fault detection for an aircraft. *22nd Congress of International Council of the Aeronautical Sciences.* Harrogate, UK: Retrieved from http://www.icas.org/ICAS_ARCHIVE/ICAS2000/ABSTRACTS/ICA0631.HTM.

Dexter, A. L., & Benouarets, M. (1997). Model-based fault diagnosis using fuzzy matching . *IEEE Transaction on Man, and Cybernetics Society, 27*(5), pp. 673 - 682.

Diana, G., Bruni, S., Cheli, F., & Resta, F. (2002). Active control of the running behaviour of a railway vehicle stability and curving performances. *Proceedings of the 17th IAVSD symposium, 37*, pp. 157-170. Lyngb, Denmark.

Ding, S. X. (2014). *Data-driven Design of Fault Diagnosis and Fault-tolerant Control Systems.* London, UK: Springer.

Djeghali, N., Ghanes, M., Djennoune, S., & Barbot, J. P. (2010). Fault tolerant control for induction motors using sliding mode observers. *11th International workshop on Variable Structure System (VSS)* (pp. 190 - 196). Mexico City, US: IEEE.

Dukkipati, R., Narayanaswamy, S., & Osman, M. (1992). Independently rotating wheel systems for railway-a state-of-the-art review. *Journal of Vehicle System Dynamics, 21*(1), pp. 297-330.

El Hachemi Benbouzid, M. (2000). A Review of Induction Motors Signature Analysis as a Medium for Faults Detection. *IEEE Transaction on Industrial Electronics, 47*(5), pp. 984 - 993.

Frank, P. (1990). Fault diagnosis in dynamic systems using analytical and knowledge-based redundancy: A survey and some new results. *Journal of Automatica, 26*(3), pp. 459–474.

Furman, C. P., Chutani, S., & Nussbaumer, H. J. (1995). Hardware/ doftware fault tolerance with multiple task modular redundancy. *Computers and Communications* (pp. 171-177). Alexandria, Egypt: IEEE.

Gallagher, P. A., Paciotti, G., Ribichini, A., & Struve, B. C. (2012). *Patent No. WO2012017195 A1*. UK.

Garg, V., & Dukkipati, R. (1984). *Dynamic of Railway Vehicle Systems.* Canada: ACADEMIC PRESS.

Gayme, D., Menon, S., Ball, C., & Mukavetz, D. (2003). Fault detection and diagnosis in turbine engines using fuzzy logic. *22nd Conference on Fuzzy Information Processing Society* (pp. 341 - 346). US: IEEE.

Gertler, J. (1998). *Fault Detection and Diagnosis in Engineering Systems.* New York, US: Marcel Dekker.

Goodall, R. M. (1997). Active Railway Suspensions: Implementation Status and Technological Trends. *Journal of Vehicle System Dynamics, 28*(2-3), pp. 87-117.

Goodall, R. M., & Li, H. (2000). Solid Axle and Independently-Rotating Railway Wheelsets - A Control Engineering Assessment of Stability. *Journal of Vehicle System Dynamics, 33*(1), pp. 57–67.

Goodall, R. M., & Kortum, W. (2002). Mechatronic developments for railway vehicles of the future. *Journal of Control Engineering Practice, 10*(8), pp. 887–898.

Goodall, R. M., & Mei, T. X. (2006a). Chapter 11: Active Suspension. In S. Iwincki, & S. Iwnicki (Ed.), *Handbook of Railway Vehicle Dynamics* (pp. 327-357). US: CRC Press.

Goodall, R. M., & Mei, T. X. (2006b). Advanced Control and Monitoring For Railway Vehicle Suspensions. *International Symposium on Speed-up and Service Technology for Railway and Maglev Systems (STECH'06), 1*, pp. 10-16. Chengdu Sichuan, China.

Goodall, R. M., Bruni, S., & Mei, T. X. (2006). Concepts and prospects for actively-controlled railway running. *Journal of Vehicle System Dynamics, 44*(1), pp. 60-70.

Goodall, R. M. (2010). Control engineering challenges for railway trains of the future. *International Conference on Control (UKACC)* (pp. 1 - 10). Coventry: IET.

Goupile, P. (2011). AIRBUS state of the art and practice on FDI and FTC in flight control system. *Journal of Control Engineering Practice, 19*(6), pp. 524-539.

Gretzschel, M., & Bose, L. (1999). A mechatronic approach for active influence on railway vehicle running behaviour. *proceedings of the 16th IAVSD symposium*, *33*, pp. 418-430. Pretoria, South Africa.

Guenab, F., Weber, P., Theilliol, D., & Zhang, Y. M. (2011). Design of a fault tolerant control system incorporating reliability analysis and dynamic behaviour constraints. *Journal of Systems Science, 42*(1), pp. 219-233.

Haggag, S., Rosa, A., Huang, K., & Cetinkunt, S. (2007). Fault tolerant real time control system for steer-by-wire electro-hydraulic systems. *Journal of Mechatronics*, *17*(2-3), pp. 129–142.

Haupt , S. E., & Haupt, R. L. (2004). *Practical Genetic Algorithms* (2nd ed.). US: John Wiley & Sons.

Henry, M. P., & Clarke, D. W. (1993). The self-validating sensor: rationale, definitions, and examples. *Journal of Control Engineering Practice, 1*(4), pp. 585-610.

Himmelblau, D. M. (1979). *Fault Diagnosis in Chemical and Petrochemical Processes (Chemical Engineering Monographs)* (Vol. 8). Amsterdam: Elsevier Science .

Hoskins, J. C., & Himmelblau, D. M. (1988). Artificial neural network models of knowledge representation in chemical engineering. *Journal of Computers & Chemical Engineering, 12*(9-10), pp. 881–890.

Ifedi, C. J., Mecrow, B. C., Brockway, S. T., Boast, G. S., Atkinson, G. J., & Kostic-Perovic, D. (2011). Fault-Tolerant In-Wheel Motor Topologies for High-Performance Electric Vehicles. *International Electric Machines & Drives Conference (IEMDC)* (pp. 1310-1315). Niagara Falls, ON, US: IEEE.

Isermann, R. (1997). Supervision, fault-detection and fault-diagnosis methods — An introduction. *Journal of Control Engineering Practice, 5*(5), pp. 639–652.

Isermann, R., Schwarz, R., & Stolzl, S. (2002). Fault-tolerant drive-by-wire systems. *IEEE Transaction on Control Systems, 22*(5), pp. 64-81.

Isermann, R. (2005). Model-based fault-detection and diagnosis- status and applications. *Journal of Annual Reviews in Control, 29*(1), pp. 71-85.

Isermann, R. (2008). Mechatronic systems—Innovative products with embedded control. *Journal of Control Engineering Practice, 16*(1), pp. 14–29.

Isermann, R. (2011). *Fault-Diagnosis Applications.* Berlin, Germany, Germany: Springer. Retrieved from 978-3-642-12766-3

Iwnicki, S. (2003). Simulation of wheel–rail contact forces. *Journal of Fatigue & Fracture of Engineering Materials & Structures, 26*(10), pp. 887-900.

Jiang, J. (2005). Fault-tolerant Control Systems- An Introduction Overview. *Journal of ACTA Automatic SINICA, 31*(1), pp. 161-174.

Kalman, R. E. (1960). A New Approach to Linear Filtering and Prediction Problems. *Journal of Basic Engineering, 82*(1), pp. 35-45.

Kortüm, W., Goodall, R., & Hedrick, J. (1998). Mechatronics in ground transportation-current trends and future possibilities. *Journal of Annual Reviews in Control, 22*, pp. 133–144.

Kwan, C., & Xu, R. (2004). A note on simultaneous isolation of sensor and actuator faults. *IEEE Transaction on Control Systems Technology*, pp. 183 - 192.

Lehrasab, N., Roberts, C., & Goodman, C. J. (2002). Industrial fault diagnosis: Pneumatic train door case study. *Journal of Rail and Rapid Transit (Part F), 216*, pp. 175-183.

Leontaritis, I., & Billings, S. A. (1985). Input-output parametric models for non-linear systems Part I: deterministic non-linear systems. *Journal of Control, 41*(2), pp. 303-328.

Li, B., Chow, M. Y., Tipsuwan, Y., & Hung, J. C. (2000). Neural-network-based motor rolling bearing fault diagnosis. *IEEE Transaction on Industrial Electronics, 47*(5), pp. 1060-1069.

Li, H. (2001). *Measuring systems for active steering of railway vehicles, A Doctoral Thesis.* Loughborough, UK: (PhD thesis), Loughborough University, Retrieved from https://dspace.lboro.ac.uk/2134/6790.

Li, H., & Goodall, R. (1998). Modelling and analysis of a railway wheelset for active control. *International Conference on Control (UKACC). 2*, pp. 1289 - 1293. Swansea, UK: IET.

Li, P., Goodall, R., Weston, P., Ling, C. S., Goodman, C., & Roberts, C. (2007). Estimation of railway vehicle suspension parameters for condition monitoring. *Journal of Control Engineering Practice, 15*(1), pp. 43–55.

Liu, X. F., & Dexter, A. (2001). Fault-tolerant supervisory control of VAV air-conditioning systems. *Journal of Energy and Buildings, 33*(4), pp. 379–389.

Lombaerts, T. J, Saili, H., & Breeman, J. (2010). Introduction. In C. Edwards, T. Lomaerts, & H. Smaili (Eds.), *Fault Tolerant Flight Control A Benchmark Challenge* (pp. 3-45). Berlin, Germany: Springer.

Lombaerts, T. J., Looye, G. H., Chu, Q. P., & Mulder, J. A. (2012). Design and simulation of fault tolerant flight control based on a physical approach. *Journal of Aerospace Science and Technology, 23*(1), pp. 151–171.

Maybeck, P. S. (1979). *Stochastic models, estimation and control* (Vol. 1). New York, US: Academic Press.

McMahan, J. (2005). Delta Flight 1080 Jammed Elevator Incident. *Journal of American Aviation Historical Society, 50*(4), pp. 270-274.

Mehrabi, M. G., Ulsoy, A. G., Koren, Y., & Heytler, P. (2002). Trends and perspectives in flexible and reconfigurable manufacturing systems. *Journal of Intelligent Manufacturing, 13*(2), pp. 23–44.

Mei, T. X., & Goodall, R. M. (1999a). Wheelset control strategies for a two axle railway vehicle. *Vehicle System Dynamics Supplement, 33*, pp. 653–664.

Mei, T. X., & Goodall, R. M. (1999b). Optimal control strategies for active steering of railway vehicles. *Proceedings of IFAC world congress 99, F*, pp. 251–256. Beijing, China.

Mei, T. X., & Goodall, R. M. (2000a). Modal Controllers for Active Steering of Railway Vehicles with Solid Axle Wheelsets. *Journal of Vehicle System Dynamics, 34*(1), pp. 25-41.

Mei, T. X., & Goodall, R. M. (2000b). LQG and GA solutions for active steering of railway vehicles. *IEE Proceedig on Control Theory and Applications, 147*(1), pp. 111 - 117.

Mei, T. X., Perez, J., & Goodall, R. M. (2000). Design of optimal PI cotrol for perfect curving of railway vehicle with solid axle wheelsete. *International conference of Control (UKACC).* Cambridge, UK.

Mei, T. X., & Goodall, R. M. (2001). Robust control for independently rotating wheelsets on a Railway Vehicle Using Practical Sensors. *IEEE Transactions on control systems technology, 9*(4), pp. 599-607.

Mei, T. X., Li, H., & Goodall , R. M. (2001). Kalman filters applied to actively controlled railway vehicle suspensions. *Transactions of the Institute of Measurement and Control, 23*, pp. 163–181.

Mei, T. X., Li, H., Goodall, R. M., & Wickens, A. H. (2002). Dynamics and control assessment of rail vehicles using permanent magnet wheel motors. *Vehicle System Dynamics Supplement, 37*, pp. 326-337.

Mei, T. X., Nagy, Z., Goodall, R. M., & Wickens, A. H. (2002). Mechatronic solutions for high-speed railway vehicles. *Journal of Control Engineering Practice, 10*(9), pp. 1023–1028.

Mei, T. X., & Goodall, R. M. (2003a). Recent development in active steering of railway vehicles. *Journal of Vehicle System Dynamics, 39*(6), pp. 415-436.

Mei, T. X., & Goodall, R. M. (2003b). Control for Railway Vehicles. *Control Systems, Robotics and Automation in Encyclopedia of Life Support Systems (EOLSS)* (pp. 1-63). Oxford, UK: Eolss.

Mei, T. X., & Goodall, R. M. (2007). Stability control of railway bogies using absolute stiffness: sky-hook spring approach. *Journal of Vehicle System Dynamics, 44*(Supplemnt(1)), pp. 83-92.

Mei, T. X., & Li, H. (2007). Control design for the active stabilisation of rail wheelsets. *Transactions of the ASME, Journal of Dynamic Systems, Measurement and Control, 130*(1), pp. 11002-11009.

Mendonça, L., Sousa, J., & Costa, J. S. (2006). Chapter 3: Fault detection and isolation of industrial processes using optimized fuzzy models. In V. Palade, L. Jain, & C. D. Bocaniala (Eds.), *Computational inteligence in fault diagnosis* (pp. 81-104). London, UK: Springer.

Meneganti, M., Saviello, F., & Tagliaferri, R. (1998). Fuzzy neural networks for classification and detection of anomalies. *IEEE Transaction on Neural Networks, 9*(5), pp. 848–861.

Mirzapour, M., Mei, T. X., & Hussain, I. (2012). Assessment of fault tolerance for actively controlled railway wheelset. *International Conference on Control (UKACC)* (pp. 631 - 636). Cadiff, UK: IEEE.

Mirzapour, M., & Mei, T. X. (2014). Detection and isolation of actuator failure for actively controlled railway wheelsets. *International Conference on Control (UKACC)* (pp. 561 - 566). Loughborough, UK: IEEE.

Mirzapour, M., Mei, T. X., & Xuesong, J. (2014). Fault detection and isolation for an active wheelset control system. *Journal of Vehicle System Dynamics, 52*(Supplement(1)), pp. 157-171.

Monk-Steel, A. D., Thompson, D. J., de Beer, F. G., & Janssen, M. H. (2006). An investigation into the influence of longitudinal creepage on railway squeal noise due to lateral creepage. *Journal of Sound and Vibration, 293*(3-5), pp. 766–776.

Montoya, R. J., Howell, W. E., Bundick, W. T., Ostroff, A. J., Hueschen, R. M., & Belcastro, C. M. (1982). Restructurable controls. *Proceedings of a workshop held at NASA Langley Research Center.* Hampton, US.

Muenchhof, M., Beck, M., & Isermann, R. (2009). Fault-tolerant actuators and drives—Structures, fault detection principles and applications. *Journal of Annual Reviews in Control, 33*(2), pp. 136–148. doi:10.1016/j.arcontrol.2009.08.002

Napolitano, M. R., An, Y., & Seanor, B. A. (2000). A fault tolerant flight control system for sensor and actuator failures using neural networks. *Journal of Aircraft Design, 3*(2), pp. 103-128.

Nelles, O. (2001). *Nonlinear System Identification.* Berlin, Germany: Springer.

Nelson, V. P. (1990). Fault-tolerant computing: fundamental concepts. *IEEE Transaction on Computer Science, 23*(7), pp. 19-25.

Pacchioni, A., Goodall, R., & Bruni, S. (2010). Active suspension for a two-axle. *Journal of Vehicle System Dynamics, 48*(1), pp. 105-120.

Patton, R. J. (1991). Fault detection and diagnosis in aerospace systems using analytical redundancy. *Journal of Computing & Control Engineering, 2*(3), pp. 127-136.

Patton, R. J. (1997). Fault-tolerant control systems: The 1997 situation. *In Proceedings of the 3rd IFAC symposium on fault detection, supervision and safety for technical processes*, (pp. 1033–1055). Hull,UK.

Patton, R. J., Chen, J., & Nielsen, S. B. (1995). Model-based methods for fault diagnosis: some guidlines. *Transactions of the Institute of Measurement and Control, 17*, pp. 73-83.

Patton, R. J., Clark, R. N., & Frank, P. M. (1989). *Fault Diagnosis in Dynamic Systems, Theory and Application* (1 ed.). London: Prentice Hall.

Patton, R. J., Frank, P., & Clark, R. (2000). *Issues of fault diagnosis for Dynamic Systems.* London, UK: Springer.

Patton, R. J., Uppal , F. J., & Lopez-Toribio, C. J. (2000). Soft computing approaches to fault diagnosis for dynamic systems: a survey. *Paper presented at the Proceedings of the 4 th IFAC Symposium* . Retrieved from University of Hull http://www.hull.ac.uk/control/downloads/softcomp.pdf.

Pau, L. F. (1981). *Failure Diagnosis and Performance Control.* New York, US: Marcel Dekker.

Pearson, J. T., Goodall, R. M., Mei, T. X., & Himmelstein, G. (2004). Active stability control strategies for a high speed bogie. *Journal of Control Engineering Practice, 12*(11), pp. 1381–1391.

Pearson, J. T., Goodall, R. M., Mei, T. X., Shuiwen, S., Kossmann, C., & Himmelstein, G. (2003). Control system design methodology of an active stabilisation system for a high speed railway vehicle. *European Control Conference (ECC)* (pp. 2396 - 2400). Cambridge, UK: IEEE.

Perez, J., Busturia, J. M., & Goodall, R. M. (2002). Control strategies for active steering of bogie-based railway vehicles. *Journal of Control Engineering Practice, 10*(9), pp. 1005-1012.

Perez, J., Stow, J. M., & Iwnicki, S. (2006). Application of active steering systems for the reduction of rolling contact fatigue on rails. *Journal of Vehicle System Dynamics, 44*(Supplement (1)), pp. 730-740.

Polach, O. (2004). Curving and Stability optimisation of locomotive bogies using interconnected wheelsets. *Vehicle System Dynamics, 41*(Supplement), pp. 53-62.

Polach, O. (2005). Creep forces in simulations of traction vehicles running on adhesion limit. *Journal of Wear, 258*(7-8), pp. 992-1000.

Rauber, T. W., Nascimento, E. M., Wandekokem, E. D., & Varejão, F. M. (2010). Pattern Recognition based Fault Diagnosis in Industrial Processes: Review and Application. In A. Herout (Ed.), *Pattern Recognition Recent Advances* (pp. 483-508). Rijeka, Croatia: InTech.

Rich, S. H., & Venkatasubramanian, V. (1987). Model-based reasoning in diagnostic expert system for chemical process plant. *Journal of Computers & Chemical Engineering, 11*(2), pp. 111-122.

Schwarz, R., Isermann, R., Böhm, J., Nell, J., & Rieth, P. (1998). Modeling and control of an electro-mechanical disk brake. *SAE Technical Paper Series, 980600,* pp. 177-189. doi:10.4271/980600

Sharma, A. B., Golubchik, L., & Govindan, R. (2010). Sensor faults: Detection methods and prevalence in real-world datasets. *ACM Transactions on Sensor Networks (TOSN), 6*(3), pp. 1-34.

Shen, G., & Goodall, R. (1997). Active Yaw Relaxation for Improved Bogie Performance. *Journal of Vehicle System Dynamics, 28*(4-5), pp. 273-289.

Simani, S. (2006). *Fault diagnosis of dynamic systems using model-based and filtering approaches.* Ferrara , Italy: Retrieved from http://www.silviosimani.it/FDI-lecture-notes.pdf.

Simani, S., Fantuzzi, C., & Patton, R. J. (2003). *Model-based Fault Diagnosis in Dynamic System Using Identification Techniques.* London, UK: Springer.

Sobhani, E. T., & Khorasani, K. (2009). *Fault Diagnosis of Nonlinear Systems Using a Hybrid Approach* (1 ed.). US: Springer.

Steinberg, M. (2005). Historical overview of research in reconfigurable flight control. *Journal of Aerospace Engineering, 219*(G), pp. 263–275.

Suda, Y., Wang, W., Nishina, M., Lin, S., & Michitsuji, Y. (2012). Self-steering ability of the proposed new concept of independently rotating wheels using inverse tread conicity. *Journal of Vehicle System Dynamics, 50*(Supplement (1)), pp. 291-302.

Tarnowski, E. (2008). Overview of potential evolutions of technologies applied in commercial transport airplanes. *In Proceedings of the 17th IFAC world congress.* COEX, South Korea.

Thompson, H. A., & Fleming, P. J. (1990). Fault-tolerant transputer-based controller configurations for gas-turbine engines. *Journal of Control Theory and Applications, 137*(4), pp. 253 - 260.

Ulieru, M., & Isermann, R. (1993). Design of fuzzy logic based diagnostic model for technical process. *Journal of Fuzzy Set and Systems, 58*(3), pp. 249–271.

Venkatasubramanian, V., & Chan, K. (1989). A neural network methodology for process fault diagnosis. *AIChE Journal, 35*(12), pp. 1993-2002.

Wickens, A. H. (1973). Stability of High Speed trains. *Journal of Physics in Technology, 4*(1), pp. 1 -17.

Wickens, A. H. (1994). Dynamic Stability of articulated and steered railway vehicles guided by lateral displacement feedback. *Journal of Vehicle System Dynamics, 23*(Supplement (1)), pp. 541–553.

Wickens, A. H. (1998). The dynamics of railway vehicles—from Stephenson to Carter. *IMechE proc (part F), 212*(F), pp. 209–217.

Wickens, A. H. (2003). *Fundamentals of Rail Vehicle Dynamics: Guidance and Stability.* The Netherlands: Swets & Zeitlinger.

Wickens, A. H. (2006). Chapter 2: A History of Railway Vehicle Dynamics. In S. Iwnicki (Ed.), *Handbook of Railway Vehicle Dynamics* (pp. 5-31). New York, US: CRC Press.

Wolfgang, B. (2015). *Bond Graph Model-based Fault Diagnosis of Hybrid Systems* (1 ed.). Switzerland: Springer.

Xu, X., Hines, J. W., & Uhrig, R. E. (1998). On-Line Sensor Calibration Monitoring And Fault Detection For Chemical Processes. *Maintenance and Reliability Conference.* University of Tennessee, USA.

Zhang, X., Foo, G., Vilathgamuwa, M. D., Tseng, K. J., Bhangu, B. S., & Gajanayake, C. (2013). Sensor fault detection, isolation and system reconfiguration based on extended Kalman filter for induction motor drives. *IET Transaction on Electric Power Applications, 7*(7), pp. 607-617.

Zhang, Y. M., & Jiang, J. (2006). Issues on integration of fault diagnosis and reconfigurable control in active fault-tolerant control. *6th IFAC Symposium on Fault Detection, Supervision and Safety of Technical Processes.*

Zhang, Y., & Jiang, J. (2008). Bibliographical review on reconfigurable fault-tolerant control systems. *Journal of Annual Reviews in Control, 32*(2), pp. 229–252.

Zheng Jiang , J., Z. Matamoros-Sanch, A., Goodall, R. M., & Smith, M. C. (2012). Passive suspensions incorporating inerters for railway vehicles. *Journal of Vehicle System Dynamics, 50*(Supplement (1)), pp. 263-276.

Zhongming , Y. (2000). A review on induction motor online fault diagnosis. *3rd Proceeding on Power Electronics and Motion Control Conference (IPEMC). 3*, pp. 1353 - 1358. Beijing: IEEE.

Zolotas, A. C., & Goodall, R. M. (2007). Modelling and control of railway vehicle suspensions. In *Lecture Notes in Control and Information Sciences* (pp. 373-412). New York, US: Springer.